NONLINEAR VIBRATION AND CONTROL OF FIBER METAL LAMINATES

by

JIANJUN LIU

A dissertation submitted to the Graduate Faculty in Engineering in partial fulfillment of the requirements for the degree of Doctor of Philosophy, The City University Of New York

2007

UMI Number: 3245093

ProQuest Information and Learning Company
300 North Zeeb Road
P.O. Box 1346
Ann Arbor, MI 48106-1346

This manuscript has been read and accepted for the Graduate Faculty in Engineering in satisfaction of the dissertation requirement for the degree of Doctor of Philosophy.

Prof. Benjamin Liaw

Date — Chair of Examining Committee

Dean Mumtaz K. Kassir

Date — Executive Officer

Prof. Benjamin Liaw, Dept of Mechanical Engineering, The City College

Prof. Charusheel Bapat, Dept of Mechanical Engineering, The City College

Prof. Yiannis Andreopoulos, Dept of Mechanical Engineering, The City College

Prof. Jackie Li, Dept of Mechanical Engineering, The City College

Prof. Vikram Kapila, Dept. of Mechanical, Aerospace and Manufacturing Engineering, Polytechnic University

Supervision Committee

THE CITY UNIVERSITY OF NEW YORK

ABSTRACT

NONLINEAR VIBRATION AND CONTROL OF FIBER METAL LAMINATES

by

Jianjun Liu

Adviser: Professor Benjamin Liaw
Co-adviser: Professor Charusheel Bapat

In this dissertation, we first studied the linear and nonlinear vibration of cantilever beams made of Fiber Metal Laminates (FMLs). An inextensible beam model with nonlinear damping was adopted to explore the nonlinearities of cantilever beams. Approximate solutions were obtained by solving an integro-differential equation via Multiple Scales method and Harmonic Balance Method. For the single-mode response, a large discrepancy in the nonlinear coefficient was found between theory and experiment. For different excitation level, a small variation in the linear natural frequency was detected. A beam model with a nonlinear spring-hinged end and the other end free was applied to tune the inextensible cantilever beam theory. While this modified mode can reasonably explain the natural frequency difference, its ability to resolve the discrepancy in the nonlinear coefficient is limited.

Then we studied the efficiency problems of using PZT patches in negative feedback control of beam. Uniform beam model was applied when the mass and stiffness of PZT patches were ignored. Stepped beam model was then derived to describe the beam-actuator structure when the effect of patches was taken into consideration. It is found that the use of PZT patches for active vibration control may degrade the control

efficiency by modifying the configuration of the structure. It is also found that the optimal positions from stepped beam model are similar to those from the uniform beam model. The ratio of control efficiency from the stepped beam model to that from the uniform beam model is associated with material properties and structural dimensions. Because the factor is a constant when the structure is determined, we propose a modified model to estimate the control efficiency. Several experiments on vibration control of a beam were conducted to verify our efficiency estimate.

Finally we extended our control efficiency estimation method to the vibration of plates. It is found that the structural modification caused by attaching PZT patches may degrade the control ability while the optimal positions are not sensitive to these structural alterations. Our proposed efficiency estimation method works well for the vibration control of plates.

ACKNOWLEDGMENTS

I would like to dedicate this work to my family, who have been giving me endless support for so many years. I would also like to acknowledge my mentors, Professors Benjamin Liaw and Charusheel Bapat, who offered continuous valuable advice, guidance and suggestions. In addition, I would like to thank Professors Yiannis Andreopoulos and Jackie Li from Department of Mechanical Engineering at City College of New York as well as Professor Vikram Kapila from Department of Mechanical, Aerospace and Manufacturing Engineering at Polytechnic University for serving on my Ph.D. Dissertation Committee.

I would also like to thank my research colleagues: Mr. Thomas Cheung, Yanxiong Liu, and all my friends who have worked in the Material Processing and Solid Mechanics Laboratory, Department of Mechanical Engineering, City College of New York.

Table of Contents

List of Tables

List of Figures

CHAPTER 1: OVERVIEW

1.1 INTRODUCTION

Fiber-metal laminates are hybrid composites formed by interlacing layers of thin metals (usually aluminum alloy) and fiber-reinforced laminae to optimize the properties of metals and fiber-reinforced laminae for better damage tolerance to fatigue crack growth, foreign body impact damage, corrosion resistance and fire retardation [205,221,280,309,337,351,352]. In addition they are relatively lightweight in comparison to their metallic counterparts. Commercially two types of fiber-metal laminates are available: Glare and ARALL, which use glass-epoxy and aramid-epoxy laminae, respectively, with thin aluminum sheets and have been adopted widely in the aerospace and spacecraft industries. While a lot of references can be found on the damage tolerance of Fiber-metal laminates, little work has been done about its dynamical properties, especially in nonlinear domain under moderate to large deformation.

Weight saving is a critical issue in almost all disciplines of engineering design and analysis. Although lightweight structures are more desirable for cost reduction and efficiency enhancement, the use of lightweight materials often results in increased flexibility and poor stability. It is therefore essential for any high-precision operation to properly control vibration and stabilize an engineering structure. In general, there are two types of techniques to reduce vibration - passive control and active control. Passive control enhances the system damping by incorporating viscoelastic materials or implanting mechanical dampers whereas active control counteracts undesirable motion by creating control forces from actuators.

It has been demonstrated by many researchers that active control is an effective way for vibration suppression and control. The study of active vibration control has attracted a great deal attention in a new discipline, which is called “smart structures, adaptive materials, and/or intelligent systems” [8]. To serve the purpose of actuation, there are several types of materials available: electrostrictive materials, magnetostrictive materials, piezoelectric materials, thermomechanical materials, shape memory alloys[84,88,107,117,185,195,201,237,266,279,292,296,380], and electrorheological fluids [124,179,194,197,287], just to name a few. Among them, lead zirconate titanate piezoceramic materials, commonly known as PZT, have been found very useful in many applications. These materials have high stiffness for resisting deformation and low time constant for rapid response. They are space resizable and can be bonded or embedded into host structures without much difficulties. Discovered in 1880 by Pierre and Jacques Curie, the theory governing typical PZT behaviors is called piezoelectric effect [2]. Although the material response of a typical PZT is nonlinear in nature [164,329,339,374], for most engineering applications the linear model of piezoelectricity is acceptable within a reasonable range of precision.

During the past two decades, the use of PZT as actuators in active vibration control has generated a lot of interest within the research community. These include, but not limited to, modeling control mechanism of PZT, implementation and verification of using PZT as actuating elements, and optimization problems in control systems involving PZT as actuators and/or sensors.

Although there are many papers studying the PZT’s applications in various areas in recent years, little work has been done about the modification of host structure due to

attachment of PZT patches. People rarely notice that this alteration could degrade the control efficiency substantially. In this study, we will concentrate on the control ability that PZT patches can provide to the host structure. By comparing the efficiency estimates with and without consideration of structural alteration because of the presence of actuators, a new method is introduced for better prediction of control ability of PZT patches.

In Chapter 2, a series of experiments were first conducted to measure the dynamic Young's moduli and damping ratios of aluminum alloys and fiber-metal laminates. Results from this preliminary study will be used as the benchmark data for nonlinear analysis and active vibration control presented in chapter 3 and chapter 4.

In Chapter 3, an inextensible beam model with nonlinear damping was presented. Approximate solutions were obtained by solving an integro-differential equation via Multiple Scales method and Harmonic Balance Method. For the single-mode response, a large discrepancy in nonlinearity coefficient was found between theory and experiment. For different excitation level, a small variation in the linear natural frequency was detected. A beam model with a nonlinear spring-hinged end and the other end free was used to fit theoretical results with the experimental outputs. While this modified mode can reasonably explain the small natural frequency variation, it is incapable to explain the large discrepancy in nonlinearity coefficients. It is also found that the damping is inherently complicate phenomena.

In Chapter 4, uniform beam model and stepped beam model were applied to describe the beam-actuator structure respectively. The efficiency functions from both models were calculated. It was found that the use of PZT patches for active vibration

control may degrade the control efficiency by modifying the configuration of the structure. A new model was proposed to simplify the procedure of solving the efficiency problem when using PZT patches as actuator. Optimal configurations of PZT patches were obtained by maximizing the efficiency functions. Several experiments were conducted to prove some of our conclusions. Then we extended our control efficiency estimation method to the vibration of plates. A numerical example was conducted to verify this combination model. A pair of PZT patches were surface-bonded as actuators. Uniform plate model was applied when the mass and stiffness of PZT patches were ignored. Finite element method was adopted when the effect of patches was taken into consideration. Optimal positions of actuators pair were obtained by maximizing the mode control authority. It is found that the structural modification caused by attaching PZT patches may degrade the control ability while the optimal positions are not sensitive to these structural alterations.

In Chapter 5, the conclusion and contributions of the present research are presented. Suggestions for future work are described.

1.2 LITERATURE REVIEW

1.2.1 Linear Beam Theories

There are mainly three beam theories in use today.

(1) The exact elasticity solutions of beam theory.

The detailed development of the theory of elasticity approach of beam problem can be found in reference [5] and [10]. They organized the works of Galileo, Bernoulli, Euler, Coulomb, Saint-Venant, Poisson, Kirchhoff, Rayleigh, and Timoshenko etc. This

approach has a major drawback however. It can only solve problems with relatively simple boundary conditions and loadings.

(2) The Euler-Bernoulli beam theory.

The Euler-Bernoulli beam theory assumes plane sections remain plane and normal to the deflected axis and do not undergo any strain in the plane. This means warping, shear deformation and normal strain are neglected. These assumptions are valid for slender beams undergoing small deflections. Under this theory the rotation of the cross sections is due to bending alone.

(3) The Timoshenko beam theory.

If the ratio of thickness to length of the beam is not small enough, the transverse shear is not negligible. Based on the Euler-Bernoulli beam theory, the Timoshenko beam theory does consider the effect of transverse shear deformation. In this theory, in order to simplify the complex nature of deformation, the shear strain is assumed to be uniform over a given cross section. A shear correction factor is introduced to account for the transverse shear effects, and its value depends on the shape of the cross section. The rotation of the cross section is due to both bending and transverse shear deformation in the Timoshenko beam theory [218]. Timoshenko later extended the theory to include the rotatory inertia effect.

When deflection is small a linear beam model would suffice. However several nonlinearities need to be considered when dealing with large deformation problems. Nonlinearities of a beam mainly come from nonlinear damping, geometric nonlinearity, inertia nonlinearity, material nonlinearity and boundary nonlinearity [218].

1.2.2 Nonlinear Beam Theories

Majority of earlier works on the nonlinearity of a transverse beam focuses on the effect of midplane stretching in the vibration of a simply supported beam. Woinowsky-Krieger [350] investigated the effect of an axial force on the vibration of hinged bars. He concluded that the nonlinearities arise from midplane stretching and nonlinear strain-displacement relations. He also found the resonant frequencies vary with the amplitude of vibration because of nonlinearity. Burgreen [60] studied the midplane stretching problem on the vibrations of a pin-ended column with constant distance between pin ends. He also considered the effects of a compressive axial load. Following a similar scheme, Eisley [116] showed the effect of an axial periodic load on the motion of a hinged beam. Ray and Bert [262] experimentally verified the midleplane stretching theory in the nonlinear vibrations of a beam with pinned ends. Evensen [118] extended their works to the vibrations of beams with simply supported and clamped ends. Busby and Weingarten [61] used a finite-element approach to analyze the nonlinearities of a beam under periodic loading.

A relatively new topic on nonlinear vibration of beams is nonlinearities coming from the nature of inextension of cantilever beams. Applying the extended Hamilton's principle, Crespo da Silva and Glynn [96,97] obtained the nonlinear integro-partial-differential equations governing the flexural-flexural-torsional motion of isotropic, inextensional beams. Nonlinearities due to inertia and geometry up to order three were kept in their derivation. Pai and Nayfeh [240] extended the model proposed by Crespo da Silva and Glynn to include the effect of shear deformation. Hodges et al. [148] addressed the issues of proper physical interpretation of the Euler angles and pointed out some common mistakes in the nonlinear modeling of a cantilever beam.

Crespo da Silva and Hodges [98,99] later derived the nonlinear differential equations of motion for a rotating beam. They investigated the influence of the nonlinear terms up to order three on the motion of a helicopter rotor blade. Further Crespo da Silva [100] studied the nonlinear flexural-flexural-torsional-extensional dynamics of beams. Pai and Nayfeh [239,240] extended the above model to include the effect of transverse shear deformation on the vibrations of slewing or rotating metallic and composite beams. Pai and Nayfeh [242] proposed a geometrically exact nonlinear beam model for naturally curved and twisted solid composite rotor blades undergoing large vibrations. In their model, both warpings and three-dimensional stress were considered.

There are other sources contributing to the nonlinearity on vibration of beams. Damping is essentially a nonlinear phenomenon. Anderson, Nayfeh, and Balachandran [13] showed that inclusion of quadratic air damping in the analytical model significantly improves the agreement between experimental and theoretical results. In the case of harmonic excitation, the energy loss for both viscous damping and structural damping is proportional to the square of the displacement amplitude. Thus, for structurally damped systems subjected to a harmonic excitation, it is convenient to replace the structural damping by an equivalent viscous damping term [6].

Nonlinearities can also appear in the boundary conditions. For example, an ideal clamped boundary condition is impossible to obtain. Tabaddor [313] found that substitution of a torsionally elastic end for the clamped-end boundary condition of a cantilever beam improves dramatically the agreement between experimental and theoretical results. The torsional spring has both linear and cubic stiffness components. Arafat and Nayfeh [26] investigated the influence of nonlinear boundary conditions on

the nonplanar autoparametric responses of an inextensible cantilever beam. They found the effective nonlinearity is related to the stiffness components of the springs.

Governing equations of nonlinear beam would also include a quadratic nonlinear term when a static deflection is present. Sato, Saito, and Otomi [276] showed the static deflection changed the effective nonlinearity of the beam while they studied the influence of gravity on the parametric resonance of a simply supported beam carrying a concentrated mass.

It is impossible to include all possible nonlinearities and secondary effects, like rotational inertia, shear deformation, warping, damping, static deformation, etc [218]. Usually insignificant nonlinearities and secondary effects are dropped. The challenge is to include enough complexity so that the problem is meaningful and, yet, apply simplifying assumptions that make the problem tractable [306].

Early works on single-mode response of nonlinear beams can be found in Ref. [7]. The characteristics of bending of the frequency-response curves, amplitude jumps, limit cycles, and hysteresis are discussed in detail for the case of a single mode under the influence of nonlinearity. Dowell et al. [113] experimentally investigated the response of a cantilever, metallic beam due to a tip load. They found experimental results agree with the nonlinear theories under small and moderate excitation. When the tip deflection is in the same order of the beam span, the nonlinear model is erratic because the assumptions of the model cannot be met. Zavodney and Nayfeh [376] conducted experiments of a cantilever beam with a lumped mass under parametrical excitation. Their theoretical model contained nonlinearities from the inertia, curvature, and axial displacement up to the third order. They found the jump points varied with increasing acceleration levels.

Using Galerkin's discretization scheme as well as multiple scales method, they obtained the approximate solutions of the governing equation.

Anderson et al. [13] investigated the nonlinear motions of cantilever beams and experimentally observed that, effective nonlinearity, which combines the inertia nonlinearity and the geometric nonlinearity, changes from hardening type in lower modes to softening type in higher modes as the natural frequency increases. Berdichevsky et al. [47] analyzed the nonlinear vibrations of a cantilever beam excited at the free end. They showed the dynamical response can be explained in terms of a dynamical potential. Moon and Holmes [227] observed chaotic motions on the vibration of a buckled elastic beam as the beam alternates between the two static equilibrium positions.

In recent years, many examples of modal interactions have been studied both experimentally and analytically. Modal interactions may be the result of internal (autoparametric) resonances, external combination resonances, parametric combination resonances, or nonresonant interactions [7].

1.2.3 Vibration Control Using PZT Patches as Actuators

There are several reviews articles about the applications and theory of piezoelectric materials [80,103,133,137,338]. Wada *et al* [338] presented a classification of adaptive structures. They categorized intelligent structures as a subset of active controlled structures. Structures with actuators distributed throughout are defined as adaptive structures or actuated structures. Conventional aircraft wings with articulated leading and trailing edge control surface is an example of adaptive structures. Structures which have sensors distributed throughout are called sensory structure. The sensors may be used to detect displacements, strains, temperature, heat flow, presence or accumulation

of damage etc. A typical example of this technology is damage detection of long life structures. The overlap structures that have sensors, actuators and controllers are classified as controlled structures. Active structures are a subset of controlled structures whose control elements (sensors and actuators) act as structural elements and are part of the load bearing system. One part of active structures with learning elements is classified as intelligent structures.

Crawley [103] presented an overview and assessment of technology leading to the development of intelligent structures. He discussed the four component technologies critical to the evolution and application of intelligent structures: actuators for intelligent structures, sensory elements, control methodology and algorithm, and controller architecture and implementation hardware.

Clinton *et al* [80] did an overview on the modeling of piezoelectric sensors and actuators incorporated in intelligent structures. They concluded that available structural models involving piezoelectric sensors and actuators fall into three broad classes: 1. Discrete (patches) piezoelectric sensors/actuators that are bonded to or embedded in structures. Their presence in the structure does not affect the overall properties of the structure when they are not activated (ignore the inertia and stiffness of sensors/actuators). 2. Distributed piezoelectric film sensors/actuators are bonded to the top and bottom of the structure. They do not affect the overall structure properties when inactivated. 3. Distributed lamina piezoelectric sensors/actuators stacked together with substrate laminae to form an active laminated composite plate. The Classic Laminated Plate Theory(CLPT) is often used to model the overall properties of the laminated composite. Giurgiutiu [133] summarize the recent achievements in the application of smart-material actuation to

counteract aeroelastic and vibration effects in helicopters and fixed wing aircraft. Gopinathan [137] reviewed different laminate theories used for the modeling and analysis of laminated composite beams or plates structures. The following review is concentrated on the PZT application in vibration control area.

1.2.3 (a) Actuation modeling

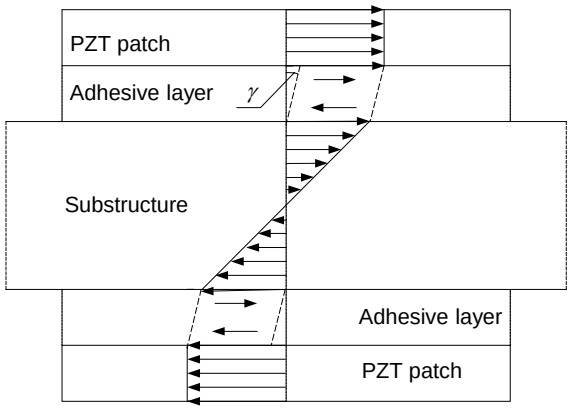

Figure 1-1 The uniform-strain model.

Two models have been explored to represent the static interaction between PZT and structures. Crawley and de Louis [101] presented uniform strain model, which is based on static case. In Fig. 1-1, two piezoelectric elements are shown bonded to an elastic substructure. If we apply voltage on both PZT patches in same amplitude and opposite phase, the substructure will be deformed in bending. It assumes uniform strain within the PZT patch and pure shear state in adhesive layer while linear strain in host structure.

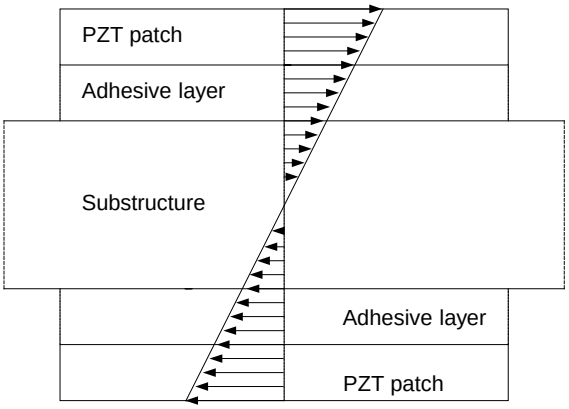

Figure 1-2 The Bernoulli-Euler model

Crawley and Anderson [102] proposed a Bernoulli-Euler model which assumes the strains distribution within actuator, adhesive layer and substrate are linear variation as shown in Fig. 1-2. Several detailed finite element models and experiments were carried out by a lot of researchers. It is found that uniform strain model is not correct when the beam is getting thinner while the Bernoulli-Euler model predicted the interaction relatively well. When extending these two models to dynamic cases, they are called pin-force model and distributed moment forcing model respectively.

Assuming the bonding is perfect and the adhesive layer is negligible, pin-force model extends uniform strain model's result to dynamic problem. It suggests the structure can be considered as beam forced by two equivalent concentrated moments acting at the edge of PZT patches. The equivalent moment [101] is

$$M_{\Lambda} = \frac{E_b b_a}{\psi + 6}\Lambda = \chi_1 V(t) \tag{1.1}$$

$$\Lambda \equiv d_{31} V / t_a \ , \qquad \psi = \frac{E_b t_b}{E_a t_a}, \qquad \chi_1 = \frac{E_b b_a}{\psi + 6}\frac{d_{31}}{t_a} \tag{1.2}$$

where E_b is the Young's modulus of the beam, t_b thickness of the beam, E_a, t_a, b_a are the Young's modulus, thickness and width of actuator respectively; d_{31} is piezoelectric coefficient corresponds to 3-1 directions, V is the voltage applied on thickness direction. Based on pin-force model, Gaudenzi *et al*[128-130] and Yang *et al* [360-368] did extensive studies from vibration suppression implementation to optimization placement of actuators.

It should be noted that this pin-force model is based on static cases, it assume the piezoelectric layer is very thin compare with the beam thickness [103,303]; it does not account for the effects of the transverse shear and axial forces in the beam. This assumption is acceptable for static case since when we bonded the piezoelectric patches to beam for shape control or other static purpose, the structures are under pure bending and piezoelectric layer is usually thin. Even if there are some other loading applied on the beam, Im and Atluri [157] proposed a revised pin-force model which accounts for the transverse loading and axial force, they derived a complicated formula for static problem which assumes the piezoelectric layer is thin and short compare the beam's and uniform strain distribution.

Distributed moment forcing model is based on Bernoulli-Euler model. This model assumes the strain distribution is linear through the entire across section and constant along the axial direction. Under this model, the effect of PZT is modeled as distributed bending moment along the contact surface.

The moment (ignore the adhesive layers) is

$$M_\Lambda = E_a \Lambda b(t_a^2 + t_b t_a) = \chi V(t) \tag{1.3}$$

$$\chi = E_a b(t_a + t_b) d_{31} \tag{1.4}$$

It was found that the distributed moment forcing model is better than pin-force model especially when the thickness of PZT is comparable with that of the beam.

Pin-force model and distributed moment forcing model are based on a pair of PZT actuators collocated on the host structure. Park *et al* [246] extended uniform stain model and Bernoulli-Euler model to one bonded piezoelectric patch case. Their method is similar to Crawley's approach [101,102]. They also presented a torsion model, which is used to control the torsional movement of beam. Strmbi *et al* [303] presented Pin-force model and Euler-Bernoulli model in a general fashion, they discussed the case of one side only actuation layer. Although Chaudhry and Rogers[79] proposed an enhanced pin-forced model, which improves the accuracy when PZT patches get thicker, majority of researchers adopt the distributed moment forcing model because the latter provides better prediction and the assumptions are generally reasonable.

Gibbs and Fuller [132] studied the actuation of piezoelectric patches on thin plates. They suggest that PZT would induce two pairs of bending moments, which bend the plate section beneath it. That is the two dimensional version of pin force modal. Tzou and Fu [325] extended the distributed moment forcing model when they investigate the segmentation of piezoelectric sensors and actuators. Ha *et al*[138] developed a finite element formulation to model the dynamic as well as static response of laminated composites containing distributed piezoelectric ceramics subjected to both mechanical and electrical loading.

1.2.3 (b) Optimization of actuators' placement and dimensions

In recent years, there are a lot of papers concentrating on PZT applications in vibration control. They implemented the available models in suppressing vibration of beam, rod [107], bar, truss [215,355], plate and shell [11,31,86,181,224,274,275,312,315, 323,326,328,329]. One branch of them is the optimization of positions and dimensions of PZT patches in vibration reduction.

It is well known that misplaced sensors and actuators lead to some problems such as lack of observability and controllability, and spillover [144,182,344]. The placements of sensors/actuators have been investigated by many researchers [21,32,34,49,51,64,76, 86,115, 128,131,140,144,152,158,180,182,202,219,229,230,271,283,301,307,344,361, 362,372,378]. Tzou and Fu [325] showed that fully covered piezoelectric sensors and actuators may not control some vibrational modes because of the lack of observability and controllability. Therefore, segmentation of the sensors and actuators is necessary to control most vibrational modes. The use of a number of small sized sensors and actuators is needed to enhance control efficiency or to control several modes simultaneously. However, as the number of independent sensors and actuators increases, the design process of the control system becomes complex and the costs and weights of the control system increase. Therefore, research on configurations of piezoelectric sensors and actuators, which guarantee sufficient degrees of controllability and observability for the vibrational modes under consideration, should be investigated

Crawley and Louis [101] used pin-force model to investigate the optimal position of PZT pairs. They suggest the optimal position of a certain mode be the anti-node of that mode. Barboni *et al* [34] extended this work using the method of modal analysis. They obtained similar results as Crawley Louis [101]. Kondoh *et al* [182] presented a strategy

of positioning sensors and actuators by minimizing the quadratic cost function in the standard optimal control. Hac and Liu [140] studied the problem of sensor and actuator locations in motion control of flexible structures. They obtained optimization criteria by considering the energy input and output. Na and Librescu [229] investigated the optimal feedback control of structure with respect to the actuator locations and power consumption. Steffen *et al* [301] used distributed moment forcing model to study the optimal problem of PZT surface bonded beams. Sadri *et al* [271] obtained two criteria for the optimal placement of piezoelectric actuators using controllability and observability of the system. Han and Lee [144] used a generic algorithm to seek the optimal locations of piezoelectric sensors and actuators of a smart composite plate from the perspective of controllability and observability. Li *et al* [51] used maximal modal force rule to find the optimal collocation of PZT pairs on the plate. They concluded that piezoelectric actuators should be bonded on the places of maximal modal strains of every order mode to produce maximal modal control forces. Aldraihem *et al* [21] proposed an optimization criterion based on modal cost and controllability index to investigate the size and placement of actuators. Ball and Jones [32] investigated the characteristics and effectiveness of shaped piezo-actuators for use in controlling the divergence of a simplified forward wing model. The effects of actuator location, size, thickness and shape were evaluated using the principle of virtue work by maximize the modal amplitude of first bending mode. They found the optimal actuator size should span the entire wing. The required actuator's thickness for divergence control decreases with increase airspeed due to the effectiveness softening of the wing in the presence of air loads. A uniform rectangle actuator is more efficient for controlling divergence; however, a linear shaped actuator is more efficient

from the standpoint of control effectiveness per actuator weight. Bhargava *et al* [49,202,203] presented optimization solution based on actuator power factor. Ip and Tse[158] presented the optimal position and orientation of a piezoelectric patch actuator for improving the controllability of isotropic plates. They found the optimal patch positions coincide exactly with anti-nodes of vibration modes for simply supported plates. Kim and Kum [180] proposed a simultaneous structural/control optimum strategy. The structural weight, the state error energy, control energy, stability robustness and electric power required for vibration control are considered as the objective function; The location of the actuators, ply orientation and thickness of composite lamina are considered as control design variables. Maln *et al*[219] investigated the optimal embedding location and thickness of PZT pair in order to get maximum bending effect from actuator. Nam *et al* [230] calculated the best geometry (placement, thickness, width and length) of piezo-actuators using numerical method. Suleman and Goncalves [307] presented the optimization of size and placement of actuator pairs on an adaptive composite beam using physical programming approach. . Yousefi-koma and Vukovich [372] proposed a simultaneous dimension and location optimization of piezoactuators. They used three different optimization criteria: maximizing overall damping ratio, minimization of the overall real part of eigenvalues of the controlled system and minimization LQR cost function. Zhang *et al* [378] applied a float-encoded genetic algorithm to the optimal control of flexible smart structure bonded with piezoelectric actuators and sensors. The objective function is based on dissipation energy due to a control action.

In all these works, the PZT patch's mass and stiffness are either assumed to be negligible, or considered but dealt with numerical methods. First they used modal expansion theorem to simplify the problem to optimization for each mode, then they combine the objective functions together to optimize several models simultaneously. If the mass and stiffness of actuators are ignored, the natural frequencies and modal functions of host structure can be calculated before optimization. And the natural frequencies and modal functions are constant during the optimizing procedure. If the host structure is simple structure like beam or plate, the analytic or semi-analytic solutions can be obtained. The objective function can be expressed specifically. It is much more complicated, however, if the structural modifications due to the presence of actuators are considered. Because the natural frequencies and modal functions keep changing in the procedure of optimization, usually there are no explicit objective functions available. At each optimization step, the natural frequencies and modal functions need to be recalculated. Furthermore, it is difficult to solve the modal problems of modified structures. Because of those difficulties most researchers resort to numerical method. Wang and Wang [344] attempted to consider the effects of PZT patches on the substructure, their model does include the actuator's stiffness, but they still ignore the inertia of PZT patches. Researchers do realize the PZT patches change the structure at certain level. However, they simply ignore the effect, thinking an analytical solution including PZT patches' inertia and stiffness may be too complicated even for simple substructures like beams and plates. They used numerical methods, such as finite element techniques, to circumvent the problem. Yang and Lee [365] proposed the stepped beam model to describe the actuator-beam structure, but they only studied the changes of

natural frequencies and modal shape functions. They did not mention those changes would influence the control efforts.

Many researchers also investigated the actuator dimensions [21,32,59,128,178, 202,219,230, 284,307,344,372] and other [158,229,301,361,378] optimization. Ip and Tse [158] studied the orientation problem of a piezoelectric patch actuator when control a simply supported plates. They developed a finite element model to include the effects of mass and stiffness of the piezoelectric patch. By allowing the patch to take on different position and orientation (ranging from 0^o to 90^o in steps of 15^o), the optimal position and orientation of actuator were found. They suggest aligning the patch (0^o) is already a good choice; the improvement by varying orientation is insignificant (less than 1%). Ball and Jones [32] investigated the effect of PZT patch effect. They concluded that a uniform rectangle actuator is more efficient for controlling divergence; however, a linear shaped actuator is more efficient from the standpoint of control effectiveness per actuator weight. Although the optimization of actuator placement and size have been studied extensively, there are only a few paper discussed the optimal thickness of PZT patches. Seeley and Chattopadhyay [284] show optimal thickness for box beams with a bimorph actuator configuration. Kim and Jones [178] investigated the effect of piezo-actuator thickness on the active vibration control of a cantilever beam. They found that there existed an optimal thickness for actuators in static excitation of beam by the piezo-actuators. It was shown that the optimal thickness is a strong function of the Young's modulus ratio of the actuator/beam configuration, becoming thinner with stiffer piezo-actuators. Then they studied the optimal thickness of actuator for dynamic case.

1.2.3 (c) Control algorithm implementation and experiment verification

The second branch of PZT applications in vibration control is algorithm implementation. Using available analytic actuation mechanism model or finite element method, many researchers were able to applied different strategies to control structures containing PZT as actuators. The popular algorithms are proportional velocity feedback control [30,130,186,213,249,290,297,324,379], LQG (linear quadratic Gaussian) control [24,25,28,30,143,207,259,278,290,332,372], IMSC (independent modal space control) [55,65,83,119,134,144,182,209,251,259,297,312] and PPF (positive position feedback) control [37,41,74,119,134,144,251,297].

Balamurugan and Narayanan [30] investigated active vibration control of piezolaminated smart beam. First they developed a finite element model based on Euler-Bernoulli beam theory. Then they implemented three classic control strategies – proportional displacement feedback control, proportional velocity feedback control and Lyapunov control (bang-bang control). Finally they applied an optimal control strategy, linear quadratic regulator (LQR) to control the beams. The control performances of different algorithms at various loading conditions were illustrated.

Baz *et al* [55] proposed an independent modal space control (IMSC) with positive position feedback (PPF) scheme to suppress vibration of flexible structure. Their model inherits the simplicity of IMSC while PPF only needs the modal position signal. They presented first order filter to achieve the PPF effect. They suggest a time-sharing strategy to give first priority to control the most vibrant mode. The effectiveness of their algorithm was validated experimentally. Baz and Hong [65] improved their model by introducing an adaptive modal positive position feedback (AMPPF) method. The parameters of AMPPF controller are adjusted in an adaptive manner in order to follow

the performance of an optimal reference model. The effectiveness and stability was verified through experiments.

Khajepour *et al* [172,173] proposed modal coupling controller (MCC) that uses internal resonance to damp out the oscillation of non-linear systems. It provides an energy link between the plant to be controlled and the controller. They introduced Upgrading Input Algorithm (UIA) to take advantage of the neck developed in the plant response when implement the modal coupling controller. They conducted the experiment to validate their model. According to their result, the proposed model MCC is more robust to noise. And MCC is able to produce a uni-directional input while maintain the same performance as velocity feedback which needs twice the peak to peak actuator effort as that in MCC.

Shen and Homaifar [290] implemented the velocity feedback control, hybrid fuzzy-PID control, genetic algorithms-designed PID control and linear quadratic Gaussian/loop transfer recovery (LQR/LQT) in vibration control of plate. The simulation results showed that these controllers perform well for controlling the Gaussian noise disturbance; GA-designed PID controller performs better at damping the sinusoidal disturbance. The stability and robustness of the four algorithms were proved. They conducted experiments based on velocity feedback control.

Prakah-Asante and Craig [252] presented multi-input-multi-output (MIMO) methods to actively control vibration transmission of disturbances using bonded piezoelectric actuators and sensors. They investigated linear/non-linear rate feedback control, linear quadratic Gaussian (LQG)/loop transfer recovery (LTR) control with augmented states to obtain disturbance accommodation, H_∞ optimization control and

adaptive feedforward control based on the least-mean-squares (LMS) algorithm. The effectiveness of those schemes was illustrated. They suggested a hybrid controller strategy, which combines the faster response characteristics of a feedback law together with a robust feedforward adaptive algorithm to obtain optimal vibration suppression for both transient and steady state vibration. Experiments on both aluminum and composite beams were conducted. They implemented linear/non-linear feedback, adaptive feedforward and hybrid of those two controllers in real time manner. According to their results, transient vibration suppression of about 20 dB can be obtained from linear/nonlinear control. Performance of adaptive feedforward alone in the presence of transient disturbance is degraded. The hybrid controller of linear/nonlinear feedback and adaptive feedforward based on LMS compensates more effectively for both the transient and steady state disturbance.

Bai and Lin [28] implemented the LQG algorithm based on floating-point DSP in active vibration control of flexible beams. They used the piezoelectric ceramic PZT as the actuator and the piezoelectric plastic PVDF as the sensor. The characteristics of the physical system were identified by a parametric modeling technique. Significant attenuation of white noise disturbance in the frequency range of approximately 100-800 Hz was shown.

Han *et al* [143] conducted experiments of vibration control of composite beams and plates. They developed an analytical model of the laminated composite beam with piezoelectric sensors and actuators based on the classical laminated beam theory and Ritz method. They implemented LQG algorithm as well as classic control method like constant gain feedback and bang-bang control. They successfully controlled the first and

second bending modes of cantilevered beam. Further they conducted experiments to control cantilevered plates. It was shown that the simultaneous control of the bending and twisting modes significantly suppresses the vibration level. The advantages of LQG in robustness to noise and control efficiency compared with classical control methods were shown.

Gaudenzi *et al* [130] used position and velocity control strategies to attenuate vibration of beam. The sensing ad actuating actions were carried out by two identical PZT piezo-patches connected at the beam in a collocated way. They performed numerical simulation as well as experiments. A finite element model was developed based on Euler–Bernoulli model and subsequent modal factorization. The results of the numerical simulations were compared with the ones obtained in the experimental tests. According to their paper, a good correspondence obtained in all the examined cases. Choi [89] performed an experiment for vibration reduction using multi-step bang-bang control algorithm. Clark *et al* [92] performed a vibration control experiment on thin plane using modal sensor.

1.2.3 (d) Finite element models and approach

Although there are several analytic models available for structures involve piezoelectric sensors/actuators, they are very specific case related. And the cases studied are usually simple structures like beam (beam-like) and plate (plate-like). It was proved that the finite element method is a powerful tool to deal with complex structures and couple disciplines. There are a growing number of papers on the finite element modeling of structures with piezoelectric elements [30,31,40,45,50,51,54,66,69-74,81,86,138,139, 145,155,167,168,170,175,186,187, 235,241,243,249,253,255,258,269,270,289,306,317,

323,324]. Most of them have same assumptions that are used in the piezoelectric modeling, linear variation of electric potential through thickness, poling direction along the thickness and only longitudinal stress or strain could be induced by monolithic piezoelectric materials, and only the transverse components of electric field and displacement are retained.

Tzou and Tseng [324] developed a finite element model for the sensors and actuators bonded to the surface of plates and shells. The element for the thin piezoelectric layer was solid element with internal degrees of freedom (DOF). Applying Hamilton principle on the whole structure, they formulate the dynamics problem in the finite element form, Using Guyan reduction they were able to condense the DOF's associated with electrical potential. The time response of the system was calculated using the Wilson-q method. Constant gain velocity feedback and constant amplitude velocity feedback were implemented respectively. The results were compared and the effect of the feedback gain was illustrated.

Hwang and Park [155] proposed a model for the plate elements with attached piezoelectric sensors and actuators. Classical laminate theory (CLT) with the induced strain actuation and Hamilton principle were used to develop their model. They introduced 4-node 12-degree of freedom quadrilateral non-conforming plate bending element. In their paper, they investigated the alteration of stiffness and damping property of composite structure and the effect of vibration control performance by different piezoelectric sensor/actuator configurations.

Lam et al [186] developed a finite element model based on the classical laminated theory (CLT) for the active vibration control of a composite plate containing distributed

piezoelectric sensors and actuators. The formulation was derived from the variational principle. A simple negative velocity feedback control algorithm was used to actively control the dynamic response of an integrated structure.

Oh et al. [236] presented a formulation for the postbuckling vibration of plates. Non-linear finite element equations based on the layerwise displacement theory were adopted to develop the equations for piezolaminated plates subject to thermal piezoelectric loads. Their paper shows that for fully distributed piezolaminates, excessive bending moments for the suppression of thermally buckled deflection may cause another type of structural instability. They also investigated the optimal placement of piezoceramic patches in suppressing thermally buckled deflection for the partially segmented piezolaminates.

Based on the classical laminated theory (CLT) and Hamilton's principle Liu et al. [213] developed a finite element model for the control of laminated composite plates containing integrated piezoelectric sensors and actuators. A four-node non-conforming rectangular plate bending element was used. With the use of negative velocity feedback control scheme, they investigated the effects of stacking sequence and position of sensors/actuators on the vibration suppression of a beam and plate.

In order to improve the accuracy of finite element model, some researchers developed their models based on higher polynomial order of the elements and nonlinear beam/plate theory. Further, higher order electrical models were proposed to better describe the non- linear electric field in the piezoelectric material. Bhattacharya et al. [50] developed a finite element model for smart beams and plates based on the Raleigh-Ritz principle and the first order shear deformation theory. They used an eight-node

isoparametric quadrilateral element to discretize the whole domain. They studied the effects of stacking sequence, boundary conditions, and electric voltage application.

Peng *et al*. [249] introduced the third order laminate theory to their finite element model for the active position control as well as vibration control of composite beams with distributed piezoelectric sensors and actuators. Negative velocity feedback control algorithm was used in a closed control loop. They also investigated the effects of the number and locations of the sensors/actuators on the control system.

Based on the third order shear theory, Zhou et al. [385] presented another development in the finite element models by introducing a three order potential field that describe the field distribution in the piezoelectric elements along the thickness direction. They found that the results from their model were significant different from other models for thick piezoelectric layers.

Kim and Moon [228] presented a finite element formulation for piezoelectric plate elements with passively shunted circuit elements that incorporated the electric circuit dynamics. They applied their model for the prediction of plate behavior subjected to aerodynamic loading (panel-flutter). They compared the results obtained from an active control model using LQR method with those obtained from a passive RL circuit. They concluded that, the suppression using the passive control is not more than that obtained using active control. However, the need of controller, power supplies, and amplifiers for the active control case would reduce its efficiency compared to the passive elements that only require the addition of a resistance and an inductance.

Saravanos [274,275] presented a formulation for the finite element problem of a composite shell with piezoelectric laminas. He proposed the “Mixed Piezoelectric Shell

Theory" [275] (MPST) that utilizes the first order shear theory for the displacement and the discrete- layer approximation for the electric potential. He used the Love assumption for shallow shells (radius is much larger than thickness). The model he developed was for an eight-node curvilinear shell element. The model is applied to different cases of composite layouts and geometric boundary conditions and concluded that the model is accurate in predicting the dynamics of the shells. Further; he included a passively shunted circuit to damp out the vibration of the shells [274]. Meanwhile, Chen et al. [86] proposed a similar finite element formulation for thin shell elements which presents a special case of the formulation presented by Saravanos [274,275].

1.2.3 (e) Other developments

In the smart structures we discussed so far the PZT element plays solely either actuation or sensation role. Recently several researchers investigated the possibility using piezoelectric materials simultaneously as sensor and actuator in vibration suppression. The primary advantages of this concept are: (1) the reduction of the weight of the piezoelectric elements involved in the structure, light weight structure is always desired in aeronautic and astronautic application; (2) the reduction of the structural alteration because of the presence of PZT patches, the modification of structure will degrade the control effectiveness; and (3) a truly collocated sensor/actuator arrangement which is preferred in control applications as it ensures the stability of the control system. The basic idea of self-sensing actuator is to extract the strain or stain rate signals from charge response of a piezoceramic actuator. The electrical charge generated in the actuator's electrodes contains two parts when the voltage applied on it: the mechanical response

term which is caused by deformation and the feedthrough charge term caused by the voltage applied across the piezoelectric capacitance.

Dosch et al [112] developed a self-sensing actuator (SSA) technique which allowing a single piece of piezoelectric element to serve as both sensor and actuator concurrently in a closed loop system. They used a simple bridge circuit to measure either strain or strain rate in the actuator. The experiments on cantilevered beams were conducted to valid the SSA technique. According to their results, five percent settling time was reduce significantly for the first two modes with rate feedback control or positive position feedback control.

In a similar work, Anderson et al [23] presented a model of a cantilever beam with strain rate feedback, positive position feedback, and LQG control. Yang and Chiu [363] developed a strain rate circuit of concurrent sensing and actuation of piezoelectric materials, and the results were successfully implemented in the dither motor of a ring laser gyroscope.

While the self-sensing actuator technique has many attractive properties, it proved very difficult to be implemented. This is because that the capacitance of PZT actuator is hard to identify. The compensator required continual readjustment according to hysteretic nonlinearities and temperature variations. In an effort to overcome those difficulties, Cole and Clark [95] proposed an adaptive approach to design the compensation. Base on the acknowledgement that piezoceramics exhibit nonlinear variations in their piezoelectric constants as a function of applied voltage and temperature, an adaptive digital compensation technique was proposed to track the unsteady capacitance. Vipperman and Clark [336] extended their analysis toward the implementation of an adaptive controller

in vibration control of a cantilever beam. They proposed a hybrid analog and digital compensator and implemented it in their experiments.

PZT has also been used in passive vibration suppression [14,27,29,40,42,141,142, 149-151,153,188,199,228,274,288,289,320-322] and shape control purpose [15,16,59, 73,163,208,300,318,342] extensively. But we will concentrate on the active vibration control in this study.

1.3 METHOD OF APPROACH

We started with the linear and nonlinear vibration of cantilever beams made of Fiber Metal Laminates (FMLs). Euler-Bernoulli beam theory and the half power method are used to investigate the dynamic Young's modulus and linear viscous damping in the linear vibration. For nonlinear vibration, an inextensible beam model with nonlinear damping is adopted to study single mode response of cantilever beams. Approximate solutions are obtained by solving an integro-differential equation via Multiple Scales method and Harmonic Balance Method. A beam model with a nonlinear spring-hinged end and the other free is applied to improve the agreements between theoretical and experimental results.

After that we studied the vibration control of a uniform beam surface-bonded with a pair of PZT patches. When the inertia and stiffness of PZT patches are ignored, the beam-actuator system is simplified into a uniform beam problem. Distributed moment forcing mode is adopted to represent the control mechanism of actuators. Using modal summation method, the vibration of beam can be decomposed into infinite modal vibrations. In each mode the natural frequencies and corresponding model shape functions are obtained. Control force from actuator is transformed to modal control

forces. The efficiency function of each mode is defined to stand for the ability that the PZT patches are able to restrain the corresponding modal oscillation. A stepped beam model is used when the modification of structure by attaching actuators is taken into consideration. Comparing the efficiency functions from uniform beam model and from stepped beam model, we find that the PZT patches not only alter the beam structure itself, but also degrade the control effort. The effect on natural frequencies and modal shape functions may be negligible; the effect on control efficiency could be significant. It is also found that the ratio of the corresponding modal efficiency functions from uniform beam model and stepped beam model is a constant related with material properties and dimensions of PZT patches and the host beam. By introducing this ratio into results from uniform beam model, the degraded control efficiency can be obtained without much difficulty. This will greatly simplify the procedure of estimating the control ability of the actuators. This ratio exists when PZT patches are used as actuators by attaching to plate, shell and many other complicate structures. The proposed method is based on attaching a pair of PZT patches. However, it can be easily extended to cases of a single patch as well as multiple patches by superimposing the efficiency functions accordingly.

At last we extended our control efficiency estimation method to the vibration of plates. A pair of PZT patches is surface-bonded as actuators. Uniform plate model is applied when the mass and stiffness of PZT patches are ignored. Finite element method is adopted when the effect of patches is taken into consideration. Optimal positions of actuators pair are obtained in both cases. It is found that the structural modification caused by attaching PZT patches may degrade the control ability while the optimal positions are not sensitive to these structural alterations.

CHAPTER 2: DYNAMIC MECHANICAL PROPERTIES OF FIBER-METAL LAMINATED BEAMS

In this chapter, effective dynamic Young's moduli and damping ratios of Fiber-metal laminates made from glass-fiber reinforced GLARE and aramid-fiber reinforced ARALL laminates interlaced with aluminum layers were obtained using resonant and nonresonant vibration tests of cantilever beams made from these materials. Dynamic Young's moduli E_n, $n = 1, 2, \cdots$, for first few natural frequencies f_n were estimated using resonant excitation and substituting f_n in $E_n = \frac{\rho A}{I}\left(\frac{2\pi f_n}{\beta_n^2}\right)^2$. Dynamic Young's modulus was also estimated by non-resonant excitation and solving a complex equation which relates strain at distance d from the fixed end and the amplitude of the base excitation. The obtained dynamic moduli were in excellent agreement with those obtained using static tests. It was found that compared to aluminum alloys, the effective Young's moduli of fiber-metal laminates are lower and are approximately proportional to the aluminum content. Young's moduli were almost constant within an experimental excitation frequency range of 0 to 5,000 Hz. Damping ratios were evaluated using half-power method and were within a narrow range of 0 to 0.02. Impulse tests conducted using an impact hammer agreed very well with theoretical simulation which used experimentally obtained Young's moduli and damping ratios.

2.1 INTRODUCTION

Fiber-metal laminates are hybrid composites formed by interlacing layers of thin metals (usually aluminum alloy) and fiber-reinforced laminae to optimize the properties

of metals and fiber-reinforced laminae for better damage tolerance to fatigue crack growth, foreign body impact damage, corrosion resistance and fire retardation [205,221,280, 337,309,351,352]. In addition they are relatively lightweight in comparison to their metallic counterparts. Commercially two types of fiber-metal laminates are available: Glare and ARALL, which use glass-epoxy and aramid-epoxy laminae, respectively, with thin aluminum sheets and have been adopted widely in the aerospace and spacecraft industries. Dynamic mechanical properties of fiber-reinforced composites have been studied quite extensively since late 1960's using vibration testing [3,281,282] or ultrasonic technique [316]. The main mechanical properties obtained in these studies were dynamic Young's modulus and damping ratio. For the vibration testing technique, the dynamic Young's modulus can be evaluated simply using formulae derived from free-vibration of a linearly elastic composite beam whereas the damping ratio can be estimated by the half-power method [281,282]. These dynamic properties can also be obtained by the more elaborate complex-modulus approach, which assumes the beam being viscoelastic [3,48,146,147, 268]. In this study, dynamic mechanical properties of these relatively novel fiber-metal laminates were obtained using the procedures proposed by Schultz and Tsai [281,282] and agreement between Young's modulus obtained using static and dynamic testing was good. Impulse tests conducted using an impact hammer agreed very well with theoretical simulation which used experimentally obtained Young's moduli. In many of these works the nonlinearity was small [281,282]. A method based on harmonic balance method is proposed to get Young's modulus and damping properties during large amplitude vibration of an inextensible cantilever Beam will be presented in Chapter 3.

2.2 THEORETICAL CONSIDERATION

The classical Euler-Bernoulli beam model has been well developed. It assumes that plane cross sections, normal to the neutral axis before deformation, continue to remain plane and normal to the neutral axis and do not undergo any strain in their planes. Euler-Bernoulli beam model would usually suffice when dealing with small deformations. Schultz and Tsai [281,282] proposed an experimental procedure to measure the effective Young's moduli of composite beams and damping ratio based on Euler-Bernoulli beam model. Methods based on resonant vibration and nonresonant vibration are used in what follows.

2.2.1 Resonant Method

This method is based on the fact that for a very lightly damped linear system amplitude at resonance and hence strains are the highest for the given input amplitude. Hence in principle a strain gage can be used to identify resonance.

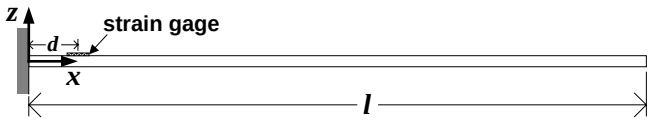

Figure 2-1 Free vibration of a cantilever beam.

The governing equation for a cantilever beam in free vibration, as shown in the Figure 2-1, is:

$$\frac{\partial^2 w}{\partial t^2} + \frac{EI}{\rho A}\frac{\partial^4 w}{\partial x^4} = 0, \tag{2.1}$$

here w is the beam deflection along *z*-direction , ρ the density, *E* the dynamic Young's modulus along the *x*-direction, *I* the second moment of inertia about the neutral axis, and

A the cross-sectional area. As shown in Appendix B, the frequency equation can be expressed as:

$$\cosh \beta l \cos \beta l + 1 = 0, \tag{2.2}$$

where

$$\beta^4 = \frac{\rho A}{EI}\left(2\pi f\right)^2 \tag{2.3}$$

is a root (i.e., eigenvalue) of the frequency equation and f is a circular frequency. The corresponding n^{th}-mode resonant frequency, f_n, can thus be expressed as:

$$f_n = \frac{\beta_n^2}{2\pi}\sqrt{\frac{EI}{\rho A}}, \tag{2.4}$$

where β_n is the corresponding n^{th}-root of the frequency equation, Equation (2.2). Hence, as shown by Schultz and Tsai [281,282], one can calculate the dynamic Young's modulus, E_n, at the n^{th}-resonant as:

$$E_n = \frac{\rho A}{I}\left(\frac{2\pi f_n}{\beta_n^2}\right)^2. \tag{2.5}$$

This last equation indicates that the accurate measurement of f_n is important in this case. The damping ratios can be obtained using the half power method [281,282]:

$$\xi_n = \frac{\Delta f}{2 f_n}. \tag{2.6}$$

Here ξ_n is the damping ratio in the n^{th}-mode and Δf is the difference between the two frequencies at which the response is 0.707 of the resonance peak.

2.2.2 Nonresonant Method

In this method an undamped beam is excited at the base as $y_b \sin(2\pi ft)$ where frequency f $(f \neq f_n)$, and is shown in Figure 2-2.

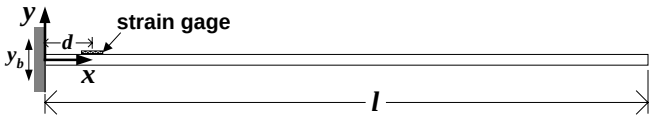

Fig 2-2 Forced vibration of a cantilever beam.

It is assumed that the resulting strain ε at location distance d from the base is known experimentally. It can be shown that strain can be expressed as:

$$\frac{\varepsilon}{y_b} = \frac{h\beta^2}{4}\frac{g_1 + g_2 + g_3 + g_4}{g_0} \quad , \quad \beta = \sqrt[4]{\frac{\rho A}{EI}(2\pi f)^2} \tag{2.7}$$

where y_b is the known amplitude of the base excitation, h is thickness of the beam, and the functions, g_i (i = 0,1,2,3,4), are given as:

$$\begin{aligned}
g_0 &= \cosh\beta l \cos\beta l + 1 \\
g_1 &= -\sin\beta d(\cos\beta l \sinh\beta l + \cosh\beta l \sin\beta l) \\
g_2 &= \cos\beta d(-\cos\beta l \cosh\beta l + \sin\beta l \sinh\beta l - 1) \\
g_3 &= -\sinh\beta d(\cos\beta l \sinh\beta l + \cosh\beta l \sin\beta l) \\
g_4 &= \cosh\beta d(\cos\beta l \cosh\beta l + \sin\beta l \sinh\beta l + 1) \ .
\end{aligned} \tag{2.8}$$

A careful examination of Equation (2.7) and Equation (2.8) indicates that as long as ε and y_b are accurately measured, one can obtain dynamic Young's modulus by solving the transcendental Equation (2.7).

2.2.3 Frequency Responses and Curve Fitting

The displacement of a point at distance d from the base of beam due to sinusoidal base excitation during the lightly damped n^{th} mode of the cantilever beam can be expressed as,

$$\upsilon(d,t) = \phi_n(d) q_n(t), \tag{2.9}$$

where $q_n(t)$ satisfies,

$$\ddot{q}_n + 2\omega_n \xi_n \dot{q}_n + \omega_n{}^2 q_n = [(2\pi f)^2 y_b \int_0^l \rho A \phi_n dx] \cos 2\pi ft \,. \tag{2.10}$$

It is assumed that experimental frequency response curve is available and ω_n and ξ_n can be obtained by using the least square algorithm to fit response obtained using Equation (2.10) to that obtained experimentally. Once the ω_n is determined, then E_n can be calculated as $E_n = \frac{\rho A}{I}\left(\frac{\omega_n}{\beta_n^2}\right)^2$.

Physical experiments were performed to obtain data required in section 2.2. The experimental apparatus and procedure is detailed next. The results of Young's modulus and damping ratio obtained here agree with previous results and to those obtained using static tests.

2.3 EXPERIMENTAL PROCEDURE

The beams tested in this study were made of 2024-T3 aluminum alloy and nine types of fiber-metal laminates and details are given in Table 2-1. In this table the notation (*m*/*n*) means lay-up configuration: *m* layers of aluminum sheets interlaced with and *n* layers of fiber-epoxy laminae. These beams were 25 mm wide x 254 mm long (or 1" x 10") and thickness varies as given in Table 2-1. The active length of each beam was 22.225 mm (8.75"). As shown in Figure 2-3 and Figure 2-4, a beam was first clamped to the a Brüel & Kjær 4802 vibration shaker and base displacement was monitored using Brüel & Kjær 2708 amplifier and wave generator. Displacement amplitude was measured using signal conditioner and computer. A strain gage signal was monitored using data acquisition system and computer. Results were obtained by sweeping through a wide range of frequencies (from 0 to 5,000 Hz) and base amplitude was held constant with in the resonant range. To excite different modes amplitude was adjusted to get reasonable strain.

Resonance was confirmed when the strain signal reached a local peak. Data was collected after system reached a steady state. The second part of experiment was to study impact responses of fiber-metal laminated beam as shown in Figure 2-5. Results and discussion follows.

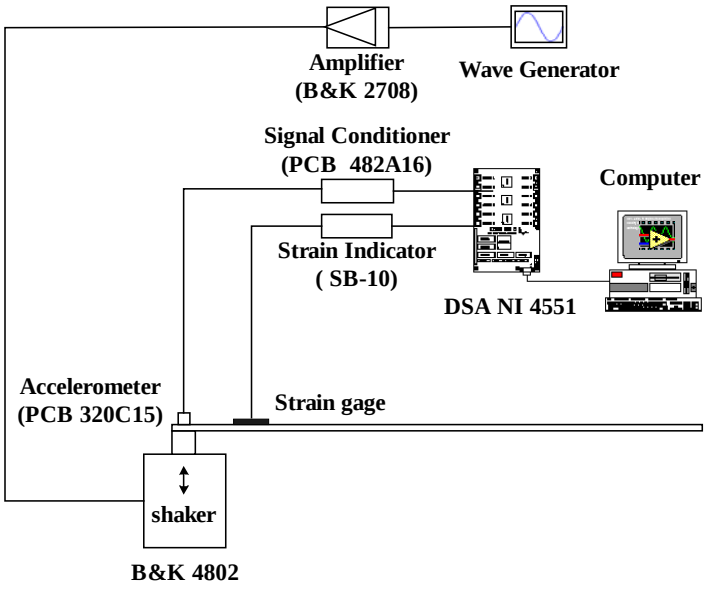

Figure 2-3 The schematic of experimental setup for vibration of a cantilever beam.

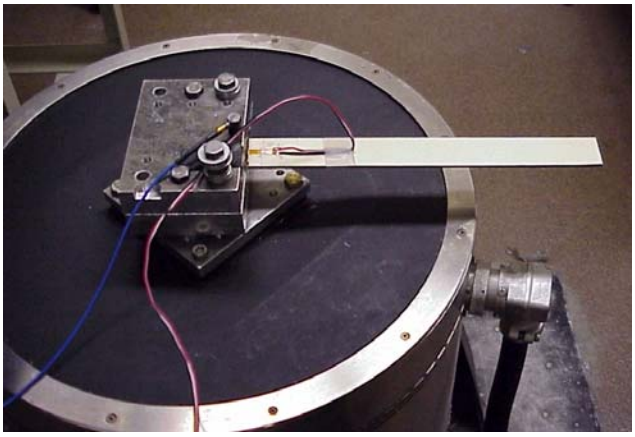

Figure 2-4 Experimental setup for vibration of a cantilever beam.

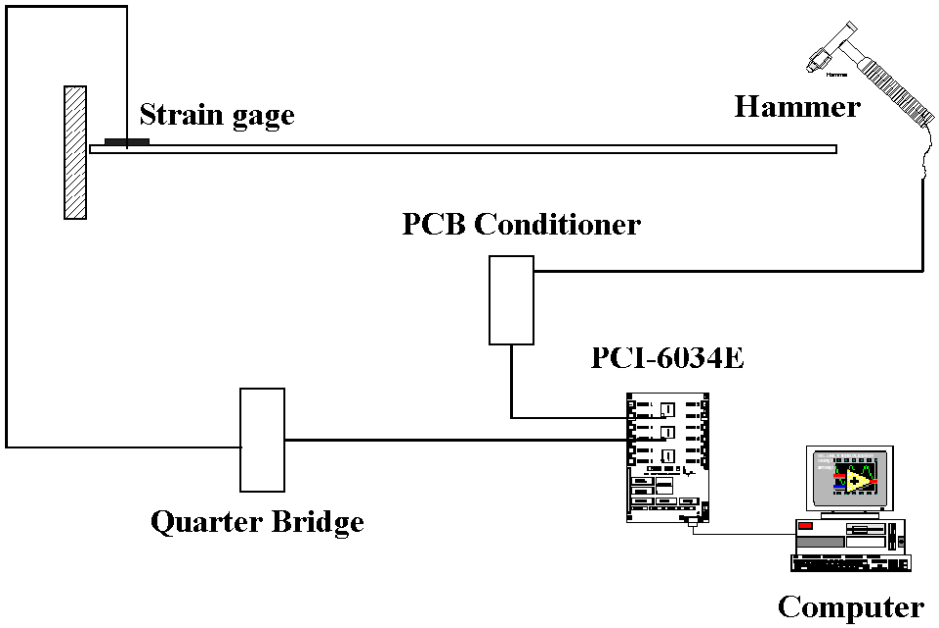

Figure 2-5 The schematic of experimental setup of impulse tests.

2.4 RESULTS AND DISCUSSION

Preliminary tests were conducted to demonstrate that the nonlinear effects in these experiments are small. Resonance Reponses of two cantilever beams made of 2024-T3 aluminum alloy and Glare 5 (3/2) respectively were tested at the fundamental frequencies. The results were plotted in Figure 2-6 and Figure 2-7 respectively. Two curves were fitted based on damped linear model, Equation (2.10) and linear model without damping. These figures indicate that the nonlinearity was small and hence neglected. The damping ratios for aluminum and Glare 5(3/2) beams in the first mode were 0.011 and 0.004 obtained from curve fitting linear model with damping and corresponding values obtained using half power point method are 0.0117 and 0.0056 respectively. Young's moduli for 2024-T3 aluminum alloy and Glare 5 (3/2) obtained using Equation (2.10) were 70 and 62 GPa, respectively.

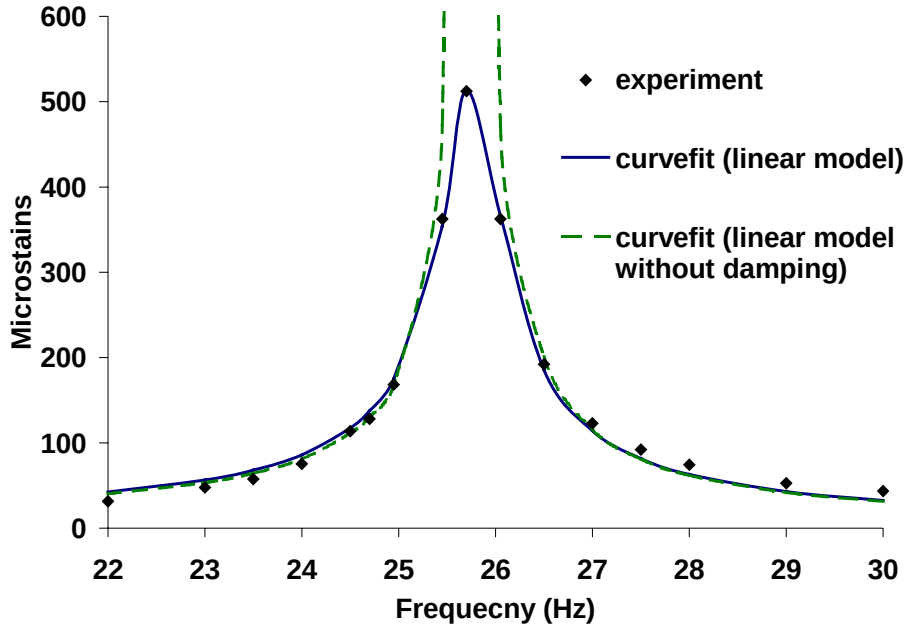

Figure 2-6 Frequency responses of a cantilever beam (2024-T3 aluminum).

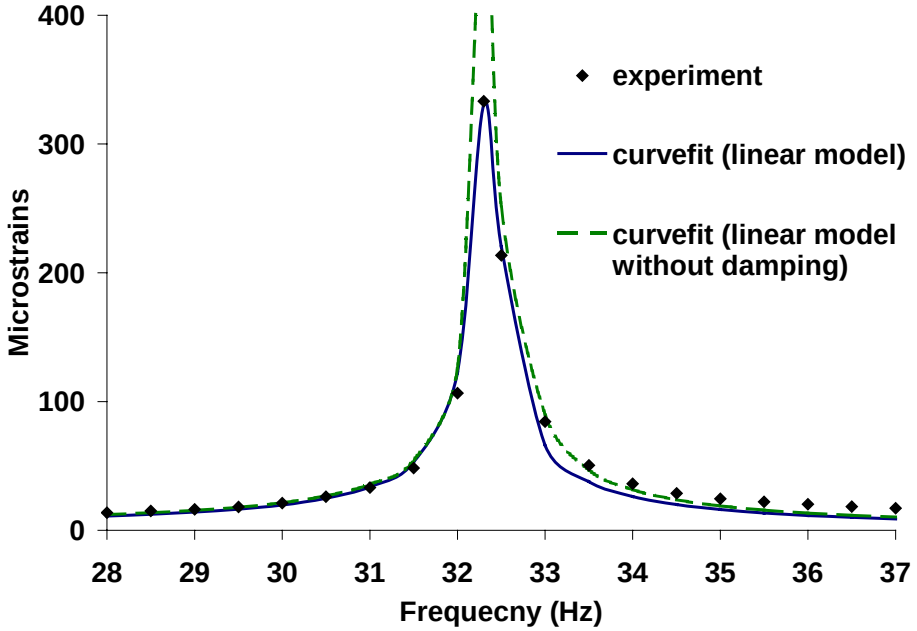

Figure 2-7 Frequency responses of a cantilever beam (Glare 5 3/2)

The resonant testing approach presented in section 2.2.1 was used to estimate Young's modulus and damping ratio by resonantly vibrating beams in the frequency range of 0-5000 Hz. and results are presented in Figures 8-11 respectively. Results for 12 different types of fiber-metal laminates with different lay-up configurations (different thickness and different content of 2024-T3 aluminum alloy) are presented in those figures. These results show that the Young's moduli are nearly constant within a frequency range of 0 - 5,000 Hz. Those having less aluminum content also possess lower dynamic Young's modulus. As an example beam made up of Glare 5 (6/5) contains 60% Aluminum by volume and the Young's modulus is 40 GPa which is nearly 60% of 70 GPa which is Young's modulus of Aluminum beam. These values are very close to those obtained using standard uniaxial tensile tests using a MTS 810 Universal Testing System. The experimental stress-strain curves for 2024-T3 aluminum and three Glare 5's with (2/1), (4/3) and (6/5) lay-up configurations are shown in Figures 2-14(a)-(d). The Young's moduli for these cases are 70, 65, 50 and 43 GPa respectively and they agree with those obtained using resonant testing presented above. The damping ratios of these materials are shown in Figures 8 and 10 are within a narrow range of 0 to 0.02.

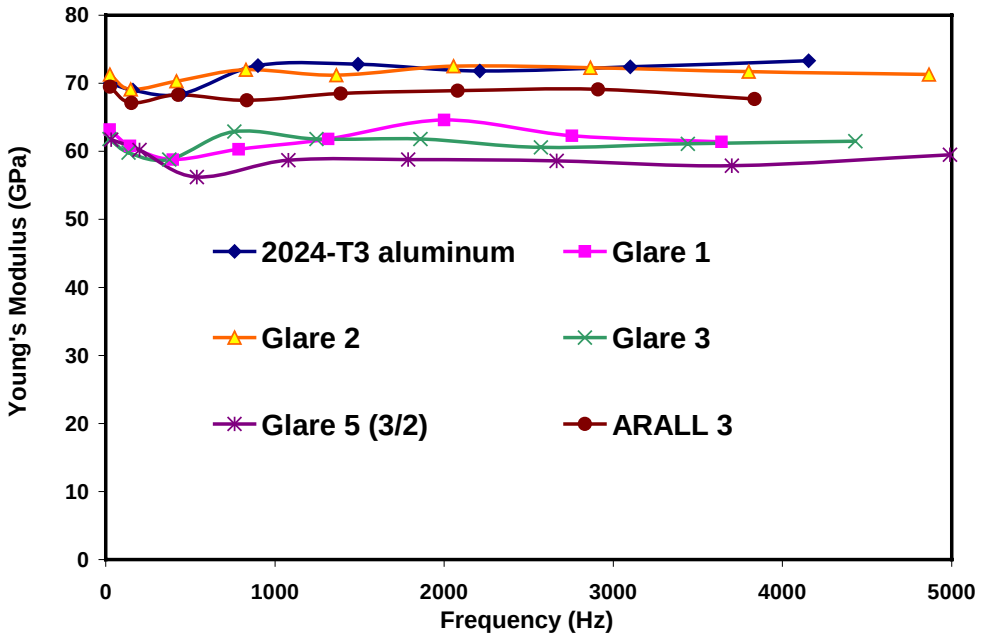

Figure 2-8 Comparison of dynamic Young's moduli of 2024-T3 aluminum and five types of fiber-metal laminates.

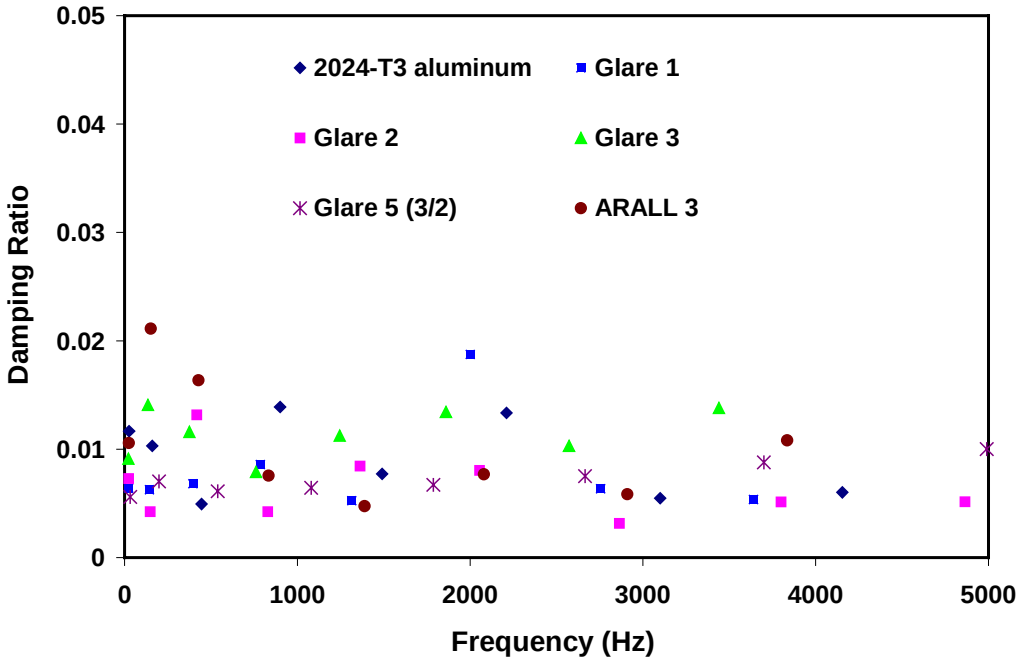

Figure 2-9 Comparison of damping ratios of 2024-T3 aluminum and five types of fiber-metal laminates.

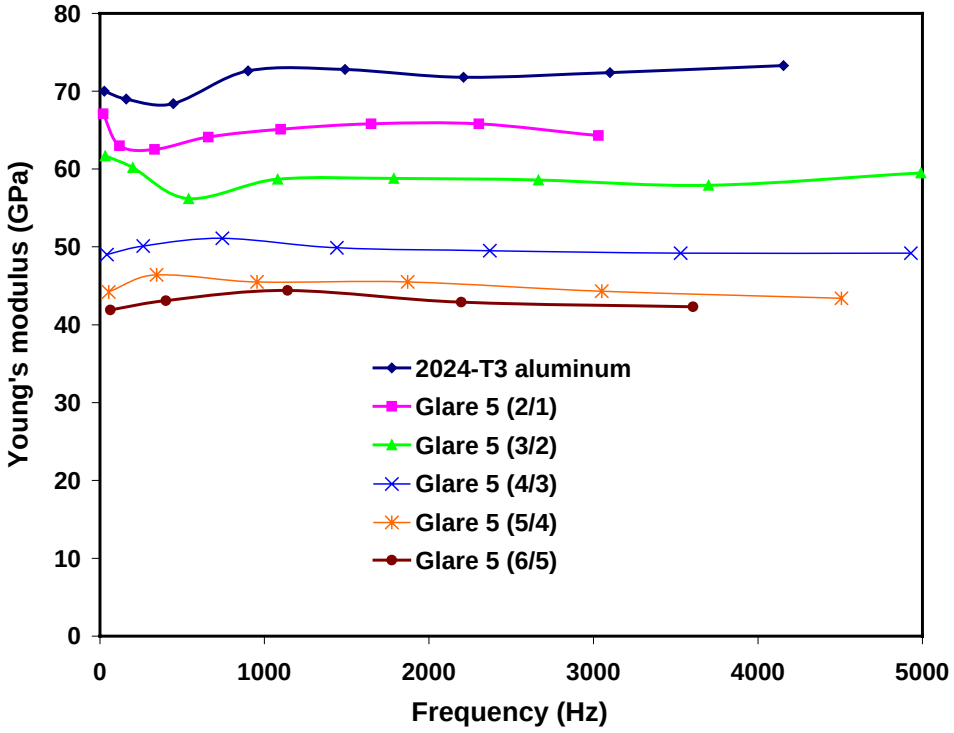

Figure 2-10 Comparison of dynamic Young's moduli of Glare 5 fiber-metal laminates with different lay-up configurations.

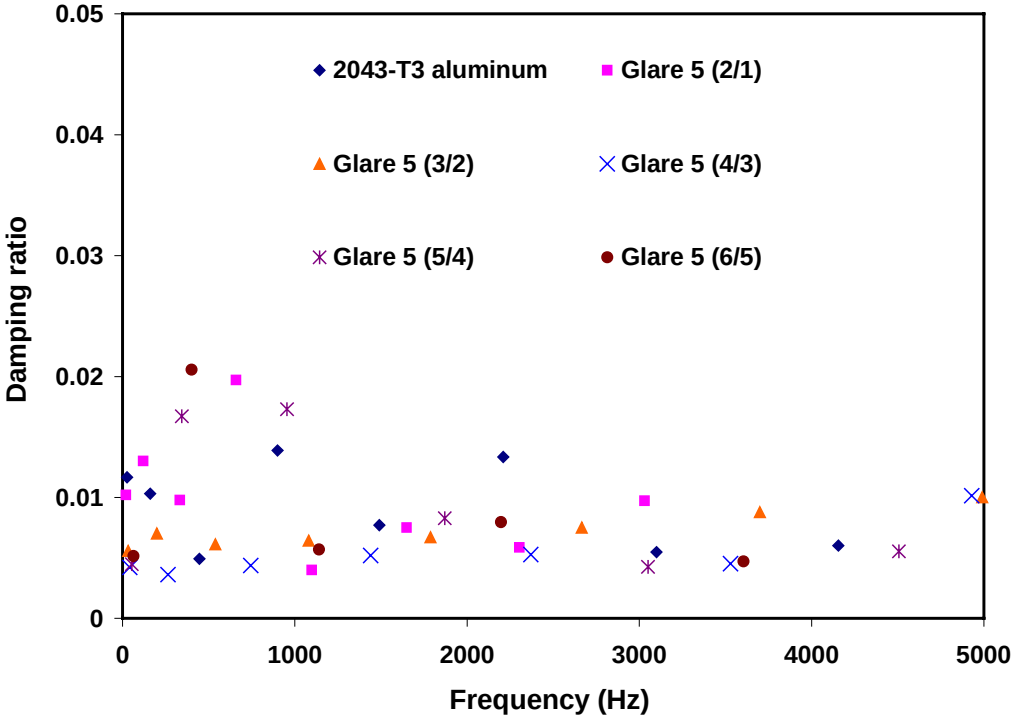

Figure 2-11 Comparison of damping ratios of Glare 5 fiber-metal laminates with different lay-up configurations.

The non-resonance approach presented in section 2.2 to estimate dynamic Young's was then used in cases of Aluminum 2024-T3 and Glare 5 (3/2) beams around their fundamental resonance of 25.80 and 32.44 Hz respectively. The strains produced at non-resonant frequencies due to base amplitude of y_b = 0.131mm and 0.026mm respectively are plotted in Figures 2-12 and 2-13 together with the estimated values of ratios of dynamic Young's moduli over those obtained by the resonance scheme presented in section 2.2.2. As shown in Figure 2-12 the dynamic Young's moduli obtained by non-resonance scheme is in excellent agreement with those obtained by resonance scheme. For Glare 5 (3/2) beam estimated values of 62 GPa are close to those obtained using resonant scheme near resonance and shows the deviation of around 10% at to ends. The advantage of this method is that it does not need to know the exact resonant frequencies, however it can be only used with very lightly damped system.

Beams were also tested under short duration impact loads. The experimental results were obtained by impacting beam using a PCB 086B03 impact hammer powered by a PCB 482A16 signal conditioner. A strain gage was mounted near the clamped end and the impulse load and strain signals were recorded through a National Instruments PCI-6034E data acquisition board at a sampling rate of 100 KHz. The Theoretical response of Glare 5 (5/4) fiber-metal laminated cantilever beam was obtained using estimated value of Young's modulus and average damping ratio and 7 modes were used in these calculations. Actual short duration load is shown in Figure 2-15(a) and comparison of experimental and theoretical results is presented in Figure 2-15(b) and they agree.

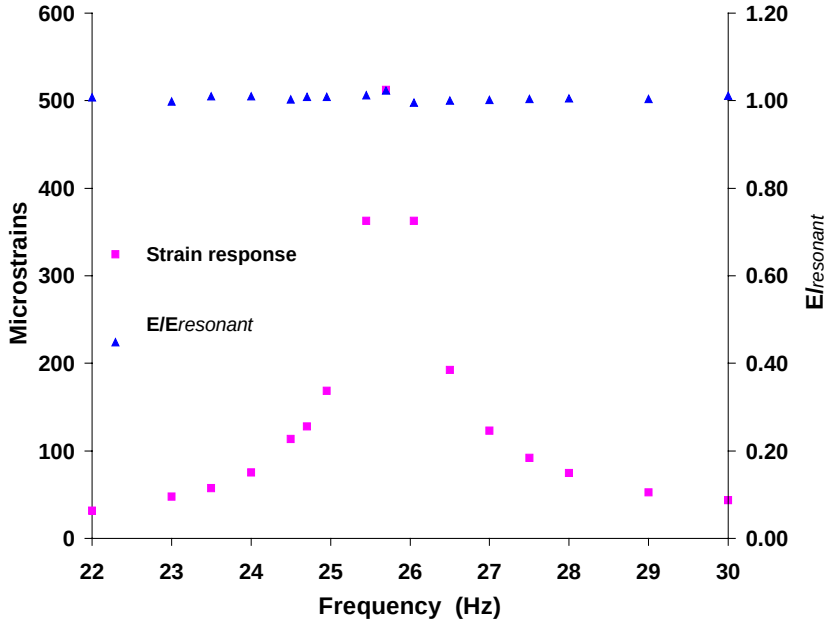

Figure 2-12 Frequency response around the fundamental mode of a vibrating cantilever beam (2024-T3 aluminum).

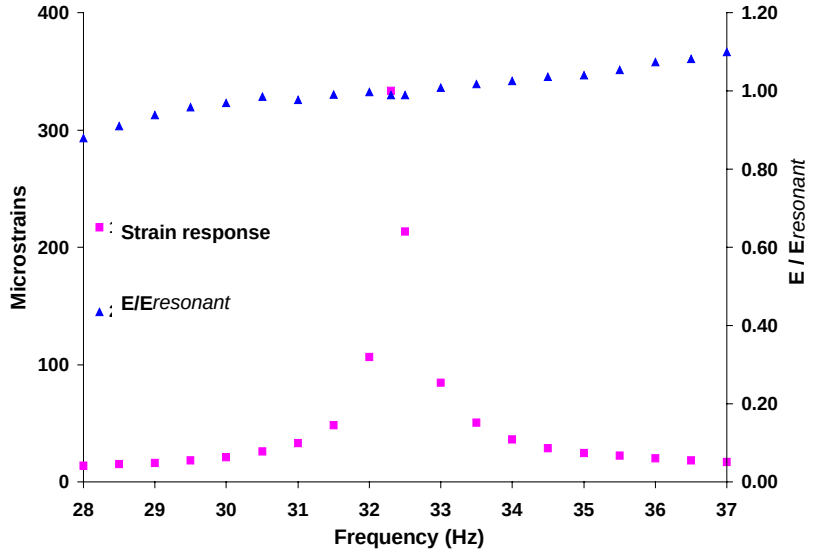

Figure 2-13 Frequency response around the fundamental mode of a vibrating cantilever beam (Glare 5 (3/2) fiber-metal laminate).

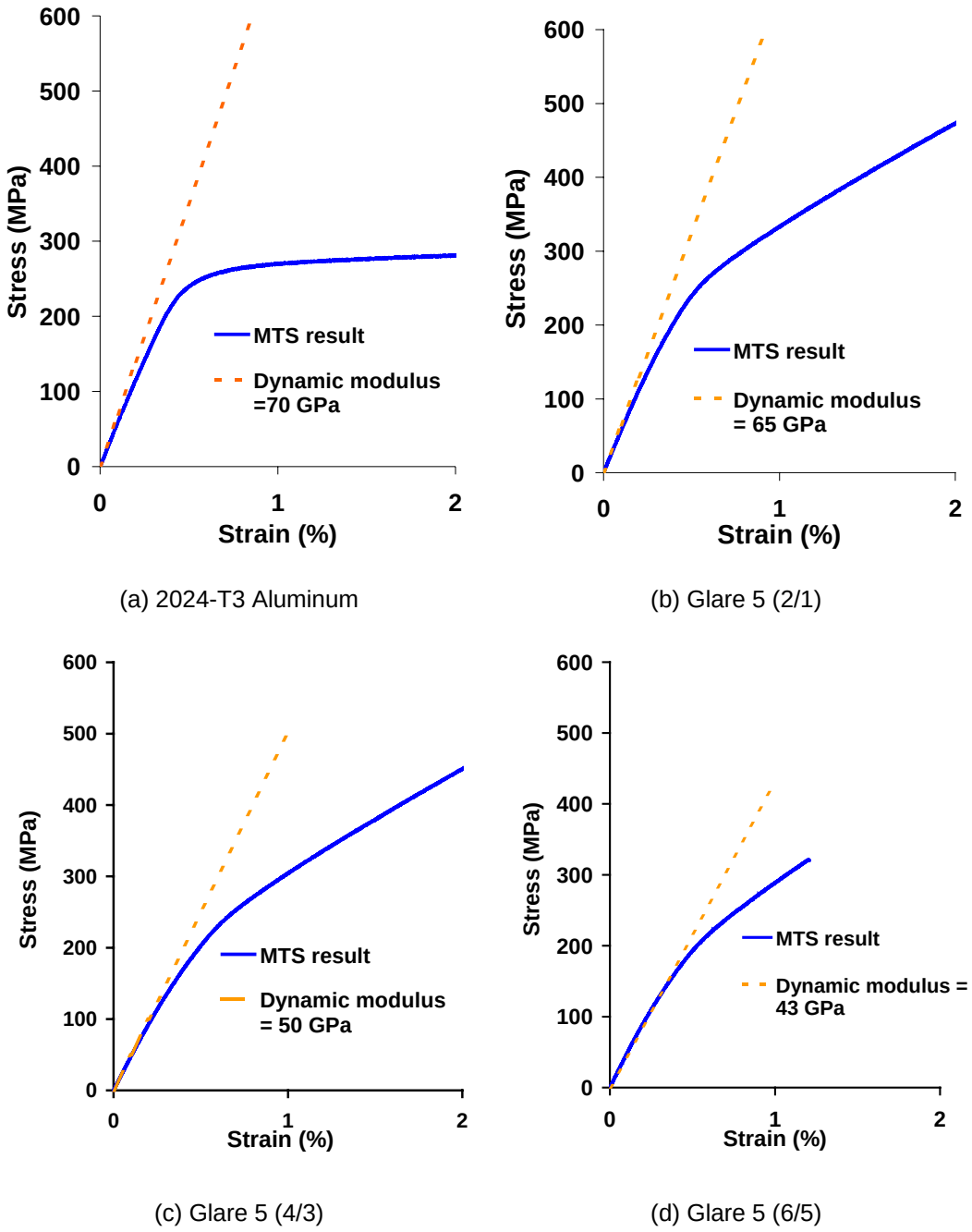

Figure 2-14 Comparison of static and dynamic Young's moduli for aluminum and three types of Glare 5 fiber-metal laminates.

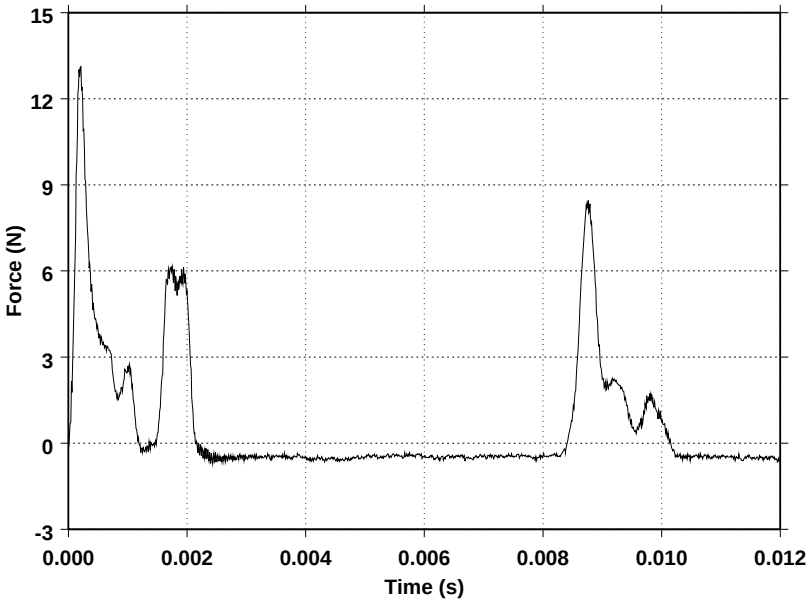

(a) Impulse force signal

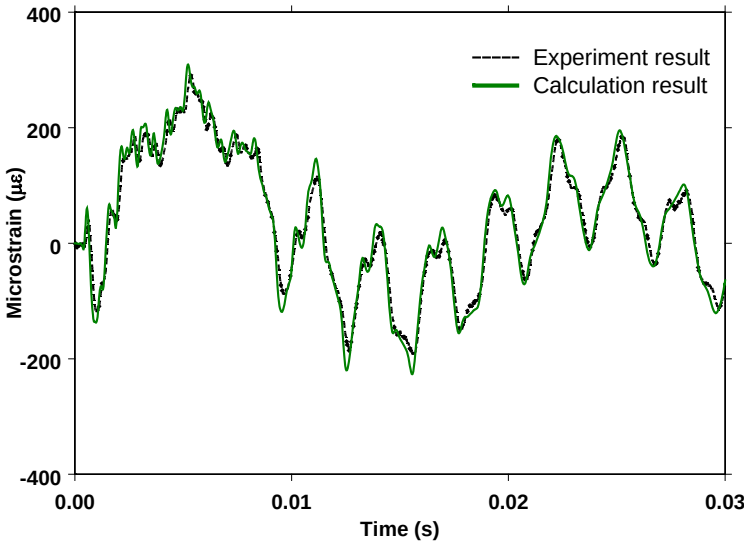

(b) Experimental strain and theoretical calculations

Figure 2-15 Impact response Glare 5 (5/4) fiber-metal laminated cantilever beam struck by an impulse force at the free end.

2.5 CONCLUSIONS

- Dynamic Young's modulus can be accurately estimated using resonant, non-resonant and curvefitting technique. For the materials tested Young's modulus are nearly proportional to the aluminum content.
- Young's modulus is nearly constant in the frequency range of 0-5000Hz. for most of the material tasted.
- Damping produced by simple composite beams made up of these materials is small (below 0.02).

Table 2-1 Material Properties Used in Preliminary Vibration Studies

Material Type	Lay-up Configuration	Metal Alloy	Metal Thickness	Prepreg Constituents
Aluminum	N/A	2024-T3	0.060"	N/A
Glare 1	3/2	7475-T76	0.012"	Glass-Epoxy
Glare 2	3/2	2024-T3	0.012"	Glass-Epoxy
Glare 3	3/2	2024-T3	0.012"	Glass-Epoxy
Glare 5	2/1	2024-T3	0.012"	Glass-Epoxy
Glare 5	3/2	2024-T3	0.012"	Glass-Epoxy
Glare 5	4/3	2024-T3	0.012"	Glass-Epoxy
Glare 5	5/4	2024-T3	0.012"	Glass-Epoxy
Glare 5	6/5	2024-T3	0.012"	Glass-Epoxy
ARALL 3	3/2	7475-T76	0.012"	Aramid-Epoxy

Material Type	Lay-up Configuration	Metal Alloy	Metal Thickness	Prepreg Constituents
Aluminum	N/A	N/A	0.060"	29.0 gm
Glare 1	$[0^\circ_2]$ Unidirectional	0.010"	0.056"	24.3
Glare 2	$[0^\circ_2]$ Unidirectional	0.010"	0.056"	24.3
Glare 3	$[0^\circ/90^\circ]$ Cross-Ply	0.010"	0.056"	25.2
Glare 5	$[0^\circ/90^\circ/90^\circ/0^\circ]$ Cross-Ply	0.020"	0.044"	18.9
Glare 5	$[0^\circ/90^\circ/90^\circ/0^\circ]$ Cross-Ply	0.020"	0.076"	32.0
Glare 5	$[0^\circ/90^\circ/90^\circ/0^\circ]$ Cross-Ply	0.020"	0.108"	43.7
Glare 5	$[0^\circ/90^\circ/90^\circ/0^\circ]$ Cross-Ply	0.020"	0.140"	59.0
Glare 5	$[0^\circ/90^\circ/90^\circ/0^\circ]$ Cross-Ply	0.020"	0.172"	69.9
ARALL 3	$[0^\circ_2]$ Unidirectional	0.0085"	0.053"	22.0

CHAPTER 3: NONLINEAR VIBRATION OF FIBER-METAL LAMINATED BEAMS

In this chapter, we derive the equations of motion and boundary conditions governing the planar vibrations of inextensible Euler-Bernoulli beams made with Fiber-Metal Laminates (FML). In the beginning the beams are assumed to be isotropic, then the effective stiffness and inertia of Fiber-Metal Laminated beams are substituted in the formulas. Here we adopt the approach used by Crespo da Silva and Glynn [96,97]. For the sake of simplicity, we restrict ourselves in two-dimensional case. This approach is based on the variational principle and the extended Hamilton principle. A similar model was proposed by Malatkar and Nayfeh [218]. In this model the effect of transverse shear deformation and rotatory inertia are ignored. These assumptions are valid if the ratio of thickness to length of the beam is small enough. The beams in this study are very thin (less than 0.06 inch). The lengths of the beams are about 12 inches. The restrictions of the model are well satisfied.

We solve the resulted integro-differential equation via Multiple Scales Method and Harmonic Balance Method respectively. While the solutions are equivalent at small vibration, a moderate discrepancy can be seen in simulations when the vibration is at large amplitude.

Based on the approximate solutions, a system identification procedure is followed. For the single-mode response, a large discrepancy in nonlinearity coefficient is found between theory and experiment. For different excitation level, a small variation in the linear natural frequency is detected. A beam model with a nonlinear spring-hinged end and the other free is applied to tune the inextensible cantilever beam theory. While this

modified mode can reasonably explain the natural frequency difference, its ability of covering the discrepancy in nonlinearity coefficient is limited. It is also found that the damping is inherently complicate phenomena. Linear damping and nonlinear damping do not change the response curve significantly as long as the equivalent damping is same.

3.1. INEXTENSIBLE BEAM MODEL WITH VISCOELASTIC DAMPING

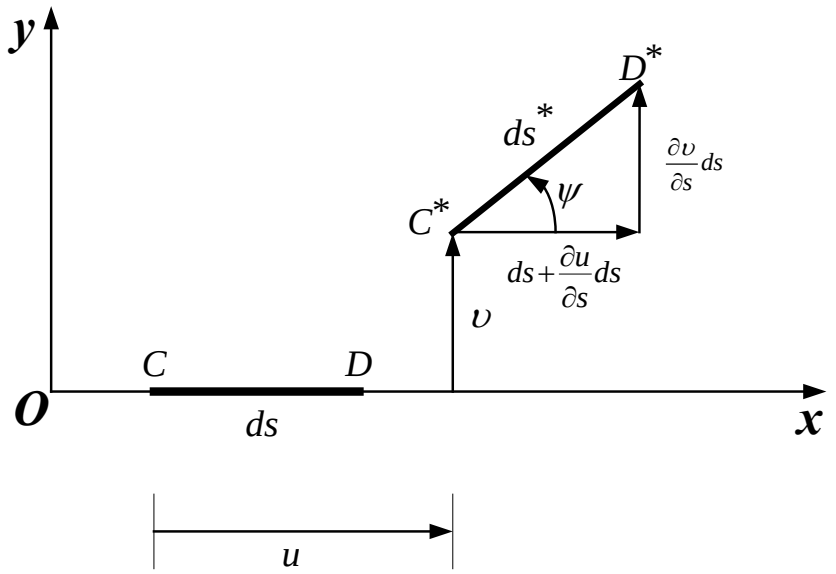

Figure 3-1 Deformation of a beam element along the neutral axis.

We consider the deformation of an element ***CD*** of the beam's neutral axis, which is of length ***ds*** and located at a distance ***s*** from the origin ***O*** of the (x, y) system as shown in Figure 3.1. After deformation, ***CD*** moves to ***C*D*.*** We denote the displacement components of ***C*** and ***D*** by $(u(s,t),\ \upsilon(s,t))$ and $(u(s,t)+\frac{\partial u(s,t)}{\partial s}ds,\ \upsilon(s,t)+\frac{\partial \upsilon(s,t)}{\partial s}ds)$, respectively. From the Figure above, the strain ***e*** at point **C** can be calculated as

$$e = \frac{ds^* - ds}{ds} = \frac{\sqrt{[ds + \frac{\partial u(s,t)}{\partial s} ds]^2 + [\frac{\partial \upsilon(s,t)}{\partial s} ds]^2} - ds}{ds}$$
$$= \sqrt{[1 + \frac{\partial u(s,t)}{\partial s}]^2 + [\frac{\partial \upsilon(s,t)}{\partial s}]^2} - 1 \qquad (3.1)$$

We assume the beam's neutral axis to be inextensional; that is, $\boldsymbol{e = 0}$. The inextensionality constraint equation thus is

$$[1 + \frac{\partial u(s,t)}{\partial s}]^2 + [\frac{\partial \upsilon(s,t)}{\partial s}]^2 = 1 \qquad (3.2)$$

It is a well-known fact that, in the absence of large axial forces, fixed-free and fixed-sliding elements are approximated as inextensional members. From the figure 3.1, we know

$$\tan\psi(s,t) = \frac{\frac{\partial \upsilon(s,t)}{\partial s}}{1 + \frac{\partial u(s,t)}{\partial s}} \qquad \psi(s,t) = \tan^{-1}\frac{\frac{\partial \upsilon(s,t)}{\partial s}}{1 + \frac{\partial u(s,t)}{\partial s}} = \tan^{-1}(\frac{\frac{\partial \upsilon(s,t)}{\partial s}}{\sqrt{1 - [\frac{\partial \upsilon(s,t)}{\partial s}]^2}}) \qquad (3.3)$$

The kinetic energy of beam (assume the rotatory effect is negligible)

$$T = \frac{1}{2}\int_0^l \rho A\{[\frac{\partial u(s,t)}{\partial t}]^2 + [\frac{\partial \upsilon(s,t)}{\partial t}]^2)ds \qquad (3.4)$$

The potential energy of beam (assume no shear deformation)

$$V(t) = \int_0^{\varepsilon}\int_0^l\int_{-h/2}^{h/2} \sigma b dy ds d\varepsilon$$
$$= \int_0^l\int_0^{\frac{\partial\psi(s,t)}{\partial s}}\int_{-h/2}^{h/2}[E\frac{\partial\psi(s,t)}{\partial s}y + E^*\frac{\partial^2\psi(s,t)}{\partial t\partial s}y]d[\frac{\partial\psi(s,t)}{\partial s}y]bdyds$$
$$= \int_0^l\int_0^{\frac{\partial\psi(s,t)}{\partial s}}\int_{-h/2}^{h/2}[E\frac{\partial\psi(s,t)}{\partial s}y^2 + E^*\frac{\partial^2\psi(s,t)}{\partial t\partial s}y^2]bdyd[\frac{\partial\psi(s,t)}{\partial s}]ds \qquad (3.5)$$
$$= \int_0^l\frac{1}{2}EI[\frac{\partial\psi(s,t)}{\partial s}]^2 dx + \int_0^l\int_0^{\frac{\partial\psi(s,t)}{\partial s}} E^* I\frac{\partial^2\psi(s,t)}{\partial t\partial s}d\frac{\partial\psi(s,t)}{\partial s}\}ds$$

where E is the Young's modulus, E^* is the loss modulus and $\psi(s,t)$ is the rotation angle of beam.

To enforce the inextensionality constraint (equation (3.2)), we use the Lagrange multiplier ***λ(s, t).*** The overall specific Lagrangian L as

$$L = \frac{1}{2}\int_0^l \{\rho A[(\frac{\partial u(s,t)}{\partial t})^2 + (\frac{\partial \upsilon(s,t)}{\partial t})^2] - EI(\frac{\partial \psi(s,t)}{\partial s})^2 + 2\int_0^{\frac{\partial \psi(s,t)}{\partial s}} E^* I \frac{\partial^2 \psi(s,t)}{\partial t \partial s} d\frac{\partial \psi(s,t)}{\partial s} + \lambda(s,t)[(1-(1+\frac{\partial u(s,t)}{\partial s})^2 - (\frac{\partial \upsilon(s,t)}{\partial s})^2]\}ds \tag{3.6}$$

Apply extended Hamilton principle

$$\int_{t_1}^{t_2} (\delta L + \delta W)dt = 0 \tag{3.7}$$

where W is the work done by non-conservative force.

$$\delta W = Q_u(s,t)\delta u(s,t) + Q_\upsilon(s,t)\delta\upsilon(s,t) \tag{3.8}$$

$$\begin{aligned}\delta L = \frac{1}{2}\int_0^l \{&\rho A(2\frac{\partial u(s,t)}{\partial t}\delta\frac{\partial u(s,t)}{\partial t} + 2\frac{\partial \upsilon(s,t)}{\partial t}\delta\frac{\partial \upsilon(s,t)}{\partial t}) \\ &-2[EI\frac{\partial \psi(s,t)}{\partial s} + E^* I\frac{\partial^2 \psi(s,t)}{\partial t \partial s}]\frac{\partial \delta\psi(s,t)}{\partial s} \\ &+\lambda(s,t)[-2(1+\frac{\partial u(s,t)}{\partial s})\delta\frac{\partial u(s,t)}{\partial s} - 2\frac{\partial \upsilon(s,t)}{\partial s}\delta\frac{\partial \upsilon(s,t)}{\partial s}]\}ds\end{aligned} \tag{3.9}$$

$$\begin{aligned}&\int_{t_1}^{t_2}\int_0^l \frac{\partial u(s,t)}{\partial t}\delta\frac{\partial u(s,t)}{\partial t}dsdt = \int_0^l\int_{t_1}^{t_2}\frac{\partial u(s,t)}{\partial t}\frac{\partial}{\partial t}(\delta u(s,t))dtds \\ &= \int_0^l(\frac{\partial u(s,t)}{\partial t}\delta u(s,t)\Big|_{t_1}^{t_2} - \int_{t_1}^{t_2}\frac{\partial^2 u(s,t)}{\partial t^2}\delta u(s,t)dt)ds = -\int_{t_1}^{t_2}\int_0^l \frac{\partial^2 u(s,t)}{\partial t^2}\delta u(s,t)dsdt\end{aligned} \tag{3.10a}$$

$$\begin{aligned}&\int_{t_1}^{t_2}\int_0^l \frac{\partial \upsilon(s,t)}{\partial t}\delta\frac{\partial \upsilon(s,t)}{\partial t}dsdt = \int_0^l\int_{t_1}^{t_2}\frac{\partial \upsilon(s,t)}{\partial t}\frac{\partial}{\partial t}(\delta \upsilon(s,t))dtds \\ &= \int_0^l(\frac{\partial \upsilon(s,t)}{\partial t}\delta \upsilon(s,t)\Big|_{t_1}^{t_2} - \int_{t_1}^{t_2}\frac{\partial^2 \upsilon(s,t)}{\partial t^2}\delta \upsilon(s,t)dt)ds = -\int_{t_1}^{t_2}\int_0^l \frac{\partial^2 \upsilon(s,t)}{\partial t^2}\delta \upsilon(s,t)dsdt\end{aligned} \tag{3.10b}$$

$$-\int_{t_1}^{t_2}\int_0^l \lambda(s,t)(1+\frac{\partial u(s,t)}{\partial s})\delta\frac{\partial u(s,t)}{\partial s}dsdt = -\int_{t_1}^{t_2}\int_0^l \lambda(s,t)(1+\frac{\partial u(s,t)}{\partial s})\frac{\partial}{\partial s}\delta u(s,t)dsdt$$
$$= -\int_{t_1}^{t_2}\{\lambda(s,t)(1+\frac{\partial u(s,t)}{\partial s})\delta u(s,t)\mid_0^l + \int_0^l \frac{\partial}{\partial s}[\lambda(s,t)(1+\frac{\partial u(s,t)}{\partial s})]\delta u ds\}dt \tag{3.10c}$$

$$-\int_{t_1}^{t_2}\int_0^l \lambda(s,t)\frac{\partial \upsilon(s,t)}{\partial s}\delta\frac{\partial \upsilon(s,t)}{\partial s}dsdt = -\int_{t_1}^{t_2}\int_0^l \lambda(s,t)\frac{\partial \upsilon(s,t)}{\partial s}\frac{\partial}{\partial s}\delta\upsilon(s,t)dsdt$$
$$= -\int_{t_1}^{t_2}\{\lambda(s,t)\frac{\partial \upsilon(s,t)}{\partial s}\delta\upsilon(s,t)\mid_0^l + \int_0^l \frac{\partial}{\partial s}[\lambda(s,t)\frac{\partial \upsilon(s,t)}{\partial s}]\delta\upsilon(s,t)ds\}dt \tag{3.10d}$$

Note by variation restriction

$$\delta u(s,t_1) = \delta u(s,t_2) = 0$$
$$\delta\upsilon(s,t_1) = \delta\upsilon(s,t_2) = 0$$

and the variation and integral operators are commutable.

From 3.3 we have

$$\tan\psi(s,t) = \frac{\frac{\partial \upsilon(s,t)}{\partial s}}{1+\frac{\partial u(s,t)}{\partial s}}$$

$$\frac{\partial\psi(s,t)}{\partial s} = \frac{\partial^2\upsilon(s,t)}{\partial s^2}[1+\frac{\partial u(s,t)}{\partial s}] - \frac{\partial\upsilon(s,t)}{\partial s}\frac{\partial^2 u(s,t)}{\partial s^2} \tag{3.11}$$

$$\delta\psi(s,t) = -\frac{\partial\upsilon(s,t)}{\partial s}\delta[\frac{\partial u(s,t)}{\partial s}] + [1+\frac{\partial u(s,t)}{\partial s}]\delta[\frac{\partial\upsilon(s,t)}{\partial s}] \tag{3.12}$$

$$-\int_{t_1}^{t_2}\int_0^l \frac{\partial\psi(s,t)}{\partial s}\delta[\frac{\partial\psi(s,t)}{\partial s}]dsdt = -\int_{t_1}^{t_2}\int_0^l \frac{\partial\psi(s,t)}{\partial s}\frac{\partial[\delta\psi(s,t)]}{\partial s}dsdt$$
$$= -\int_{t_1}^{t_2}(\frac{\partial\psi(s,t)}{\partial s}\delta\psi(s,t)\mid_0^l + \int_0^l \frac{\partial^2\psi(s,t)}{\partial s^2}\delta\psi(s,t)ds)dt \tag{3.13}$$

$$-\int_{t_1}^{t_2}\int_0^l \frac{\partial^2\psi(s,t)}{\partial t\partial s}\delta[\frac{\partial\psi(s,t)}{\partial s}]dsdt = -\int_{t_1}^{t_2}\int_0^l \frac{\partial^2\psi(s,t)}{\partial t\partial s}\frac{\partial[\delta\psi(s,t)]}{\partial s}dsdt$$
$$= -\int_{t_1}^{t_2}(\frac{\partial^2\psi(s,t)}{\partial t\partial s}\delta\psi(s,t)\mid_0^l + \int_0^l \frac{\partial^3\psi(s,t)}{\partial t\partial s^2}\delta\psi(s,t)ds)dt \tag{3.14}$$

Substitute the results of Equations (3.10a-3.10d) and (3.13-3.14) into Equation (3.7), and perform a few integrations by parts in Equation (3.13-3.14), we get

$$\begin{aligned}
&\rho A\frac{\partial^2 u(s,t)}{\partial t^2} - Q_u(s,t) \\
&= \frac{\partial}{\partial s}\{EI\frac{\partial \upsilon(s,t)}{\partial s}\frac{\partial}{\partial s}\{\frac{\partial^2 \upsilon(s,t)}{\partial s^2}[1+\frac{\partial u(s,t)}{\partial s}] - \frac{\partial \upsilon(s,t)}{\partial s}\frac{\partial^2 u(s,t)}{\partial s^2}\} \\
&\quad + E^* I\frac{\partial \upsilon(s,t)}{\partial s}\frac{\partial}{\partial t}\frac{\partial}{\partial s}\{\frac{\partial^2 \upsilon(s,t)}{\partial s^2}[1+\frac{\partial u(s,t)}{\partial s}] - \frac{\partial \upsilon(s,t)}{\partial s}\frac{\partial^2 u(s,t)}{\partial s^2}\} \\
&\quad + \lambda(s,t)(1+\frac{\partial u(s,t)}{\partial s})\}
\end{aligned} \tag{3.15a}$$

$$\begin{aligned}
&\rho A\frac{\partial^2 \upsilon(s,t)}{\partial t^2} - Q_\upsilon(s,t) = \\
&\frac{\partial}{\partial s}\{-EI\frac{\partial}{\partial s}\{\frac{\partial^2 \upsilon(s,t)}{\partial s^2}[1+\frac{\partial u(s,t)}{\partial s}] - \frac{\partial \upsilon(s,t)}{\partial s}\frac{\partial^2 u(s,t)}{\partial s^2}\}[1+\frac{\partial u(s,t)}{\partial s}] \\
&-E^* I\frac{\partial}{\partial t}\frac{\partial}{\partial s}\{\frac{\partial^2 \upsilon(s,t)}{\partial s^2}[1+\frac{\partial u(s,t)}{\partial s}] - \frac{\partial \upsilon(s,t)}{\partial s}\frac{\partial^2 u(s,t)}{\partial s^2}\}[1+\frac{\partial u(s,t)}{\partial s}]\} \\
&+\lambda(s,t)\frac{\partial \upsilon(s,t)}{\partial s}\}
\end{aligned} \tag{3.15b}$$

Boundary conditions:

$$\begin{aligned}
&-\{EI\frac{\partial \upsilon(s,t)}{\partial s}\frac{\partial}{\partial s}\{\frac{\partial^2 \upsilon(s,t)}{\partial s^2}[1+\frac{\partial u(s,t)}{\partial s}] - \frac{\partial \upsilon(s,t)}{\partial s}\frac{\partial^2 u(s,t)}{\partial s^2}\} \\
&+E^* I\frac{\partial \upsilon(s,t)}{\partial s}\frac{\partial}{\partial t}\frac{\partial}{\partial s}\{\frac{\partial^2 \upsilon(s,t)}{\partial s^2}[1+\frac{\partial u(s,t)}{\partial s}] - \frac{\partial \upsilon(s,t)}{\partial s}\frac{\partial^2 u(s,t)}{\partial s^2}\} \\
&+\lambda(s,t)(1+\frac{\partial u(s,t)}{\partial s})\}\delta u(s,t)\|_0^l = 0
\end{aligned} \tag{3.16a}$$

$$\begin{aligned}
&\{EI\frac{\partial}{\partial s}\{\frac{\partial^2 \upsilon(s,t)}{\partial s^2}[1+\frac{\partial u(s,t)}{\partial s}] - \frac{\partial \upsilon(s,t)}{\partial s}\frac{\partial^2 u(s,t)}{\partial s^2}\}[1+\frac{\partial u(s,t)}{\partial s}] \\
&+E^* I\frac{\partial}{\partial t}\frac{\partial}{\partial s}\{\frac{\partial^2 \upsilon(s,t)}{\partial s^2}[1+\frac{\partial u(s,t)}{\partial s}] - \frac{\partial \upsilon(s,t)}{\partial s}\frac{\partial^2 u(s,t)}{\partial s^2}\}[1+\frac{\partial u(s,t)}{\partial s}] \\
&-\lambda(s,t)\frac{\partial \upsilon(s,t)}{\partial s}\}\delta \upsilon(s,t)\|_0^l = 0
\end{aligned} \tag{3.16b}$$

$$\{EI\{\frac{\partial^2 \upsilon(s,t)}{\partial s^2}[1+\frac{\partial u(s,t)}{\partial s}]-\frac{\partial \upsilon(s,t)}{\partial s}\frac{\partial^2 u(s,t)}{\partial s^2}\}\frac{\partial \upsilon(s,t)}{\partial s}$$
$$+E^* I\frac{\partial}{\partial t}\{\frac{\partial^2 \upsilon(s,t)}{\partial s^2}[1+\frac{\partial u(s,t)}{\partial s}]-\frac{\partial \upsilon(s,t)}{\partial s}\frac{\partial^2 u(s,t)}{\partial s^2}\}\frac{\partial \upsilon(s,t)}{\partial s}\}\delta[\frac{\partial u(s,t)}{\partial s}]\Big|_0^l = 0 \quad (3.16c)$$

$$-\{EI\{\frac{\partial^2 \upsilon(s,t)}{\partial s^2}[1+\frac{\partial u(s,t)}{\partial s}]-\frac{\partial \upsilon(s,t)}{\partial s}\frac{\partial^2 u(s,t)}{\partial s^2}\}[1+\frac{\partial u(s,t)}{\partial s}]$$
$$+E^* I\frac{\partial}{\partial t}\{\frac{\partial^2 \upsilon(s,t)}{\partial s^2}[1+\frac{\partial u(s,t)}{\partial s}]-\frac{\partial \upsilon(s,t)}{\partial s}\frac{\partial^2 u(s,t)}{\partial s^2}\}[1+\frac{\partial u(s,t)}{\partial s}]\}\delta[\frac{\partial \upsilon(s,t)}{\partial s}]\Big|_0^l = 0 \quad (3.16d)$$

Those eight boundary conditions are either satisfied by geometry (variation term equals zero, called geometry condition) or balanced by terms other than variation term equal zero (called natural boundary condition).

Using the boundary condition 3.16a (natural boundary condition), we get

$$-\{EI\frac{\partial \upsilon(s,t)}{\partial s}\frac{\partial}{\partial s}\{\frac{\partial^2 \upsilon(s,t)}{\partial s^2}[1+\frac{\partial u(s,t)}{\partial s}]-\frac{\partial \upsilon(s,t)}{\partial s}\frac{\partial^2 u(s,t)}{\partial s^2}\}$$
$$+E^* I\frac{\partial \upsilon(s,t)}{\partial s}\frac{\partial}{\partial t}\frac{\partial}{\partial s}\{\frac{\partial^2 \upsilon(s,t)}{\partial s^2}[1+\frac{\partial u(s,t)}{\partial s}]-\frac{\partial \upsilon(s,t)}{\partial s}\frac{\partial^2 u(s,t)}{\partial s^2}\} \quad (3.17)$$
$$+\lambda(s,t)(1+\frac{\partial u(s,t)}{\partial s})\}\Big|_0^l = 0$$

Integrate both sides of Equation (3.15a) from ***l*** to ***s***, we obtain

$$\int_l^s \rho A\frac{\partial^2 u(s,t)}{\partial t^2}ds-\int_l^s Q_u(s,t)ds$$
$$=EI\frac{\partial \upsilon(s,t)}{\partial s}\frac{\partial}{\partial s}\{\frac{\partial^2 \upsilon(s,t)}{\partial s^2}[1+\frac{\partial u(s,t)}{\partial s}]+E^* I\frac{\partial \upsilon(s,t)}{\partial s}\frac{\partial}{\partial t}\frac{\partial}{\partial s}\{\frac{\partial^2 \upsilon(s,t)}{\partial s^2}[1+\frac{\partial u(s,t)}{\partial s}]$$
$$-\frac{\partial \upsilon(s,t)}{\partial s}\frac{\partial^2 u(s,t)}{\partial s^2}\}+\lambda(s,t)(1+\frac{\partial u(s,t)}{\partial s}) \quad (3.18)$$

Use Taylor series expansion, keep the terms up to order three, we get

assume $u(s,t)=O(\varepsilon^2)$ $\upsilon(s,t)=O(\varepsilon)$

$$
\begin{aligned}
&[1+\frac{\partial u(s,t)}{\partial s}]^2+[\frac{\partial \upsilon(s,t)}{\partial s}]^2=1\\
&\Rightarrow 1+\frac{\partial u(s,t)}{\partial s}=\sqrt{1-[\frac{\partial \upsilon(s,t)}{\partial s}]^2}=1-\frac{1}{2}[\frac{\partial \upsilon(s,t)}{\partial s}]^2+o(\varepsilon^3)\\
&\Rightarrow \frac{\partial u(s,t)}{\partial s}\approx -\frac{1}{2}[\frac{\partial \upsilon(s,t)}{\partial s}]^2\\
&\Rightarrow \frac{\partial^2 u(s,t)}{\partial s^2}\approx -\frac{\partial \upsilon(s,t)}{\partial s}\frac{\partial^2 \upsilon(s,t)}{\partial s^2}
\end{aligned}
\tag{3.19}
$$

Equation (3.15a) becomes

$$
\begin{aligned}
&\int_l^s \rho A\frac{\partial^2 u(s,t)}{\partial t^2}ds-\int_l^s Q_u(s,t)ds\\
&=EI\,\frac{\partial \upsilon(s,t)}{\partial s}\frac{\partial^3 \upsilon(s,t)}{\partial s^3}+E^*I\,\frac{\partial \upsilon(s,t)}{\partial s}\frac{\partial}{\partial t}\frac{\partial^3 \upsilon(s,t)}{\partial s^3}+\lambda(s,t)(1+\frac{\partial u(s,t)}{\partial s})
\end{aligned}
\tag{3.20a}
$$

Equation (3.15b) becomes

$$
\begin{aligned}
&\rho A\frac{\partial^2 \upsilon(s,t)}{\partial t^2}-Q_\upsilon(s,t)\\
&=\frac{\partial}{\partial s}\{-EI\{\frac{\partial^3 \upsilon(s,t)}{\partial s^3}+[\frac{\partial^2 \upsilon(s,t)}{\partial s^2}]^2\frac{\partial \upsilon(s,t)}{\partial s}-E^*I\,\frac{\partial}{\partial t}\{\frac{\partial^3 \upsilon(s,t)}{\partial s^3}+[\frac{\partial^2 \upsilon(s,t)}{\partial s^2}]^2\frac{\partial \upsilon(s,t)}{\partial s}\}\\
&+\lambda(s,t)\frac{\partial \upsilon(s,t)}{\partial s}\}+o(\varepsilon^3)
\end{aligned}
\tag{3.20b}
$$

From inextensionality constraint equations (3.2) and (3.19), we have

$$
\begin{aligned}
&\Rightarrow \frac{\partial u(s,t)}{\partial s}\approx -\frac{1}{2}[\frac{\partial \upsilon(s,t)}{\partial s}]^2\\
&\Rightarrow u(s,t)\approx \int_0^s -\frac{1}{2}[\frac{\partial \upsilon(s,t)}{\partial s}]^2 ds
\end{aligned}
\tag{3.21}
$$

Substitute Equation (3.21) into Equation (3.20a), we get

$$
\begin{aligned}
&\lambda(s,t)=-\int_l^s \rho A\frac{\partial^2}{\partial t^2}\int_0^s \frac{1}{2}[\frac{\partial \upsilon(s,t)}{\partial s}]^2 dsds-\int_l^s Q_u(s,t)ds\\
&-EI\,\frac{\partial \upsilon(s,t)}{\partial s}\frac{\partial^3 \upsilon(s,t)}{\partial s^3}-E^*I\,\frac{\partial \upsilon(s,t)}{\partial s}\frac{\partial}{\partial t}\frac{\partial^3 \upsilon(s,t)}{\partial s^3}+o(\varepsilon^3)
\end{aligned}
\tag{3.22}
$$

Substitute Equation (3.22) into Equation (3.20b)

$$\begin{aligned}
&\rho A\frac{\partial^2\upsilon(s,t)}{\partial t^2}+EI\frac{\partial^4\upsilon(s,t)}{\partial s^4}+E^*I\frac{\partial^5\upsilon(s,t)}{\partial t\partial s^4}-Q_\upsilon(s,t)=\\
&-EI\frac{\partial}{\partial s}\{\frac{\partial\upsilon(s,t)}{\partial s}\frac{\partial}{\partial s}[\frac{\partial\upsilon(s,t)}{\partial s}\frac{\partial^2\upsilon(s,t)}{\partial s^2}]\}\\
&-E^*I\frac{\partial}{\partial s}\{\frac{\partial}{\partial t}\frac{\partial\upsilon(s,t)}{\partial s}[\frac{\partial^2\upsilon(s,t)}{\partial s^2}]^2+[\frac{\partial\upsilon(s,t)}{\partial s}]^2\frac{\partial}{\partial t}\frac{\partial^3\upsilon(s,t)}{\partial s^3}\}\\
&-\frac{\partial}{\partial s}\{\{\int_l^s\rho A\frac{\partial^2}{\partial t^2}\int_0^s\frac{1}{2}[\frac{\partial\upsilon(s,t)}{\partial s}]^2dsds+\int_l^s Q_u(s,t)ds\}\frac{\partial\upsilon(s,t)}{\partial s}\}
\end{aligned}\tag{3.23}$$

If there is no non-conservative force, then

$$Q_u(s,t)=0$$
$$Q_\upsilon(s,t)=0$$

$$\begin{aligned}
&\rho A\frac{\partial^2\upsilon(s,t)}{\partial t^2}+EI\frac{\partial^4\upsilon(s,t)}{\partial s^4}+E^*I\frac{\partial^5\upsilon(s,t)}{\partial t\partial s^4}=\\
&-EI\frac{\partial}{\partial s}\{\frac{\partial\upsilon(s,t)}{\partial s}\frac{\partial}{\partial s}[\frac{\partial\upsilon(s,t)}{\partial s}\frac{\partial^2\upsilon(s,t)}{\partial s^2}]\}\\
&-E^*I\frac{\partial}{\partial s}\{\frac{\partial}{\partial t}\frac{\partial\upsilon(s,t)}{\partial s}[\frac{\partial^2\upsilon(s,t)}{\partial s^2}]^2+[\frac{\partial\upsilon(s,t)}{\partial s}]^2\frac{\partial}{\partial t}\frac{\partial^3\upsilon(s,t)}{\partial s^3}\}\\
&-\frac{\partial}{\partial s}\{\{\int_l^s\rho A\frac{\partial^2}{\partial t^2}\int_0^s\frac{1}{2}[\frac{\partial\upsilon(s,t)}{\partial s}]^2dsds\}
\end{aligned}\tag{3.24}$$

When the beam is subjected to a transverse base excitation in the y-direction

$$\upsilon(s,t)=\overline{\upsilon}(s,t)+\frac{a_b}{\Omega^2}\cos\Omega t \tag{3.25}$$

where $\overline{\upsilon}(s,t)$ is the transverse displacement respect to the base, Ω is the excitation frequency. Substitute Equation (3.25) into Equation (3.24),

$$\begin{aligned}
&\rho A\frac{\partial^2\overline{\upsilon}(s,t)}{\partial t^2}-\rho Aa_b\cos\Omega t+EI\frac{\partial^4\overline{\upsilon}(s,t)}{\partial s^4}+E^*I\frac{\partial^5\overline{\upsilon}(s,t)}{\partial t\partial s^4}\\
&=-EI\frac{\partial}{\partial s}\{\frac{\partial\overline{\upsilon}(s,t)}{\partial s}\frac{\partial}{\partial s}[\frac{\partial\overline{\upsilon}(s,t)}{\partial s}\frac{\partial^2\overline{\upsilon}(s,t)}{\partial s^2}]\}\\
&-E^*I\frac{\partial}{\partial s}\{\frac{\partial}{\partial t}\frac{\partial\overline{\upsilon}(s,t)}{\partial s}[\frac{\partial^2\overline{\upsilon}(s,t)}{\partial s^2}]^2+[\frac{\partial\overline{\upsilon}(s,t)}{\partial s}]^2\frac{\partial}{\partial t}\frac{\partial^3\overline{\upsilon}(s,t)}{\partial s^3}\}\\
&-\frac{1}{2}\rho A\frac{\partial}{\partial s}\{\frac{\partial\overline{\upsilon}(s,t)}{\partial s}\int_l^s\frac{\partial^2}{\partial t^2}\int_0^s[\frac{\partial\overline{\upsilon}(s,t)}{\partial s}]^2dsds\}
\end{aligned}$$

Use $\upsilon(s,t)$ as the transverse displacement respect to the base, we obtain

$$\begin{aligned}
&\rho A\frac{\partial^2\upsilon(s,t)}{\partial t^2}+EI\frac{\partial^4\upsilon(s,t)}{\partial s^4}+E^*I\frac{\partial^5\upsilon(s,t)}{\partial t\partial s^4}\\
&=\rho Aa_b\cos\Omega t-EI\frac{\partial}{\partial s}\{\frac{\partial\upsilon(s,t)}{\partial s}\frac{\partial}{\partial s}[\frac{\partial\upsilon(s,t)}{\partial s}\frac{\partial^2\upsilon(s,t)}{\partial s^2}]\}\\
&-E^*I\frac{\partial}{\partial s}\{\frac{\partial}{\partial t}\frac{\partial\upsilon(s,t)}{\partial s}[\frac{\partial^2\upsilon(s,t)}{\partial s^2}]^2+[\frac{\partial\upsilon(s,t)}{\partial s}]^2\frac{\partial}{\partial t}\frac{\partial^3\upsilon(s,t)}{\partial s^3}\}\\
&-\frac{1}{2}\rho A\frac{\partial}{\partial s}\{\frac{\partial\upsilon(s,t)}{\partial s}\int_l^s\frac{\partial^2}{\partial t^2}\int_0^s[\frac{\partial\upsilon(s,t)}{\partial s}]^2dsds\}
\end{aligned}\tag{3.26}$$

If we introduce the linear and quadratic damping force as non-conservative force, then

$$Q_\upsilon(s,t)=-(c_\upsilon\frac{\partial}{\partial t}\upsilon(s,t)+\overline{c}\frac{\partial}{\partial t}\upsilon(s,t)\,|\frac{\partial}{\partial t}\upsilon(s,t)\,|)$$

$$\begin{aligned}
&\rho A\frac{\partial^2\upsilon(s,t)}{\partial t^2}+c_\upsilon\frac{\partial}{\partial t}\upsilon(s,t)+\overline{c}\frac{\partial}{\partial t}\upsilon(s,t)\,|\frac{\partial}{\partial t}\upsilon(s,t)\,|+EI\frac{\partial^4\upsilon(s,t)}{\partial s^4}+E^*I\frac{\partial^5\upsilon(s,t)}{\partial t\partial s^4}\\
&=\rho Aa_b\cos\Omega t-EI\frac{\partial}{\partial s}\{\frac{\partial\upsilon(s,t)}{\partial s}\frac{\partial}{\partial s}[\frac{\partial\upsilon(s,t)}{\partial s}\frac{\partial^2\upsilon(s,t)}{\partial s^2}]\}\\
&-E^*I\frac{\partial}{\partial s}\{\frac{\partial}{\partial t}\frac{\partial\upsilon(s,t)}{\partial s}[\frac{\partial^2\upsilon(s,t)}{\partial s^2}]^2+[\frac{\partial\upsilon(s,t)}{\partial s}]^2\frac{\partial}{\partial t}\frac{\partial^3\upsilon(s,t)}{\partial s^3}\}\\
&-\frac{1}{2}\rho A\frac{\partial}{\partial s}\{\frac{\partial\upsilon(s,t)}{\partial s}\int_l^s\frac{\partial^2}{\partial t^2}\int_0^s[\frac{\partial\upsilon(s,t)}{\partial s}]^2dsds\}
\end{aligned}\tag{3.27}$$

We notice that $\frac{E^*}{E}<<1$, hence the cubic viscoelastic term is a highest order term if $\upsilon(s,t)=O(\varepsilon)$, here $\varepsilon<<1$ is a bookkeeping parameter that is introduced to keep track of the different orders of approximation. Accordingly the nonlinear viscoelastic term is neglected. It will be shown later the linear viscoelastic term can be replaced with the equivalent viscous damping. Let $E^*=0$, Equation (3.27) becomes

$$\rho A\frac{\partial^2\upsilon(s,t)}{\partial t^2}+c_\upsilon\frac{\partial}{\partial t}\upsilon(s,t)+\overline{c}\frac{\partial}{\partial t}\upsilon(s,t)\left|\frac{\partial}{\partial t}\upsilon(s,t)\right|+EI\frac{\partial^4\upsilon(s,t)}{\partial s^4}$$
$$=\rho Aa_b\cos\Omega t-EI\frac{\partial}{\partial s}\{\frac{\partial\upsilon(s,t)}{\partial s}\frac{\partial}{\partial s}[\frac{\partial\upsilon(s,t)}{\partial s}\frac{\partial^2\upsilon(s,t)}{\partial s^2}]\} \tag{3.28}$$
$$-\frac{1}{2}\rho A\frac{\partial}{\partial s}\{\frac{\partial\upsilon(s,t)}{\partial s}\int_l^s\frac{\partial^2}{\partial t^2}\int_0^s[\frac{\partial\upsilon(s,t)}{\partial s}]^2dsds\}$$

3.2. MULTIPLE SCALES METHOD

The governing equation of nonlinear inextensible cantilever beam

$$\rho A\frac{\partial^2\upsilon(s,t)}{\partial t^2}+c_\upsilon\frac{\partial}{\partial t}\upsilon(s,t)+\overline{c}\frac{\partial}{\partial t}\upsilon(s,t)\left|\frac{\partial}{\partial t}\upsilon(s,t)\right|+EI\frac{\partial^4\upsilon(s,t)}{\partial s^4}$$
$$=\rho Aa_b\cos\Omega t-EI\frac{\partial}{\partial s}\{\frac{\partial\upsilon(s,t)}{\partial s}\frac{\partial}{\partial s}[\frac{\partial\upsilon(s,t)}{\partial s}\frac{\partial^2\upsilon(s,t)}{\partial s^2}]\} \tag{3.29}$$
$$-\frac{1}{2}\rho A\frac{\partial}{\partial s}\{\frac{\partial\upsilon(s,t)}{\partial s}\int_l^s\frac{\partial^2}{\partial t^2}\int_0^s[\frac{\partial\upsilon(s,t)}{\partial s}]^2dsds\}$$

And the boundary conditions are

$$\upsilon(0,t)=0,\qquad EI\frac{\partial^2}{\partial s^2}\upsilon(0,t)=k_1\frac{\partial}{\partial s}\upsilon(0,t)+k_2[\frac{\partial}{\partial s}\upsilon(0,t)]^2+k_3[\frac{\partial}{\partial s}\upsilon(0,t)]^3 \tag{3.30}$$
$$\frac{\partial^2}{\partial s^2}\upsilon(l,t)=0,\qquad \frac{\partial^3}{\partial s^3}(l,t)=0$$

where ρ is the material density of beam and A is cross section area, l is the beam length, E is Young's modulus, I is the area moment of inertia, s is the arc length, t is time, $\upsilon(s,t)$ is the transverse displacement, a_b is the acceleration of the supported end of the beam, c_υ is the coefficient of linear viscous damping per unit length, $\overline{c}$ is the coefficient of quadratic damping per unit length, and Ω is the excitation frequency. k_1, k_2 and k_3 represent the linear, quadratic and cubic rotational stiffness coefficients respectively. And, the prime indicates differentiation with respect to the arc length s, whereas the overdot indicates differentiation with respect to time t.

We scale the nonlinearity and response as following:

$$\begin{aligned}
&\upsilon(s,t) = \varepsilon\upsilon_1(s,t) + \varepsilon^2\upsilon_2(s,t) + \varepsilon^3\upsilon_3(s,t) \\
&\frac{c_\upsilon}{2\rho A} = \varepsilon^2\mu_1 \\
&\frac{\overline{c}}{\rho A} = \varepsilon\mu_2 \\
&a_b = \varepsilon^3\overline{f}
\end{aligned} \tag{3.31}$$

Equation (3.30) becomes

$$\begin{aligned}
&\frac{\partial^2\upsilon(s,t)}{\partial t^2} + \varepsilon^2 2\mu_1\frac{\partial}{\partial t}\upsilon(s,t) + \varepsilon\mu_2\frac{\partial}{\partial t}\upsilon(s,t)\left|\frac{\partial}{\partial t}\upsilon(s,t)\right| + \frac{EI}{\rho A}\frac{\partial^4\upsilon(s,t)}{\partial s^4} \\
&= \varepsilon^3\overline{f}\cos\Omega t - \frac{EI}{\rho A}\frac{\partial}{\partial s}\{\frac{\partial\upsilon(s,t)}{\partial s}\frac{\partial}{\partial s}[\frac{\partial\upsilon(s,t)}{\partial s}\frac{\partial^2\upsilon(s,t)}{\partial s^2}]\} - \frac{1}{2}\frac{\partial}{\partial s}\{\frac{\partial\upsilon(s,t)}{\partial s}\int_l^s\frac{\partial^2}{\partial t^2}\int_0^s[\frac{\partial\upsilon(s,t)}{\partial s}]^2 dsds\}
\end{aligned} \tag{3.32}$$

Apply the method of multiple scales, which assume response q_n can be expressed as the function of slow time $T_0 = t$ and faster time $T_1 = \varepsilon t \quad T_2 = \varepsilon^2 t \quad \cdots$

Here we only consider faster time $T_1 = \varepsilon t \quad T_2 = \varepsilon^2 t$ and slow time $T_0 = t$

$$\upsilon(s,t) = \varepsilon\upsilon_1(s,T_0,T_1,T_2) + \varepsilon^2\upsilon_2(s,T_0,T_1,T_2) + \varepsilon^3\upsilon_3(s,T_0,T_1,T_2) \tag{3.33}$$

$$\frac{\partial}{\partial t} = \frac{\partial}{\partial T_0}\frac{dT_0}{dt} + \frac{\partial}{\partial T_1}\frac{dT_1}{dt} + \frac{\partial}{\partial T_2}\frac{dT_2}{dt} = \frac{\partial}{\partial T_0} + \varepsilon\frac{\partial}{\partial T_1} + \varepsilon^2\frac{\partial}{\partial T_2} \tag{3.34}$$

$$\frac{\partial^2}{\partial t^2} = \frac{\partial^2}{\partial T_0^2} + 2\varepsilon\frac{\partial}{\partial T_0}\frac{\partial}{\partial T_1} + \varepsilon^2\frac{\partial^2}{\partial T_1^2} + 2\varepsilon^2\frac{\partial}{\partial T_0}\frac{\partial}{\partial T_2} + H.O.T. \tag{3.35}$$

Define

$$D_0 = \frac{\partial}{\partial T_0} \quad D_1 = \frac{\partial}{\partial T_1} \quad D_2 = \frac{\partial}{\partial T_2}$$

then we have

$$\frac{\partial}{\partial t} = D_0 + \varepsilon D_1 + \varepsilon^2 D_2$$
$$\frac{\partial^2}{\partial t^2} = D_0^2 + 2\varepsilon D_0 D_1 + \varepsilon^2 D_1^2 + 2\varepsilon^2 D_0 D_2 \tag{3.37}$$

Substitute them into equation (3.37) into (3.32), we get

Order ε:

$$D_0^2 \upsilon_1(s,T_0,T_1,T_2) + \frac{EI}{\rho A}\frac{\partial^4 \upsilon_1(s,T_0,T_1,T_2)}{\partial s^4} = 0 \tag{3.38}$$

$$\upsilon_1(s,T_0,T_1,T_2)\,|_{s=0} = 0$$

$$EI\frac{\partial^2}{\partial s^2}\upsilon_1(s,T_0,T_1,T_2)\,|_{s=0} = k_1\frac{\partial}{\partial s}\upsilon_1(s,T_0,T_1,T_2)\,|_{s=0}$$

$$\frac{\partial^2}{\partial s^2}\upsilon_1(s,T_0,T_1,T_2)\,|_{s=l} = 0$$

$$\frac{\partial^3}{\partial s^3}\upsilon_1(s,T_0,T_1,T_2)\,|_{s=l} = 0$$

Order ε^2:

$$D_0^2 \upsilon_2(s,T_0,T_1,T_2) + \frac{EI}{\rho A}\frac{\partial^4 \upsilon_2(s,T_0,T_1,T_2)}{\partial s^4} = -2D_0 D_1 \upsilon_1(s,T_0,T_1,T_2) \tag{3.39}$$

$$\upsilon_2(s,T_0,T_1,T_2)\,|_{s=0} = 0$$

$$EI\frac{\partial^2}{\partial s^2}\upsilon_2(s,T_0,T_1,T_2)\,|_{s=0} = k_1\frac{\partial}{\partial s}\upsilon_2(s,T_0,T_1,T_2)\,|_{s=0} + k_2[\frac{\partial}{\partial s}\upsilon_1(s,T_0,T_1,T_2)]^2\,|_{s=0}$$

$$\frac{\partial^2}{\partial s^2}\upsilon_2(s,T_0,T_1,T_2)\,|_{s=l} = 0$$

$$\frac{\partial^3}{\partial s^3}\upsilon_2(s,T_0,T_1,T_2)\,|_{s=l} = 0$$

Order ε^3:

$$D_0^2\upsilon_3(s,T_0,T_1,T_2)+\frac{EI}{\rho A}\frac{\partial^4\upsilon_3(s,T_0,T_1,T_2)}{\partial s^4}=$$
$$\frac{\overline{f}}{2}(e^{i\Omega t}+e^{-i\Omega t})-\frac{EI}{\rho A}\frac{\partial}{\partial s}\{\frac{\partial\upsilon_1(s,T_0,T_1,T_2)}{\partial s}\frac{\partial}{\partial s}[\frac{\partial\upsilon_1(s,T_0,T_1,T_2)}{\partial s}\frac{\partial^2\upsilon_1(s,T_0,T_1,T_2)}{\partial s^2}]\}$$
$$\frac{1}{2}\frac{\partial}{\partial s}\{\frac{\partial\upsilon_1(s,T_0,T_1,T_2)}{\partial s}\int_l^s D_0^2\int_0^s[\frac{\partial\upsilon_1(s,T_0,T_1,T_2)}{\partial s}]^2 dsds\} \qquad (3.40)$$
$$-2D_0D_1\upsilon_2(s,T_0,T_1,T_2)-D_1^2\upsilon_1(s,T_0,T_1,T_2)-2D_0D_2\upsilon_1(s,T_0,T_1,T_2)$$
$$-2\mu_1(D_0\upsilon_1(s,T_0,T_1,T_2)-\mu_2D_0\upsilon_1(s,T_0,T_1,T_2)^*|D_0\upsilon_1(s,T_0,T_1,T_2)|$$

$$\upsilon_3(s,T_0,T_1,T_2)|_{s=0}=0$$

$$EI\frac{\partial^2}{\partial s^2}\upsilon_3(s,T_0,T_1,T_2)|_{s=0}=k_1\frac{\partial}{\partial s}\upsilon_3(s,T_0,T_1,T_2)|_{s=0}$$
$$+2k_2\frac{\partial}{\partial s}\upsilon_1(s,T_0,T_1,T_2)\frac{\partial}{\partial s}\upsilon_2(s,T_0,T_1,T_2)|_{s=0}+k_3[\frac{\partial}{\partial s}\upsilon_1(s,T_0,T_1,T_2)]^3|_{s=0}$$

$$\frac{\partial^2}{\partial s^2}\upsilon_3(s,T_0,T_1,T_2)|_{s=l}=0$$

$$\frac{\partial^3}{\partial s^3}\upsilon_3(s,T_0,T_1,T_2)|_{s=l}=0$$

The first-order equation with the boundary conditions, is a linear problem whose solution is assumed in the following form,

$$\upsilon(s,t)=\sum_{n=1}^{\infty}\phi_n(s)q_n(t)$$

The n^{th} mode normalized modal function $\phi_n(s)$ is:

$$\phi_n(s)=\frac{1}{\sqrt{S}}\left[(\cosh\beta_n s-\cos\beta_n s)+C_3(\sinh\beta_n s+\sin\beta_n s)+C_4(\sin\beta_n s-\sinh\beta_n s)\right]$$
$$C_3=\frac{EId_n}{k_1 l} \qquad (3.41)$$
$$C_4=-\frac{(\sinh d_n-\sin d_n)+\frac{EId_n}{k_1 l}(\cosh d_n-\cos d_n)}{(\cosh d_n+\cos d_n)}$$

$$S = \int_0^l \left[\left(\cosh \beta_n s - \cos \beta_n s\right) + C_3 \left(\sinh \beta_n s + \sin \beta_n s\right) + C_4 \left(\sin \beta_n s - \sinh \beta_n s\right) \right]^2 ds$$

where $d_n = {}_n l$ is the n^{th} root of the frequency equation

$$\frac{k_1 l}{EI} = \frac{d_n(\cosh d_n \sin d_n - \sinh d_n \cos d_n)}{1 + \cosh d_n \cos d_n} \qquad \beta_n^4 = \frac{\rho A}{EI} \omega_n^2$$

$$\int_0^l \phi_m(s)\phi_n(s)ds = \delta_{mn}$$

where δ_{mn} is the Dirac delta function.

Here we only consider one mode vibration, so

$$\upsilon(s,t) = \phi_n(s) q_n(t)$$

From Equation (3.38) we have

$$\upsilon_1(s, T_0, T_1, T_2) = \phi_n(s)[A(T_1, T_2)e^{i\omega_n T_0} + \underline{A}(T_1, T_2)e^{-i\omega_n T_0}] \tag{3.42}$$

where $\underline{A}(T_1, T_2)$ is the complex conjugate $A(T_1, T_2)$

Substitute Equation (3.42) into Equation (3.39)

$$D_0^2 \upsilon_2(s, T_0, T_1, T_2) + \frac{EI}{\rho A} \frac{\partial^4 \upsilon_2(s, T_0, T_1, T_2)}{\partial s^4} = -2i\omega_n \phi_n(s)[D_1 A(T_1, T_2)e^{i\omega_n T_0} + cc] \tag{3.43}$$

Here cc means complex conjugate of previous terms.

Boundary conditions:

$$\upsilon_2(s, T_0, T_1, T_2)|_{s=0} = 0$$

$$EI \frac{\partial^2}{\partial s^2} \upsilon_2(s, T_0, T_1, T_2)|_{s=0} = k_1 \frac{\partial}{\partial s} \upsilon_2(s, T_0, T_1, T_2)|_{s=0} + k_2 [\frac{\partial}{\partial s} \upsilon_1(s, T_0, T_1, T_2)]^2 |_{s=0}$$

$$\frac{\partial^2}{\partial s^2} \upsilon_2(s, T_0, T_1, T_2)|_{s=l} = 0$$

$$\frac{\partial^3}{\partial s^3} \upsilon_2(s, T_0, T_1, T_2)|_{s=l} = 0$$

The solution at each order must insure uniformity of the expansion (3.33). This is known as the solvability condition.

We assume Equation (3.39) has the following solution (primary response)

$$\upsilon_2(s,T_0,T_1,T_2) = V_2(s,T_1,T_2)e^{i\omega_n T_0} \tag{3.44}$$

Equation (3.39) becomes

$$-\omega_n^2 V_2(s,T_1,T_2) + \frac{EI}{\rho A}\frac{\partial^4 V_2(s,T_1,T_2)}{\partial s^4} = -2i\omega_n \phi_n(s) D_1 A(T_1,T_2) \tag{3.45}$$

$$V_2(s,T_1,T_2)\,|_{s=0} = 0$$

$$EI\frac{\partial^2}{\partial s^2}V_2(s,T_1,T_2)\,|_{s=0} = k_1\frac{\partial}{\partial s}V_2(s,T_1,T_2)\,|_{s=0} + k_2[\frac{\partial}{\partial s}V_1(s,T_1,T_2)]^2\,|_{s=0}$$

$$\frac{\partial^2}{\partial s^2}V_2(s,T_1,T_2)\,|_{s=l} = 0$$

$$\frac{\partial^3}{\partial s^3}V_2(s,T_1,T_2)\,|_{s=l} = 0$$

since

$$k_2[\frac{\partial}{\partial s}\upsilon_1(s,T_0,T_1,T_2)]^2\,|_{s=0} = k_2[\frac{\partial}{\partial s}\phi_n(s)[A(T_1,T_2)e^{i\omega_n T_0} + \underline{A}(T_1,T_2)e^{-i\omega_n T_0}]]^2\,|_{s=0}$$
$$= k_2[\frac{\partial}{\partial s}\phi_n(s)]^2[A^2(T_1,T_2)e^{i2\omega_n T_0} + \underline{A}^2(T_1,T_2)e^{-2i\omega_n T_0} + 2A(T_1,T_2)\underline{A}(T_1,T_2)]$$

There is no $e^{\pm i\omega_n T_0}$ term, so boundary condition becomes

$$EI\frac{\partial^2}{\partial s^2}V_2(s,T_1,T_2)\,|_{s=0} = k_1\frac{\partial}{\partial s}V_2(s,T_1,T_2)\,|_{s=0}$$

Multiplying Equation (3.45) with $\phi_n(s)$ on both sides and integrate from 0 to *l*, we obtain

$$\int_0^l \phi_n(s)[-\omega_n^2 V_2(s,T_1,T_2) + \frac{EI}{\rho A}\frac{\partial^4 V_2(s,T_1,T_2)}{\partial s^4}]ds$$
$$= \int_0^l [-2i\omega_n \phi_n(s) D_1 A(T_1,T_2)\phi_n(s)]ds \tag{3.46}$$

$$\int_0^l \phi_n(s)\frac{\partial^4 V_2(s,T_1,T_2)}{\partial s^4}]ds = \int_0^l \frac{\partial^4 \phi_n(s)}{\partial s^4} V_2(s,T_1,T_2)]ds$$

Equation (3.46) becomes

$$\int_0^l [-\omega_n^2 V_2(s,T_1,T_2)\phi_n(s) + \frac{EI}{\rho A}\frac{\partial^4 \phi_n(s)}{\partial s^4} V_2(s,T_1,T_2)]]ds$$
$$= \int_0^l [-2i\omega_n \phi_n(s) D_1 A(T_1,T_2)\phi_n(s)]ds$$

$$\int_0^l V_2(s,T_1,T_2)[-\omega_n^2\phi_n(s) + \frac{EI}{\rho A}\frac{\partial^4 \phi_n(s)}{\partial s^4}]ds = \int_0^l [-2i\omega_n \phi_n(s) D_1 A(T_1,T_2)\phi_n(s)]ds$$

$$\int_0^l [-2i\omega_n \phi_n(s) D_1 A(T_1,T_2)\phi_n(s)]ds = 0$$

This leads to $D_1 A(T_1,T_2)$ =0 and $\upsilon_2(s,T_0,T_1,T_2) = 0$

$$D_0 D_1 \upsilon_2(s,T_0,T_1,T_2) = 0$$
$$D_1^2 \upsilon_1(s,T_0,T_1,T_2) = 0$$

Now consider the third order Equation (3.40)

We assume $\upsilon_3(s,T_0,T_1,T_2) = V_3(s,T_1,T_2)e^{i\omega_n T_0}$

We get

$$-\omega_n^2 V_3(s,T_1,T_2)e^{i\omega_n T_0} + \frac{EI}{\rho A}\frac{\partial^4 V_3(s,T_1,T_2)}{\partial s^4} e^{i\omega_n T_0}$$
$$= \frac{\overline{f}}{2}e^{i\Omega t} - 2i\omega_n \phi_n(s) D_2 A(T_2) e^{i\omega_n T_0} - 2\mu_1 i\omega_n \phi_n(s) A(T_2) e^{i\omega_n T_0}$$
$$-\frac{EI}{\rho A}\frac{\partial}{\partial s}\{\frac{\partial \phi_n(s)}{\partial s}\frac{\partial}{\partial s}[\frac{\phi_n(s)}{\partial s}\frac{\partial^2 \phi_n(s)}{\partial s^2}](A(T_2)^3 e^{i3\omega_n T_0} + 3A(T_2)^2 \underline{A}(T_2)e^{i\omega_n T_0}) \qquad (3.47)$$
$$+2\omega_n^2 \frac{\partial}{\partial s}\{\frac{\partial \phi_n(s)}{\partial s}\int_l^s \int_0^s [\frac{\partial \phi_n(s)}{\partial s}]^2 dsds\}(A(T_2)^3 e^{i3\omega_n T_0} + A(T_2)^2 \underline{A}(T_2)e^{i\omega_n T_0}) + cc$$
$$-\mu_2 \omega_n^2 \phi_n(s)(iA(T_2)e^{i\omega_n T_0} - i\underline{A}(T_2)e^{-i\omega_n T_0}) \,|\, \phi_n(s)[iA(T_2)e^{i\omega_n T_0} - i\underline{A}(T_2)e^{-i\omega_n T_0}]\,|$$

To express the nearness of excitation frequency Ω to natural frequency ω, we introduce the detuning parameter σ defined by.

$$\Omega = \omega_n + \varepsilon^2 \sigma \tag{3.48}$$

Then $\frac{\overline{f}}{2} e^{i\Omega t} = \frac{\overline{f}}{2} e^{iT_2} e^{i\omega_n T_0}$

We expand the quadratic damping term into Fourier series

$$\begin{aligned} &-\mu_2 \omega_n^2 (iA(T_2)e^{i\omega_n T_0} - i\underline{A}(T_2)e^{-i\omega_n T_0}) \,|\, iA(T_2)e^{i\omega_n T_0} - i\underline{A}(T_2)e^{-i\omega_n T_0} \,| = -\mu_2 \omega_n^2 \sum_{m=-\infty}^{\infty} g_m(T_2) e^{im\omega_n T_0} \\ &g_m(T_2) = \frac{\omega_n}{2\pi} \int_0^{2\pi/\omega_n} (iA(T_2)e^{i\omega_n T_0} - i\underline{A}(T_2)e^{-i\omega_n T_0}) \,|\, iA(T_2)e^{i\omega_n T_0} - i\underline{A}(T_2)e^{-i\omega_n T_0} \,| e^{-im\omega_n T_0} dT_0 \end{aligned} \tag{3.49}$$

$$\begin{aligned} g_m(T_2) &= \frac{1}{2\pi} \int_0^{2\pi} (iA(T_2)e^{i\omega_n T_0} - i\underline{A}(T_2)e^{-i\omega_n T_0}) \,|\, iA(T_2)e^{i\omega_n T_0} - i\underline{A}(T_2)e^{-i\omega_n T_0} \,| e^{-im\omega_n T_0} d\omega_n T_0 \\ &= \frac{1}{2\pi} \int_0^{2\pi} (iA(T_2)e^{i\theta} - i\underline{A}(T_2)e^{-i\theta}) \,|\, iA(T_2)e^{i\theta} - i\underline{A}(T_2)e^{-i\theta} \,| e^{-im\theta} d\theta, \qquad \theta = \omega_n T_0 \end{aligned}$$

We ignore the terms other than $e^{\pm i\omega_n T_0}$ terms

Equation (3.47) becomes

$$\begin{aligned} &-\omega_n^2 V_3(s,T_1,T_2) + \frac{EI}{\rho A} \frac{\partial^4 V_3(s,T_1,T_2)}{\partial s^4} = H \\ &H = \frac{\overline{f}}{2} e^{i\sigma T_2} - 2i\omega_n \phi_n(s)(D_2 A(T_2) + \mu_1 A(T_2)) - \mu_2 \omega_n^2 \phi_n(s) \,|\, \phi_n(s) \,|\, g_1(T_2) \\ &-[3\frac{EI}{\rho A}\frac{\partial}{\partial s}\{\frac{\partial \phi_n(s)}{\partial s}\frac{\partial}{\partial s}[\frac{\phi_n(s)}{\partial s}\frac{\partial^2 \phi_n(s)}{\partial s^2}] - 2\omega_n^2 \frac{\partial}{\partial s}\{\frac{\partial \phi_n(s)}{\partial s}\int_l^s \int_0^s [\frac{\partial \phi_n(s)}{\partial s}]^2 dsds\}]A(T_2)^2 \underline{A}(T_2) \end{aligned} \tag{3.50}$$

Note that satisfying Equation (3.50) automatically satisfies its complex conjugate.

Boundary conditions:

$$\upsilon_3(s,T_0,T_1,T_2)\,|_{s=0} = 0$$

$$EI \frac{\partial^2}{\partial s^2} \upsilon_3(s,T_0,T_1,T_2)\,|_{s=0} = k_1 \frac{\partial}{\partial s} \upsilon_3(s,T_0,T_1,T_2)\,|_{s=0} + k_3 [\frac{\partial}{\partial s} \upsilon_1(s,T_0,T_1,T_2)]^3\,|_{s=0}$$

$$\frac{\partial^2}{\partial s^2} \upsilon_3(s,T_0,T_1,T_2)\,|_{s=l} = 0$$

$$\frac{\partial^3}{\partial s^3}\upsilon_3(s,T_0,T_1,T_2)\,|_{s=l}=0$$

$$k_3[\frac{\partial}{\partial s}\upsilon_1(s,T_0,T_1,T_2)]^3\,|_{s=0}=k_3[\frac{\partial\phi_n(s)}{\partial s}]^3[A(T_2)e^{i\omega_n T_0}+\underline{A}(T_2)e^{-i\omega_n T_0}]^3$$
$$=k_3[\frac{\partial\phi_n(s)}{\partial s}]^3(A(T_2)^3e^{i3\omega_n T_0}+3A(T_2)^2\underline{A}(T_2)e^{i\omega_n T_0}+cc)$$

So

$$V_3(s,T_1,T_2)\,|_{s=0}=0$$

$$EI\frac{\partial^2}{\partial s^2}V_3(s,T_1,T_2)\,|_{s=0}=k_1\frac{\partial}{\partial s}V_3(s,T_1,T_2)\,|_{s=0}+k_3 3A(T_2)^2\underline{A}(T_2)[\frac{\partial\phi_n(s)}{\partial s}]^3\,|_{s=0}$$

$$\frac{\partial^2}{\partial s^2}V_3(s,T_1,T_2)\,|_{s=l}=0$$

$$\frac{\partial^3}{\partial s^3}V_3(s,T_1,T_2)\,|_{s=l}=0$$

Multiplying Equation (3.50) with $\phi_n(s)$ on both sides and integrate from 0 to *l*, we obtain

$$\int_0^l\phi_n(s)[-\omega_n^2V_3(s,T_1,T_2)+\frac{EI}{\rho A}\frac{\partial^4V_3(s,T_1,T_2)}{\partial s^4}]ds$$
$$=\int_0^l H\phi_n(s)ds \qquad (3.51)$$

$$\int_0^l\phi_n(s)\frac{\partial^4V_3(s,T_1,T_2)}{\partial s^4}]ds$$
$$=\phi_n(s)\frac{\partial^3V_3(s,T_1,T_2)}{\partial s^3}\,|_0^l-\int_0^l\frac{\partial\phi_n(s)}{\partial s}\frac{\partial^3V_3(s,T_1,T_2)}{\partial s^3}]ds$$
$$=\phi_n(s)\frac{\partial^3V_3(s,T_1,T_2)}{\partial s^3}\,|_0^l-\frac{\partial\phi_n(s)}{\partial s}\frac{\partial^2V_3(s,T_1,T_2)}{\partial s^2}\,|_0^l+\int_0^l\frac{\partial^2\phi_n(s)}{\partial s^2}\frac{\partial^2V_3(s,T_1,T_2)}{\partial s^2}]ds$$

$$= \phi_n(s)\frac{\partial^3 V_3(s,T_1,T_2)}{\partial s^3}\Big|_0^l - \frac{\partial \phi_n(s)}{\partial s}\frac{\partial^2 V_3(s,T_1,T_2)}{\partial s^2}\Big|_0^l +$$
$$\frac{\partial^2 \phi_n(s)}{\partial s^2}\frac{\partial V_3(s,T_1,T_2)}{\partial s}\Big|_0^l - \int_0^l \frac{\partial^3 \phi_n(s)}{\partial s^3}\frac{\partial V_3(s,T_1,T_2)}{\partial s}]ds$$
$$= \phi_n(s)\frac{\partial^3 V_3(s,T_1,T_2)}{\partial s^3}\Big|_0^l - \frac{\partial \phi_n(s)}{\partial s}\frac{\partial^2 V_3(s,T_1,T_2)}{\partial s^2}\Big|_0^l +$$
$$\frac{\partial^2 \phi_n(s)}{\partial s^2}\frac{\partial V_3(s,T_1,T_2)}{\partial s}\Big|_0^l - \frac{\partial^3 \phi_n(s)}{\partial s^3}V_3(s,T_1,T_2)\Big|_0^l + \int_0^l \frac{\partial^4 \phi_n(s)}{\partial s^4}V_3(s,T_1,T_2)]ds$$

$$= \phi_n(s)\frac{\partial^3 V_3(s,T_1,T_2)}{\partial s^3}\Big|_0^l - \frac{\partial \phi_n(s)}{\partial s}\frac{\partial^2 V_3(s,T_1,T_2)}{\partial s^2}\Big|_0^l +$$
$$\frac{\partial^2 \phi_n(s)}{\partial s^2}\frac{\partial V_3(s,T_1,T_2)}{\partial s}\Big|_0^l - \frac{\partial^3 \phi_n(s)}{\partial s^3}V_3(s,T_1,T_2)\Big|_0^l + \int_0^l \frac{\partial^4 \phi_n(s)}{\partial s^4}V_3(s,T_1,T_2)]ds$$
$$= 0 + \frac{\partial \phi_n(s)}{\partial s}\frac{\partial^2 V_3(s,T_1,T_2)}{\partial s^2}\Big|_{s=0} - \frac{\partial^2 \phi_n(s)}{\partial s^2}\frac{\partial V_3(s,T_1,T_2)}{\partial s}\Big|_{s=0}$$
$$-0 + \int_0^l \frac{\partial^4 \phi_n(s)}{\partial s^4}V_3(s,T_1,T_2)]ds$$

$$\frac{\partial^2}{\partial s^2}\phi_n(s,T_0,T_1,T_2)\Big|_{s=0} = \frac{k_1}{EI}\frac{\partial}{\partial s}\phi_n(s,T_0,T_1,T_2)\Big|_{s=0}$$
$$\frac{\partial^2}{\partial s^2}V_3(s,T_1,T_2)\Big|_{s=0} = \frac{k_1}{EI}\frac{\partial}{\partial s}V_3(s,T_1,T_2)\Big|_{s=0} + \frac{k_3}{EI}3A(T_2)^2\underline{A}(T_2)[\frac{\partial \phi_n(s)}{\partial s}]^3\Big|_{s=0}$$

$$\frac{\partial \phi_n(s)}{\partial s}\frac{\partial^2 V_3(s,T_1,T_2)}{\partial s^2}\Big|_{s=0} - \frac{\partial^2 \phi_n(s)}{\partial s^2}\frac{\partial V_3(s,T_1,T_2)}{\partial s}\Big|_{s=0}$$
$$= \frac{\partial \phi_n(s)}{\partial s}\frac{k_1}{EI}\frac{\partial}{\partial s}V_3(s,T_1,T_2)\Big|_{s=0} + \frac{\partial \phi_n(s)}{\partial s}\frac{k_3}{EI}3A(T_2)^2\underline{A}(T_2)[\frac{\partial \phi_n(s)}{\partial s}]^3\Big|_{s=0}$$
$$-\frac{k_1}{EI}\frac{\partial}{\partial s}\phi_n(s,T_0,T_1,T_2)\frac{\partial V_3(s,T_1,T_2)}{\partial s}\Big|_{s=0}$$
$$= \frac{k_3}{EI}3A(T_2)^2\underline{A}(T_2)[\frac{\partial \phi_n(s)}{\partial s}]^4\Big|_{s=0}$$

So we have:

$$\int_0^l \phi_n(s)\frac{\partial^4 V_3(s,T_1,T_2)}{\partial s^4}]ds = 3\frac{k_3}{EI}A(T_2)^2\underline{A}(T_2)[\frac{\partial \phi_n(s)}{\partial s}]^3\Big|_{s=0} + \int_0^l \frac{\partial^4 \phi_n(s)}{\partial s^4}V_3(s,T_1,T_2)]ds$$

Equation (3.51) becomes

$$\int_0^l [-\omega_n^2 V_3(s,T_1,T_2)\phi_n(s) + \frac{EI}{\rho A}\frac{\partial^4 \phi_n(s)}{\partial s^4} V_3(s,T_1,T_2)]]ds$$
$$= \int_0^l H\,\phi_n(s)ds - 3\frac{k_3}{EI} A(T_2)^2 \underline{A}(T_2)\frac{\partial \phi_n(s)}{\partial s}[\frac{\partial \phi_n(s)}{\partial s}]^3 \mid_{s=0} \tag{3.52}$$

Since

$$-\omega_n^2 \phi_n(s) + \frac{EI}{\rho A}\frac{\partial^4 \phi_n(s)}{\partial s^4} = 0$$

$$\int_0^l [-\omega_n^2 V_3(s,T_1,T_2)\phi_n(s) + \frac{EI}{\rho A}\frac{\partial^4 \phi_n(s)}{\partial s^4} V_3(s,T_1,T_2)]]ds =$$
$$\int_0^l V_3(s,T_1,T_2)[-\omega_n^2 \phi_n(s) + \frac{EI}{\rho A}\frac{\partial^4 \phi_n(s)}{\partial s^4}]ds = 0$$

Equation (3.52) becomes

$$\int_0^l H\,\phi_n(s)ds - 3\frac{k_3}{EI} A(T_2)^2 \underline{A}(T_2)[\frac{\partial \phi_n(s)}{\partial s}]^4 \mid_{s=0} = 0 \tag{3.53}$$

We define

$$\alpha_g = \frac{EI}{\rho A}\int_0^l \phi_n(s)\frac{\partial}{\partial s}\{\frac{\partial \phi_n(s)}{\partial s}\frac{\partial}{\partial s}[\frac{\phi_n(s)}{\partial s}\frac{\partial^2 \phi_n(s)}{\partial s^2}]ds$$

$$\alpha_i = \int_0^l \phi_n(s)\frac{\partial}{\partial s}\{\frac{\partial \phi_n(s)}{\partial s}\int_l^s \int_0^s [\frac{\partial \phi_n(s)}{\partial s}]^2 dsds\}ds$$

$$\alpha = 3\alpha_g - 2\omega_n^2 \alpha_i + 3\frac{k_3}{EI}[\frac{\partial \phi_n(0)}{\partial s}]^4$$

$$\alpha_d = \int_0^l \phi_n^2(s) \mid \phi_n(s) \mid ds$$

$$f = \overline{f}\int_0^l \phi_n(s)ds$$

Equation (3.53) becomes

$$\frac{f}{2}e^{i\sigma T_2} - 2i\omega_n(D_2 A(T_2) + \mu_1 A(T_2)) - \mu_2 \omega_n^2 \alpha_d g_1(T_2) - \alpha A(T_2)^2 \underline{A}(T_2) = 0 \tag{3.54}$$

Using the polar form of $A = \frac{a(T_2)}{2} e^{i\beta(T_2)}$

$$g_1(T_2) = \frac{1}{8\pi} \int_0^{2\pi} (ia(T_2)e^{i(\beta(T_2)+\theta)} - ia(T_2)e^{-i(\beta(T_2)+\theta)}) \mid ia(T_2)e^{i(\beta(T_2)+\theta)} - ia(T_2)e^{-i(\beta(T_2)+\theta)} \mid e^{-i\theta} d\theta$$

$$= \frac{1}{8\pi} a(T_2)^2 e^{i\beta} \int_0^{2\pi} (ie^{i(\beta(T_2)+\theta)} - ie^{-i(\beta(T_2)+\theta)}) \mid ie^{i(\beta(T_2)+\theta)} - ie^{-i(\beta(T_2)+\theta)} \mid e^{-i(\theta+\beta(T_2))} d\theta$$

$$= \frac{1}{8\pi} a(T_2)^2 e^{i\beta(T_2)} \int_0^{2\pi} (-2\sin(\beta(T_2)+\theta)) \mid 2\sin(\beta(T_2)+\theta) \mid e^{-i(\theta+\beta(T_2))} d\theta$$

$$= \frac{-1}{2\pi} a(T_2)^2 e^{i\beta(T_2)} \int_0^{2\pi} \sin x \mid \sin x \mid e^{-ix} dx$$

$$-\int_0^{2\pi} i \sin x \sin x \mid \sin x \mid dx = -2i \int_0^{\pi} \sin^2 x \sin x dx = -2i \int_0^{\pi} (\cos^2 x - 1) d\cos x$$

$$= -2i \int_{-1}^{1} (1 - y^2) dy = -\frac{8}{3} i$$

$$\int_0^{2\pi} \sin x \cos x \mid \sin x \mid dx = \int_0^{\pi} \sin^2 x \cos x dx - \int_{2\pi}^{\pi} \sin^2 (2\pi - x) \cos(2\pi - x) d(2\pi - x)$$

$$= \int_0^{\pi} \sin^2 x \cos x dx - \int_0^{\pi} \sin^2 y \cos y dy = 0$$

So

$$g_1(T_2) = \frac{4i}{3\pi} a(T_2)^2 e^{i\beta(T_2)} \tag{3.55}$$

Equation (3.54) becomes

$$\begin{aligned} &\frac{f}{2} e^{i\sigma T_2} - i\omega_n \left(\left(\frac{da(T_2)}{dT_2} + ia(T_2) \frac{d\beta(T_2)}{dT_2} \right) e^{i\beta(T_2)} + \mu_1 a(T_2) e^{i\beta(T_2)} \right) \\ &- \frac{\alpha}{8} a(T_2)^3 e^{i\beta(T_2)} - \mu_2 \alpha_d \omega_n^2 \frac{4i}{3\pi} a(T_2)^2 e^{i\beta(T_2)} = 0 \end{aligned} \tag{3.56}$$

Divide both sides of Equation (3.56) by $e^{i\beta(T_2)}$ we get

$$\frac{f}{2}e^{i(\sigma T_2-\beta(T_2))}-i\omega_n(\frac{da(T_2)}{dT_2}+ia(T_2)\frac{d\beta(T_2)}{dT_2}+\mu_1 a(T_2))$$
$$-\frac{\alpha}{8}a(T_2)^3-\mu_2\alpha_d\omega_n^2\frac{4i}{3\pi}a(T_2)^2=0$$

We define $\gamma(T_2)=\sigma T_2-\beta(T_2)$ then

$$\beta(T_2)=\sigma T_2-\gamma(T_2)$$
$$\frac{d\beta(T_2)}{dT_2}=\sigma-\frac{d\gamma(T_2)}{dT_2}$$

Equation (3.56) becomes

$$\frac{f}{2}e^{i\gamma(T_2)}-i\omega_n\{\frac{da(T_2)}{dT_2}+ia(T_2)[\sigma-\frac{d\gamma(T_2)}{dT_2}]+\mu_1 a(T_2)\}$$
$$-\frac{\alpha}{8}a(T_2)^3-\mu_2\alpha_d\omega_n^2\frac{4i}{3\pi}a(T_2)^2=0 \qquad (3.57)$$

Separating real and imaginary parts, we obtain:

$$\frac{da(T_2)}{dT_2}=-\mu_1 a(T_2)-\mu_2\alpha_d\frac{4\omega_n}{3\pi}a(T_2)^2+\frac{f}{2\omega_n}\sin\gamma(T_2)$$
$$a(T_2)\frac{d\gamma(T_2)}{dT_2}=\sigma a(T_2)-\frac{\alpha a(T_2)^3}{8\omega_n}+\frac{f}{2\omega_n}\cos\gamma(T_2) \qquad (3.58)$$

So the beam response is given by

$$\upsilon(s,t)=\varepsilon\upsilon_1(s,t)=\varepsilon\phi_n(s)\frac{a(T_2)}{2}e^{i\beta(T_2)}e^{i\omega_n t}$$

$$A(T_2)=\frac{a(T_2)}{2}e^{i\beta(T_2)}$$

$$\Omega=\omega_n+\varepsilon^2\sigma\Rightarrow\omega_n=\Omega-\varepsilon^2\sigma$$

$$\upsilon(s,t)=\varepsilon a(T_2)\cos(\Omega t-\gamma(T_2))\phi(s)$$

When the response is steady, $\frac{da(T_2)}{dT_2}=0,\quad \frac{d\gamma(T_2)}{dT_2}=0$

we get

$$-\mu_1 a - \mu_2 \alpha_d \frac{4\omega_n}{3\pi} a^2 + \frac{f}{2\omega_n}\sin\gamma = 0$$

$$\sigma a - \frac{\alpha a^3}{8\omega_n} + \frac{f}{2\omega_n}\cos\gamma = 0$$

$$\frac{f}{2\omega_n}\sin\gamma = \mu_1 a + \mu_2 \alpha_d \frac{4\omega_n}{3\pi} a^2$$

$$\frac{f}{2\omega_n}\cos\gamma = -\sigma a + \frac{\alpha a^3}{8\omega_n}$$

Square and add the two equations above, we get

$$\left(\frac{f}{2\omega_n}\right)^2 = \left(\mu_1 a + \mu_2 \alpha_d \frac{4\omega_n}{3\pi} a^2\right)^2 + \left(\sigma a - \frac{\alpha a^3}{8\omega_n}\right)^2 \tag{3.59}$$

$$\begin{aligned} f &= 2\omega_n a \sqrt{\left(\mu_1 + \mu_2 \alpha_d \frac{4\omega_n}{3\pi} a\right)^2 + \left(\sigma - \frac{\alpha a^2}{8\omega_n}\right)^2} \\ \sigma &= \frac{\alpha a^2}{8\omega_n} \pm \sqrt{\frac{f^2}{4\omega_n^2 a^2} - \left(\mu_1 + \mu_2 \alpha_d \frac{4\omega_n}{3\pi} a\right)^2} \end{aligned} \tag{3.60}$$

Equation (3.60) agrees with equations (3.24) and (3.25) in Ref. [218].

If we define the amplitude of q_n as $\bar{q}_n$ after the response is stable

$$q_n = \bar{q}_n \cos(\Omega t - \gamma) = \varepsilon a \cos(\Omega t - \gamma)$$

then

$$\bar{q}_n = \varepsilon a \quad \Rightarrow \quad a = \frac{\bar{q}_n}{\varepsilon}$$

By definition we have

$$\begin{aligned} a &= \frac{\bar{q}_n}{\varepsilon} & \mu_1 &= \frac{\bar{\mu}_1}{\varepsilon^2} \\ \mu_2 &= \frac{\bar{\mu}_2}{\varepsilon} & f &= \frac{\bar{f}}{\varepsilon^3} \\ \sigma &= \frac{\Omega - \omega_n}{\varepsilon^2} \end{aligned} \tag{3.61}$$

Substitute Equation (3.61) into Equation (3.60)

we have

$$\begin{aligned} \bar{f} &= 2\omega_n \bar{q}_n \sqrt{(\bar{\mu}_1 + \bar{\mu}_2 \alpha_d \frac{4\omega_n}{3\pi} \bar{q}_n)^2 + (\Omega - \omega_n - \frac{\alpha \bar{q}_n^{\,2}}{8\omega_n})^2} \\ \Omega - \omega_n &= \frac{\alpha \bar{q}_n^{\,2}}{8\omega_n} \pm \sqrt{\frac{\bar{f}^2}{4\omega_n^2 \bar{q}_n^{\,2}} - (\bar{\mu}_1 + \bar{\mu}_2 \alpha_d \frac{4\omega_n}{3\pi} \bar{q}_n)^2} \end{aligned} \tag{3.62}$$

3.3 VISCOELASTIC DAMPING AND VISCOUS DAMPING

3.3.1 Linear Beam Model with Viscoelastic Damping and Viscous Damping

The governing equation of linear cantilever beam is

$$\rho A \ddot{\upsilon} + c_\upsilon \dot{\upsilon} + EI\upsilon'''' = \rho A a_b \cos \Omega t \tag{3.63}$$

And the boundary conditions are

$$\upsilon(0,t) = 0, \qquad \upsilon'(0,t) = 0$$
$$\upsilon''(l,t) = 0, \qquad \upsilon'''(l,t) = 0$$

where ρ is the material density of beam and A is cross section area, l is the beam length, E is Young's modulus, I is the area moment of inertia, s is the arc length, t is time, $\upsilon(s,t)$ is the transverse displacement, a_b is the acceleration of the supported end of the beam, c_υ is the coefficient of linear viscous damping per unit length, and Ω is the excitation frequency. And, the prime indicates differentiation with respect to the arc length s, whereas the overdot indicates differentiation with respect to time t.

Apply elastic-viscoelastic correspondence principal, Equation (3.63) becomes

$$\rho A \ddot{\upsilon} + c_\upsilon \dot{\upsilon} + EI(1 + \eta i)\upsilon'''' = \rho A a_b e^{i\Omega t} \tag{3.64}$$

where i is imaginary symbol, η is the loss factor.

Assume:

$$\upsilon(s,t) = \sum_{n=1}^{\infty} \phi_n(s) q_n(t)$$

here we only consider one mode vibration, so

$$\upsilon(s,t) = \phi(s) q(t)$$

Substitute it into Equation (3.63), times $\phi(s)$ on both sides then integrate from 0 to *l*, we get

$$\ddot{q} + 2\xi\omega\dot{q} + \omega^2(1+i\eta)q = F_0 e^{i\Omega t} \tag{3.65}$$

where

$$\omega^2 = \frac{EI}{\rho A},\ 2\omega\xi = \frac{c_\upsilon}{\rho A},\ F_0 = a_b \int_0^l \phi(s) ds$$

For the steady-state solution we assume

$$q = \bar{Q}(\Omega) e^{i\Omega t}$$

Substitute it into Equation (3.65), we get

$$\frac{\left|\bar{Q}(\Omega)\right|}{F_0/\omega^2} = \frac{1}{\sqrt{(1-\frac{\Omega^2}{\omega^2})^2 + (2\xi\frac{\Omega}{\omega} + \eta)^2}} \tag{3.66}$$

From the Equation (3.66), it shows that the viscous damping tilts the frequency response curve and influences the peak frequency. However, these effects are very small within narrow frequency range for a single mode response.

3.3.2 Inextensible Beam Model with Viscoelastic Damping and Viscous Damping

From Equation (3.27), ignoring the nonlinear viscoelastic term, we have

$$\rho A\frac{\partial^2 \upsilon(s,t)}{\partial t^2}+c_\upsilon\frac{\partial}{\partial t}\upsilon(s,t)+\overline{c}\frac{\partial}{\partial t}\upsilon(s,t)|\frac{\partial}{\partial t}\upsilon(s,t)|+EI\frac{\partial^4\upsilon(s,t)}{\partial s^4}+E^*I\frac{\partial^5\upsilon(s,t)}{\partial t\partial s^4}$$
$$=\rho Aa_b\cos\Omega t-EI\frac{\partial}{\partial s}\{\frac{\partial\upsilon(s,t)}{\partial s}\frac{\partial}{\partial s}[\frac{\partial\upsilon(s,t)}{\partial s}\frac{\partial^2\upsilon(s,t)}{\partial s^2}]\} \tag{3.67}$$
$$-\frac{1}{2}\rho A\frac{\partial}{\partial s}\{\frac{\partial\upsilon(s,t)}{\partial s}\int_l^s\frac{\partial^2}{\partial t^2}\int_0^s[\frac{\partial\upsilon(s,t)}{\partial s}]^2dsds\}$$

It is convenient to introduce the complex young's modulus to study the frequency response of the system. Equation (3.67) becomes

$$\rho A\frac{\partial^2 \upsilon(s,t)}{\partial t^2}+c_\upsilon\frac{\partial}{\partial t}\upsilon(s,t)+\overline{c}\frac{\partial}{\partial t}\upsilon(s,t)|\frac{\partial}{\partial t}\upsilon(s,t)|+EI(1+\overline{\eta}i)\frac{\partial^4\upsilon(s,t)}{\partial s^4}$$
$$=\rho Aa_be^{i\Omega t}-EI\frac{\partial}{\partial s}\{\frac{\partial\upsilon(s,t)}{\partial s}\frac{\partial}{\partial s}[\frac{\partial\upsilon(s,t)}{\partial s}\frac{\partial^2\upsilon(s,t)}{\partial s^2}]\} \tag{3.68}$$
$$-\frac{1}{2}\rho A\frac{\partial}{\partial s}\{\frac{\partial\upsilon(s,t)}{\partial s}\int_l^s\frac{\partial^2}{\partial t^2}\int_0^s[\frac{\partial\upsilon(s,t)}{\partial s}]^2dsds\}$$

where i is imaginary symbol, $\overline{\eta}=\frac{E^*}{E}$ is the loss factor.

Assume:

$$\upsilon(s,t)=\sum_{n=1}^{\infty}\phi_n(s)q_n(t)$$

Here we only consider one mode vibration, so

$$\upsilon(s,t)=\phi(s)q(t)$$

Substitute it into Equation (3.68), times $\phi(s)$ on both sides then integrate from 0 to *l*, we get

$$\ddot{q}+2\overline{\mu}_1\dot{q}+\overline{\mu}_2\dot{q}|\dot{q}|+\omega^2(1+\overline{\eta}i)q=\overline{f}e^{i\Omega t}-\overline{\alpha}_gq^3-\alpha_i(q\dot{q}^2+q^2\ddot{q}) \tag{3.69}$$

where

$$\overline{\mu}_1 = \omega\zeta = \frac{c_v}{2\rho A} \qquad \overline{\mu}_2 = \hat{c}\int_0^l \phi^2 \mid \phi \mid ds$$

$$\overline{f} = a_b \int_0^l \rho A \phi ds$$

$$\overline{\alpha}_g = 2EI\int_0^l \phi'^2 \phi''^2 ds$$

$$\alpha_i = \rho A \int_0^l (\int_0^s \phi'^2 ds)^2 ds$$

The overdot indicates differentiation with respect to time *t*.

We scale the nonlinearity and response as following:

$$q = \varepsilon q_1 + \varepsilon^3 q_3$$
$$\overline{\mu}_1 = \varepsilon^2 \mu_1$$
$$\overline{\eta} = \varepsilon^2 \eta$$
$$\overline{\mu}_2 = \varepsilon \mu_2$$
$$\overline{f} = \varepsilon^3 f$$

Apply the method of multiple scales, which assume response *q* can be expressed as the function of slow time $T_0 = t$ and faster time $T_1 = \varepsilon t \quad T_2 = \varepsilon^2 t \quad \cdots$

Here we only consider one faster time $T_2 = \varepsilon^2 t$ and slow time $T_0 = t$

$$\frac{d}{dt} = D_0 + \varepsilon^2 D_2$$
$$\frac{d^2}{dt^2} = D_0^2 + 2\varepsilon^2 D_0 D_2 + \varepsilon^4 D_2^2$$

Substitute them into Equation (3.65), we get

Order ε: $D_0^2 q_1 + \omega^2 q_1 = 0$ (3.70)

Order ε^3:
$$D_0^2 q_3 + \omega^2 q_3 = fe^{i\Omega t} - 2D_0 D_2 q_1 - 2\mu_1 D_0 q_1 - \mu_2 D_0 q_1 \mid D_0 q_1 \mid - \alpha_g q_1^3 - i\omega^2 \eta q_1 - \frac{\alpha_i}{2}[q_1 D_0^2 q_1^2] \quad (3.71)$$

Since Equation (3.69) has complex term, we cannot express the solution from Equation (3.70) as

$$q_1 = A(T_2)e^{i\omega T_0} + \overline{A}(T_2)e^{-i\omega T_0}$$

Which is the key element of the perturbation dealing with this kind of high order terms.

We notice that the viscoelastic damping can be found an equivalent viscous damping term for linear cases.

If we ignore all nonlinear terms in Equation (3.69-3.71)

We have

$$\ddot{q} + 2\overline{\mu}_1\dot{q} + \omega^2(1 + i\overline{\eta})q = \overline{f}e^{i\Omega t} \tag{3.72}$$

$$D_0^2 q_1 + \omega^2 q_1 = 0 \tag{3.73}$$

$$D_0^2 q_3 + \omega^2 q_3 = fe^{i\Omega t} - 2D_0 D_2 q_1 - 2\mu_1 D_0 q_1 - i\omega^2 \eta q_1 \tag{3.74}$$

From Equation (3.69) we have

$$q_1 = A(T_2)e^{i\omega T_0}$$

Substitute it into Equation (3.70) get

$$D_0^2 q_3 + \omega^2 q_3 = fe^{i\Omega t} - 2i\omega A' e^{i\omega T_0} - 2\mu_1 i\omega A e^{i\omega T_0} - i\omega^2 \eta A e^{i\omega T_0} \tag{3.75}$$

We can combine the viscoelastic damping term $-i\omega^2\eta Ae^{i\omega T_0}$ and viscous damping term $-2\mu_1 i\omega Ae^{i\omega T_0}$ as

$$-i\omega(2\mu_1 - \omega\eta)Ae^{i\omega T_0} = -i\omega(2\xi\omega - \omega\eta)Ae^{i\omega T_0} = -i\omega 2u_e Ae^{i\omega T_0}$$

Where

$$u_e = \omega(\xi + \frac{\eta}{2})$$

If we study the Equation (3.71) and following perturbation procedure, we can find the nonlinear terms will not interfere with the linear damping. Hence it is valid to use the equivalent damping $u_e = \omega(\xi + \frac{\eta}{2})$ to get the perturbation solution of Equation (3.69).

3.4 HARMONIC BALANCE METHOD FOR LINEAR AND NON-LINEAR DAMPING MODEL

The governing equation for nonlinear cantilever beam (assume linear damping)

$$\ddot{q} + 2\xi\omega\dot{q} + \mu_2\dot{q}\,|\dot{q}| + \omega^2 q = \overline{f}\cos\Omega t - \overline{\alpha}_g q^3 - \alpha_i(q\dot{q}^2 + q^2\ddot{q}) \tag{3.77}$$

$$\overline{\mu}_2 = \overline{c}\int_0^l \phi^2\,|\phi|\,ds$$

$$\overline{f} = a_b\int_0^l \rho A\phi ds$$

$$\alpha_g = 2EI\int_0^l \phi'^2\phi''^2 ds$$

$$\alpha_i = \rho A\int_0^l (\int_0^s \phi'^2 ds)^2 ds$$

Let $\tau = \omega t$

$$\frac{dq}{dt} = \frac{dq}{d\tau}\frac{d\tau}{dt} = \omega\frac{dq}{d\tau}$$

$$\frac{d^2q}{dt^2} = \omega^2\frac{d^2q}{d\tau^2}$$

Equation (3.77) becomes

$$\ddot{q} + 2\xi\dot{q} + \mu_2\dot{q}\,|\dot{q}| + q + \alpha_g q^3 + \alpha_i(q\dot{q}^2 + q^2\ddot{q}) = f\cos r\tau \tag{3.78}$$

Where

$$\alpha_g = \frac{\overline{\alpha}_g}{\omega^2} \quad f = \frac{\overline{f}}{\omega^2} \quad r = \frac{\Omega}{\omega} \quad \mu_2 = \frac{\overline{\mu}_2}{\omega^2}$$

Overdot denotes differentiate respect to τ

Let us first consider a harmonic steady state solution with no transient part.

$$q_0 = a\sin r\tau + b\cos r\tau = Ae^{ir\tau} + \overline{A}e^{-ir\tau}$$

$$A = \frac{X}{2}e^{i\beta} \qquad X^2 = a^2 + b^2 \qquad \beta = \tan^{-1}\frac{-a}{b} \tag{3.79}$$

$$\mu_2\dot{q}_0\,|\dot{q}_0| = \mu_2 r^2(iAe^{ir\tau} - i\overline{A}e^{-ir\tau})\,|iAe^{ir\tau} - i\overline{A}e^{-ir\tau}| = \mu_2 r^2\sum_{n=-\infty}^{\infty} g_n e^{inr\tau}$$

$$
\begin{aligned}
g_n &= \frac{r}{2\pi}\int_0^{2\pi/r}(iAe^{ir\tau}-i\bar{A}e^{-ir\tau})\,|\,iAe^{ir\tau}-i\bar{A}e^{-ir\tau}\,|e^{-inr\tau}d\tau \\
&= \frac{1}{2\pi}\int_0^{2\pi}(iAe^{i\theta}-i\bar{A}e^{-i\theta})\,|\,iAe^{i\theta}-i\bar{A}e^{-i\theta}\,|e^{-in\theta}d\theta \\
&= \frac{1}{2\pi}\frac{X^2}{4}\int_0^{2\pi}(ie^{i\theta+i\beta}-ie^{-i\theta-i\beta})\,|\,ie^{i\theta+i\beta}-ie^{-i\theta-i\beta}\,|e^{-in\theta}d\theta \\
&= \frac{1}{2\pi}\frac{X^2}{4}e^{in\beta}\int_0^{2\pi}(ie^{ix}-ie^{-ix})\,|\,ie^{ix}-ie^{-ix}\,|e^{-inx}dx \\
&= -\frac{1}{2\pi}X^2e^{in\beta}\int_0^{2\pi}\sin x\,|\sin x\,|e^{-inx}dx
\end{aligned}
\tag{3.80}
$$

Since we only consider the primary resonance, $g_1e^{ir\tau}$ and $g_{-1}e^{-ir\tau}$ are the determining terms.

$$
\begin{aligned}
g_1 &= -\frac{1}{2\pi}X^2e^{i\beta}\int_0^{2\pi}\sin x\,|\sin x\,|e^{-ix}dx \\
&= \frac{4i}{3\pi}X^2e^{i\beta} \\
g_1e^{ir\tau}+g_{-1}e^{-ir\tau} &= \frac{4i}{3\pi}X^2e^{i(r\tau+\beta)}-\frac{4i}{3\pi}X^2e^{-i(r\tau+\beta)} = \frac{-8}{3\pi}X^2\sin(r\tau+\beta) \\
&= \frac{-8}{3\pi}X^2(\sin r\tau\cos\beta+\cos r\tau\sin\beta) \\
&= \frac{-8}{3\pi}X(b\sin r\tau-a\cos r\tau)
\end{aligned}
\tag{3.81}
$$

Use the following triangle relationship:

$$
\begin{aligned}
\cos^3 r\tau &= \cos^2 r\tau\cos r\tau = \frac{1+\cos 2r\tau}{2}\cos r\tau = \frac{1}{2}\cos r\tau+\frac{1}{2}\cos 2r\tau\cos r\tau \\
&= \frac{1}{2}\cos r\tau+\frac{1}{4}\cos 3r\tau+\frac{1}{4}\cos r\tau = \frac{3}{4}\cos r\tau+\frac{1}{4}\cos 3r\tau \\
\sin^3 r\tau &= \sin^2 r\tau\sin r\tau = \frac{1-\cos 2r\tau}{2}\sin r\tau = \frac{1}{2}\sin r\tau-\frac{1}{2}\sin r\tau\cos 2r\tau \\
&= \frac{1}{2}\sin r\tau-\frac{1}{4}(\sin 3r\tau-\sin r\tau) = \frac{3}{4}\sin r\tau-\frac{1}{4}\sin 3r\tau
\end{aligned}
\tag{3.82}
$$

$$\begin{aligned}
\sin r\tau\cos^2 r\tau &= \frac{1+\cos 2r\tau}{2}\sin r\tau = \frac{1}{2}\sin r\tau + \frac{1}{2}\cos 2r\tau\sin r\tau \\
&= \frac{1}{2}\sin r\tau + \frac{1}{4}\sin 3r\tau - \frac{1}{4}\sin r\tau = \frac{1}{4}\sin r\tau + \frac{1}{4}\sin 3r\tau \\
\sin^2 r\tau\cos r\tau &= \frac{1-\cos 2r\tau}{2}\cos r\tau = \frac{1}{2}\cos r\tau - \frac{1}{2}\cos r\tau\cos 2r\tau \\
&= \frac{1}{2}\cos r\tau - \frac{1}{4}(\cos 3r\tau + \cos r\tau) = \frac{1}{4}\cos r\tau - \frac{1}{4}\cos 3r\tau
\end{aligned} \tag{3.83}$$

$$\begin{aligned}
&q_0\dot{q}_0^2 + q_0^2\ddot{q}_0 = r^2(a\sin r\tau + b\cos r\tau)(a\cos r\tau - b\sin r\tau)^2 - r^2(a\sin r\tau + b\cos r\tau)^3 \\
&(a\sin r\tau + b\cos r\tau)(a\cos r\tau - b\sin r\tau)^2 \\
&= (a\sin r\tau + b\cos r\tau)(a^2\cos^2 r\tau + b^2\sin^2 r\tau - 2ab\sin r\tau\cos r\tau)^2 \\
&= a^3\sin r\tau\cos^2 r\tau + ab^2\sin^3 r\tau - 2a^2b\sin^2 r\tau\cos r\tau \\
&+ b^3\sin^2 r\tau\cos r\tau + a^2b\cos^3 r\tau - 2ab^2\sin r\tau\cos^2 r\tau \\
&= ab^2\sin^3 r\tau + a^2b\cos^3 r\tau + (b^3 - 2a^2b)\sin^2 r\tau\cos r\tau + (a^3 - 2ab^2)\sin r\tau\cos^2 r\tau
\end{aligned} \tag{3.84}$$

Substituting Equation (3.79) into Equation (3.78), using the results of Equation (3.80)-(3.84) we get

$$\begin{aligned}
&-r^2 a\sin r\tau - r^2 b\cos r\tau + 2\xi ar\cos r\tau - 2\xi br\sin r\tau \\
&-\frac{8}{3\pi}X\mu_2 r^2 b\sin r\tau + \frac{8}{3\pi}X\mu_2 r^2 a\cos r\tau + a\sin r\tau + b\cos r\tau \\
&+[(\alpha_g - r^2\alpha_i)a^3 + r^2\alpha_i ab^2](\frac{3}{4}\sin r\tau - \frac{1}{4}\sin 3r\tau) \\
&+[(\alpha_g - r^2\alpha_i)b^3 + r^2\alpha_i a^2 b](\frac{3}{4}\cos r\tau + \frac{1}{4}\cos 3r\tau) \\
&+[3(\alpha_g - r^2\alpha_i)a^2 b + r^2\alpha_i(b^3 - 2a^2 b)](\frac{1}{4}\cos r\tau - \frac{1}{4}\cos 3r\tau) \\
&+[3(\alpha_g - r^2\alpha_i)ab^2 + r^2\alpha_i(a^3 - 2ab^2)](\frac{1}{4}\sin r\tau + \frac{1}{4}\sin 3r\tau) = f\cos r\tau
\end{aligned} \tag{3.85}$$

We now separate the $\sin r\tau$ and $\cos r\tau$ terms to obtain

$$
\begin{aligned}
&-r^2 a - 2\xi b r - \frac{8}{3\pi} X \mu_2 r^2 b + a \\
&\quad + \frac{3}{4}[(\alpha_g - r^2\alpha_i)a^3 + r^2\alpha_i a b^2] + \frac{1}{4}[3(\alpha_g - r^2\alpha_i)ab^2 + r^2\alpha_i(a^3 - 2ab^2)] = 0 \\
&-r^2 b + 2\xi a r + \frac{8}{3\pi} X \mu_2 r^2 a + b \\
&\quad + \frac{3}{4}[(\alpha_g - r^2\alpha_i)b^3 + r^2\alpha_i a^2 b] + \frac{1}{4}[3(\alpha_g - r^2\alpha_i)a^2 b + r^2\alpha_i(b^3 - 2a^2 b)] = f
\end{aligned}
\tag{3.86}
$$

Let us define

$$
\begin{aligned}
&A = r^2 - 1 - \frac{1}{4}(3\alpha_g - 2r^2\alpha_i)X^2 \\
&X^2 = a^2 + b^2
\end{aligned}
\tag{3.87}
$$

Then Equation (3.86) becomes

$$
\begin{aligned}
&Aa + 2r\xi b + \frac{8}{3\pi} X \mu_2 r^2 b = 0 \\
&2r\xi a + \frac{8}{3\pi} X \mu_2 r^2 a - Ab = f
\end{aligned}
\tag{3.88}
$$

Squaring and adding both sides in Equations (3.88) we get

$$
[A^2 + (2r\xi + \frac{8}{3\pi} X \mu_2 r^2)^2]X^2 = f^2 \tag{3.89}
$$

It should be noted that *A* is a function of *X*. In obtaining the solution for Equation (3.78), we balance the harmonic terms and ignored the higher harmonics. Hence this method is called Harmonic Balance Procedure. For free vibrations, $f = 0$ and hence

$$
(A^2 + (2r\xi + \frac{8}{3\pi} X \mu_2 r^2)^2) = 0 \quad or \quad X^2 = 0 \tag{3.90}
$$

For force vibration,

$$
\begin{aligned}
&\frac{9}{16}(\alpha_g - \frac{2}{3}r^2\alpha_i)^2 X^6 + [\frac{3}{2}(\alpha_g - \frac{2}{3}r^2\alpha_i)(1 - r^2) + (\frac{8}{3\pi}\mu_2 r^2)^2]X^4 \\
&\quad + \frac{32}{3\pi}\xi\mu_2 r^3 X^3 + [r^4 - 2r^2(1 - 2\xi^2) + 1]X^2 - f^2 = 0
\end{aligned}
\tag{3.91}
$$

For the cantilever beam subjected to force provided by PZT excitation,

$$
\ddot{q} + 2\xi\dot{q} + \mu_2\dot{q}\,|\,\dot{q}\,| + q + \alpha_g q^3 + \alpha_i(q\dot{q}^2 + q^2\ddot{q}) = f\cos r\tau \tag{3.92}
$$

$$
\begin{aligned}
&f = \frac{bU}{\omega^2} = \frac{\chi[\phi_n'(x_2) - \phi_n'(x_1)]}{\omega^2}U \\
&\chi = E_a b(t_a + t_b)d_{31}
\end{aligned}
$$

Here $\int_0^l \rho A \phi_n^2(x)dx = 1$, $\boldsymbol{U}$ is the input voltage aptitude.

The results obtained by solving Equation (3.91) are compared with those obtained in with Equations (3.62) and are shown in Figure 3.2(a), (b) and (c) for moderate damping, large amplitude motions and for light damping respectively. Parameters used in calculation for Figure 3.2(a) are $E = 207GPa$, $\rho = 7810kg.m^{-3}$, $t = 0.79375mm$, $b = 12.7mm$, $l = 485.14mm$, $a_b = 0.216g$, $\xi = 6.262*10^{-4}$, $\mu_2 = 5.1759$, $\alpha_i = 1.1078*10^5$, $\alpha_g = 7.6836*10^3$. In large amplitude motions case, Figure 3.2(b), we use same parameters as those used in moderate damping case except $a_b = 2.16g$. In light damping case, Figure 3.2(c), we use same parameters as those used in moderate damping case except $\xi = 6.262*10^{-5}$ and $\mu_2 = 0.51759$. It can be seen that the results obtained using Harmonic Balance Method and the Multiple Scale Method are very close. At large amplitudes, small differences in results can be seen in Figure 3.2(b) and 3.2(c) due to different approximate methods used in respective analyses.

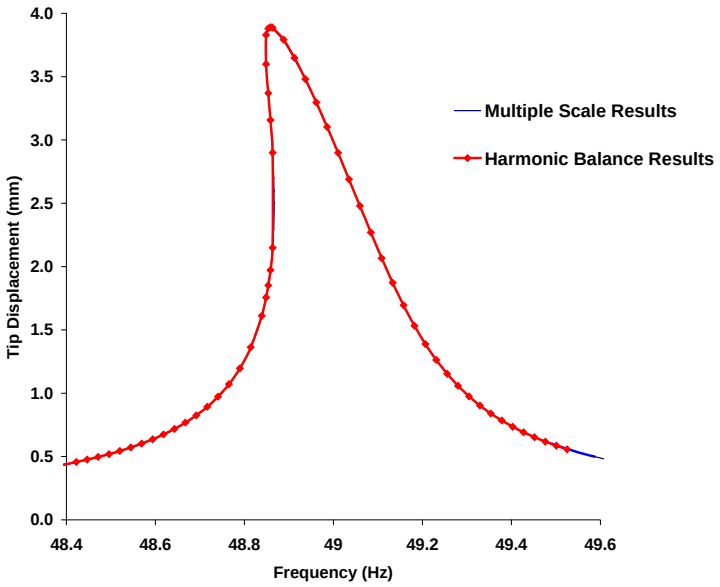

(a) moderate damping case

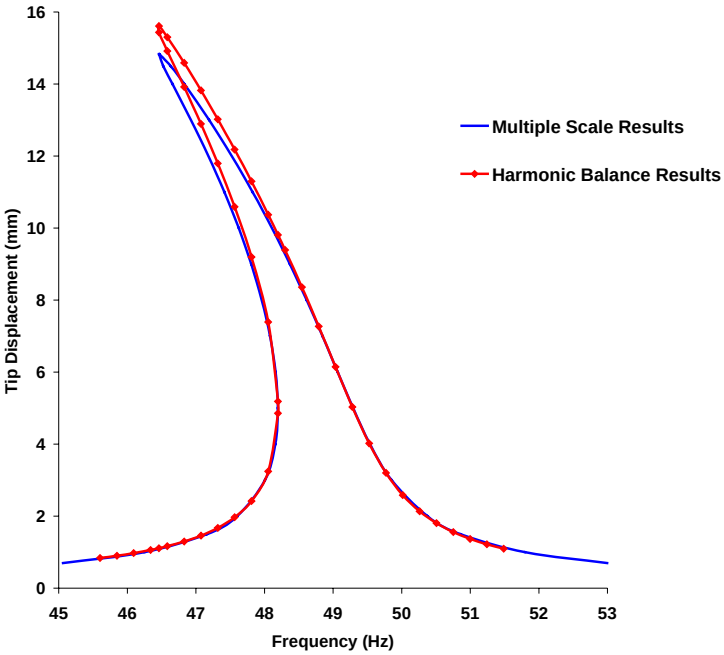

(b) large amplitude motions case

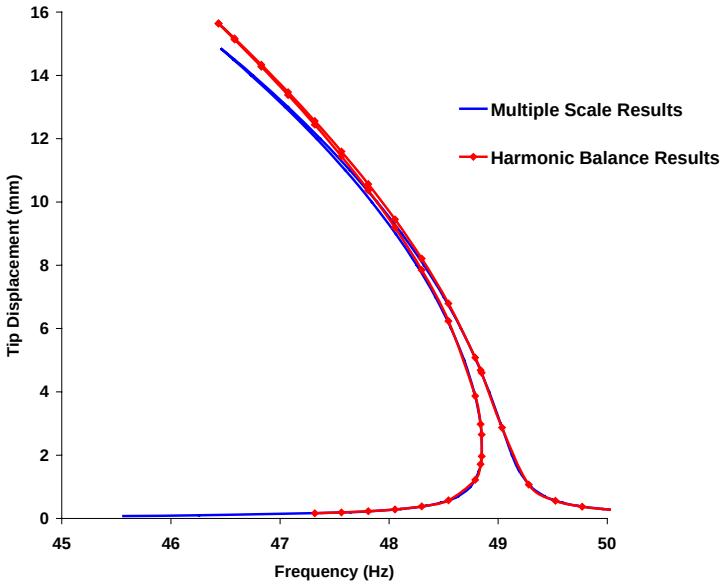

(c) light damping case

Figure 3-2 The comparison of solutions from Harmonic Balance Method and Multiple Scale Method.

3.5 EXPERIMENTAL PROCEDURE

The beams tested in this study were made of 2024-T3 aluminum alloy and three types of fiber-metal laminates – GLARE2 (0^o), GLARE2 (90^o) and GLARE3.The details are given in Table 2- 1. These beams were 25 mm wide x 381 mm long (or 1" x 15") and thickness varies as given in Table 1. The active length of each beam was 305 mm (12"). The beam was mounted vertically on an aluminum clamping fixture attached to a Brüel & Kjær 4802 vibration shaker. The excitation level was controlled by Data Physics through a PCB accelerometer placed on the clamping fixture. The accelerometer signal was conditioned with a PCB 482A10 amplifier before fed to Data Physics controller. The controller then generates appropriate output voltage to drive the Brüel & Kjær 2708 amplifier. The response of the cantilever beam was measured with three 350 Ohm strain gages mounted on the beam. The distances from the fixed end of the beam to the stain gages are approximately 12.7 mm (0.5"), 94.0 mm (3.7") and 161.0 mm (6.34") respectively as seen in Figure 3.3. Each strain gage formed one arm of a quarter bridge circuit, and its signal was conditioned using a Measurements Group 2310 signal conditioning amplifier. The signal from strain gage conditioner was fed to a digital computer through a National Instruments data acquisition board (PCI 6052). The voltage was monitored and recorded by Labview7.0.

We conducted experiments to investigate the frequency responses near the first three resonant frequencies for each type of beams. For each mode, we used a new beam with the same configuration to prevent beams from fatigue damage. We conducted several testing sequences on one beam regarding the specific mode. For each testing sequences, the frequency was swept while the excitation amplitude was held constant.

The excitation amplitude itself was different for each sequence. These sweeps allowed for characterization of the nonlinear dynamics of the beam by capturing jumps and multiple solutions. At each increment of the frequency, we waited for a long time to ensure steady state before recording the response.

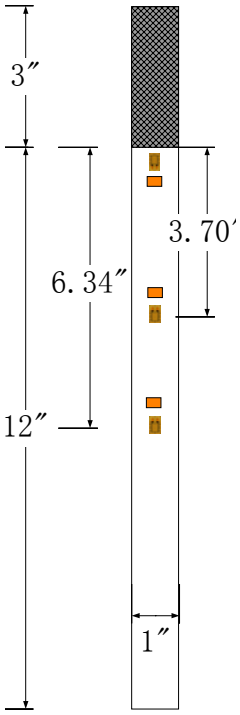

Figure 3-3 Specimen configurations for nonlinear vibration tests

3.6 RESULTS AND DISCUSSIONS

The experimental results of frequency response of a cantilevered beam made of GLARE 2 (0^o) were shown in Figure 3-4. In the first place, we assume the beam was perfectly fixed on the fixture. When the excitation acceleration was 0.5g the vibrations were very small. Hence the nonlinearities can be ignored. From the linear vibration theory described in Chapter 2, we find the natural frequency is 216.25hz and linear

damping is 0.001634. Then we attempt to match the experimental results with the theoretical analysis for the test sequence with excitation acceleration at 25g. The results are shown in Figure 3-5. There are some differences between the experimentally and theoretically obtained frequency-response curves. The dot line shows the theoretical results when the third natural frequency is set to 216.25hz. We observe in Fig. 3-5 that the theoretically obtained frequency-response curve is to the right of the experimental one. This indicates that the natural frequency needs to be lowered. Also, we observe that the spike in the experimental frequency-response curve is wider than the theoretical one. This indicates that excitation level needs to be increased.

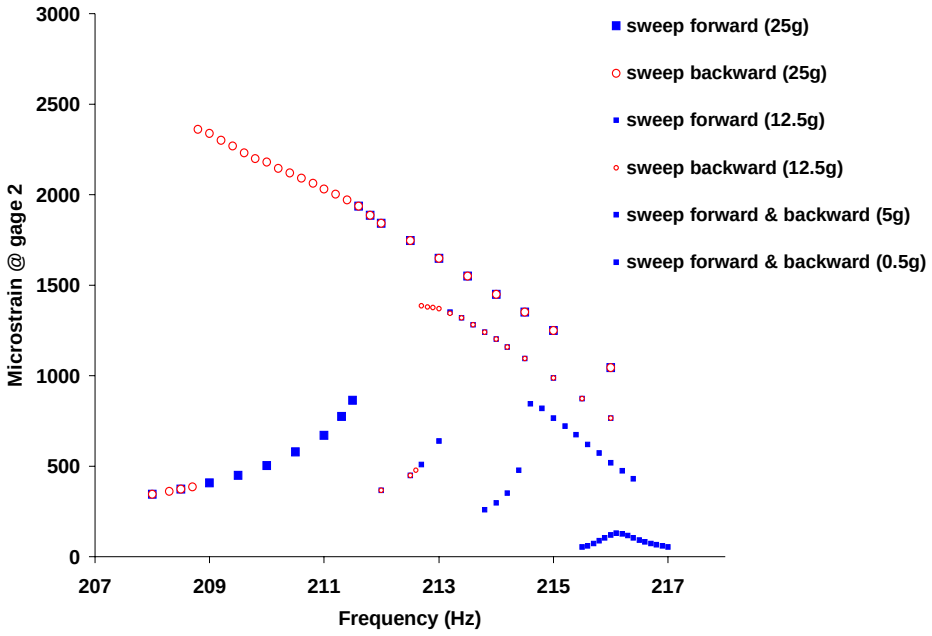

Figure 3-4 Frequency response of a cantilevered beam made of GLARE 2 (0^o).

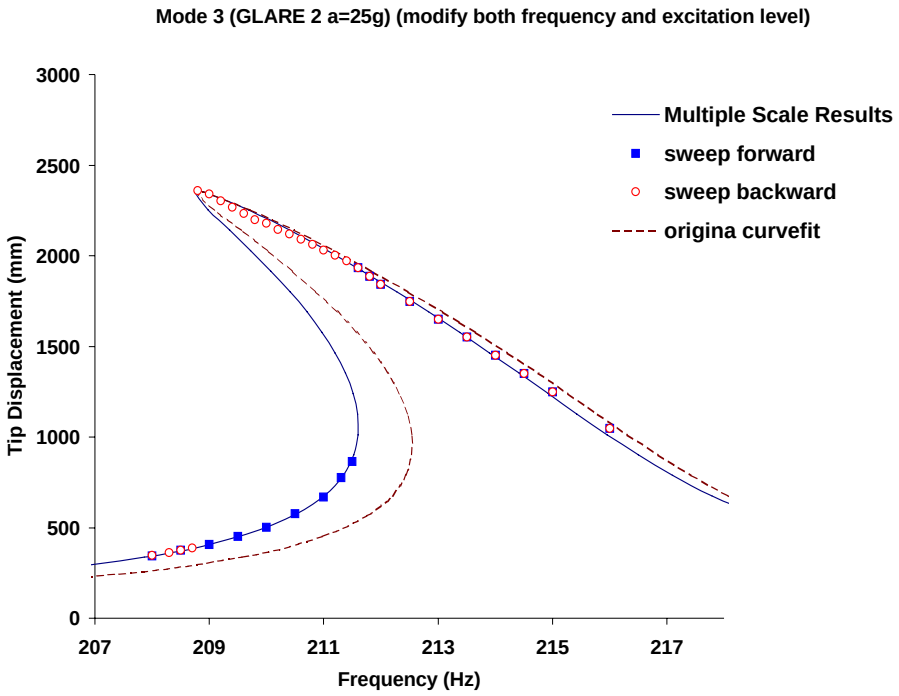

Figure 3-5 Experimental and theoretical results of frequency response of a cantilevered beam made of GLARE 2 (0^o) at the third mode for excitation acceleration at 25g

For better agreement between the third-mode experimental and theoretical frequency-response results, we had to lower natural frequency by nearly 1.37 Hz, which is around 0.6% of the natural frequency at small vibration, and we had to increase the value of acceleration nearly 4%. For test sequences with excitation accelerations at 5g and 12.5g, we had to lower natural frequency by nearly 0.75Hz and 0.90Hz respectively. In the mean time we had to modify the excitation acceleration accordingly. The reason for small adjustment of excitation level could be improper calibration of the accelerometer and/or an error in the measurement of the strain-gage and acceleration. But the natural frequency shift for the same beam is unacceptable. The most likely reason is the beam was damaged. But it was later confirmed that this was not the case. We believe the assumption of ideal-clamp boundary condition could be contributing to the shift in the

natural frequency. Tabaddor [313] studied the influence of nonideal-clamp boundary conditions and found significant changes in the model behavior.

Next we consider the case of a torsional spring with linear and cubic stiffness terms in the theoretical analysis. By incorporating the boundary flexibility, we have introduced two additional unknowns into our analysis, the linear and cubic stiffness coefficients. The linear stiffness coefficients can be found by taking the first experimentally obtained linear natural frequency and substituting it into Equation (3.41). This will well account for the natural frequency shift in our experiments. Then we adjust the value of the cubic stiffness term by curve fitting the theoretically obtained frequency-response curve for one excitation amplitude. We find that by appropriately choosing the linear stiffness coefficients and adjusting the excitation level accordingly (within 5%), the experimentally and theoretically obtained frequency-response curves are in excellent agreement for beams made of GLARE2 (0 degree) (shown in Figures 3-6, 3-7, 3-8), GLARE2 (90 degree) (shown in Figures 3-9, 3-10, 3-11) and GLARE 3 (shown in Figures 3-12, 3-13, 3-14). For the aluminum beam, the experimental results do not fit the nonlinear theory very well (shown in Figures 3-15, 3-16, 3-17). This could be explained by the fact that aluminum is susceptive to fatigue damage and the beam might not be able to survive the large vibration. We also find there is a large discrepancy in the nonlinear coefficient between theory and experiment. The order of the cubic stiffness term calculated from this discrepancy is beyond the assumption of the theory. The order analysis is presented in Appendix C.

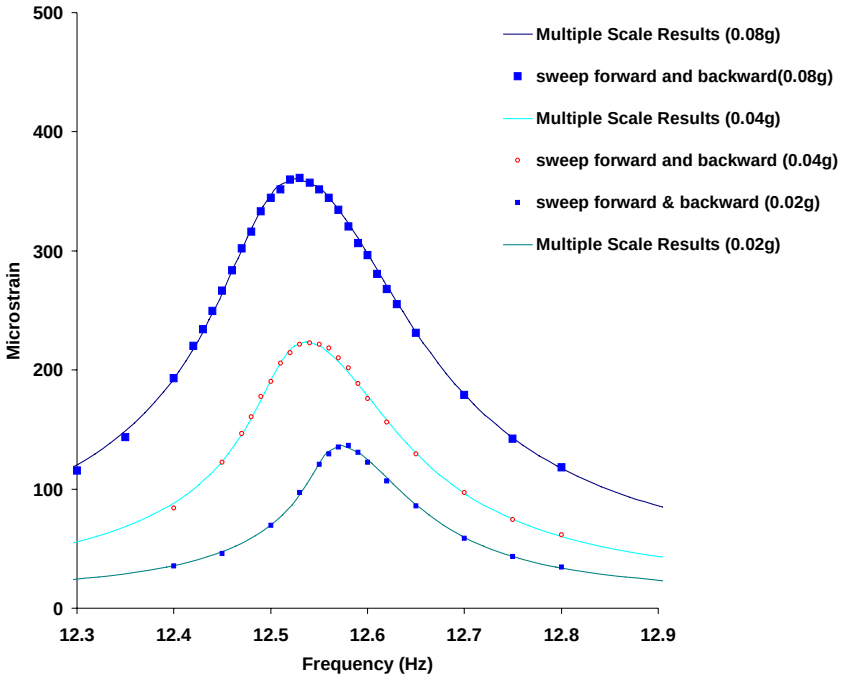

Figure 3-6 Experimentally and theoretically obtained first-mode frequency-response curves for the beam made of GLARE 2 at a_b = 0.02g, 0.04g, and 0.08g

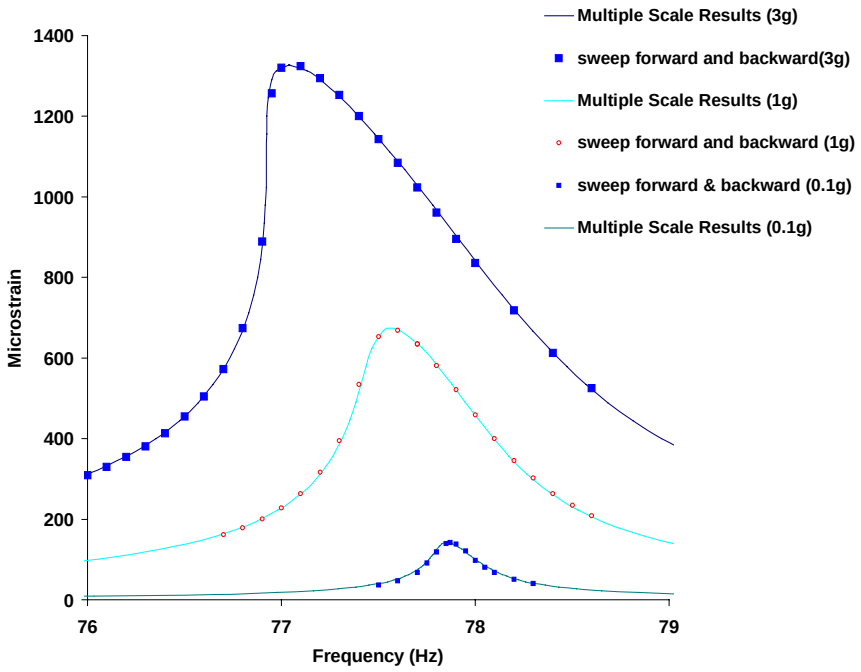

Figure 3-7 Experimentally and theoretically obtained second-mode frequency-response curves for the beam made of GLARE 2 at a_b = 0.1g, 1g, and 3g

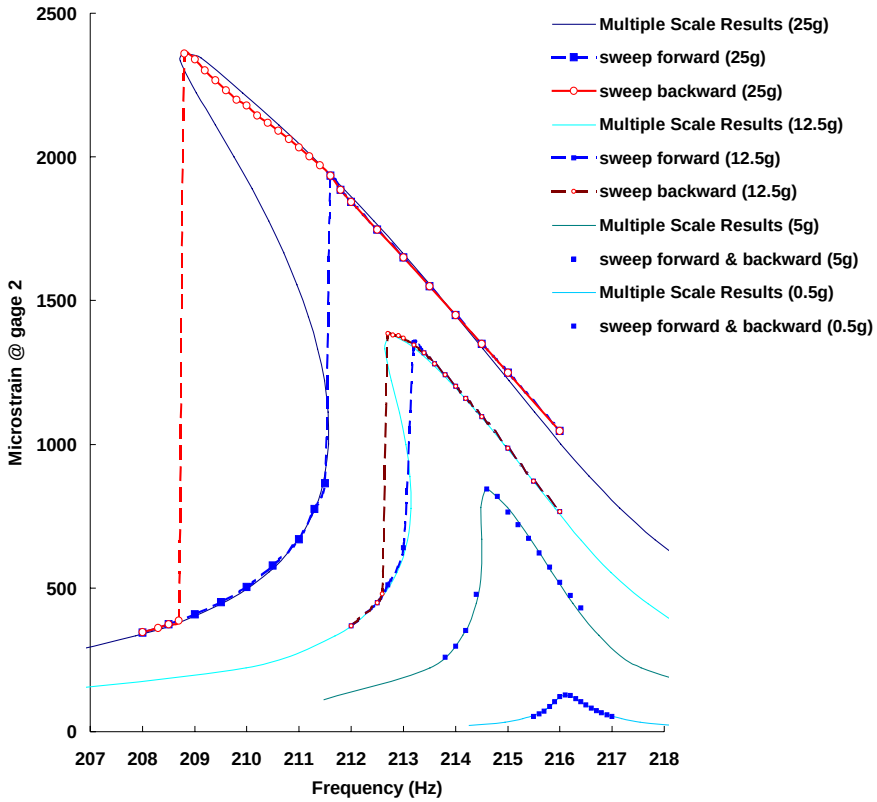

Figure 3-8 Experimentally and theoretically obtained third-mode frequency-response curves for the beam made of GLARE 2 at a_b = 0.5g, 5g, 12.5g and 25g

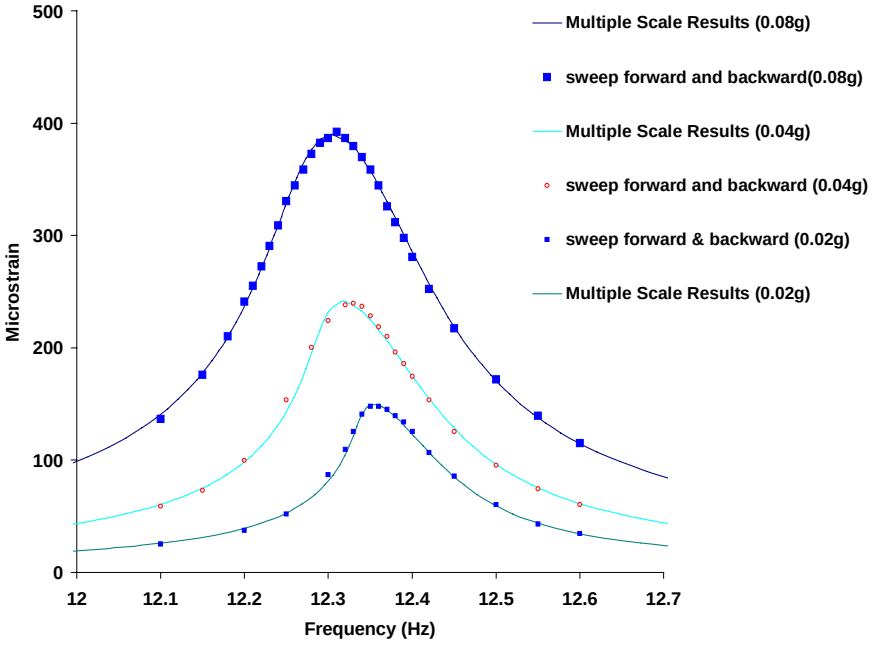

Figure 3-9 Experimentally and theoretically obtained first-mode frequency-response curves for the beam made of GLARE 2 (90 degree) at a_b = 0.02g, 0.04g and 0.08g

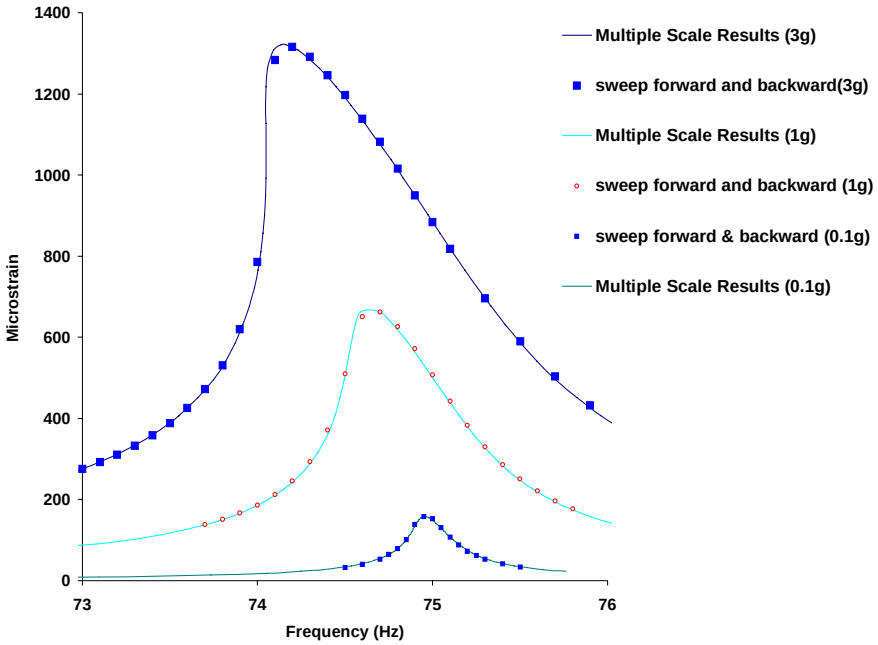

Figure 3-10 Experimentally and theoretically obtained second -mode frequency-response curves for the beam made of GLARE 2 (90 degree) at a_b = 0.1g, 1g, and 3g

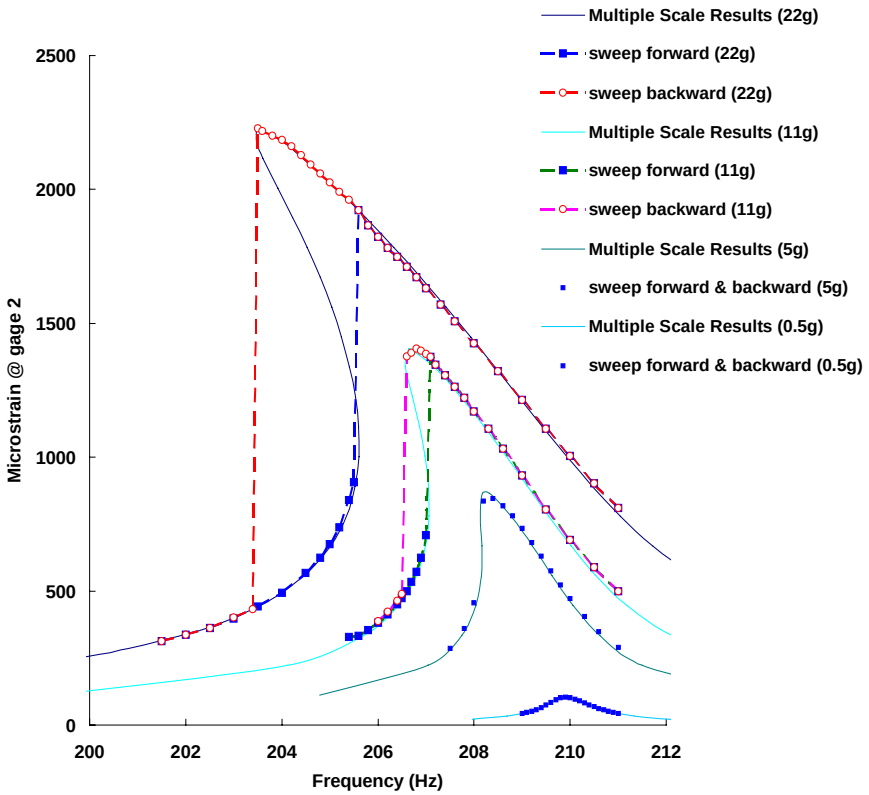

Figure 3-11 Experimentally and theoretically obtained third-mode frequency-response curves for the beam made of GLARE 2 (90 degree) at a_b = 0.5g, 5g, 11g and 22g

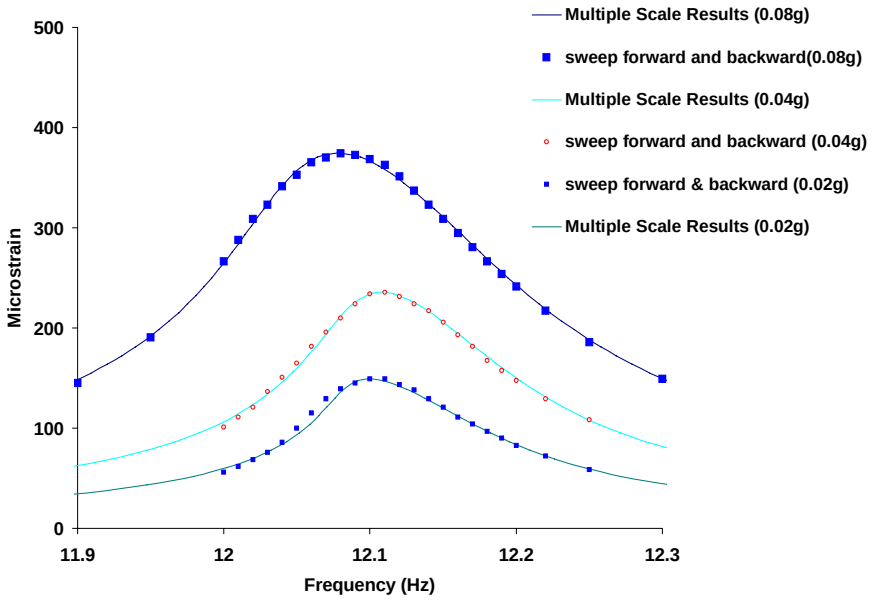

Figure 3-12 Experimentally and theoretically obtained first-mode frequency-response curves for the beam made of GLARE 3 at a_b = 0.02g, 0.04g, and 0.08g

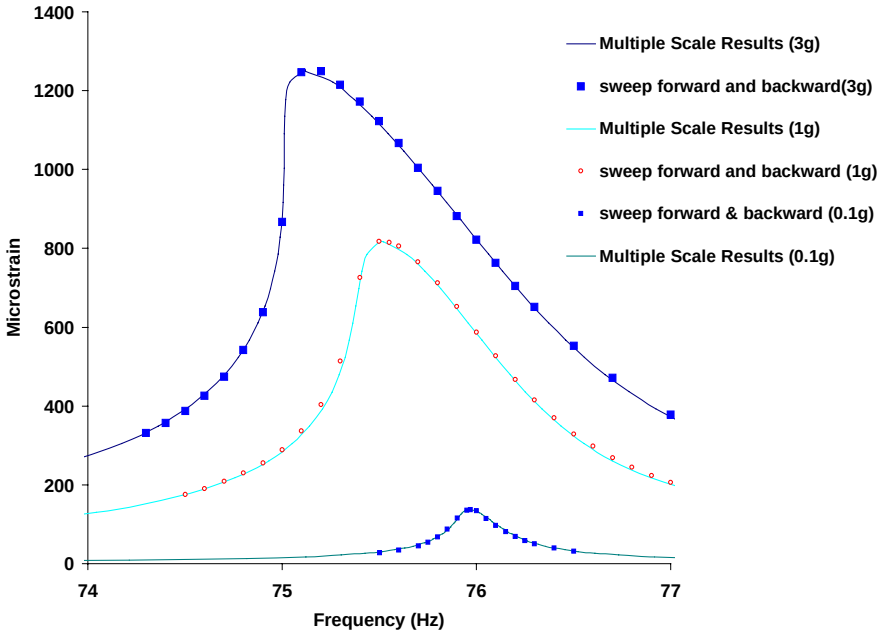

Figure 3-13 Experimentally and theoretically obtained second-mode frequency-response curves for the beam made of GLARE 3 at a_b = 0.1g, 1g, and 3g

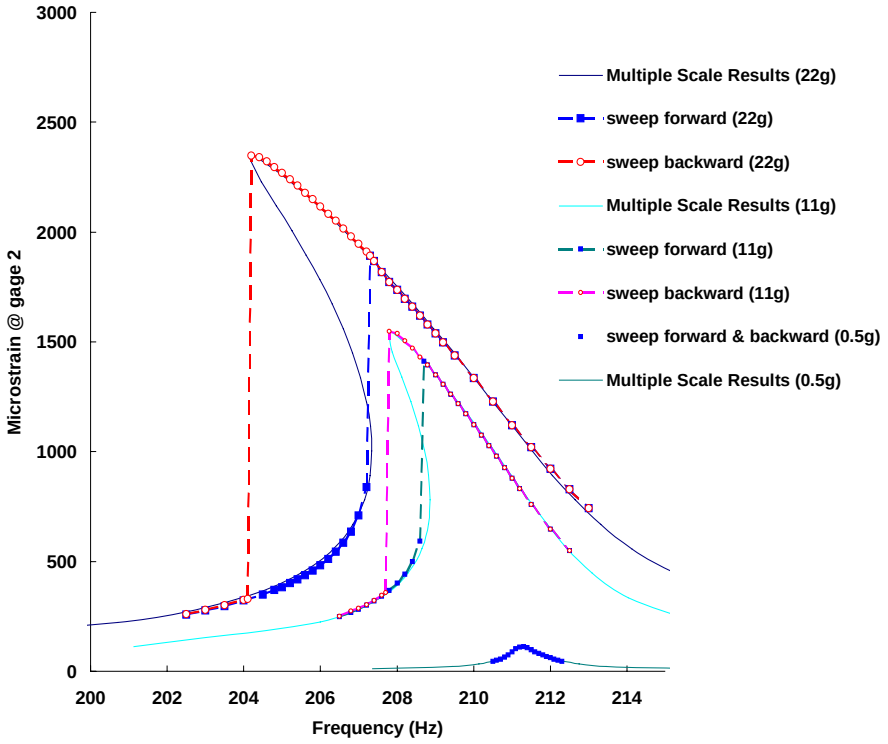

Figure 3-14 Experimentally and theoretically obtained third-mode frequency-response curves for the beam made of GLARE 3 at a_b = 0.5g, 5g, 11g and 22g

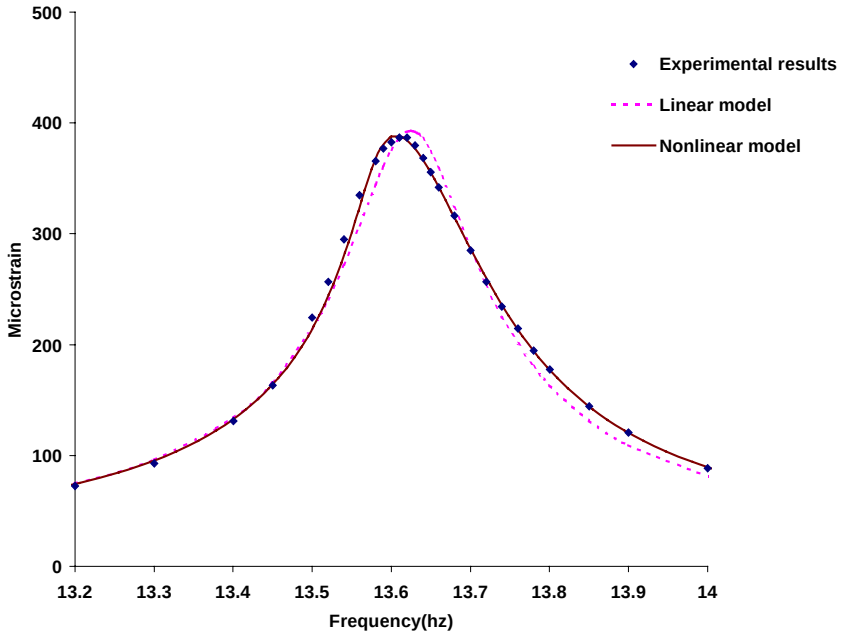

Figure 3-15 Experimentally and theoretically obtained first-mode frequency-response curves for the beam made of aluminum at a_b = 0.084g using linear and nonlinear model

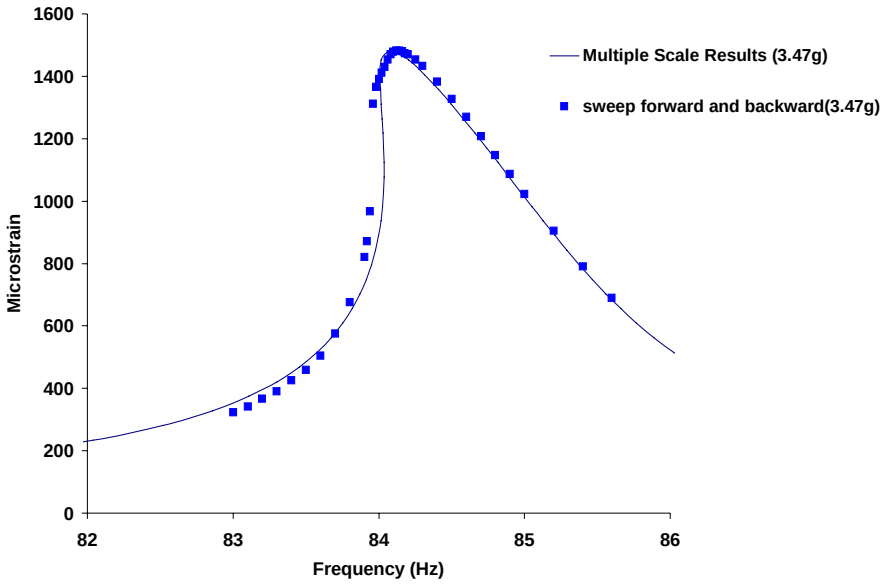

Figure 3-16 Experimentally and theoretically obtained second-mode frequency-response curves for the beam made of aluminum at a_b = 3.47g

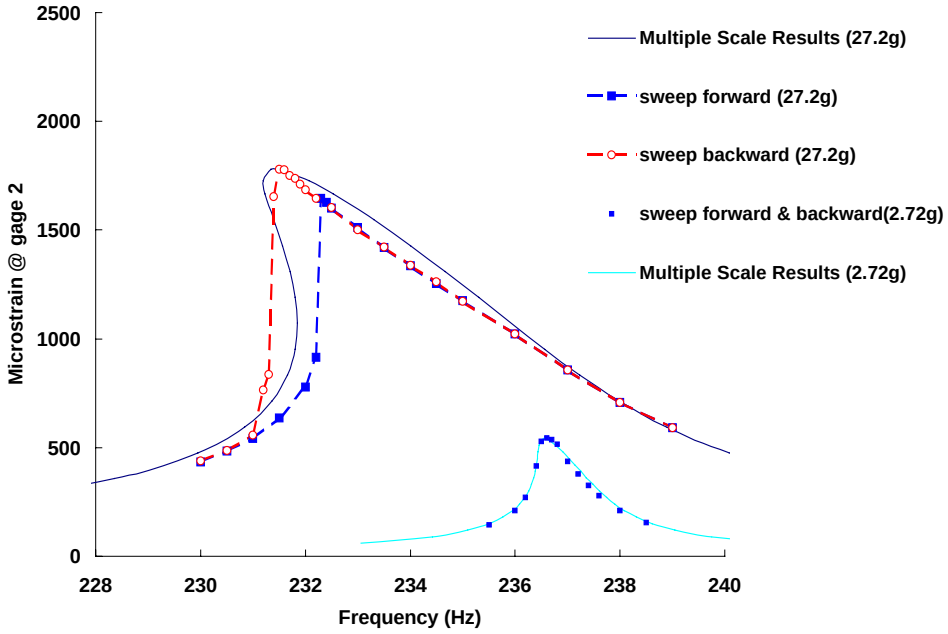

Figure 3-17 Experimentally and theoretically obtained third-mode frequency-response curves for the beam made of aluminum at a_b = 2.72g and 27.2g

CHAPTER 4 VIBRATION CONTROL EFFICIENCY OF BEAMS AND PLATES USING PZT PATCHES

4.1 THE UNIFORM-BEAM MODEL

When the model ignores the inertia and stiffness of PZT patches, we called it the uniform beam model. First we start with a beam attached with one pair of PZT patches. Using the distributed moment forcing model, the dynamic of beam with actuator can be described as:

$$EIw'''' + \rho A\ddot{w} + c\dot{w} = M_{\Lambda}''$$

$$\begin{aligned} M_{\Lambda} &= \chi[H(x-x_1) - H(x-x_2)]V(t) \\ \chi &= E_a b(t_a + t_b)d_{31} \end{aligned} \tag{4.1}$$

Here $H(x)$ is Heaviside step function. If we ignore the mass and stiffness of PZT patches, using mode summation method, we can represent the solution, $w(x,t)$, in terms of normal modes, $\phi_n(x)$, (n = 1,2,3,…) as:

$$w(x,t) = \sum_{n=1}^{\infty} \phi_n(x) q_n(t)$$

$$\ddot{q}_n(t) + 2\zeta_n \omega_n \dot{q}_n(t) + \omega_n^2 q_n(t) = \frac{\chi V(t)}{\rho A} \int_0^l \phi_n(x) \frac{\partial^2 [H(x-x_1) - H(x-x_2)]}{\partial x^2} dx \tag{4.2}$$

Since we can simplify the integration term as

$$\int_0^l \phi_n(x) \frac{\partial^2 [H(x-x_1) - H(x-x_2)]}{\partial x^2} dx = \phi_n'(x_2) - \phi_n'(x_1)$$

From Equation (4.2), we have

$$\ddot{q}_n(t) + 2\zeta_n \omega_n \dot{q}_n(t) + \omega_n^2 q_n(t) = \frac{\chi[\phi_n'(x_2) - \phi_n'(x_1)]}{\rho A} V(t) \tag{4.3}$$

4.1.1 Single-mode Consideration

If only considering a particular mode of beam, in order to get the most efficient control effort, we must maximize $|\phi_n'(x_2)-\phi_n'(x_1)|$:

$$\phi_n'(x_2)-\phi_n'(x_1)=\phi_n'(x_a+\frac{l}{2})-\phi_n'(x_a-\frac{l}{2}) \tag{4.4}$$

Here x_a is the position of PZT patches center, l is the length of PZT pair.

First we assume the length of PZT is constant, x_a is the only optimal variable. Take the derivative of Equation (4.4) with respect to x_a, we have:

$$\frac{\partial}{\partial x_a}(\phi_n'(x_a+\frac{l}{2})-\phi_n'(x_a-\frac{l}{2}))=\frac{d}{dx_a}(\phi_n'(x_a+\frac{l}{2})-\phi_n'(x_a-\frac{l}{2}))$$
$$=\phi_n''(x_a+\frac{l}{2})-\phi_n''(x_a-\frac{l}{2}) \qquad (\frac{l}{2}\le x_a\le L-\frac{l}{2})$$

When $\phi_n''(x_a+\frac{l}{2})-\phi_n''(x_a-\frac{l}{2})=0$, we get the maximal value:

$$\frac{\partial}{\partial x_a}(\phi_n'(x_a+\frac{l}{2})-\phi_n'(x_a-\frac{l}{2}))=0$$

hence

$$\phi_n''(x_a+\frac{l}{2})=\phi_n''(x_a-\frac{l}{2}) \tag{4.5}$$

Conclusion 1: If the PZT length is fixed, the modal curvatures at the two ends of attachment must be equal when the position of patches is optimal for that mode; or the PZT pair reaches the boundary of beam.

Next we assume the position of PZT x_a is constant. Then l is the only optimal variable. Take the derivative of Eq. (4.4) with respect to l, we have:

$$\frac{\partial}{\partial l}(\phi_n'(x_a+\frac{l}{2})-\phi_n'(x_a-\frac{l}{2}))=\frac{d}{dl}(\phi_n'(x_a+\frac{l}{2})-\phi_n'(x_a-\frac{l}{2}))$$
$$=\phi_n''(x_a+\frac{l}{2})\frac{d(x_a+\frac{l}{2})}{dl}-\phi_n''(x_a-\frac{l}{2})\frac{d(x_a-\frac{l}{2})}{dl}$$
$$=\frac{1}{2}[\phi_n''(x_a+\frac{l}{2})+\phi_n''(x_a-\frac{l}{2})]$$

When $\phi_n''(x_a+\frac{l}{2})+\phi_n''(x_a-\frac{l}{2})=0$, we get the maximal value:

$$\frac{\partial}{\partial l}(\phi_n'(x_a+\frac{l}{2})-\phi_n'(x_a-\frac{l}{2}))=0$$

hence

$$\phi_n''(x_a+\frac{l}{2})=-\phi_n''(x_a-\frac{l}{2}) \tag{4.6}$$

Conclusion 2: If the PZT position is fixed, the modal curvatures at the two ends of attachment must be opposite when the length of patches is optimal for that mode; or the PZT pair reaches the boundary of beam.

If x_a, l are two optimal variables, Eqs (4.5) and (4.6) must stand simultaneously for a maximal value to exist. Hence we have

$$\phi_n''(x_a+\frac{l}{2})=\phi_n''(x_a-\frac{l}{2})=0 \tag{4.7}$$

Conclusion 3: The two ends of attachment must be either nodes or the ends of beam when the length and position of PZT pair are both optimal for the corresponding mode.

From the mathematical perspective view, the absolute maximum of $\phi_n'(x_a+\frac{l}{2})-\phi_n'(x_a-\frac{l}{2})$ is equal to the maximum of $\int_{x_a-\frac{l}{2}}^{x_a+\frac{l}{2}}\phi''(x)dx$, where $x_a+\frac{l}{2}$ and $x_a-\frac{l}{2}$

are either nodes or boundaries of the beam. We need to compare the values for all possible combinations to find the maximal one.

From the practical perspective view, we only need to compare the values of two adjacent nodes or boundaries. Even without the consideration of computational cost, one may always use two or more PZT patches (segment actuators) to get better performance.

In this study, the length ratio of a PZT patch to a beam is less than 0.2. The optimization procedure is reduced to find maximum area underneath the curvature curve of certain model function. It is always at the neighborhood of maximal curvature or second maximal curvature if the boundary limit exists.

4.1.2 Multiple-mode Consideration

The full vibration of a beam is the summation of all infinite modal vibrations. In practice, we can account for only the first N modes. For one modal vibration, we might define Equation (4.4) as the control effective function. However for multiple modes consideration, it is more convenient to define effective function as following:

From Equation (4.3)

$$\ddot{q}_n(t) + 2\zeta_n\omega_n\dot{q}_n(t) + \omega_n^2 q_n(t) = \frac{\chi[\phi_n'(x_a + \frac{l}{2}) - \phi_n'(x_a - \frac{l}{2})]}{\rho A} V(t)$$

If we use negative velocity feedback, then $V(t) = -k\dot{q}_n(t)$, or

$$\ddot{q}_n(t) + 2\omega_n\{\zeta_n + k\chi\frac{\phi_n'(x_2) - \phi_n'(x_1)}{2\omega_n\rho A}\}\dot{q}_n(t) + \omega_n^2 q_n(t) = 0 \tag{4.8}$$

where

$$\omega_n = \beta_n^2\sqrt{\frac{EI}{\rho A}} = (\beta_n L)^2\sqrt{\frac{EI}{\rho AL^4}} = \lambda_n^2\sqrt{\frac{EI}{\rho AL^4}} \tag{4.9}$$

and $\lambda_n = \beta_n L$ is the n^{th} root of the frequency equation.

If we define the active damping ratio as ζ_a, from the equation above, we have

$$\begin{aligned}(\zeta_a)_n &= k\chi \frac{\phi_n'(x_a + \frac{l}{2}) - \phi_n'(x_a - \frac{l}{2})}{2\omega_n \rho A} = k\chi \frac{L^2}{2\sqrt{\rho AEI}} \frac{\phi_n'(x_a + \frac{l}{2}) - \phi_n'(x_a - \frac{l}{2})}{\lambda_n^2} \\ &= k\chi \frac{L^2}{2\sqrt{\rho AEI}} (f_{effective})_n\end{aligned} \tag{4.10}$$

here $(f_{effective})_n \equiv \frac{\phi_n'(x_a + \frac{l}{2}) - \phi_n'(x_a - \frac{l}{2})}{\lambda_n^2}$ is the effective function of the n^{th} mode. It is worthy to notice that for the uniform beam mode, the modal effective function is not related to material properties, such as Young modulus and density.

One reasonable optimal criterion is to maximize the sum of the active damping ratios corresponding to the first N modes. We define

$$g(x) = \sum_{n=1}^{N} \alpha_n (\zeta_a)_n = k\chi \frac{L^2}{2\sqrt{\rho AEI}} \sum_{n=1}^{N} \alpha_n (f_{effective})_n$$

as the objective function to be optimized, where α_n is the mode weigh factor, N is the number of modes taken into account. Here we use N=5 and $\alpha_n = 1$. Since $\chi \frac{L^2}{2\sqrt{\rho AEI}}$ is a constant for a particular beam and k is restrained by the PZT depolarization voltage, it is equivalent to optimize the function $f(x) = \sum_{n=1}^{m} (f_{effective})_n$. In order to avoid losing the controllability on certain mode, the value of $(f_{effective})_n$ should not be less than some

factor (e.g., one third used in this study) of the maximum possible value when only that mode is considered. The result is shown in Figure 4-1.

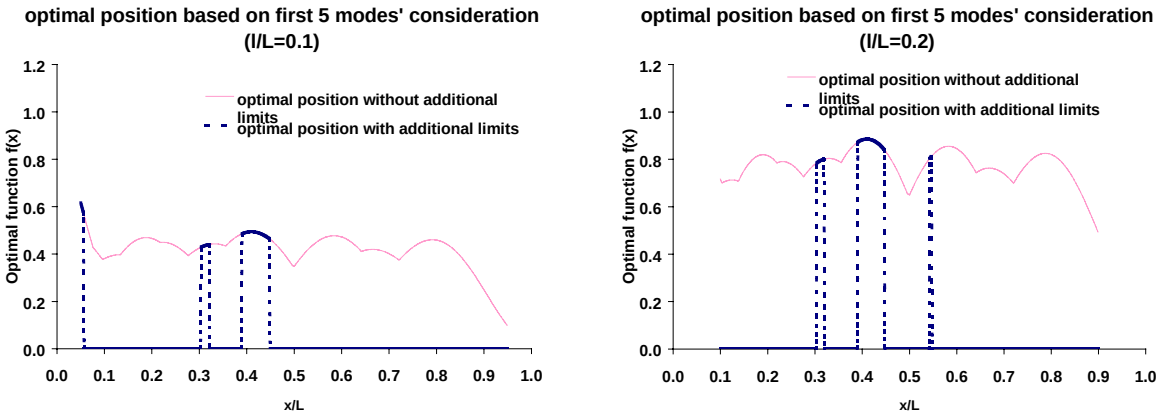

Figure 4-1 Position optimization of a cantilever beam.

4.2 THE STEPPED-BEAM MODEL

If the mass or stiffness of PZT cannot be ignored, we can use stepped beam model to deal with the beam-actuator structure. The beam is divided into thee uniform-section beams as shown in Figure 4-2.

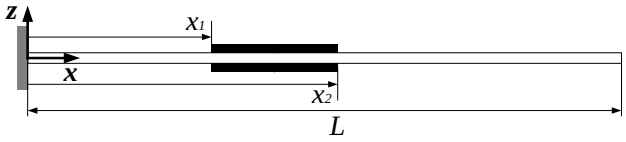

Figure 4-2 The stepped-beam model with a pair of PZT patches.

The governing equations for each section are

$$(EI)_i w_i'''' + (\rho A)_i \ddot{w}_i = 0 \qquad i = 1,2,3 \tag{4.11}$$

where

$$(EI)_1 = E_b I_b = \frac{1}{12} E_b b t_b^3$$

$$(EI)_2 = E_b I_b + 2E_a I_a = \frac{1}{12}[E_b bt_b^3 + 2E_a bt_a^3] + \frac{1}{2}E_a bt_a(t_b + t_a)^2$$

$$(EI)_3 = E_b I_b = \frac{1}{12}E_b bt_b^3$$

$$(\rho A)_1 = \rho_b bt_b$$

$$(\rho A)_2 = \rho_b bt_b + 2\rho_a bt_a$$

$$(\rho A)_3 = \rho_b bt_b$$

Solving the governing equations, we get

$$w_i = A_i \cosh \beta_i x + B_i \sinh \beta_i x + C_i \cos \beta_i x + D_i \sin \beta_i x \qquad i = 1, 2, 3$$

where $\beta_i^4 = \dfrac{(\rho A)_i}{(EA)_i}\omega^2$

Since we have 12 variables; we need to find 12 boundary equations.

For cantilever beam case:

At $x = 0$ $\quad w_1 = 0$, $w_1' = 0$

At $x = L$ $\quad w_3'' = 0$, $w_3''' = 0$

At $x = x_1$ $\quad w_1 = w_2$, $w_1' = w_2'$

$$(EI)_1 w_1'' = (EI)_2 w_2'' \tag{4.12a}$$

$$(EI)_1 w_1''' = (EI)_2 w_2''' \tag{4.12b}$$

At $x = x_2$ $\quad w_2 = w_3$, $w_2' = w_3'$

$$(EI)_2 w_2'' = (EI)_3 w_3'' \tag{4.12c}$$

$$(EI)_2 w_2''' = (EI)_3 w_3''' \tag{4.12d}$$

From the 12 boundary equations we get the corresponding characteristic equation. Solving the equations, we get the natural circular frequency ω. Substituting ω we can get all 12 variables and the corresponding model functions.

After we get the frequencies and model functions, we can use model summation method to solve the dynamic problem of the structure.

$$EIw'''' + \rho A\ddot{w} + c\dot{w} = M''_{\Lambda}$$

$$M_{\Lambda} = \chi[H(x-x_1) - H(x-x_2)]V(t)$$

here $H(x)$ is the Heaviside step function.

Since we include the mass and stiffness of PZT patch, $EI, \rho A$ are not constant. By using the Principle of Virtual Work, we can get

$$w(x,t) = \sum_{n=1}^{\infty} \phi_n(x) q_n(t)$$

$$\ddot{q}_n(t) + 2\zeta_n \omega_n \dot{q}_n(t) + \omega_n^2 q_n(t) = \frac{\chi[\phi_n'(x_2) - \phi_n'(x_1)]}{\int_0^L \rho A \phi_n^2(x) dx} V(t) \tag{4.13}$$

$$\omega_n^2 = \frac{\int_0^L EI\phi_n''^2(x)dx}{\int_0^L \rho A \phi_n^2(x) dx} \tag{4.14}$$

$$\begin{aligned}(\zeta_a)_n &= k\chi \frac{\phi_n'(x_2) - \phi_n'(x_1)}{2\omega_n \int_0^L \rho A \phi_n^2(x)dx} = k\chi \frac{L^2}{2\sqrt{(\rho A)_1 (EI)_1}} \frac{\sqrt{(\rho A)_1 (EI)_1}}{L^2} \frac{\phi_n'(x_2) - \phi_n'(x_1)}{\omega_n \int_0^L \rho A \phi_n^2(x)dx} \\ &= k\chi \frac{L^2}{2\sqrt{(\rho A)_1 (EI)_1}} (f_{effective})_n\end{aligned} \tag{4.15}$$

here

$$(f_{effective})_n = \frac{\sqrt{(\rho A)_1 (EI)_1}}{L^2} \frac{\phi_n'(x_2) - \phi_n'(x_1)}{\omega_n \int_0^L \rho A \phi_n^2(x)dx} \tag{4.16}$$

Comparing Equation (4.10) and Equation (4.16), we can see the relationships between active damping ratio and effective function for both model are very similar. The effective function in stepped beam mode is associated with the material properties and the structural dimensions

Thus, in stepped beam modal, the PZT patches not only change the natural frequencies of beam, but also model shape functions. The effective function $f_{effective}$ is structural dimension dependable. In order to demonstrate the structure alteration caused by PZT patches, a cantilever beam with a pair PZT patches bonded in the fix end is considered. The material properties and dimensions of beam and PZT patches are listed in Table 4-1.

Table 4-1 Material properties and structural dimensions of the beam.

E_b	72 GPa
E_a	66 GPa
ρ_b	2900 $kg.m^{-3}$
ρ_a	7800 $kg.m^{-3}$
t_b	0.06 inch
t_a	0.02 inch
b	0.5 inch
l	1.25 inch
L	8.75 inch

Using the stepped beam model, we can get the normalized nondimensional modal functions:

$$\phi_1(x)=\begin{cases}0.353*[\cosh(1.875x)-\cos(1.875x)]-0.251*[\sinh(1.875x)-\sin(1.875x)] & 0<x<0.143\\ 1.052*[\cosh(2.093(x-1))+\cos(2.093(x-1))]+0.768*[\sinh(2.093(x-1))+\sin(2.093(x-1))] & 0.143<x<1\end{cases}$$

$$\phi_2(x)=\begin{cases}-0.465*[\cosh(4.611x)-\cos(4.611x)]+0.370*[\sinh(4.611x)-\sin(4.611x)] & 0<x<0.143\\ 1.032*[\cosh(5.146(x-1))+\cos(5.146(x-1))]+1.053*[\sinh(5.146(x-1))+\sin(5.146(x-1))] & 0.143<x<1\end{cases}$$

$$\phi_3(x)=\begin{cases}0.586*[\cosh(7.557x)-\cos(7.557x)]-0.442*[\sinh(7.557x)-\sin(7.557x)] & 0<x<0.143\\ 1.010*[\cosh(8.434(x-1))+\cos(8.434(x-1))]+1.009*[\sinh(8.434(x-1))+\sin(8.434(x-1))] & 0.143<x<1\end{cases}$$

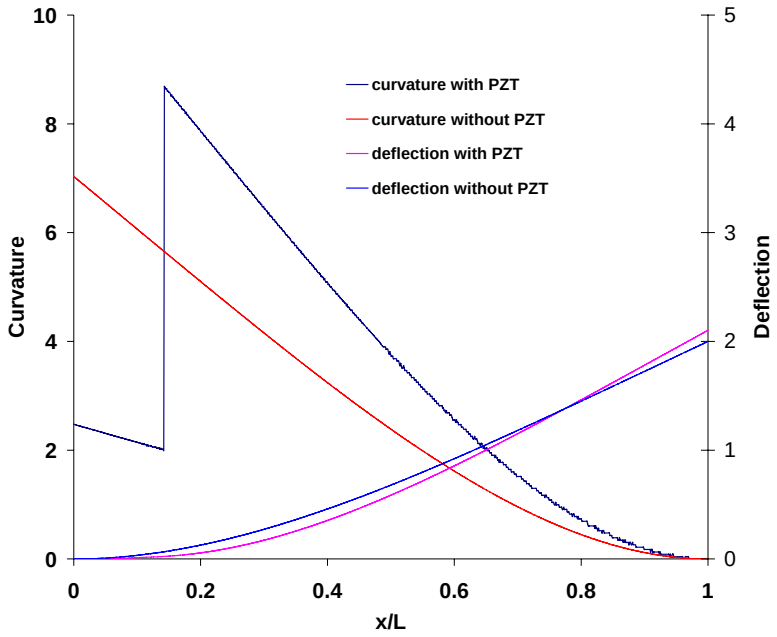

Figure 4-3 First modal deflection and curvature function of a cantilever beam with PZT.

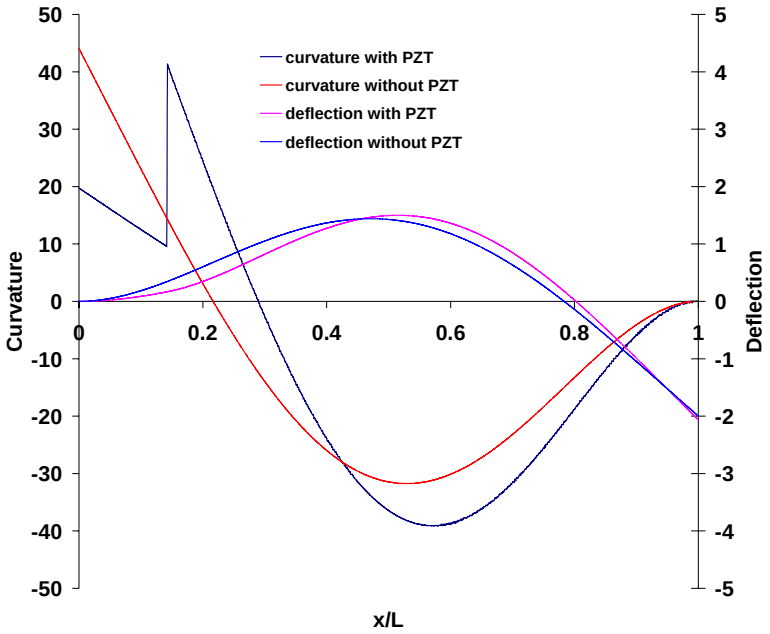

Figure 4-4 Second modal deflection and curvature function of a cantilever beam with PZT.

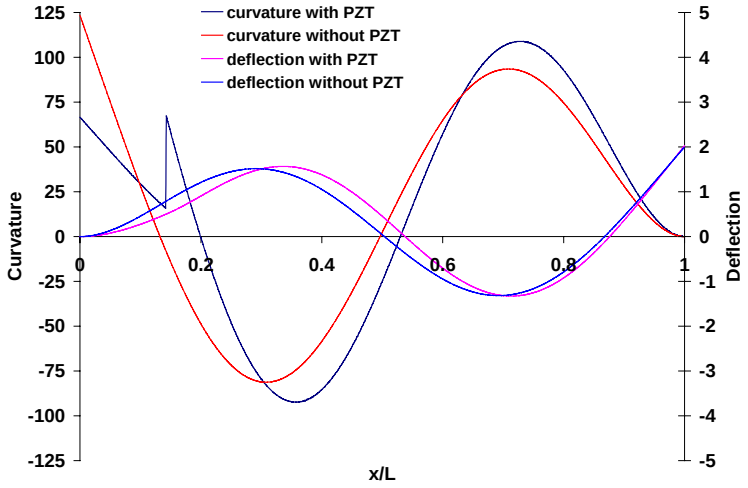

Figure 4-5 Third modal deflection and curvature function of a cantilever beam with PZT.

From Figures 4-3 to 4-5, we can see that although PZT patches do not change the modal deflection that much, they do change the curvature a lot. The curvature drops significantly within the area covered by PZT pair, which is consistent with the boundary

conditions we use in stepped beam modal. Equation (4.16) shows the effective function $(f_{effective})_n$ is proportional to the slope difference between two edges of PZT pair. And the slope difference equals the area underneath the curvature curve. Hence $(f_{effective})_n$ will drop substantially because of the modal curvature alteration, great cares must be taken when we estimate the PZT pair's control ability.

Calculations of cantilever beams with different PZT patch positions were carried out. Using Equation (4.16), the effective functions of each case are evaluated. From Figures 4-6 to 4-8, one can find that although the patches change the host structures, hence change the effective function's value; the trends of effective functions are similar with those of beams without patches. However, the effective function degrades least when the PZT patches are bonded near the fixed end.

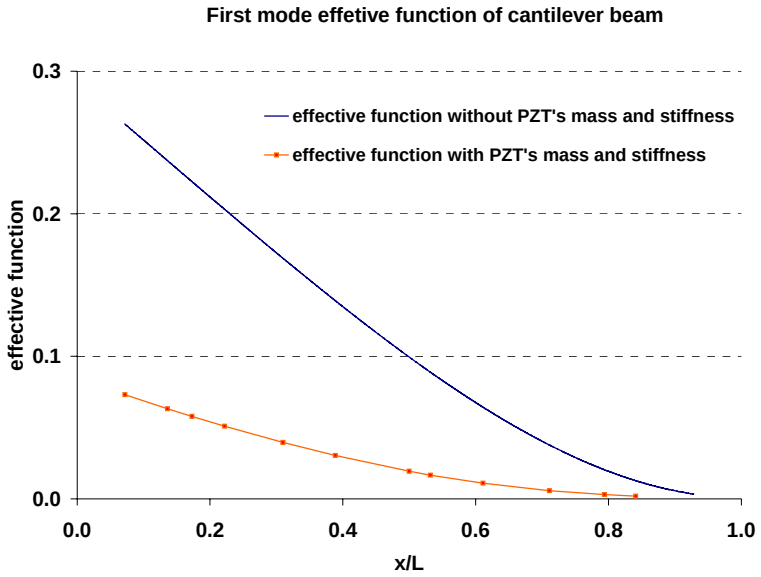

Figure 4-6 Comparison of effective functions of first mode of a cantilever beam w/o PZT patches.

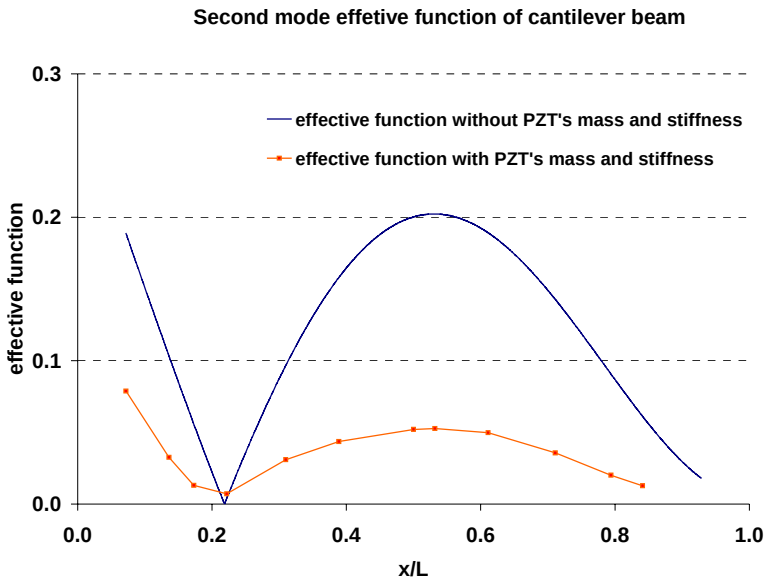

Figure 4-7 Comparison of effective functions of second mode of a cantilever beam w/o PZT patches.

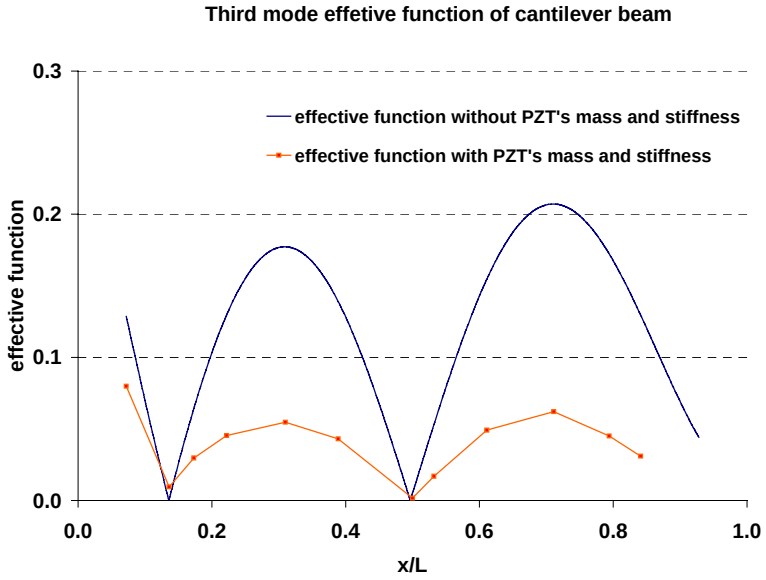

Figure 4-8 Comparison of effective functions of third mode of a cantilever beam w/o PZT patches.

Conclusion: the optimal positions from stepped beam model are similar as those from uniform beam model. However, the effective function and active damping ratios from

former model are smaller than those from latter model. The ratio of results from stepped beam model to from uniform beam model is between $\frac{E_b I_b}{E_b I_b + 2E_a I_a}$ and 1.

$$\frac{E_b I_b}{E_b I_b + 2E_a I_a} = \frac{\frac{1}{12} E_b b t_b^3}{\frac{1}{12}[E_b b t_b^3 + 2E_a b t_a^3] + \frac{1}{2} E_a b t_a (t_b + t_a)^2}$$
$$= \frac{E_b t_b^3}{E_b t_b^3 + 2E_a t_a^3 + 6E_a t_a (t_b + t_a)^2}$$

If we define $\alpha = \frac{E_a}{E_b}$, $\beta = \frac{t_a}{t_b}$

then we have

$$\frac{E_b I_b}{E_b I_b + 2E_a I_a} = \frac{1}{1 + 2\alpha\beta^3 + 6\alpha\beta(1+\beta)^2} \tag{4.18}$$

For the cases we investigate here:

$\alpha = \frac{E_a}{E_b} = \frac{66}{72}$, $\beta = \frac{t_a}{t_b} = \frac{0.02}{0.06}$, and $\frac{E_b I_b}{E_b I_b + 2E_a I_a} = \frac{72}{312} = 0.23$. We can see the control efficiency is degraded substantially because of the changes of modal shape functions caused by PZT patches. Even the thickness ratio β is small; this kind of degradation may still not be negligible. Let β=0.1, $\frac{E_b I_b}{E_b I_b + 2E_a I_a} = 0.60$, this effect is significant.

From the studies above, we can see if the PZT pair's position is optimal, the control efficiency is proportional to $\chi \frac{E_b I_b}{E_b I_b + 2E_a I_a}$ (here we make the conservative estimation)

$$\chi \frac{E_b I_b}{E_b I_b + 2E_a I_a} = E_b t_b b d_{31} \frac{\alpha(\beta+1)}{1 + 2\alpha\beta^3 + 6\alpha\beta(1+\beta)^2} = E_b t_b b d_{31} f_{index}$$

$$f_{index1} = \frac{\alpha(\beta+1)}{1+2\alpha\beta^3+6\alpha\beta(1+\beta)^2} \tag{4.19}$$

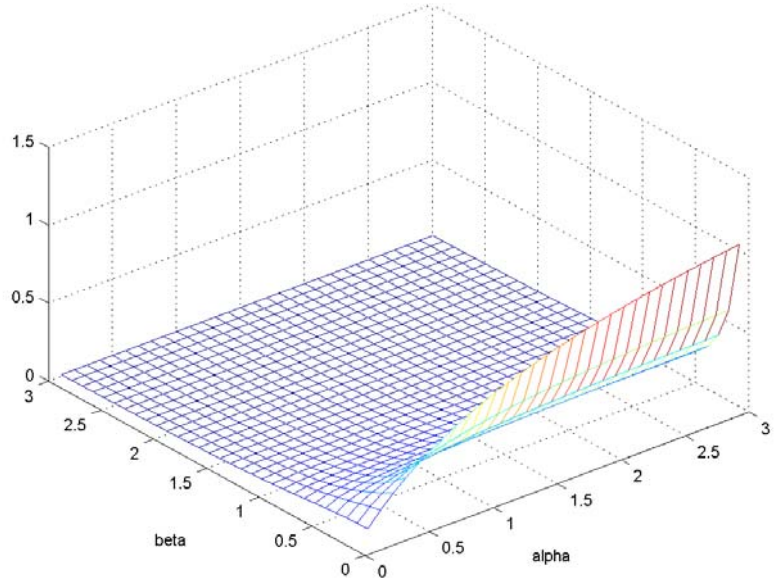

Figure 4-9 The optimization index function Equation (4.19) versus Young's modulus ratio alpha and thickness ratio beta

Here we assume the voltage is constant. At this case the field $E = V / t_p$ should be smaller than depolarization field E_0 of PZT while varying the actuator's thickness. When the PZT patches available are relatively thick but the maximum voltage of power supplier (liner amplifier) is limited, the smart material is still safe even applied the maximum voltage, we can choose the proper PZT Young's modulus and thickness so that $\frac{\alpha(\beta+1)}{1+2\alpha\beta^3+6\alpha\beta(1+\beta)^2}$ gets the maximum value. Usually PZT Young's modulus is constant, we can adjust the thickness ratio to maximize the control efficiency.

In practice, the PZT is usually thin; the polarization field is the main concern. In this case, we set the field as the polarization field E_0, hence $\Lambda_0 \equiv d_{31}E_0$. The potential control ability is proportional to

$$\chi V_{\max}\frac{E_bI_b}{E_bI_b+2E_aI_a}=E_p\Lambda_0 b(t_a^2+t_bt_a)\frac{E_bI_b}{E_bI_b+2E_aI_a}$$
$$=E_bt_b^2b\Lambda_0\frac{\alpha\beta(\beta+1)}{1+2\alpha\beta^3+6\alpha\beta(1+\beta)^2}=E_bt_b^2b\Lambda_0 f_{index2}$$

$$f_{index2}=\frac{\alpha\beta(\beta+1)}{1+2\alpha\beta^3+6\alpha\beta(1+\beta)^2} \tag{4.20}$$

For a specific beam, Young's modulus E_b, dimension t_b and b are fixed; for a particular PZT material, Λ_0 is constant for particular PZT material, so the potential control ability of a PZT patch pair is proportional to f_{index2}.

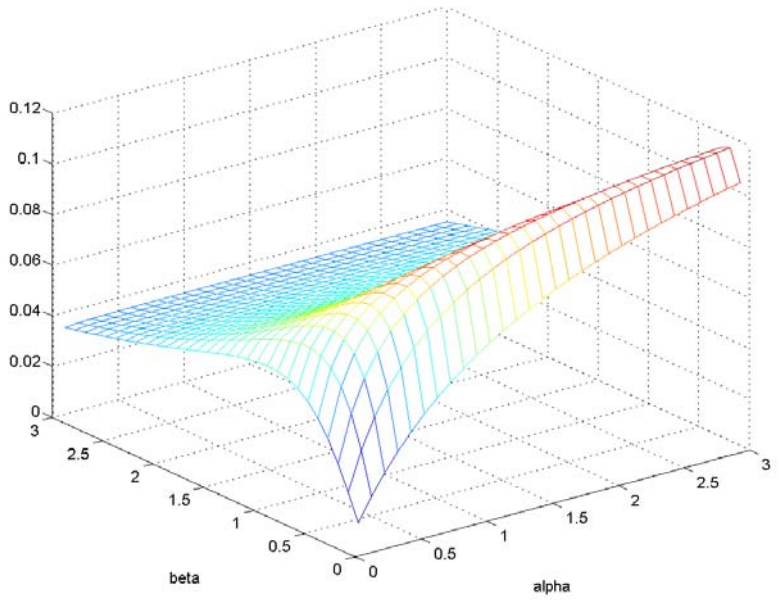

Figure 4-10 The optimization index function Equation (4.20) versus Young's modulus ratio alpha and thickness ratio beta

As shown in Figures 4-11 to 4-19, similar studies were carried out for the beam with other boundary conditions (see Appendix B). It is found that the PZT patches change the modal effective functions significantly. The optimal positions remain same as those from uniform model for pinned-pinned beam. If the beam has at least one fixed end, the optimal positions are more likely at the fixed end, the exact solution must be obtained from careful study using stepped beam model.

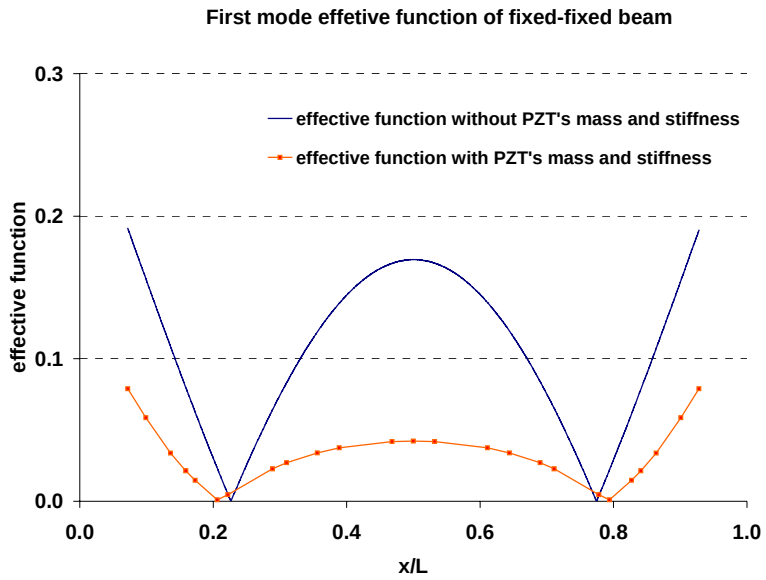

Figure 4-11 Comparison of effective functions of first mode of a fixed-fixed beam w/o PZT patches.

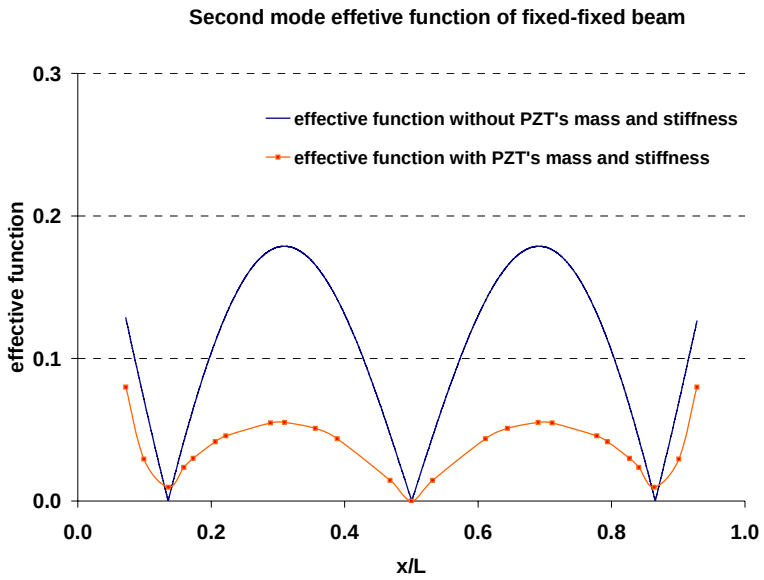

Figure 4-12 Comparison of effective functions of second mode of a fixed-fixed beam w/o PZT patches.

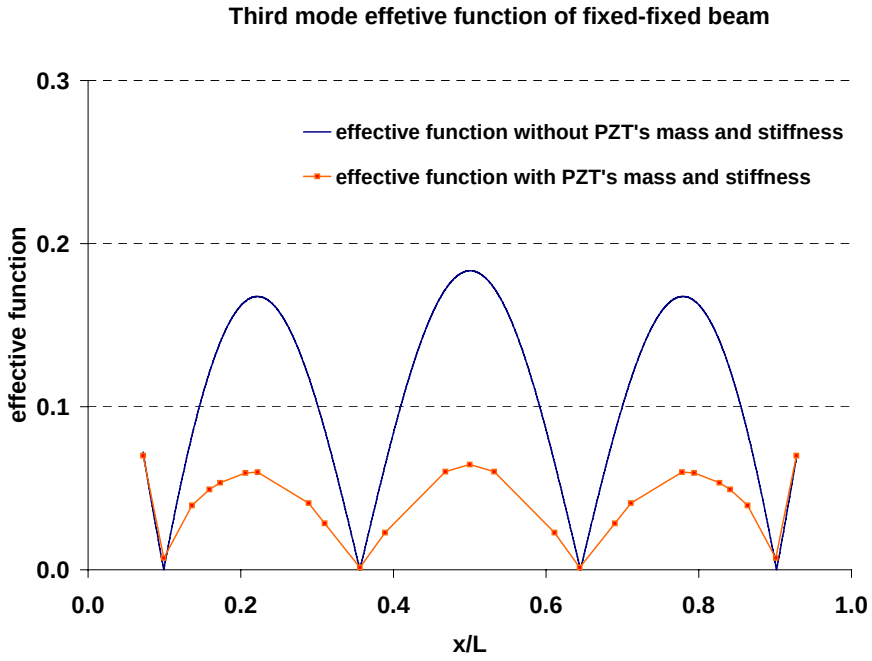

Figure 4-13 Comparison of effective functions of third mode of a fixed-fixed beam w/o PZT patches.

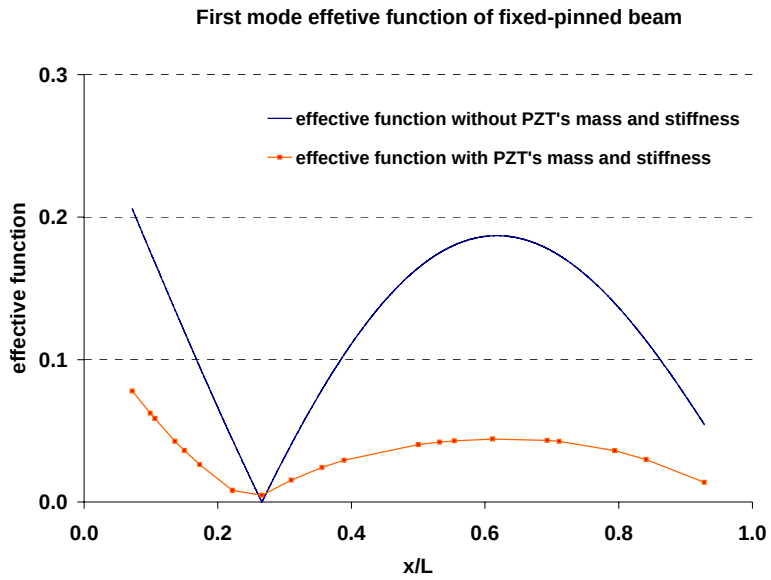

Figure 4-14 Comparison of effective functions of first mode of a fixed-pinned beam w/o PZT patches.

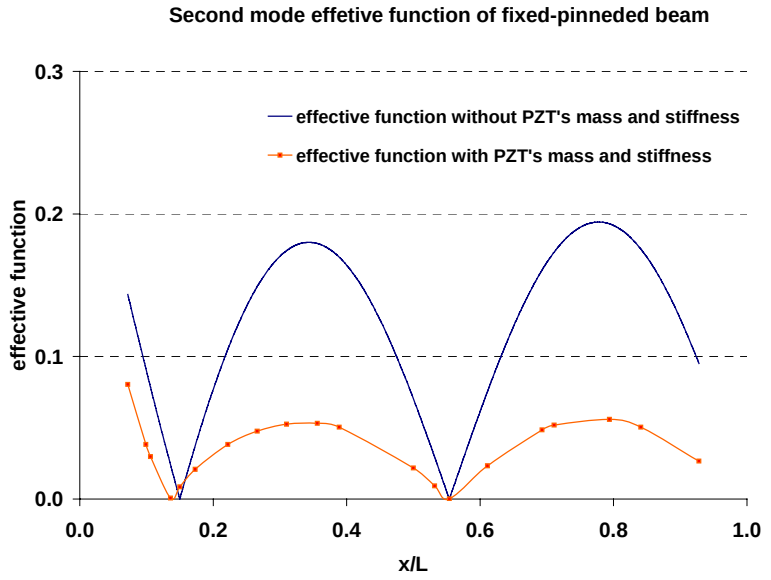

Figure 4-15 Comparison of effective functions of second mode of a fixed-pinned beam w/o PZT patches.

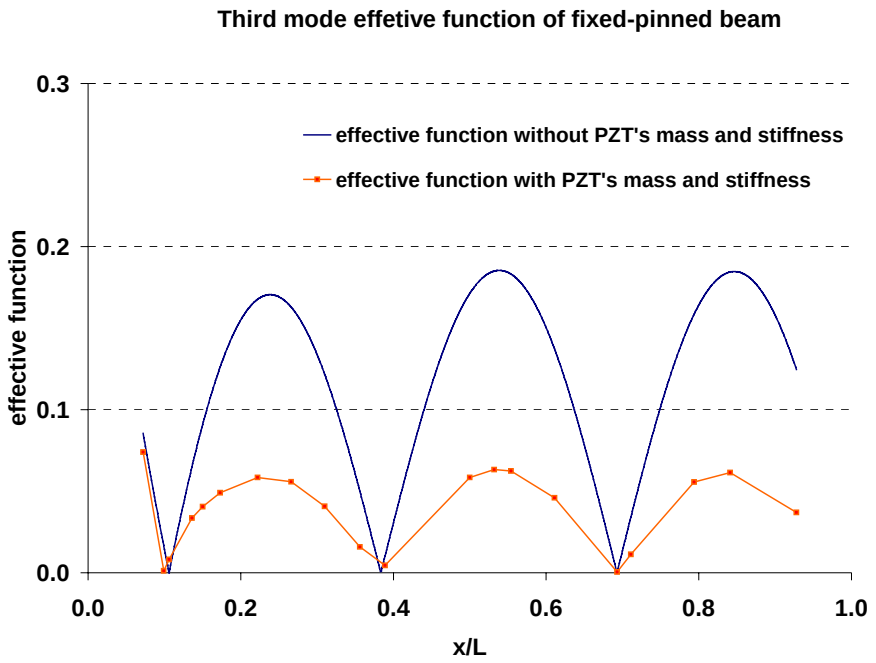

Figure 4-16 Comparison of effective functions of third mode of a fixed-pinned beam w/o PZT patches.

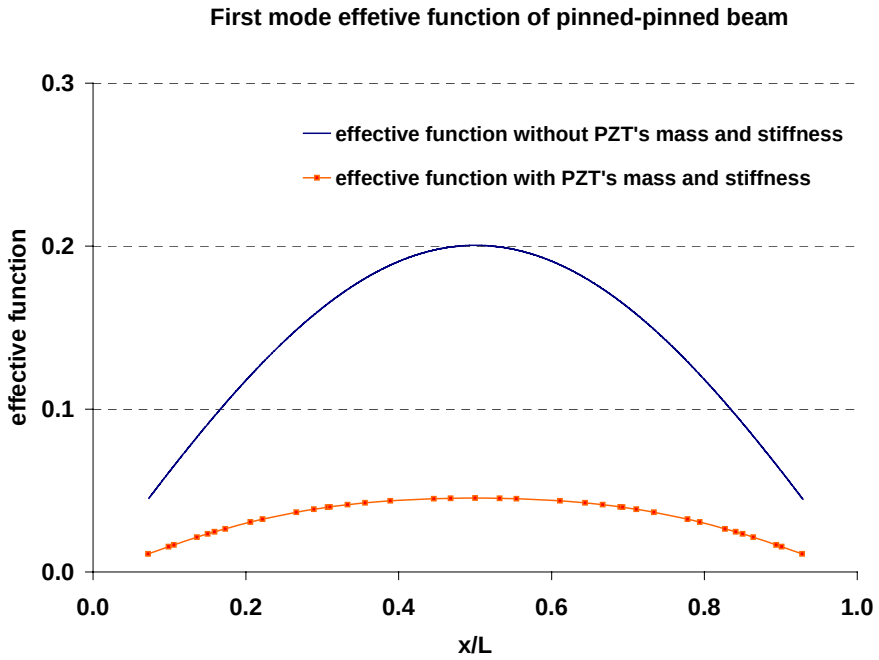

Figure 4-17 Comparison of effective functions of first mode of a pinned-pinned beam w/o PZT patches.

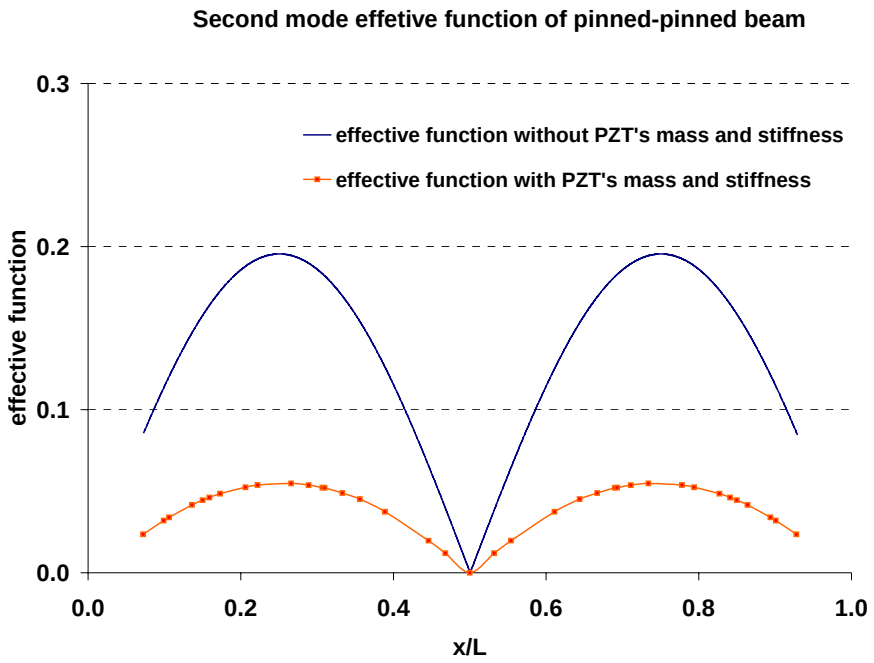

Figure 4-18 Comparison of effective functions of second mode of a pinned-pinned beam w/o PZT patches.

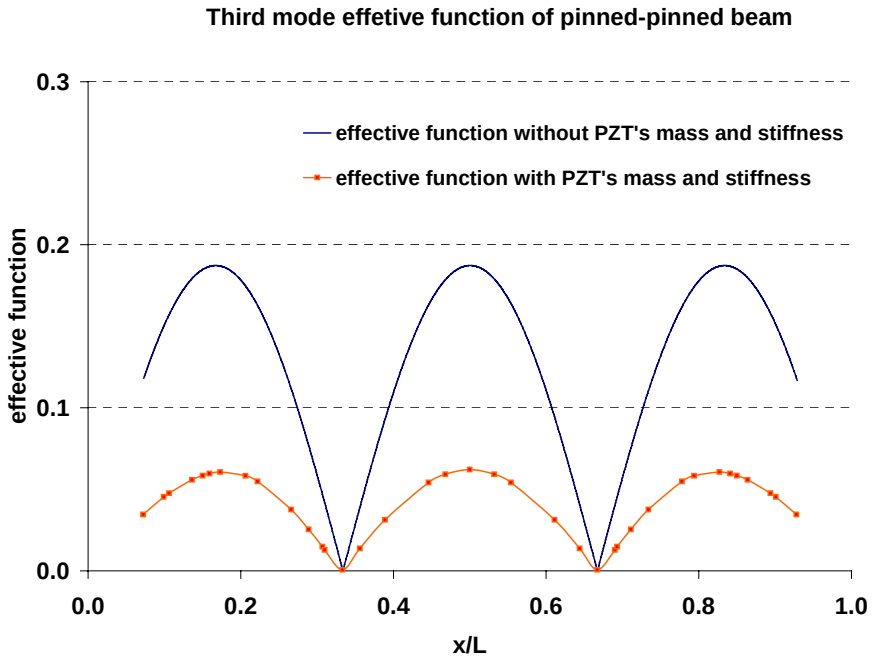

Figure 4-19 Comparison of effective functions of third mode of a pinned-pinned beam w/o PZT patches.

4.3 BEAMS BONDED WITH ONE PZT PATCH

If only one PZT patch is bonded, the beam-actuator system is not straight beam anymore. The neutral line is broken into three sections. The load imposed by the actuator includes a bending moment as well as an axial force. Those effects are negligible, however, if the length of actuator is relatively small compared with that of beam. We can still use stepped beam model to describe the beam-actuator structure as shown in Figure 4-20. In this case, the width of actuator is not required to be same as that of the beam.

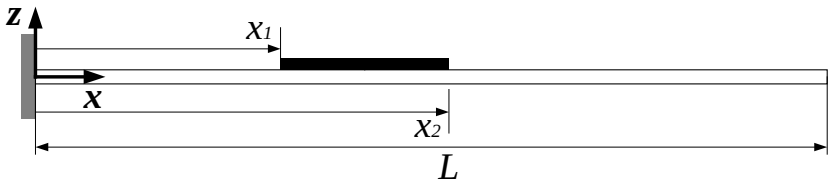

Figure 4-20 The stepped-beam model with one PZT patch.

The governing equations for each section are

$$(EI)_i w_i'''' + (\rho A)_i \ddot{w}_i = 0 \qquad i = 1,2,3$$

where

$$(EI)_1 = E_b I_b = \frac{1}{12} E_b b t_b^3 \tag{4.21a}$$

$$(EI)_2 = E_b I_b + E_a I_a = \frac{1}{12}[E_b b t_b^3 + E_a b_a t_a^3] + \frac{1}{4} E_a b_a t_a (t_b + t_a)^2 \tag{4.21b}$$

$$(EI)_3 = E_b I_b = \frac{1}{12} E_b b t_b^3 \tag{4.21c}$$

$$(\rho A)_1 = \rho_b b t_b \tag{4.21d}$$

$$(\rho A)_2 = \rho_b b t_b + \rho_a b t_a \tag{4.21e}$$

$$(\rho A)_3 = \rho_b b t_b \tag{4.21f}$$

The boundary conditions are same as those of collocate case. Natural frequencies and corresponding modal functions can be obtained from similar procedure. All conclusions discussed in Section 4.2 are applicable in one patch case where the bending moment is updated with

$$M_{\Lambda} = \frac{1}{2} E_a \Lambda b_a (t_a^2 + t_b t_a) = \frac{1}{2} \chi V(t) \tag{4.22}$$

4.4 Experimental Verification of Active Vibration Control of Beams

Figure 4-21 shows the experimental setup of active vibration control of an aluminum cantilever beam conducted in this study. The beam was bonded with a pair of PZT patches as the actuator. A strain gage was mounted near the clamped end for measuring the dynamic response. The material properties and structural dimensions are shown in Table 4-1.

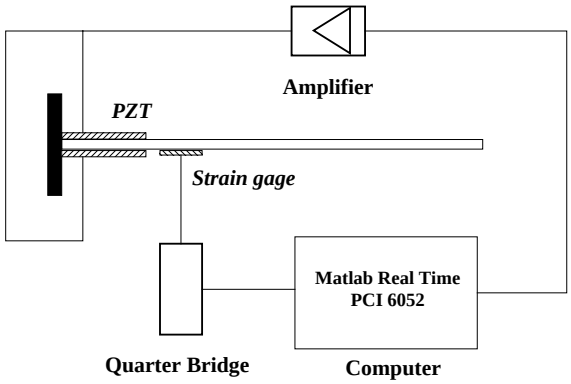

Figure 4-21 Experimental set up of active vibration control of a cantilever beam.

4.4.1 Resonance Excitation

As shown in Figure 4-22, a sinusoidal voltage was applied on PZT pair out of phase. The beam was excited near first natural frequency. The amplitude of the steady response was measured.

First mode excitation:

Excitation voltage $u = 20\sin(2\pi * 30.6t)$

The amplitude of strain response $94\mu\varepsilon$

Theoretical calculation

$$\ddot{q}_1(t) + 2\zeta_1\omega_1\dot{q}_1(t) + \omega_1^2 q_1(t) = b_1 u$$

$$at\ resonance\ \ q_1 = \frac{1}{2\zeta_1}\frac{b_1 u}{\omega_1^2}$$

$$y = \varepsilon(d,t) = c_1 q_1 = \frac{c_1}{2\zeta_1}\frac{b_1 u}{\omega_1^2} = \frac{0.276498*1.762*10^{-2}*20}{2*0.0111*(2*\pi*30.77)^2}$$

$$= 117\mu\varepsilon$$

Matlab simulation shows the strain response is 114 $\mu\varepsilon$

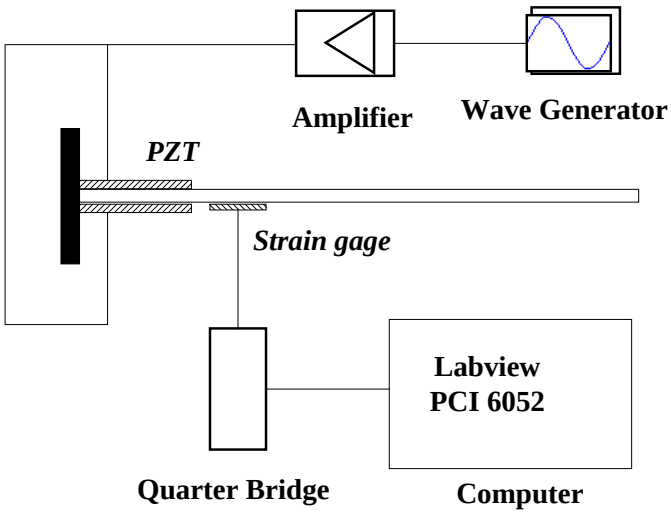

Figure 4-22 Cantilever beam excited by PZT pair

It shows we over estimate the control ability of PZT patches. These may be attributed to the imperfect bonding, viscoelastic behavior of adhesive layers and the piezo-coefficient error. Nevertheless it is appropriate to introduce a factor in our simulation model to represent our system. This factor is $\frac{94}{114} = 82.5\%$.

4.4.2 Measurement of Active Damping Ratio

The same cantilever beam was first displaced at the tip then released. This is to simulate free vibration. A Pentium 4 1.6 GHz PC is used for the data processing and digital control. The controller is designed and implemented using Matlab/Simulink and Real Time Toolbox. The signals are converted from Analog-to-Digital and Digital-to-Analog using a National Instruments data acquisition board (PCI 6052). At first the voltage signal from quarter bridge circuit was transformed into strain. A low pass filter was employed to filter the noise and response from higher modes. Then strain signal was differentiated into strain rate, which is proportional to the velocity. The output voltage signal was generated by multiplying the strain rate with an appropriate gain, so that the output signal was in the range of –10V to +10V. By imposing a saturation block (limits set to -10 and 10), the signal from the controller was guaranteed in the safe range. A linear power amplifier was used to magnify the output signal into an effective voltage command for the PZT actuator. The magnify factor of amplifier was set to 20(maximum), so the aptitude of control voltage applied to PZT was less than 200V, which was within the range of the maximum permissible actuator voltage 254V. Figure 4-23 shows the block diagram of velocity feedback control. It should be noted that the low pass filter will introduce a phase lag which will degrade the control efficiency. In our experiments the

cut off frequency was set to 35Hz, the phase lag happened to be 180 degree. This can be counteracted by switch the proportional gain.

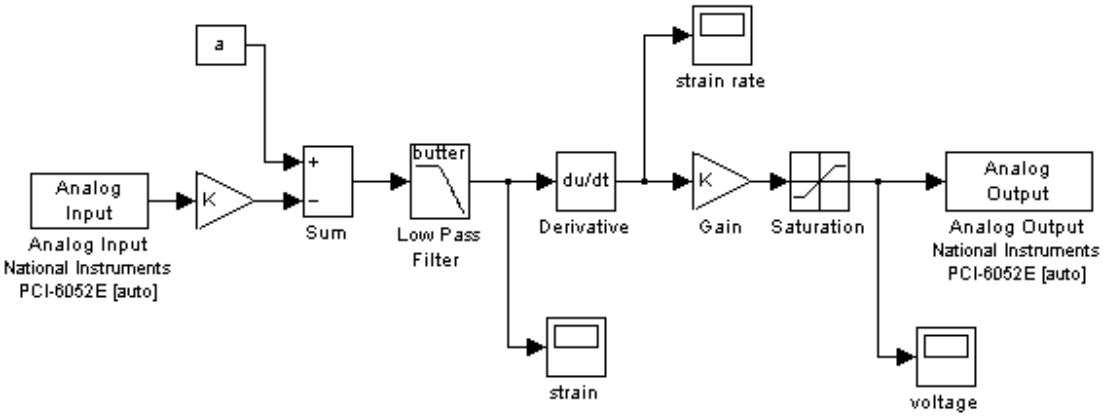

Figure 4-23 Block diagram of velocity feedback controller

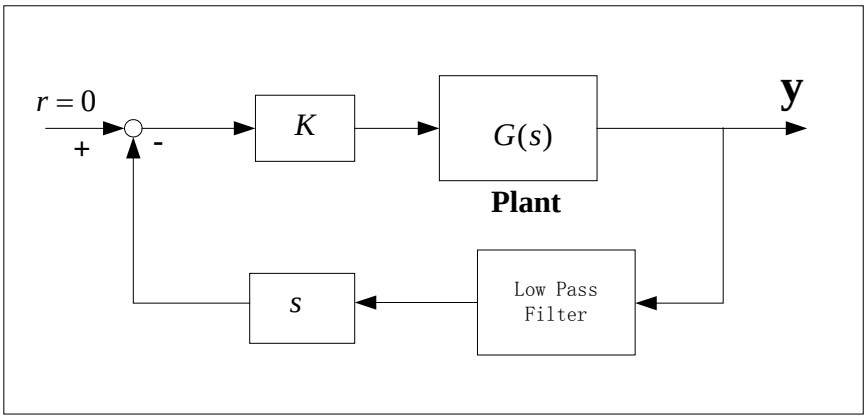

Figure 4-24 Velocity feedback controller

When the beam is in free vibration, the first mode is dominating the oscillation. Since the response from higher modes is filtered, we can consider only first mode's contribution. From the result derived above, we have

$$w(x,t) = \phi_1(x) q_1(t)$$

$$\ddot{q}_1(t) + 2\zeta_1 \omega_1 \dot{q}_1(t) + \omega_1^2 q_1(t) = \frac{\chi[\phi_1'(x_2) - \phi_1'(x_1)]}{\rho A} V(t)$$

When apply velocity feedback control algorithm, the control voltage is

$$V(t) = -k\dot{q}_1(t)$$

If we ignore the modification of structure by attaching PZT patch, we can use uniform beam mode to calculate the active damping ratio as shown in Equation (4-10).

On the other side, when the mass and stiffness of PZT patch are taken into consideration, the stepped beam mode predicts the active damping ratio as Equation (4-15).

Our proposed mode to estimate the active damping ratio as following:

$$(\zeta_a)_1 = \frac{E_b I_b}{E_b I_b + E_a I_a} * k\chi \frac{\phi_1'(x_2) - \phi_1'(x_1)}{2\omega_1 \rho A}$$

where the natural frequency and modal function are from uniform beam mode.

At first, the gain was set to zero. The beam-actuator system was vibrating with the inherent structural damping, as shown in Figure 4-25. The damping ratio was calculated by logarithmic decrement method. For this test, it is found to be 0.0111.

The gain was then set to 1000. A free vibration test was again conducted with the result shown in Figure 4-25. The damping ratio with the active vibration control was estimated as 0.1085. The difference between the damping ratios with and without PZT control: 0.097 (=0.1085–0.0111) is the experimental active damping ratio. The input voltage applied on the PZT pair in the experiment was used in the simulation as shown in Figure 4-26. The response of the beam in the simulation indicates the active damping ratio is 0.103 as shown in Figure 4-27.

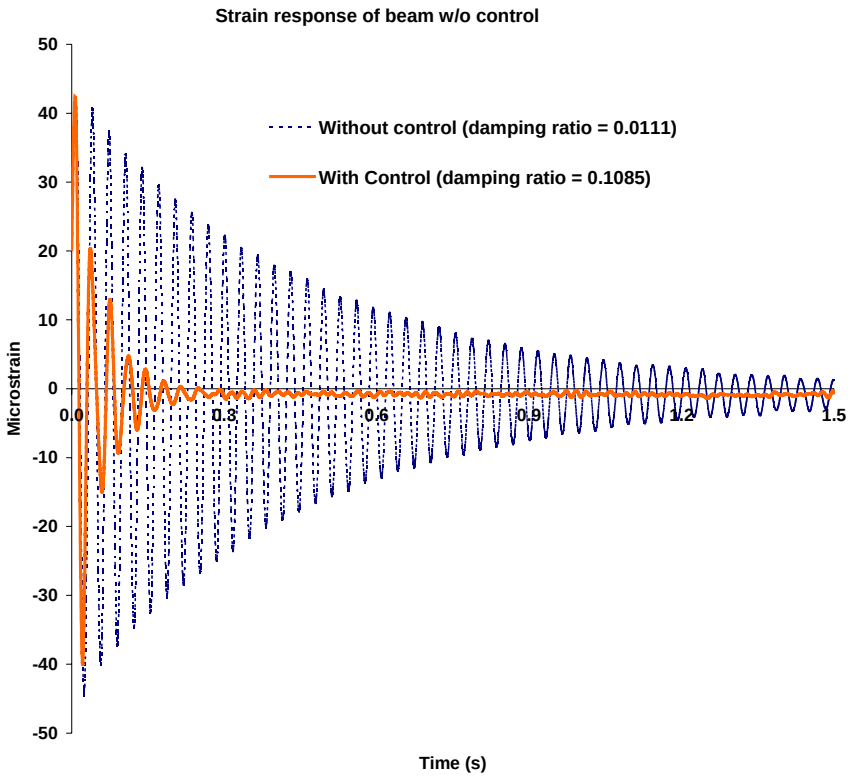

Figure 4-25 Vibration of a cantilever beam w/o control.

The theoretical active damping ratio can be determined by uniform beam mode is 0.242, 0.103 by stepped beam mode, 0.09 by our proposed mode in this study. In comparison with the estimated damping ratio obtained by these three modes, the damping ratio evaluated by the stepped beam mode is very close to the experimental results, our proposed mode is a good approximation of stepped beam mode. The uniform beam modal, as predicted, overestimates the PZT control ability.

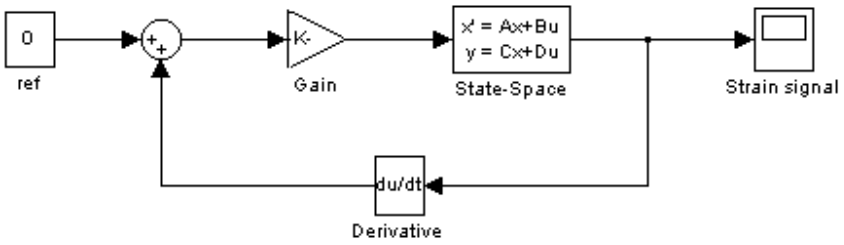

Figure 4-26 Simulink block diagram

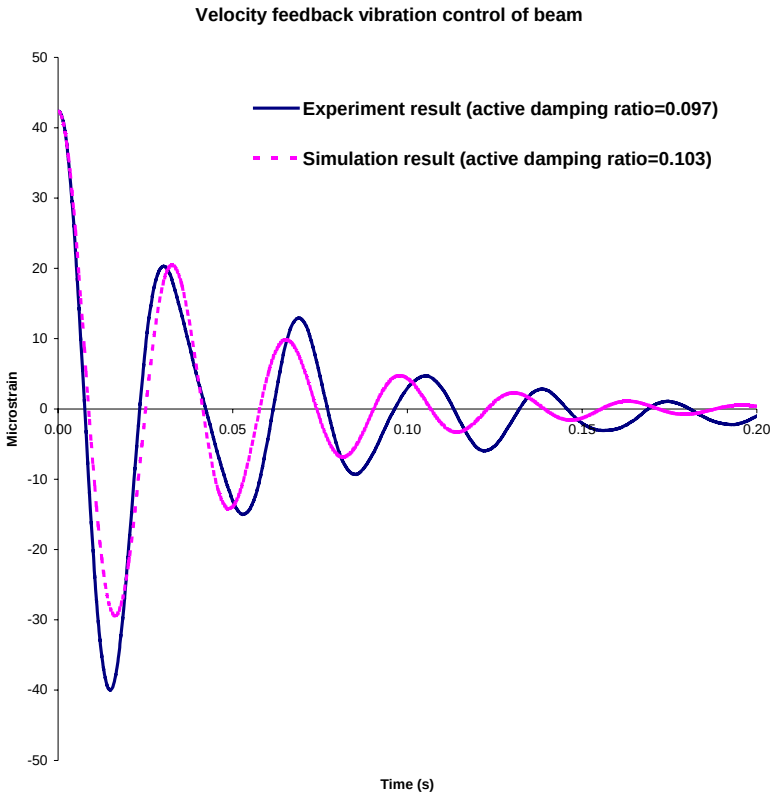

Figure 4-27 Velocity Feedback Control Simulink Result

Next the active vibration control was conducted for a cantilever beam subject to a special type of forced vibration: base-excitation vibration. The experimental setup is shown in Figure 4-28. The beam was fixed on the top of a shaker, which was vibrating at constant amplitude near the first natural frequency of the beam-actuator system.

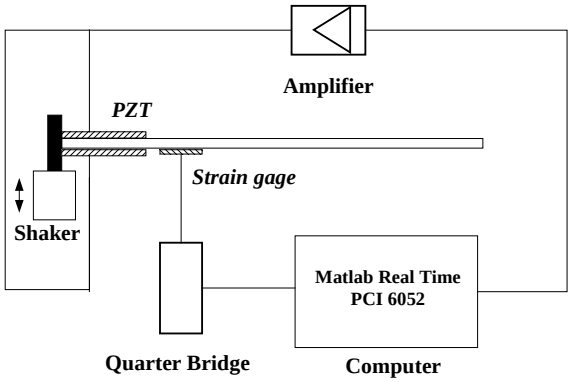

Figure 4-28 Experimental setup of active vibration control of a cantilever beam subject to base excitation.

As expected, the strain gage mounted near the clamped end recorded a constant amplitude strain signal (45.5 microstrains). The same controller as above was then applied. The ensuing strain oscillation suddenly drops to 4.26 microstrains, indicating about 90% of vibration suppression due to this control mechanism, as shown in Figure 4-29.

The stead strain response to base excitation is

$$y = \varepsilon(d,t) = c_1 q_1 = \frac{c_1}{2\zeta_1}\frac{b_1 u}{\omega_1^2}$$

The amplitude of strain response is proportional to damping ratio. We have

$$\frac{amp(\varepsilon_{before})}{amp(\varepsilon_{after})} = \frac{45.5}{4.26} = 10.7 = \frac{\zeta_{after}}{\zeta_{before}}$$

We know the inherent damping

$$\zeta_{before} = 0.0111$$
$$\Rightarrow \zeta_{after} = 0.1186$$
$$\zeta_{active} = 0.108$$

The active damping ratio from base excitation is close to that from free vibration test. Both are consistent with theoretic result.

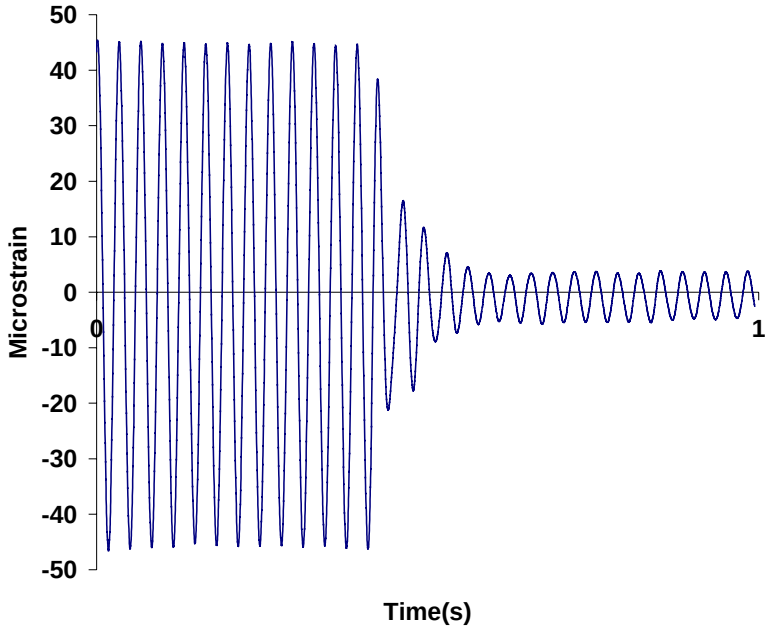

Figure 4-29 Verification of the effect of active vibration control using a PZT patch.

4.5 ACTIVE VIBRATION CONTROL OF PLATES USING PZT PATCHES AS ACTUATORS

From the studies of control authority of PZT patches in beam vibration, we know control efficiency is degraded substantially because of the change of modal shape functions caused by the presence of PZT patches. However, it may be very tedious, if not impossible, to calculate all the modal shape functions of a plate-actuator structure. This is especially true since numerous cases need to be taken into consideration when one intends to find the optimal positions or dimensions of PZT patches. These difficulties may be overcome if one uses the similar model proposed for beam vibration control (see Chapter 4.3). In this study, we will compute the control authority of PZT patches, assuming the mass and stiffness of the actuators are negligible. When considering the effect of PZT patches on the structural configuration, we can multiply the results obtained

from conventional plate theory without PZTs with the factor that will be defined in this chapter to get an approximate control authority.

4.5.1 Basic Equations

Consider a thin rectangular plate bonded with a pair of rectangular piezoelectric patches (Figure 4-30). Assume that the piezoelectric elements are perfectly bonded, and the effects of the bonding layers on the stiffness and mass of the plate-actuator system can be ignored.

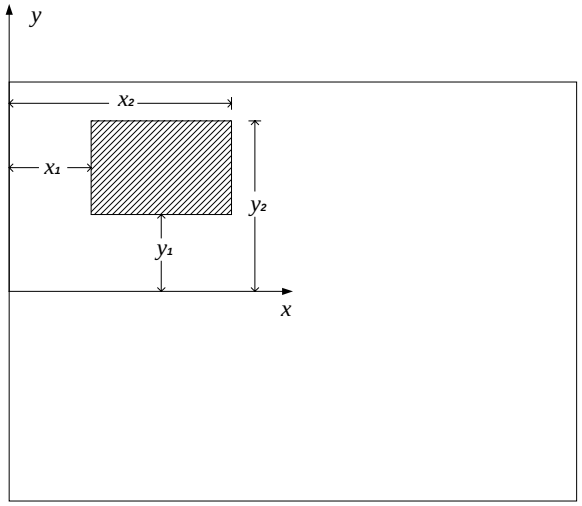

Figure 4-30 A PZT-patch pair bonded to a thin plate.

The free body of a typical plate element is shown in Figure 4-31. Here M_x and M_y are the bending moment intensities along the x- and y-directions, respectively; M_{xy} the twisting moment intensity; Q_x and Q_y the transverse shear force intensities along the x- and y-directions, respectively; $q(x,y)$ the external force intensity; m_x and m_y the external bending moment intensities along the x- and y-directions, respectively; and m_{xy} the external twisting moment intensity. In this study, it is assumed that there are no in-plane forces.

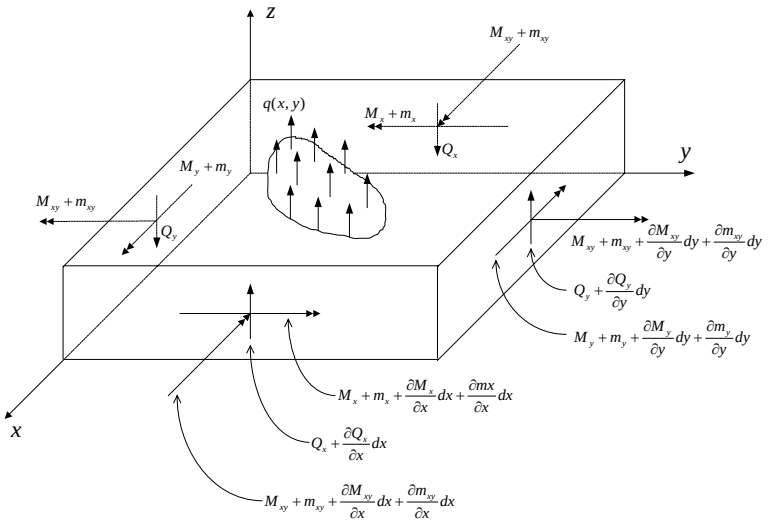

Figure 4-31 The free body of a plate element.

Summing all forces in the *z*-direction yields the following equation:

$$\frac{\partial Q_x}{\partial x}+\frac{\partial Q_y}{\partial y}+q=\rho h\ddot{w} \tag{4.23}$$

Similarly, summing all moments about the *x*- and *y*-directions will yield the following equations:

$$\begin{aligned} Q_x-\frac{\partial M_x}{\partial x}-\frac{\partial M_{xy}}{\partial y}-\frac{\partial m_x}{\partial x}-\frac{\partial m_{xy}}{\partial y}&=\frac{\rho h^2}{12}\frac{\partial^3 w}{\partial x\partial t^2}\approx 0\\ Q_y-\frac{\partial M_{xy}}{\partial x}-\frac{\partial M_y}{\partial y}-\frac{\partial m_{xy}}{\partial x}-\frac{\partial m_y}{\partial y}&=\frac{\rho h^2}{12}\frac{\partial^3 w}{\partial y\partial t^2}\approx 0 \end{aligned} \tag{4.24}$$

where the terms on the right-hand side are the rotary inertias of the element. They can be neglected if only the low frequencies are the concern.

Apply the classic plate theory, which assume normal to the midplane of the undeformed plate remains straight and normal to the midplane during deformation, we have

$$
\begin{aligned}
M_x &= -D\left(\frac{\partial^2 w}{\partial x^2} + \nu \frac{\partial^2 w}{\partial y^2}\right) \\
M_y &= -D\left(\frac{\partial^2 w}{\partial y^2} + \nu \frac{\partial^2 w}{\partial x^2}\right) \\
M_{xy} &= -D(1-\nu)\frac{\partial^2 w}{\partial x \partial y}
\end{aligned}
\tag{4.25}
$$

where $D = \dfrac{Eh^3}{12(1-\nu^2)}$

The plate bonded with PZT patches is not homogeneous, however, we can always find the equivalent bending stiffness $D(x, y)$. Substituting the transverse shears and the bending moments in Equations (4.24) and (4.25) into Equation (4.23), we get

$$
\begin{aligned}
\frac{\partial Q_x}{\partial x} + \frac{\partial Q_y}{\partial y} = &\frac{\partial}{\partial x}\left(\frac{\partial M_x}{\partial x} + \frac{\partial M_{xy}}{\partial y}\right) + \frac{\partial}{\partial y}\left(\frac{\partial M_{xy}}{\partial x} + \frac{\partial M_y}{\partial y}\right) \\
&+ \left(\frac{\partial^2 m_x}{\partial x^2} + 2\frac{\partial^2 m_{xy}}{\partial x \partial y} + \frac{\partial^2 m_y}{\partial y^2}\right)
\end{aligned}
\tag{4.26a}
$$

$$
\begin{aligned}
&\nabla^2(D\nabla^2 w) - (1-\nu)\left(\frac{\partial^2 D}{\partial y^2}\frac{\partial^2 w}{\partial x^2} - 2\frac{\partial^2 D}{\partial x \partial y}\frac{\partial^2 w}{\partial x \partial y} + \frac{\partial^2 D}{\partial x^2}\frac{\partial^2 w}{\partial y^2}\right) \\
&\quad - \left(\frac{\partial^2 m_x}{\partial x^2} + 2\frac{\partial^2 m_{xy}}{\partial x \partial y} + \frac{\partial^2 m_y}{\partial y^2}\right) - q(x, y) + \rho h \ddot{w} = 0
\end{aligned}
\tag{4.26b}
$$

where $\nabla^2 = \dfrac{\partial^2}{\partial x^2} + \dfrac{\partial^2}{\partial y^2}$. We can see it is extremely difficult to solve Equation (4.26) analytically.

However, if the PZT patches are relatively thin, their mass and stiffness can be ignored. $q(x, y)$ is usually zero when the plate is actuated by PZT patches. The equivalent bending stiffness D will be a constant. The differential equation of motion of such plate can be described as

$$D\nabla^4 w + \rho h\ddot{w} = \frac{\partial^2 m_x}{\partial x^2} + 2\frac{\partial^2 m_{xy}}{\partial x \partial y} + \frac{\partial^2 m_y}{\partial y^2} \tag{4.27}$$

where the external moment intensities $m(x, y, t)$ is the bending moment distribution induced by the actuator elements, which can be expressed as:

$$m_{xy} = 0$$

$$m_x = m_y = \chi V(t)[H(x-x_1) - H(x-x_2)][H(y-y_1) - H(y-y_2)]$$

Here $V(t)$ is the input voltage applied on the PZT patches, $\chi = E_a(t_a + t_p)d_{31}$ is the factor related to actuator ability, and $H(x)$ is the Heavside function.

Applying mode summation method, we can represent the solution, $w(x, y, t)$, in terms of normal modes, $\phi_n(x, y)$, (n = 1,2,3,…) as:

$$w(x, y, t) = \sum_{n=1}^{\infty} \phi_n(x, y) q_n(t)$$

$$\ddot{q}_n(t) + \omega_n^2 q_n(t) = \frac{1}{\rho h} \iint \phi_n(x, y)\left(\frac{\partial^2 m_x}{\partial x^2} + \frac{\partial^2 m_y}{\partial y^2}\right) dxdy$$

$$\iint \phi_n(x, y)\left(\frac{\partial^2 m_x}{\partial x^2} + \frac{\partial^2 m_y}{\partial y^2}\right) dxdy = \chi V(t) \iint \phi_n(x, y)[H(y-y_1) - H(y-y_2)] \frac{\partial^2 [H(x-x_1) - H(x-x_2)]}{\partial x^2} dxdy$$
$$+ \chi V(t) \iint \phi_n(x, y)[H(x-x_1) - H(x-x_2)] \frac{\partial^2 [H(y-y_1) - H(y-y_2)]}{\partial y^2} dxdy$$

$$\iint \phi_n(x, y)[H(x-x_1) - H(x-x_2)] \frac{\partial^2 [H(y-y_1) - H(y-y_2)]}{\partial y^2} dxdy$$
$$= \int_{x_1}^{x_2} \left(\frac{\partial \phi_n(x, y_2)}{\partial y} - \frac{\partial \phi_n(x, y_1)}{\partial y}\right) dx$$

$$\iint \phi_n(x, y)[H(y-y_1) - H(y-y_2)] \frac{\partial^2 [H(x-x_1) - H(x-x_2)]}{\partial x^2} dxdy$$
$$= \int_{y_1}^{y_2} \left(\frac{\partial \phi_n(x_2, y)}{\partial x} - \frac{\partial \phi_n(x_1, y)}{\partial x}\right) dy$$

So we have

$$\ddot{q}_n(t)+\omega_n^2 q_n(t)=\frac{\chi V(t)}{\rho h}[\int_{x_1}^{x_2}(\frac{\partial\phi_n(x,y_2)}{\partial y}-\frac{\partial\phi_n(x,y_1)}{\partial y})dx + \int_{y_1}^{y_2}(\frac{\partial\phi_n(x_2,y)}{\partial x}-\frac{\partial\phi_n(x_1,y)}{\partial x})dy] \tag{4.28}$$

It is appropriate to introduce the internal damping factor ζ_n

$$\ddot{q}_n(t)+2\zeta_n\omega_n\dot{q}_n(t)+\omega_n^2 q_n(t)= \frac{\chi V(t)}{\rho h}[\int_{x_1}^{x_2}(\frac{\partial\phi_n(x,y_2)}{\partial y}-\frac{\partial\phi_n(x,y_1)}{\partial y})dx+\int_{y_1}^{y_2}(\frac{\partial\phi_n(x_2,y)}{\partial x}-\frac{\partial\phi_n(x_1,y)}{\partial x})dy] \tag{4.29}$$

The terms on the right-hand side stands for the modal control authority.

When the thickness of the PZT pairs is comparable with the plate thickness, the mass and stiffness of actuators can no longer be ignored. Using the similar procedure used in chapter 4.2, we find the real control authority is degraded to

$$\frac{\chi V(t)}{\rho h}[\frac{E_pI_p}{E_pI_p+\frac{b_a}{b_p}E_aI_a}\int_{x_1}^{x_2}(\frac{\partial\phi_n(x,y_2)}{\partial y}-\frac{\partial\phi_n(x,y_1)}{\partial y})dx+\frac{E_pI_p}{E_pI_p+\frac{l}{L}E_aI_a}\int_{y_1}^{y_2}(\frac{\partial\phi_n(x_2,y)}{\partial x}-\frac{\partial\phi_n(x_1,y)}{\partial x})dy]$$

where $\frac{b_a}{b_p}$, $\frac{l}{L}$ are the width ratio and the length ratio of the actuators and the plate respectively. Similar optimization procedure can then be carried out to investigate the active control of plate vibration.

4.5.2 Optimization Problems in Active Vibration Control of Plates Using PZT Patches as Actuators

Optimal positions of actuators pair are obtained by maximizing the mode control authority. An aluminum cantilever plate excited by a pair of PZT patches is studied in this paper. The PZT pair is used as actuators. The material properties and structural dimensions are shown in Table 4-2.

Table 4-2 Material properties and structural dimensions of the plate.

E_p	72 GPa
E_a	66 GPa
ρ_p	2900 $kg.m^{-3}$
ρ_a	7800 $kg.m^{-3}$
t_p	0.06 inch
t_a	0.02 inch
b_p	4 inch
b_a	0.5 inch
l	1.25 inch
L	4 inch

We define the n[th] modal control index as

$$\Theta = \frac{E_p I_p}{E_p I_p + \frac{b_a}{b_p} E_a I_a} \int_{x_1}^{x_2} \left(\frac{\partial \phi_n(x, y_2)}{\partial y} - \frac{\partial \phi_n(x, y_1)}{\partial y}\right) dx + \frac{E_p I_p}{E_p I_p + \frac{l}{L} E_a I_a} \int_{y_1}^{y_2} \left(\frac{\partial \phi_n(x_2, y)}{\partial x} - \frac{\partial \phi_n(x_1, y)}{\partial x}\right) dy$$

The control index Θ is calculated while the position of actuators was varying. Each time the PZT pair is mounted at 0.25 inch apart (horizontal or vertical) from the last position. The cantilever plate is fixed along y-axis. The control indexes of first three modes from three theoretic models (uniform plate model, FEM model and combination model) are shown in Figure 4-32 – Figure 4-40. For the n[th] mode, the optimal position to attach the PZT pair is where the control index Θ gets its peak value.

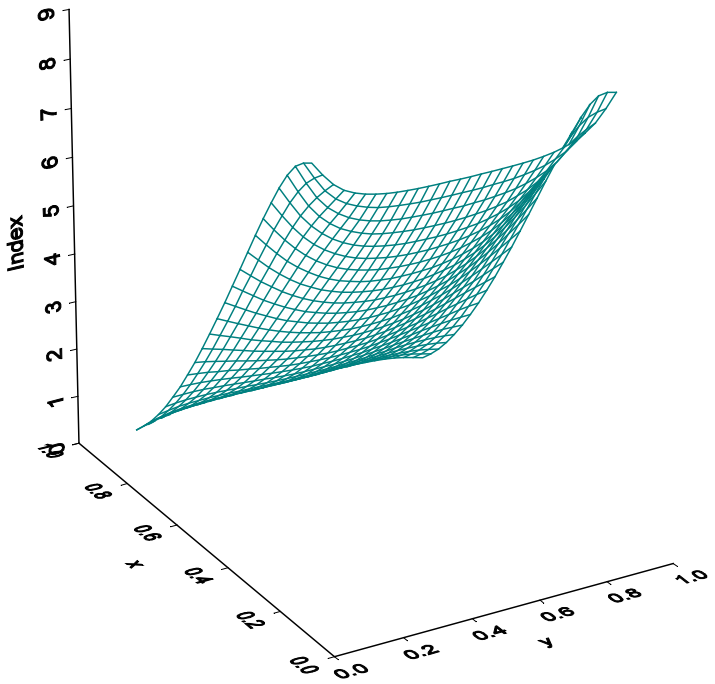

Figure 4-32 Position optimization for mode 1 (uniform plate model)

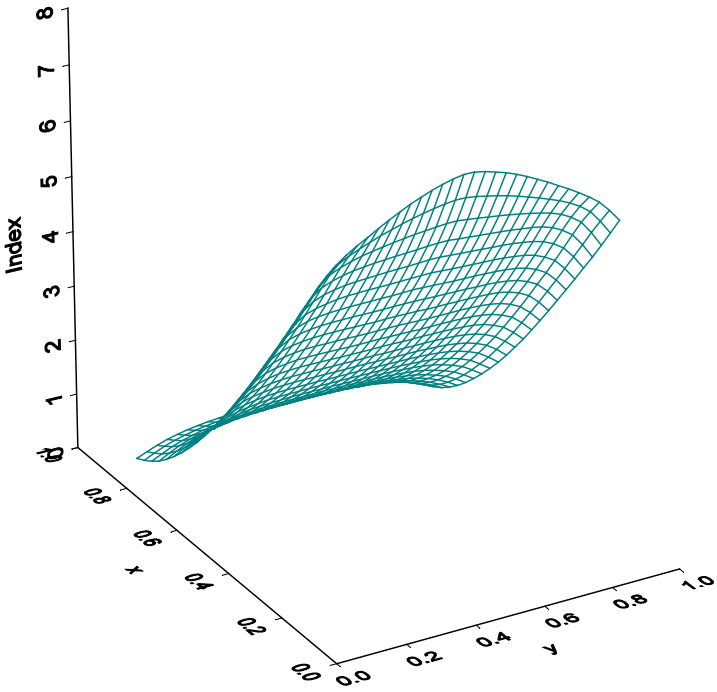

Figure 4-33 Position optimization for mode 1 (FEM model)

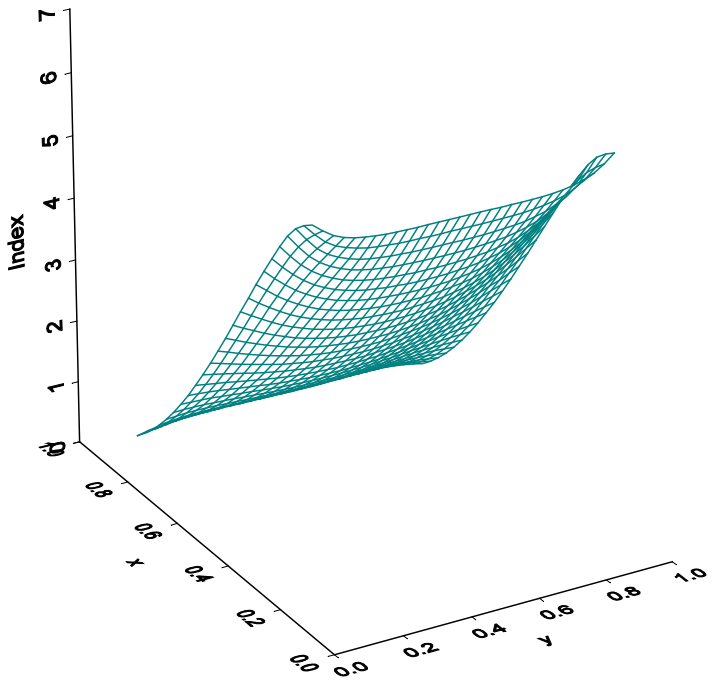

Figure 4-34 Position optimization for mode 1 (combination model)

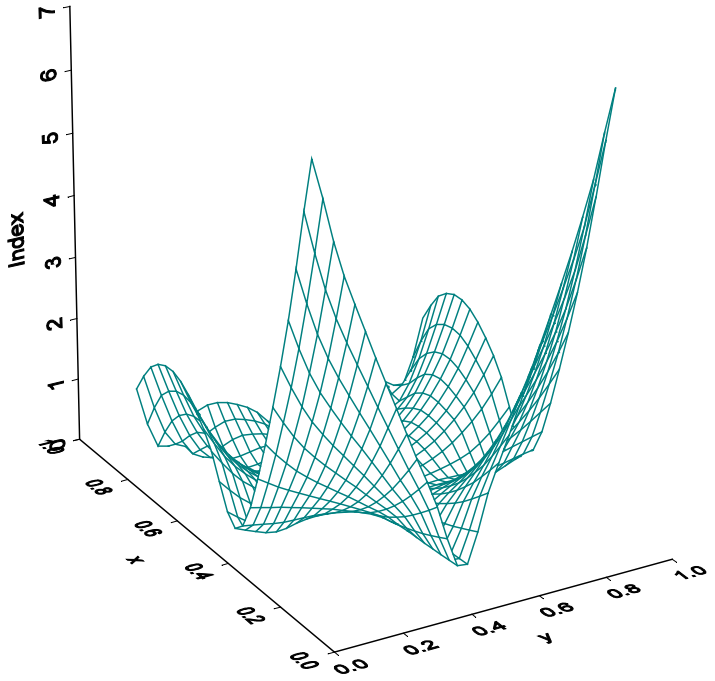

Figure 4-35 Position optimization for mode 2 (uniform plate model)

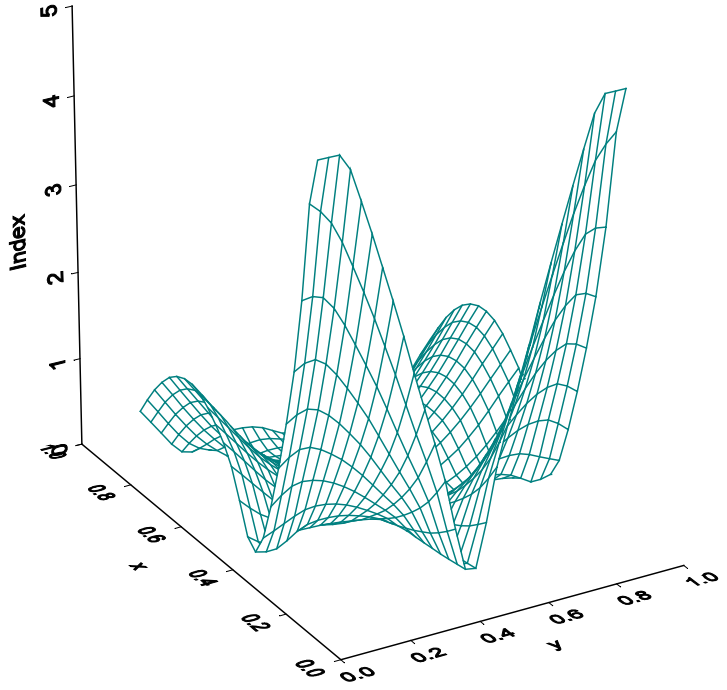

Figure 4-36 Position optimization for mode 2 (FEM model)

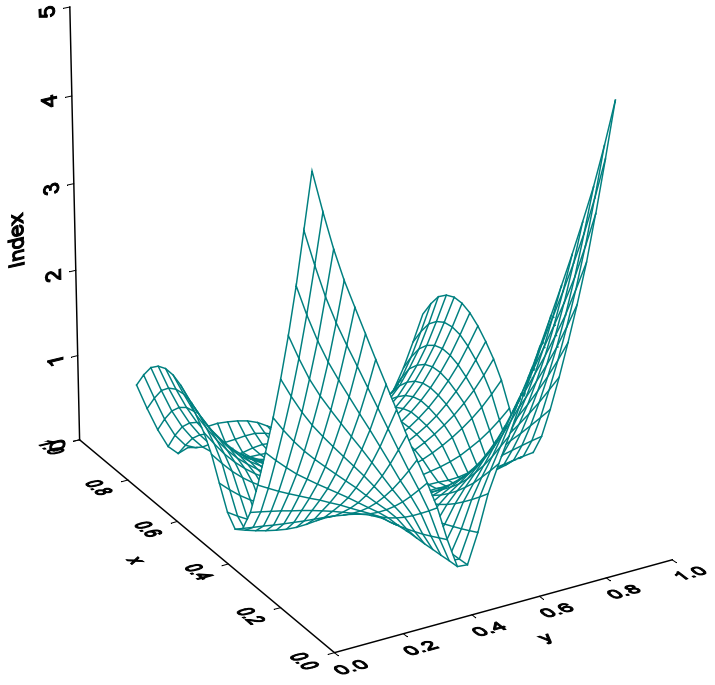

Figure 4-37 Position optimization for mode 2 (combination model)

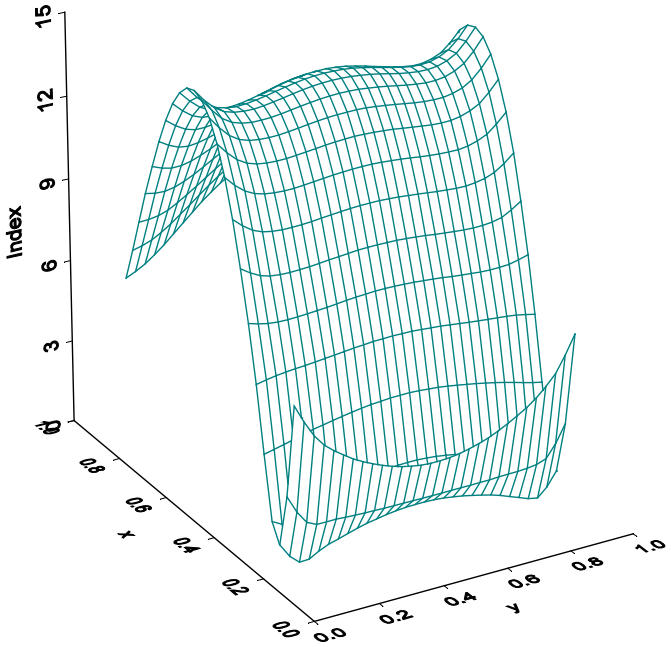

Figure 4-38 Position optimization for mode 3 (uniform plate model)

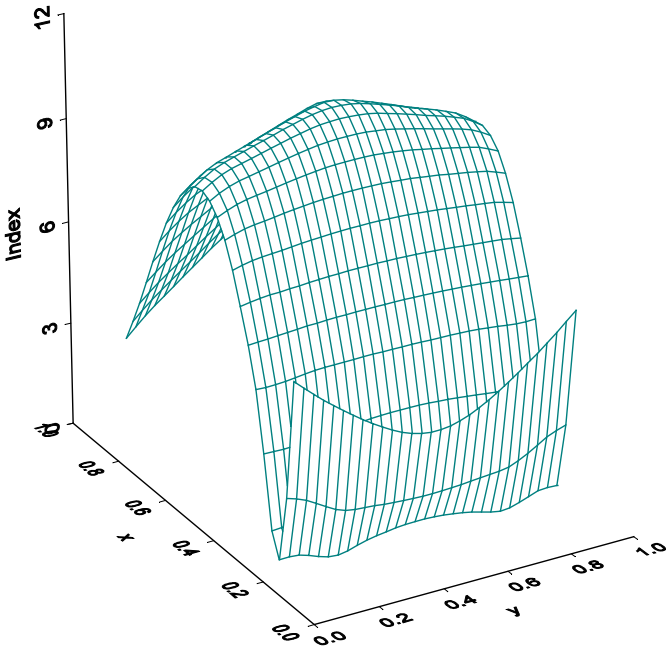

Figure 4-39 Position optimization for mode 3 (FEM model)

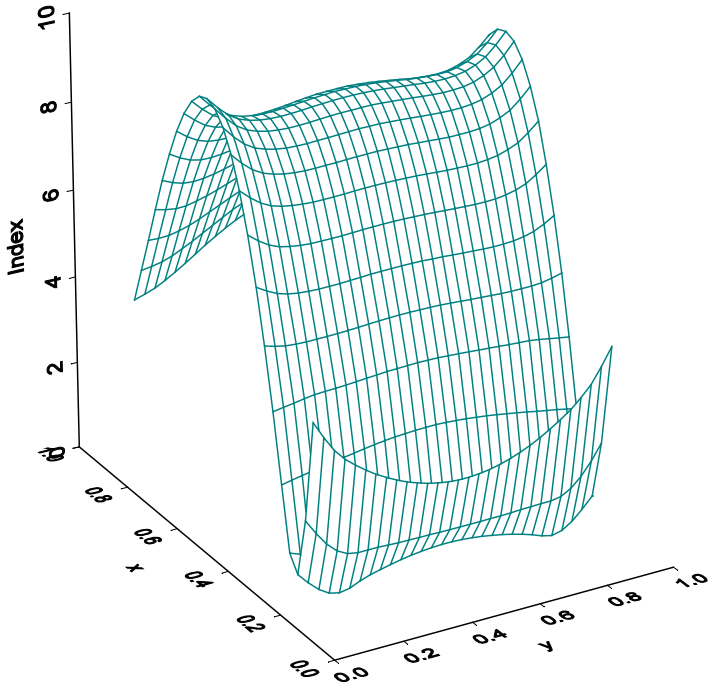

Figure 4-40 Position optimization for mode 3 (combination model)

We can see that the uniform plate model, which ignores the effects of patches, overestimates the control authority of actuators; while the combination model we propose presents a low limit of the real control ability of actuators. The results from combination model are closer to the FEM results than from uniform plate model. Considering the bonding between plates and PZT patches can not be perfect, the lower limit of control ability makes more sense to engineers. The control authority calculated from uniform beam model always larger than the actual value. In other words, the structural modification caused by attaching PZT patches degrades the control ability. Although these degradations are sometimes significant, the optimal positions are not sensitive to these structural alterations.

4. 5. 3 Conclusions

In this study the position optimization of PZT actuators in active vibration control of plates are explored. A pair of PZT patches is surface-bonded as actuators. At first, uniform plate model, which ignores the mass and stiffness of PZT patches, is used to estimate the control authority. Then finite element method is applied when the effect of patches is taken into consideration. It is found that the structural modification caused by attaching PZT patches may degrade the control ability. Base on those two models, a combination model is presented. This combination model, while taking advantage of simplicity of the uniform plate model, yet accounts for the effect of PZT patch's inertia and stiffness.

A numerical example is conducted to verify this combination model. It is found that the uniform plate model, which ignores the effects of patches, overestimates the control authority of actuators; while the combination model we propose presents a better estimation of the real control ability of actuators. It is also found that the structural modification caused by attaching PZT patches may degrade the control ability while the optimal positions are not sensitive to these structural alterations

CHAPTER 5: CONCLUSIONS AND RECOMMENDATIONS FOR FUTURE STUDIES

5.1 SUMMARY

In this dissertation we investigated the linear and nonlinear vibration and control of cantilever beams and plates subjected to transverse harmonic excitations. In the vibration part, we focused on the linear and nonlinear responses of the beams made of Fiber Metal Laminates (FMLs). Euler-Bernoulli beam theory and the half power method were used to investigate the dynamic Young's modulus and linear viscous damping in the linear vibration while the excitation levels were kept low. It was found that compared to aluminum alloys, the effective Young's moduli of fiber-metal laminates are lower and are approximately proportional to the aluminum content. Young's moduli were almost constant within an experimental excitation frequency range of 0 to 5,000 Hz. An inextensible beam model with nonlinear damping was applied to explore the nonlinearities of cantilever beams. Approximate solutions were obtained by solving an integro-differential equation via Multiple Scales Method and Harmonic Balance Method. For the single-mode response, a large discrepancy in nonlinearity coefficient was found between theoretical and experimental results. For different excitation levels, a small variation in the linear natural frequency was detected. A beam model with a nonlinear spring-hinged end and the other end free was then applied to tune the inextensible cantilever beam theory. While this modified mode could reasonably explain the natural frequency difference, its ability of covering the discrepancy in nonlinearity coefficient was limited.

In the control part, we studied the efficiency problems of using PZT patches in negative feedback control of aluminum beams and plates. The PZT patches were surface-

bonded as actuators and strain gages were used as sensors. The uniform beam model was applied when the mass and stiffness of PZT patches were ignored. The stepped beam model was then derived to describe the beam-actuator structure when the effect of patches was taken into consideration. It was found that the use of PZT patches for active vibration control might degrade the control efficiency by modifying the configuration of the structure. The optimal positions from stepped beam model were similar as those from the uniform beam model. The ratio of control efficiency from the stepped beam model to that from the uniform beam model was associated with material properties and structural dimensions. Based on those findings a modified model to estimate the control efficiency was presented and the optimal thickness of PZT patches was obtained. This modified model, while taking advantage of simplicity of the uniform beam model, accounts for the effect of PZT patch's inertia and stiffness. The efficiency estimate technique was confirmed both numerically and experimentally. By applying the proposed estimate method, the degraded control efficiency can be obtained without much difficulty. The proposed method is based on attaching a pair of PZT patches. However, it can be easily extended to cases of a single patch as well as multiple patches by superimposing the efficiency functions accordingly. Furthermore we extended our control efficiency estimation method to the vibration control of plates. Finite element method was adopted when the effect of patches was taken into consideration. Optimal positions of an actuator pair were obtained by maximizing the mode control authority. While the optimal positions were not sensitive to these structural alterations, the control ability of PZT patches was reduced substantially as expected. Our proposed efficiency estimation method works very well for the vibration control of plates.

5.2 CONTRIBUTIONS

- Extensively studied the dynamical properties of fiber-metal laminates made from glass-fiber reinforced (GLARE) and aramid-fiber reinforced (ARALL) laminates interlaced with aluminum layers.
- Fully investigated the accuracy of the inextensible beam model in the large vibration of cantilevered beams.
- Introduced the viscoelastic damping together with linear damping and nonlinear damping in the inextensible beam model.
- Evaluated the effectiveness and limitation of the beam model with a nonlinear spring-hinged end and the other end free.
- Discovered the degradation of control efficiency of actuators because of the structural alteration caused by attaching the PZT panels.
- Proposed a control efficiency estimate technique. The technique greatly simplifies the procedure of dimension and position optimization of actuators.
- Obtained the optimal positions and thickness of PZT pairs for a particular beam and plate structure respectively.

5.3 RECOMMENDATION FOR FUTURE STUDIES

The nonlinearity is inherently a complicate and case-related topic. Much more experimental works are needed to confirm the effectiveness of the inextensible beam model proposed by Crespo da Silva and Glynn [96,97]. The nonlinearity coefficients obtained from experiments are not consistent with the theoretical results based on this model. Although this could be explained by the fact that there are other possible sources

of nonlinearity in our specimens such as existing pre-damage, non-ideal clamping and skewed fixture etc., there remain a lot of issues for improvement in the model itself.

The current studies are limited to the linear vibration control of cantilever beam on the basis of single input and single output (SISO). It could be interesting to conduct some experiments based on the multi-input multi-output (MIMO) scheme. In the meantime it is always challenging to implement robust and optimal control algorithms to subside the nonlinear vibration under large external excitations. The similar control efficiency estimate method based on the nonlinear vibration of structure could also be exploited.

APPENDIX A: INTRODUCTION TO PZT

PZT is the acronym for lead zirconate titanate, which is a wildly used piezoelectric ceramic material. Piezoelectricity is a coupling phenomenon between mechanical and electrical behaviors in certain kind of materials. These materials induce an electrical charge when mechanically deformed (direct effect), and physically deform in the presence of an electric field (converse effect). There are a wide variety of materials that exhibit this phenomenon to some degree, including natural quartz crystals, semi-crystalline polyvinylidene polymers, polycrystalline piezoceramics, and even human bone (Piezo System Catalog).

Piezoelectricity was discovered by Jacques and Pierre Curie in the 1880s. They found some crystals (tourmaline, quartz, topaz, cane sugar and Rochelle salt) generated surface charges when subjected to mechanical stress. The Curie brothers asserted there was an inner relationship between the electrical effects and mechanical stress in a given crystal. However they did not predict that crystals exhibiting the direct piezoelectric effect (electricity from applied stress) would also exhibit the converse piezoelectric effect (stress in response to applied electric field). This property was mathematically deduced from fundamental thermodynamic principles by Lippmann in 1881. Since then, the core of piezoelectric theory was established. Much more work was done to make this core grow into a versatile and complete framework in the following 30 years. Twenty natural crystal classes were found existing piezoelectric effects, and all 18 possible macroscopic piezoelectric coefficients were defined accompanying a rigorous thermodynamic treatment of crystal solids using appropriate tensorial analysis.

This natural piezoelectricity is due to the spontaneous separation of charge within certain crystal structures under the right conditions. This phenomenon, referred to as spontaneous polarization, is caused by a displacement of the electron clouds relative to their individual atomic centers. Such a situation produces an electric dipole.

Between 1920 and 1940 the success of sonar stimulated intense development activity on all kinds of piezoelectric devices, both resonating and non-resonating. However, the materials available at the time often limited device performance and certainly limited commercial exploitation.

In the second half of 20th century metal oxide-based piezoelectric ceramics (called piezoceramics) enabled designers to employ the piezoelectric effect and the inverse piezoelectric effect in many new applications. These materials generally are physically strong and chemically inert, and they are relatively inexpensive to manufacture. The composition, shape, and dimensions of a piezoelectric ceramic element can be tailored to meet the requirements of a specific purpose.

Piezoceramics materials mainly include the barium titanate family and the lead zirconate titanate family (PZT). Barium titanate piezoceramics were first developed and later the lead zirconate titanate piezoceramics were created. The latter exhibits greater sensitivity and higher operating temperatures, relative to ceramics of other compositions. The PZT materials currently are the most widely used piezoelectric ceramics.

Piezoelectric ceramics have crystal microstructures. Each crystal consists of a small, tetravalent metal ion, usually titanium or zirconium, in a lattice of larger, divalent metal ions, usually lead or barium, and O_2 ions ("Piezo theory" from www. americanpiezo.com). Above a critical temperature, called the Curie point, each crystal

exhibits a simple cubic symmetry with no dipole moment, as shown in Fig. A-1(a). At temperatures below the Curie point, however, each crystal has tetragonal or rhombohedral symmetry and a dipole moment, as depicted in Fig. A-1(b). Adjoining dipoles form regions of local alignment called domains. The alignment gives a net dipole moment to the domain, and thus a net polarization. However the direction of polarization among neighboring domains is random, so the ceramic element has no overall polarization, as illustrated in Fig. A-2(a).

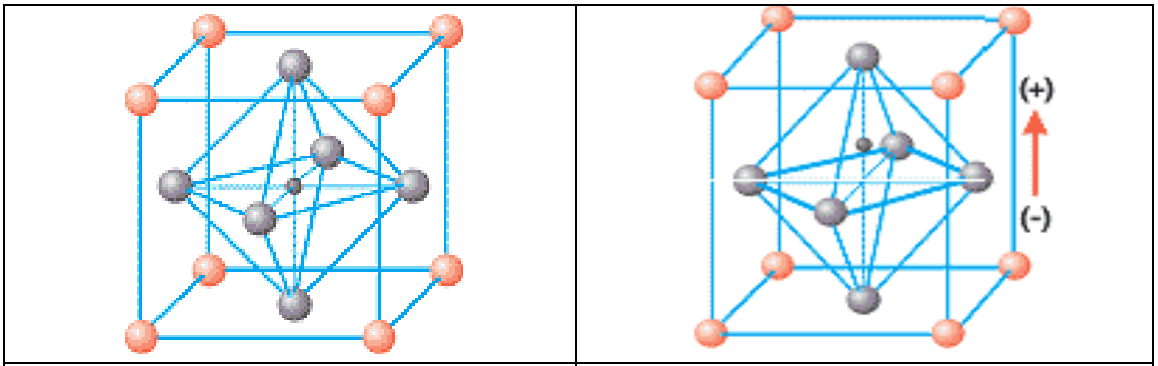

(a) above Curie point (b) below Curie point

Figure A-1. Crystal structure of piezoceramic versus Curie point

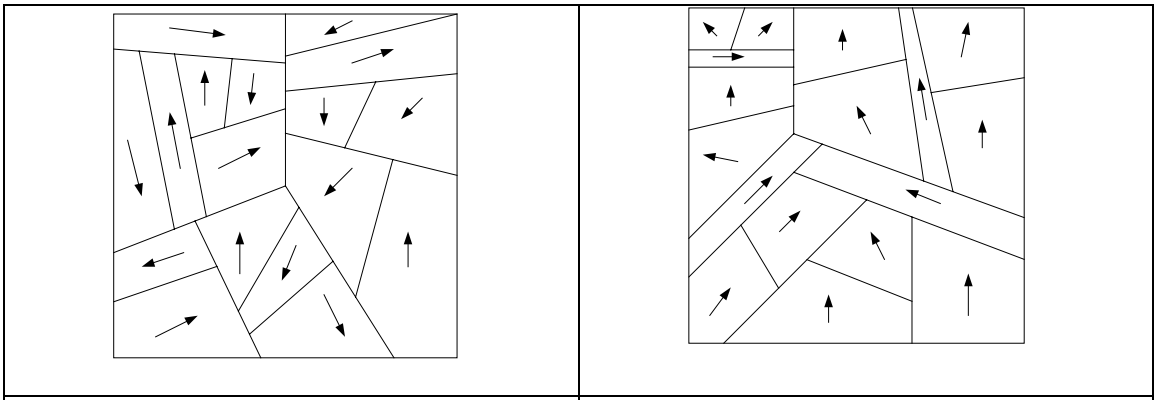

(a) before polarization (b) after polarization

Figure A-2. Neighboring domains before and after polarization.

As shown in Fig. A-2(b), the material may be induced to exhibit macroscopic polarization in any given direction by subjecting it to a strong electric field, called the

poling voltage. During electrical polarization the material becomes permanently elongated in the direction of the poling field and reduced in the transverse direction. When voltage is subsequently applied in the same direction as the poling voltage, the material experiences further elongation along the polar axis and the transverse contraction as stipulated by Poisson's ratio. When the voltage is removed, the piece reverts to its original poled dimensions. When voltage is applied opposite to the poled direction, the piece contracts along the polar axis and expands in the transverse direction. Again it reverts to its original poled dimensions after removing the voltage. If too large a voltage is applied in the depoling direction, the original polarization will be degraded (called depolarization), or the electric dipoles may be partially or completely flipped around 180 degree, causing the piece to be repoled in the opposite direction. The maximum depoling field a piece can withstand without experiencing depolarization effects is its coercive field, E_c.

When stress is applied along the poling axis, an electric field arises within the body, which tends to oppose the force acting upon it. Compressive stress generates an electric field with the same orientation as the original poling field, inducing the piece to elongate in opposition to the compressive forces. The piece reverts to its original poled dimensions after removing the stress. By the same token, tensile stress generates an electric field with an orientation opposite to that of the original poling field.

Under small field conditions, the constitutive relations for a piezoceramic are (IEEE Standard, 1987):

$$\begin{aligned} D_i &= e_{ij}^{\sigma} E_j + d_{im} \sigma_m \\ \varepsilon_k &= d_{jk} E_j + s_{km}^{E} \sigma_m \end{aligned} \tag{A-1}$$

where the vector D_i of size (3x1) is the electric displacement, ε_k the (6x1) strain vector, E_j the (3x1) applied electric field vector, and σ_m the (6x1) stress vector. The piezoelectric constants are the (3x3) dielectric permittivity e_{ij}^{σ}, the piezoelectric coefficients d_{im} (3x6) and d_{jk} (6x3), and the elastic compliance s_{km}^{E} (6x6). The superscripts and E indicate that the quantity is measured at constant stress and constant electric field, respectively. The poling direction, which is along the thickness, is denoted as the 3-axis whereas the 1- and 2-axes are in the plane of the piezoceramic sheet. The material is normally assumed transversely isotropic in the 1-2 plane. The d_{jk} matrix can then be expressed as:

$$[d] = \begin{bmatrix} 0 & 0 & d_{31} \\ 0 & 0 & d_{32} \\ 0 & 0 & d_{33} \\ 0 & d_{24} & 0 \\ d_{15} & 0 & 0 \\ 0 & 0 & 0 \end{bmatrix} \tag{A-2}$$

Here d_{3k} (k = 1,2,3) relates the normal strain in the k direction to an electric field, E_3, along the poling direction; d_{24} relates the shear strain in the 1-3 plane to a transverse electric field, E_2; d_{15} relates the shear strain in the 2-3 planes to a transverse electric field, E_1. There is no shear in the 1-2 plane relating to any electrical field. Note that $d_{24} = d_{15}$ and $d_{31} = d_{32}$ because the piezoelectric material is considered transversely isotropic. For the PZT material used in this study: PSI-5A4E from Piezo Systems, Inc., Cambridge MA, hese piezoelectric coefficients are:

$d_{24} = d_{15} = 0$
$d_{31} = d_{32} = -190 \text{ x } 10^{-12}$ m/V
$d_{33} = 390 \text{ x } 10^{-12}$ m/V

APPENDIX B: FREE VIBRATION OF BEAMS WITH VARIOUS BOUNDARY CONDITIONS

The governing equation for a beam in free vibration is:

$$\frac{\partial^2 w(x,t)}{\partial t^2} + \frac{EI}{\rho A}\frac{\partial^4 w(x,t)}{\partial x^4} = 0$$

here $w(x,t)$ is the time-varying beam deflection at location x, ρ the density, E the dynamic Young's modulus along the x-direction, I the second moment of inertia about the neutral axis, and A the cross-sectional area. Applying the method of separation of variables:

$$w(x,t) = W(x)T(t)$$

where

$$W(x) = C_1(\cosh\beta x + \cos\beta x) + C_2(\cosh\beta x - \cos\beta x) + C_3(\sinh\beta x + \sin\beta x) + C_4(\sinh\beta x - \sin\beta x)$$

and

$$T(t) = \sin(2\pi ft)$$

here $\beta^4 = \frac{\rho A}{EI}(2\pi f)^2$ (B-1)

and f is the frequency.

B.1 Cantilever Beams

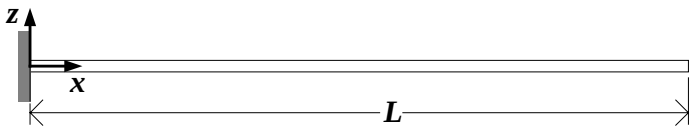

Figure B-1. Free vibration of a cantilever beam.

For the case of a cantilever beam in free vibration, as shown in Fig. B-1, we can apply the boundary conditions at the clamped end:

$$w(x,t)\big|_{x=0} = 0 \quad \Rightarrow \quad W(0) = 0 \quad \Rightarrow \quad C_1 = 0$$

$$\left.\frac{\partial w(x,t)}{\partial x}\right|_{x=0} = 0 \quad \Rightarrow \quad W'(0) = 0 \quad \Rightarrow \quad C_3 = 0$$

thus $W(x) = C_2\left(\cosh\beta x - \cos\beta x\right) + C_4\left(\sinh\beta x - \sin\beta x\right)$

Applying the boundary conditions at the free end, we have:

$$\left.\frac{\partial^2 w(x,t)}{\partial x^2}\right|_{L=0} = 0 \;\Rightarrow\; W''(0) = 0 \quad \Rightarrow$$

$$C_2\left(\cosh\beta L + \cos\beta L\right) + C_4\left(\sinh\beta L + \sin\beta L\right) = 0$$

$$\left.\frac{\partial^3 w(x,t)}{\partial x^3}\right|_{L=0} = 0 \;\Rightarrow\; W'''(0) = 0 \quad \Rightarrow$$

$$C_2\left(\sinh\beta L - \sin\beta L\right) + C_4\left(\cosh\beta L + \cos\beta L\right) = 0$$

For a non-trivial solution, the determinant of the above two equations should be zero. Thus, we have the following frequency equation:

$$\cosh\beta L\cos\beta L + 1 = 0 \tag{B-2}$$

The n^{th} mode normalized modal function is:

$$\phi_n(x) = \frac{1}{\sqrt{L}}\left[\left(\cosh\beta_n x - \cos\beta_n x\right) - \frac{\sinh k_n - \sin k_n}{\cosh k_n + \cos k_n}\left(\sinh\beta_n x - \sin\beta_n x\right)\right] \quad 0 \le x \le L \tag{B-3}$$

and the corresponding nondimensionalized modal function becomes:

$$\Phi_n(\eta) = \left(\cosh k_n\eta - \cos k_n\eta\right) - \frac{\sinh k_n - \sin k_n}{\cosh k_n + \cos k_n}\left(\sinh k_n\eta - \sin k_n\eta\right) \quad 0 \le \eta \le 1 \tag{B-4}$$

where $k_n = \beta_n L$ is the n^{th} root of the frequency equation. For the first four modes, k_n has the values of 1.857104, 4.694091, 7.854757, and 10.995541, respectively.

B.2 Fixed-Fixed Beams

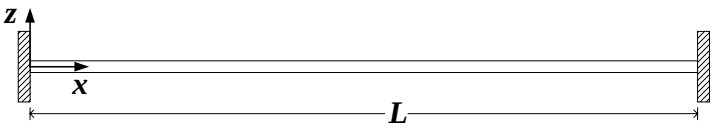

Figure B-2. Free vibration of a fixed-fixed beam.

For the case of a fixed-fixed beam in free vibration, as shown in Fig. B-2, we can apply the boundary conditions at the left fixed end:

$$w(x,t)\big|_{x=0} = 0 \quad \Rightarrow \quad W(0) = 0 \quad \Rightarrow \quad C_1 = 0$$

$$\left.\frac{\partial w(x,t)}{\partial x}\right|_{x=0} = 0 \quad \Rightarrow \quad W'(0) = 0 \quad \Rightarrow \quad C_3 = 0$$

thus $W(x) = C_2(\cosh \beta x - \cos \beta x) + C_4(\sinh \beta x - \sin \beta x)$

Applying the boundary conditions at the right fixed end, we have:

$$w(x,t)\big|_{x=L} = 0 \quad \Rightarrow \; W(L) = 0 \quad \Rightarrow$$

$$C_2(\cosh \beta L - \cos \beta L) + C_4(\sinh \beta L - \sin \beta L) = 0$$

$$\left.\frac{\partial w(x,t)}{\partial x}\right|_{L=0} = 0 \quad \Rightarrow \; W'(L) = 0 \quad \Rightarrow$$

$$C_2(\sinh \beta L + \sin \beta L) + C_4(\cosh \beta L - \cos \beta L) = 0$$

For a non-trivial solution, the determinant of the above two equations should be zero. Thus, we have the following frequency equation:

$$\cosh \beta L \cos \beta L = 1 \tag{B-5}$$

The n^{th} mode normalized modal function is:

$$\phi_n(x) = \frac{1}{\sqrt{L}}\left[\left(\cosh\beta_n x - \cos\beta_n x\right) - \frac{\sinh k_n - \sin k_n}{\cosh k_n - \cos k_n}\left(\sinh\beta_n x - \sin\beta_n x\right)\right] \quad 0 \le x \le L \qquad \text{(B-6)}$$

and the corresponding nondimensionalized modal function becomes:

$$\Phi_n(\eta) = \left(\cosh k_n\eta - \cos k_n\eta\right) - \frac{\sinh k_n - \sin k_n}{\cosh k_n - \cos k_n}\left(\sinh k_n\eta - \sin k_n\eta\right) \quad 0 \le \eta \le 1 \qquad \text{(B-7)}$$

where $k_n = \beta_n L$ is the n^{th} root of the frequency equation. For the first four modes, k_n has the values of 4.730041, 7.853205, 10.995608, and 14.137165, respectively.

B.3 Fixed-Pinned Beams

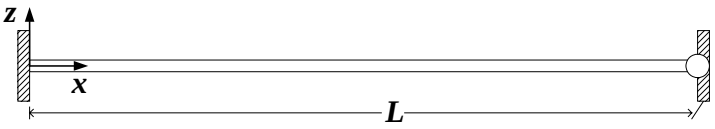

Figure B-3. Free vibration of a fixed-pinned beam.

For the case of a fixed-pinned beam in free vibration, as shown in Fig. B-3, we can apply the boundary conditions at the fixed end:

$$w(x,t)\big|_{x=0} = 0 \quad \Rightarrow \quad W(0) = 0 \quad \Rightarrow \quad C_1 = 0$$

$$\left.\frac{\partial w(x,t)}{\partial x}\right|_{x=0} = 0 \quad \Rightarrow \quad W'(0) = 0 \quad \Rightarrow \quad C_3 = 0$$

thus $W(x) = C_2\left(\cosh\beta x - \cos\beta x\right) + C_4\left(\sinh\beta x - \sin\beta x\right)$

Applying the boundary conditions at the pinned end, we have:

$$w(x,t)\big|_{x=L} = 0 \quad \Rightarrow \; W(L) = 0 \quad \Rightarrow$$

$$C_2\left(\cosh\beta L - \cos\beta L\right) + C_4\left(\sinh\beta L - \sin\beta L\right) = 0$$

$$\left.\frac{\partial^2 w(x,t)}{\partial x^2}\right|_{L=0} = 0 \;\Rightarrow\; W''(L) = 0 \qquad \Rightarrow$$

$$C_2\left(\cosh\beta L + \cos\beta L\right) + C_4\left(\sinh\beta L + \sin\beta L\right) = 0$$

For a non-trivial solution, the determinant of the above two equations should be zero. Thus, we have the following frequency equation:

$$\tanh\beta L = \tan\beta L \tag{B-8}$$

The n^{th} mode normalized modal function is:

$$\phi_n(x) = \frac{1}{\sqrt{L}}\left[\left(\cosh\beta_n x - \cos\beta_n x\right) - \frac{\cosh k_n - \cos k_n}{\sinh k_n - \sin k_n}\left(\sinh\beta_n x - \sin\beta_n x\right)\right] \quad 0 \le x \le L \tag{B-9}$$

and the corresponding nondimensionalized modal function becomes:

$$\Phi_n(\eta) = \left(\cosh k_n\eta - \cos k_n\eta\right) - \frac{\cosh k_n - \cos k_n}{\sinh k_n - \sin k_n}\left(\sinh k_n\eta - \sin k_n\eta\right) \quad 0 \le \eta \le 1 \tag{B-10}$$

where $k_n = \beta_n L$ is the n^{th} root of the frequency equation. For the first four modes, k_n has the values of 3.926602, 7.068583, 10.210176, and 13.351768, respectively.

B.4 Pinned-Pinned Beams

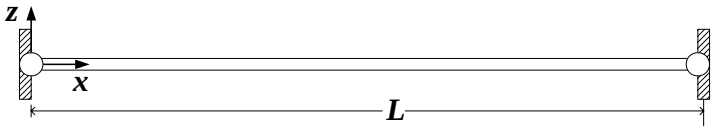

Figure B-4. Free vibration of a pinned-pinned beam.

For the case of a pinned- pinned beam in free vibration, as shown in Fig. B-4, we can apply the boundary conditions at the left pinned end:

$$w(x,t)\big|_{x=0} = 0 \qquad \Rightarrow \qquad W(0) = 0 \qquad \Rightarrow \qquad C_1 = 0$$

$$\left.\frac{\partial^2 w(x,t)}{\partial x^2}\right|_{x=0} = 0 \quad \Rightarrow \qquad W''(0) = 0 \qquad \Rightarrow \qquad C_2 = 0$$

thus $W(x) = C_3(\sinh \beta x + \sin \beta x) + C_4(\sinh \beta x - \sin \beta x)$

Applying the boundary conditions at the right pinned end, we have:

$$w(x,t)\big|_{x=L} = 0 \qquad \Rightarrow \; W(L) = 0 \qquad \Rightarrow$$

$$C_3(\sinh \beta L + \sin \beta L) + C_4(\sinh \beta L - \sin \beta L) = 0$$

$$\left.\frac{\partial^2 w(x,t)}{\partial x^2}\right|_{L=0} = 0 \quad \Rightarrow \; W''(L) = 0 \qquad \Rightarrow$$

$$C_3(\sinh \beta L - \sin \beta L) + C_4(\sinh \beta L + \sin \beta L) = 0$$

For a non-trivial solution, the determinant of the above two equations should be zero. Thus, we have the following frequency equation:

$$\sinh \beta L \sin \beta L = 0 \qquad \text{or} \quad k_n = \beta_n L = n\pi \tag{B-11}$$

The n^{th} mode normalized modal function is:

$$\phi_n(x) = \sqrt{\frac{2}{L}} \sin \frac{n\pi x}{L} \quad 0 \le x \le L \tag{B-12}$$

and the corresponding nondimensionalized modal function becomes:

$$\Phi_n(\eta) = \sqrt{2} \sin n\pi\eta \quad 0 \le \eta \le 1 \tag{B-13}$$

APPENDIX C: THE ORDER ANALYSIS OF MULTIPLE SCALES METHOD

In our theoretical analysis $\varepsilon << 1$ is an expansion parameter to keep track of the different orders of approximation. Since the choice of the expansion parameter affects the coefficients of the terms in the expansion, a final step is required. The forcing frequency, forcing amplitude, and linear viscous damping were the experimentally obtained parameters that were fed into the theoretical model by scaling the values according to the transformations outlined in previous sections. However, the scalings and perturbation solution require a numerical value for one last parameter, the perturbation parameter ε: Though in some cases, the perturbation parameter is a physical variable, in this case, it is only an expansion parameter whose choice is not entirely arbitrary. For our case, to complete the perturbation analysis, we need to evaluate the relative smallness of our perturbation terms. We substitute the experimentally obtained value into equation 3.29, estimate the potential maximal value of each term in the equation. We compare the orders of each term relative to the inertia term and calculate the perturbation parameter to check if the value is small enough. In order to insure the validity of our perturbation expansion, the expansion parameter must be small enough.

$$\rho A\frac{\partial^2 \upsilon(s,t)}{\partial t^2} + c_\upsilon \frac{\partial}{\partial t}\upsilon(s,t) + \overline{c}\frac{\partial}{\partial t}\upsilon(s,t)\left|\frac{\partial}{\partial t}\upsilon(s,t)\right| + EI\frac{\partial^4 \upsilon(s,t)}{\partial s^4}$$
$$= \rho A a_b \cos\Omega t - EI\frac{\partial}{\partial s}\{\frac{\partial \upsilon(s,t)}{\partial s}\frac{\partial}{\partial s}[\frac{\partial \upsilon(s,t)}{\partial s}\frac{\partial^2 \upsilon(s,t)}{\partial s^2}]\} - \frac{1}{2}\rho A\frac{\partial}{\partial s}\{\frac{\partial \upsilon(s,t)}{\partial s}\int_l^s \frac{\partial^2}{\partial t^2}\int_0^s [\frac{\partial \upsilon(s,t)}{\partial s}]^2 ds ds\}$$

And the boundary conditions are

$$\upsilon(0,t)=0, \qquad EI\frac{\partial^2}{\partial s^2}\upsilon(0,t)=k_1\frac{\partial}{\partial s}\upsilon(0,t)+k_3[\frac{\partial}{\partial s}\upsilon(0,t)]^3$$

$$\frac{\partial^2}{\partial s^2}\upsilon(l,t)=0, \qquad \frac{\partial^3}{\partial s^3}(l,t)=0$$

Unit:

c_υ $\quad \frac{kg/s^2}{m/s}=kg/ms$ $\qquad\qquad$ $\frac{\overline{c}}{\rho A}$ $\quad \frac{kg/m^2}{kg/m}=1/m$

$\overline{c}$ $\quad \frac{kg/s^2}{m^2/s^2}=kg/m^2$

$$\frac{\partial^2\upsilon(s,t)}{\partial t^2}+\frac{c_\upsilon}{\rho A}\frac{\partial}{\partial t}\upsilon(s,t)+\frac{\overline{c}}{\rho A}\frac{\partial}{\partial t}\upsilon(s,t)\,|\frac{\partial}{\partial t}\upsilon(s,t)\,|+\frac{EI}{\rho A}\frac{\partial^4\upsilon(s,t)}{\partial s^4}$$
$$=a_b\cos\Omega t-\frac{EI}{\rho A}\frac{\partial}{\partial s}\{\frac{\partial\upsilon(s,t)}{\partial s}\frac{\partial}{\partial s}[\frac{\partial\upsilon(s,t)}{\partial s}\frac{\partial^2\upsilon(s,t)}{\partial s^2}]\}-\frac{1}{2}\frac{\partial}{\partial s}\{\frac{\partial\upsilon(s,t)}{\partial s}\int_l^s\frac{\partial^2}{\partial t^2}\int_0^s[\frac{\partial\upsilon(s,t)}{\partial s}]^2dsds\}$$

In modal space order analyses, we define:

Term 1: $\int_0^l\frac{\partial^2\upsilon(s,t)}{\partial t^2}\phi(s)ds$ $\qquad$ Term 2: $\int_0^l\frac{c_\upsilon}{\rho A}\frac{\partial}{\partial t}\upsilon(s,t)\phi(s)ds$

Term 3: $\int_0^l\frac{\overline{c}}{\rho A}\frac{\partial}{\partial t}\upsilon(s,t)\,|\frac{\partial}{\partial t}\upsilon(s,t)\,|\phi(s)ds$ $\qquad$ Term 4: $\int_0^l\frac{EI}{\rho A}\frac{\partial^4\upsilon(s,t)}{\partial s^4}\phi(s)ds$

Term 5: $\int_0^l a_b\cos\Omega t\phi(s)ds$

Term 6: $-\int_0^l\frac{EI}{\rho A}\frac{\partial}{\partial s}\{\frac{\partial\upsilon(s,t)}{\partial s}\frac{\partial}{\partial s}[\frac{\partial\upsilon(s,t)}{\partial s}\frac{\partial^2\upsilon(s,t)}{\partial s^2}]\}\frac{\partial}{\partial s}\phi(s)ds$

Term 7: $-\int_0^l\frac{1}{2}\frac{\partial}{\partial s}\{\frac{\partial\upsilon(s,t)}{\partial s}\int_l^s\frac{\partial^2}{\partial t^2}\int_0^s[\frac{\partial\upsilon(s,t)}{\partial s}]^2dsds\}\frac{\partial}{\partial s}\phi(s)ds$

Aluminum (mode 1)

Unit $[m/s^2]$	$\frac{\partial^2 \upsilon(s,t)}{\partial t^2}$	$\frac{c_\upsilon}{\rho A}\frac{\partial}{\partial t}\upsilon(s,t)$	$\frac{\overline{c}}{\rho A}\frac{\partial}{\partial t}\upsilon(s,t)\lvert\frac{\partial}{\partial t}\upsilon(s,t)\rvert$	$\frac{EI}{\rho A}\frac{\partial^4 \upsilon(s,t)}{\partial s^4}$	$a_b \cos\Omega t$
$a_b = 0.085g$	115	1.4	0	115	0.87

	$\frac{\frac{c_\upsilon}{\rho A}\frac{\partial}{\partial t}\upsilon(s,t)}{\frac{\partial^2 \upsilon(s,t)}{\partial t^2}}$	$\frac{\frac{\overline{c}}{\rho A}\frac{\partial}{\partial t}\upsilon(s,t)\lvert\frac{\partial}{\partial t}\upsilon(s,t)\rvert}{\frac{\partial^2 \upsilon(s,t)}{\partial t^2}}$	$\frac{\frac{EI}{\rho A}\frac{\partial^4 \upsilon(s,t)}{\partial s^4}}{\frac{\partial^2 \upsilon(s,t)}{\partial t^2}}$	$\frac{a_b \cos\Omega t}{\frac{\partial^2 \upsilon(s,t)}{\partial t^2}}$
$a_b = 0.085g$	$O(\varepsilon^2)$ $\varepsilon = 0.11$	0	$O(1)$	$O(\varepsilon^2)$ $\varepsilon = 0.087$

Evaluate at $s = l$	$\frac{EI}{\rho A}\frac{\partial}{\partial s}\{\frac{\partial \upsilon(s,t)}{\partial s}\frac{\partial}{\partial s}[\frac{\partial \upsilon(s,t)}{\partial s}\frac{\partial^2 \upsilon(s,t)}{\partial s^2}]\}$	$\frac{1}{2}\frac{\partial}{\partial s}\{\frac{\partial \upsilon(s,t)}{\partial s}\int_l^s \frac{\partial^2}{\partial t^2}\int_0^s [\frac{\partial \upsilon(s,t)}{\partial s}]^2 dsds\}$
$a_b = 0.085g$	-1.7	0.94

Evaluate at $s = l$	$\frac{\frac{EI}{\rho A}\frac{\partial}{\partial s}\{\frac{\partial \upsilon(s,t)}{\partial s}\frac{\partial}{\partial s}[\frac{\partial \upsilon(s,t)}{\partial s}\frac{\partial^2 \upsilon(s,t)}{\partial s^2}]\}}{\frac{\partial^2 \upsilon(s,t)}{\partial t^2}}$	$\frac{\frac{1}{2}\frac{\partial}{\partial s}\{\frac{\partial \upsilon(s,t)}{\partial s}\int_l^s \frac{\partial^2}{\partial t^2}\int_0^s [\frac{\partial \upsilon(s,t)}{\partial s}]^2 dsds\}}{\frac{\partial^2 \upsilon(s,t)}{\partial t^2}}$
$a_b = 0.085g$	$O(\varepsilon^2)$ $\varepsilon = 0.12$	$O(\varepsilon^2)$ $\varepsilon = 0.090$

Evaluate at $s = 0$	$\frac{EI}{\rho A}\frac{\partial}{\partial s}\{\frac{\partial \upsilon(s,t)}{\partial s}\frac{\partial}{\partial s}[\frac{\partial \upsilon(s,t)}{\partial s}\frac{\partial^2 \upsilon(s,t)}{\partial s^2}]\}$	$\frac{1}{2}\frac{\partial}{\partial s}\{\frac{\partial \upsilon(s,t)}{\partial s}\int_l^s \frac{\partial^2}{\partial t^2}\int_0^s [\frac{\partial \upsilon(s,t)}{\partial s}]^2 dsds\}$
$a_b = 0.085g$	-2.8	-0.86

Evaluate at $s = 0$	$\frac{\frac{EI}{\rho A}\frac{\partial}{\partial s}\{\frac{\partial \upsilon(s,t)}{\partial s}\frac{\partial}{\partial s}[\frac{\partial \upsilon(s,t)}{\partial s}}{\frac{\partial^2 \upsilon(s,t)}{\partial t^2}}$	$\frac{\frac{1}{2}\frac{\partial}{\partial s}\{\frac{\partial \upsilon(s,t)}{\partial s}\int_l^s \frac{\partial^2}{\partial t^2}\int_0^s [\frac{\partial \upsilon(s,t)}{\partial s}]}{\frac{\partial^2 \upsilon(s,t)}{\partial t^2}}$
$a_b = 0.085g$	$O(\varepsilon^2)$ $\varepsilon = 0.16$	$O(\varepsilon^2)$ $\varepsilon = 0.086$

Moment $[[N*m]$	$EI\frac{\partial^2}{\partial s^2}\upsilon(0,t)$	$k_1\frac{\partial}{\partial s}\upsilon(0,t)$	$k_3[\frac{\partial}{\partial s}\upsilon(0,t)]^3$
$a_b = 0.085g$	0.33	0.33	-0.73

	$\frac{EI\frac{\partial^2}{\partial s^2}\upsilon(0,t)}{EI\frac{\partial^2}{\partial s^2}\upsilon(0,t)}$	$\frac{k_1\frac{\partial}{\partial s}\upsilon(0,t)}{EI\frac{\partial^2}{\partial s^2}\upsilon(0,t)}$	$\frac{k_3[\frac{\partial}{\partial s}\upsilon(0,t)]^3}{EI\frac{\partial^2}{\partial s^2}\upsilon(0,t)}$
$a_b = 0.085g$	1	$O(1)$	$O(\varepsilon^2)$ $\varepsilon = 1.5$

	f_0 (hz)	$\xi = \frac{c_\upsilon}{2\omega\rho A}$	$\frac{\overline{c}}{\rho A}[\frac{1}{m}]$	Nonlinear factor α	$k_1\,[N*m]$	$k_3\,[N*m]$
$a_b =$ $0.085g$	13.64	0.00628	0	$-4.3*10^6$	194	$-1.5*10^8$

Modal space order analyses

Unit $[m^2/s^2]$	Term 1	Term 2	Term 3	Term 4	Term 5	Term 6	Term 7
$a_b = 0.085g$	32	0.40	0	32	0.38	-0.20	0.040

	$\frac{\text{Term 2}}{\text{Term 1}}$	$\frac{\text{Term 3}}{\text{Term 1}}$	$\frac{\text{Term 4}}{\text{Term 1}}$	$\frac{\text{Term 5}}{\text{Term 1}}$	$\frac{\text{Term 6}}{\text{Term 1}}$	$\frac{\text{Term 7}}{\text{Term 1}}$
$a_b =$ $0.085g$	$O(\varepsilon^2)$ $\varepsilon = 0.11$	$O(\varepsilon^2)$ $\varepsilon = 0.052$	$O(1)$	$O(\varepsilon^2)$ $\varepsilon = 0.11$	$O(\varepsilon^2)$ $\varepsilon = 0.079$	$O(\varepsilon^2)$ $\varepsilon = 0.035$

Aluminum (mode 2)

Unit $[m/s^2]$	$\frac{\partial^2 \upsilon(s,t)}{\partial t^2}$	$\frac{c_\upsilon}{\rho A}\frac{\partial}{\partial t}\upsilon(s,t)$	$\frac{\overline{c}}{\rho A}\frac{\partial}{\partial t}\upsilon(s,t)\lvert\frac{\partial}{\partial t}\upsilon(s,t)\rvert$	$\frac{EI}{\rho A}\frac{\partial^4 \upsilon(s,t)}{\partial s^4}$	$a_b \cos\Omega t$
$a_b =$ $3.47g$	-3246	-35	0	-3246	41

	$\frac{\frac{c_\upsilon}{\rho A}\frac{\partial}{\partial t}\upsilon(s,t)}{\frac{\partial^2 \upsilon(s,t)}{\partial t^2}}$	$\frac{\frac{\overline{c}}{\rho A}\frac{\partial}{\partial t}\upsilon(s,t)\lvert\frac{\partial}{\partial t}\upsilon(s,t)\rvert}{\frac{\partial^2 \upsilon(s,t)}{\partial t^2}}$	$\frac{\frac{EI}{\rho A}\frac{\partial^4 \upsilon(s,t)}{\partial s^4}}{\frac{\partial^2 \upsilon(s,t)}{\partial t^2}}$	$\frac{a_b \cos\Omega t}{\frac{\partial^2 \upsilon(s,t)}{\partial t^2}}$
$a_b =$ $3.47g$	$O(\varepsilon^2)$ $\varepsilon = 0.10$	0	$O(1)$	$O(\varepsilon^2)$ $\varepsilon = 0.11$

Evaluate at $s = l$	$\frac{EI}{\rho A}\frac{\partial}{\partial s}\{\frac{\partial \upsilon(s,t)}{\partial s}\frac{\partial}{\partial s}[\frac{\partial \upsilon(s,t)}{\partial s}\frac{\partial^2 \upsilon(s,t)}{\partial s^2}]\}$	$\frac{1}{2}\frac{\partial}{\partial s}\{\frac{\partial \upsilon(s,t)}{\partial s}\int_l^s \frac{\partial^2}{\partial t^2}\int_0^s [\frac{\partial \upsilon(s,t)}{\partial s}]^2 dsds\}$
$a_b =$ $3.47g$	311	-352

Evaluate at $s = l$	$\frac{\frac{EI}{\rho A}\frac{\partial}{\partial s}\{\frac{\partial \upsilon(s,t)}{\partial s}\frac{\partial}{\partial s}[\frac{\partial \upsilon(s,t)}{\partial s}\frac{\partial^2 \upsilon(s,t)}{\partial s^2}]\}}{\frac{\partial^2 \upsilon(s,t)}{\partial t^2}}$	$\frac{\frac{1}{2}\frac{\partial}{\partial s}\{\frac{\partial \upsilon(s,t)}{\partial s}\int_l^s \frac{\partial^2}{\partial t^2}\int_0^s [\frac{\partial \upsilon(s,t)}{\partial s}]^2 dsds\}}{\frac{\partial^2 \upsilon(s,t)}{\partial t^2}}$
$a_b =$ $3.47g$	$O(\varepsilon^2)$ $\varepsilon = 0.31$	$O(\varepsilon^2)$ $\varepsilon = 0.33$

Evaluate at $s = 0$	$\frac{EI}{\rho A}\frac{\partial}{\partial s}\{\frac{\partial \upsilon(s,t)}{\partial s}\frac{\partial}{\partial s}[\frac{\partial \upsilon(s,t)}{\partial s}\frac{\partial^2 \upsilon(s,t)}{\partial s^2}]\}$	$\frac{1}{2}\frac{\partial}{\partial s}\{\frac{\partial \upsilon(s,t)}{\partial s}\int_l^s \frac{\partial^2}{\partial t^2}\int_0^s [\frac{\partial \upsilon(s,t)}{\partial s}]^2 dsds\}$
$a_b =$ $3.47g$	-286	-438

Evaluate at $s = 0$	$\frac{EI}{\rho A}\frac{\partial}{\partial s}\{\frac{\partial \upsilon(s,t)}{\partial s}\frac{\partial}{\partial s}[\frac{\partial \upsilon(s,t)}{\partial s}$ $\frac{\partial^2 \upsilon(s,t)}{\partial t^2}$	$\frac{1}{2}\frac{\partial}{\partial s}\{\frac{\partial \upsilon(s,t)}{\partial s}\int_l^s \frac{\partial^2}{\partial t^2}\int_0^s [\frac{\partial \upsilon(s,t}{\partial s}$ $\frac{\partial^2 \upsilon(s,t)}{\partial t^2}$
$a_b =$ $3.47g$	$O(\varepsilon^2)$ $\varepsilon = 0.30$	$O(\varepsilon^2)$ $\varepsilon = 0.37$

Moment $[[N*m]$	$EI\frac{\partial^2}{\partial s^2}\upsilon(0,t)$	$k_1\frac{\partial}{\partial s}\upsilon(0,t)$	$k_3[\frac{\partial}{\partial s}\upsilon(0,t)]^3$
$a_b = 3.47g$	1.5	1.5	-71

	$\frac{EI\frac{\partial^2}{\partial s^2}\upsilon(0,t)}{EI\frac{\partial^2}{\partial s^2}\upsilon(0,t)}$	$\frac{k_1\frac{\partial}{\partial s}\upsilon(0,t)}{EI\frac{\partial^2}{\partial s^2}\upsilon(0,t)}$	$\frac{k_3[\frac{\partial}{\partial s}\upsilon(0,t)]^3}{EI\frac{\partial^2}{\partial s^2}\upsilon(0,t)}$
$a_b = 3.47g$	1	$O(1)$	$O(\varepsilon^2)$ $\varepsilon = 7.0$

	f_0 (hz)	$\xi = \frac{c_\upsilon}{2\omega\rho A}$	$\frac{\overline{c}}{\rho A}[\frac{1}{m}]$	Nonlinear factor α	$k_1\,[N*m]$	$k_3\,[N*m]$
$a_b = 3.47g$	84.90	0.00534	0	$-1.1*10^9$	1280	$-4.8*10^{10}$

Modal space order analyses

Unit $[m^2/s^2]$	Term 1	Term 2	Term 3	Term 4	Term 5	Term 6	Term 7
$a_b = 3.47g$	901	9.6	0	901	9.6	-18	11

	$\frac{\text{Term 2}}{\text{Term 1}}$	$\frac{\text{Term 3}}{\text{Term 1}}$	$\frac{\text{Term 4}}{\text{Term 1}}$	$\frac{\text{Term 5}}{\text{Term 1}}$	$\frac{\text{Term 6}}{\text{Term 1}}$	$\frac{\text{Term 7}}{\text{Term 1}}$
$a_b = 3.47g$	$O(\varepsilon^2)$ $\varepsilon = 0.10$	0	$O(1)$	$O(\varepsilon^2)$ $\varepsilon = 0.10$	$O(\varepsilon^2)$ $\varepsilon = 0.14$	$O(\varepsilon^2)$ $\varepsilon = 0.11$

Aluminum (mode 3)

Unit $[m/s^2]$	$\frac{\partial^2 \upsilon(s,t)}{\partial t^2}$	$\frac{c_\upsilon}{\rho A}\frac{\partial}{\partial t}\upsilon(s,t)$	$\frac{\bar{c}}{\rho A}\frac{\partial}{\partial t}\upsilon(s,t)\left\|\frac{\partial}{\partial t}\upsilon(s,t)\right\|$	$\frac{EI}{\rho A}\frac{\partial^4 \upsilon(s,t)}{\partial s^4}$	$a_b \cos \Omega t$
$a_b = 27.2g$	11754	45	239	11754	267
$a_b = 2.72g$	3601	14	0	3601	27

	$\frac{\frac{\partial^2 \upsilon(s,t)}{\partial t^2}}{\frac{\partial^2 \upsilon(s,t)}{\partial t^2}}$	$\frac{\frac{c_\upsilon}{\rho A}\frac{\partial}{\partial t}\upsilon(s,t)}{\frac{\partial^2 \upsilon(s,t)}{\partial t^2}}$	$\frac{\frac{\bar{c}}{\rho A}\frac{\partial}{\partial t}\upsilon(s,t)\left\|\frac{\partial}{\partial t}\upsilon(s,t)\right\|}{\frac{\partial^2 \upsilon(s,t)}{\partial t^2}}$	$\frac{\frac{EI}{\rho A}\frac{\partial^4 \upsilon(s,t)}{\partial s^4}}{\frac{\partial^2 \upsilon(s,t)}{\partial t^2}}$	$\frac{a_b \cos \Omega t}{\frac{\partial^2 \upsilon(s,t)}{\partial t^2}}$
$a_b = 27.2g$	1	$O(\varepsilon^2)$ $\varepsilon = 0.062$	$O(\varepsilon^2)$ $\varepsilon = 0.14$	$O(1)$	$O(\varepsilon^2)$ $\varepsilon = 0.15$
$a_b = 2.72g$	1	$O(\varepsilon^2)$ $\varepsilon = 0.062$	0	$O(1)$	$O(\varepsilon^2)$ $\varepsilon = 0.086$

Evaluate at $s = l$	$\frac{EI}{\rho A}\frac{\partial}{\partial s}\{\frac{\partial \upsilon(s,t)}{\partial s}\frac{\partial}{\partial s}[\frac{\partial \upsilon(s,t)}{\partial s}\frac{\partial^2 \upsilon(s,t)}{\partial s^2}]\}$	$\frac{1}{2}\frac{\partial}{\partial s}\{\frac{\partial \upsilon(s,t)}{\partial s}\int_l^s \frac{\partial^2}{\partial t^2}\int_0^s [\frac{\partial \upsilon(s,t)}{\partial s}]^2 dsds\}$
$a_b = 27.2g$	-671	1124
$a_b = 2.72g$	-19	31

Evaluate at $s = l$	$\frac{\frac{EI}{\rho A}\frac{\partial}{\partial s}\{\frac{\partial \upsilon(s,t)}{\partial s}\frac{\partial}{\partial s}[\frac{\partial \upsilon(s,t)}{\partial s}\frac{\partial^2 \upsilon(s,t)}{\partial s^2}]\}}{\frac{\partial^2 \upsilon(s,t)}{\partial t^2}}$	$\frac{\frac{1}{2}\frac{\partial}{\partial s}\{\frac{\partial \upsilon(s,t)}{\partial s}\int_l^s \frac{\partial^2}{\partial t^2}\int_0^s [\frac{\partial \upsilon(s,t)}{\partial s}]^2 dsds\}}{\frac{\partial^2 \upsilon(s,t)}{\partial t^2}}$
$a_b = 27.2g$	$O(\varepsilon^2)$ $\varepsilon = 0.24$	$O(\varepsilon^2)$ $\varepsilon = 0.31$
$a_b = 2.72g$	$O(\varepsilon^2)$ $\varepsilon = 0.072$	$O(\varepsilon^2)$ $\varepsilon = 0.093$

Evaluate at $s=0$	$\frac{EI}{\rho A}\frac{\partial}{\partial s}\{\frac{\partial \upsilon(s,t)}{\partial s}\frac{\partial}{\partial s}[\frac{\partial \upsilon(s,t)}{\partial s}\frac{\partial^2 \upsilon(s,t)}{\partial s^2}]\}$	$\frac{1}{2}\frac{\partial}{\partial s}\{\frac{\partial \upsilon(s,t)}{\partial s}\int_l^s \frac{\partial^2}{\partial t^2}\int_0^s [\frac{\partial \upsilon(s,t)}{\partial s}]^2 dsds\}$
$a_b =$ $27.2g$	-694	-2866
$a_b =$ $2.72g$	-19	-80

Evaluate at $s=0$	$\frac{\frac{EI}{\rho A}\frac{\partial}{\partial s}\{\frac{\partial \upsilon(s,t)}{\partial s}\frac{\partial}{\partial s}[\frac{\partial \upsilon(s,t)}{\partial s}\frac{\partial^2 \upsilon(s,t)}{\partial s^2}]\}}{\frac{\partial^2 \upsilon(s,t)}{\partial t^2}}$	$\frac{\frac{1}{2}\frac{\partial}{\partial s}\{\frac{\partial \upsilon(s,t)}{\partial s}\int_l^s \frac{\partial^2}{\partial t^2}\int_0^s [\frac{\partial \upsilon(s,t)}{\partial s}]^2 dsds\}}{\frac{\partial^2 \upsilon(s,t)}{\partial t^2}}$
$a_b =$ $27.2g$	$O(\varepsilon^2)$ $\varepsilon = 0.24$	$O(\varepsilon^2)$ $\varepsilon = 0.49$
$a_b =$ $2.72g$	$O(\varepsilon^2)$ $\varepsilon = 0.073$	$O(\varepsilon^2)$ $\varepsilon = 0.15$

Moment $[[N*m]$	$EI\frac{\partial^2}{\partial s^2}\upsilon(0,t)$	$k_1\frac{\partial}{\partial s}\upsilon(0,t)$	$k_3[\frac{\partial}{\partial s}\upsilon(0,t)]^3$
$a_b = 27.2g$	1.9	1.9	-39
$a_b = 2.72g$	0.58	0.58	108

	$\frac{EI\frac{\partial^2}{\partial s^2}\upsilon(0,t)}{EI\frac{\partial^2}{\partial s^2}\upsilon(0,t)}$	$\frac{k_1\frac{\partial}{\partial s}\upsilon(0,t)}{EI\frac{\partial^2}{\partial s^2}\upsilon(0,t)}$	$\frac{k_3[\frac{\partial}{\partial s}\upsilon(0,t)]^3}{EI\frac{\partial^2}{\partial s^2}\upsilon(0,t)}$
$a_b = 27.2g$	1	$O(1)$	$O(\varepsilon^2)$ $\varepsilon = 4.6$
$a_b = 2.72g$	1	$O(1)$	$O(\varepsilon^2)$ $\varepsilon = 14$

	f_0 (hz)	$\xi = \frac{c_\upsilon}{2\omega\rho A}$	$\frac{\overline{c}}{\rho A}[\frac{1}{m}]$	Nonlinear factor α	$k_1\,[N*m]$	$k_3\,[N*m]$
$a_b = 27.2g$	235.30	0.00190	3.79	$-6.5*10^{10}$	457	$-5.8*10^{8}$
$a_b = 2.72g$	237.1	0.00190	0	$-1.0*10^{11}$	$2.8*10^{4}$	$-1.2*10^{16}$

Modal space order analyses

Unit $[m^2/s^2]$	Term 1	Term 2	Term 3	Term 4	Term 5	Term 6	Term 7
$a_b = 27.2g$	3266	12	13	3266	38	-26	142
$a_b = 2.72g$	999	3.8	0	999	3.8	-0.72	4.0

	$\frac{\text{Term 2}}{\text{Term 1}}$	$\frac{\text{Term 3}}{\text{Term 1}}$	$\frac{\text{Term 4}}{\text{Term 1}}$	$\frac{\text{Term 5}}{\text{Term 1}}$	$\frac{\text{Term 6}}{\text{Term 1}}$	$\frac{\text{Term 7}}{\text{Term 1}}$
$a_b = 27.2g$	$O(\varepsilon^2)$ $\varepsilon = 0.062$	$O(\varepsilon^2)$ $\varepsilon = 0.063$	$O(1)$	$O(\varepsilon^2)$ $\varepsilon = 0.11$	$O(\varepsilon^2)$ $\varepsilon = 0.089$	$O(\varepsilon^2)$ $\varepsilon = 0.21$
$a_b = 2.72g$	$O(\varepsilon^2)$ $\varepsilon = 0.066$	0	$O(1)$	$O(\varepsilon^2)$ $\varepsilon = 0.062$	$O(\varepsilon^2)$ $\varepsilon = 0.027$	$O(\varepsilon^2)$ $\varepsilon = 0.063$

Glare 2 (mode 1)

Unit $[m/s^2]$	$\frac{\partial^2 \upsilon(s,t)}{\partial t^2}$	$\frac{c_\upsilon}{\rho A}\frac{\partial}{\partial t}\upsilon(s,t)$	$\frac{\bar{c}}{\rho A}\frac{\partial}{\partial t}\upsilon(s,t)\lvert\frac{\partial}{\partial t}\upsilon(s,t)\rvert$	$\frac{EI}{\rho A}\frac{\partial^4 \upsilon(s,t)}{\partial s^4}$	$a_b \cos \Omega t$
$a_b =$ $0.08g$	93	0.78	4.4	93	0.81
$a_b =$ $0.04g$	58	0.49	1.2	58	0.39
$a_b =$ $0.02g$	35	0.30	0	35	0.19

	$\frac{\frac{\partial^2 \upsilon(s,t)}{\partial t^2}}{\frac{\partial^2 \upsilon(s,t)}{\partial t^2}}$	$\frac{\frac{c_\upsilon}{\rho A}\frac{\partial}{\partial t}\upsilon(s,t)}{\frac{\partial^2 \upsilon(s,t)}{\partial t^2}}$	$\frac{\frac{\bar{c}}{\rho A}\frac{\partial}{\partial t}\upsilon(s,t)\lvert\frac{\partial}{\partial t}\upsilon(s,t)\rvert}{\frac{\partial^2 \upsilon(s,t)}{\partial t^2}}$	$\frac{\frac{EI}{\rho A}\frac{\partial^4 \upsilon(s,t)}{\partial s^4}}{\frac{\partial^2 \upsilon(s,t)}{\partial t^2}}$	$\frac{a_b \cos \Omega t}{\frac{\partial^2 \upsilon(s,t)}{\partial t^2}}$
$a_b =$ $0.08g$	1	$O(\varepsilon^2)$ $\varepsilon = 0.092$	$O(\varepsilon^2)$ $\varepsilon = 0.22$	$O(1)$	$O(\varepsilon^2)$ $\varepsilon = 0.093$
$a_b =$ $0.04g$	1	$O(\varepsilon^2)$ $\varepsilon = 0.092$	$O(\varepsilon^2)$ $\varepsilon = 0.14$	$O(1)$	$O(\varepsilon^2)$ $\varepsilon = 0.082$
$a_b =$ $0.02g$	1	$O(\varepsilon^2)$ $\varepsilon = 0.092$	0	$O(1)$	$O(\varepsilon^2)$ $\varepsilon = 0.073$

Evaluate at $s = l$	$\frac{EI}{\rho A}\frac{\partial}{\partial s}\{\frac{\partial \upsilon(s,t)}{\partial s}\frac{\partial}{\partial s}[\frac{\partial \upsilon(s,t)}{\partial s}\frac{\partial^2 \upsilon(s,t)}{\partial s^2}]\}$	$\frac{1}{2}\frac{\partial}{\partial s}\{\frac{\partial \upsilon(s,t)}{\partial s}\int_l^s \frac{\partial^2}{\partial t^2}\int_0^s [\frac{\partial \upsilon(s,t)}{\partial s}]^2 dsds\}$
$a_b =$ $0.08g$	-1.3	0.71
$a_b =$ $0.04g$	-0.30	0.17
$a_b =$ $0.02g$	-0.068	0.038

Evaluate at $s = l$	$\frac{\frac{EI}{\rho A}\frac{\partial}{\partial s}\{\frac{\partial \upsilon(s,t)}{\partial s}\frac{\partial}{\partial s}[\frac{\partial \upsilon(s,t)}{\partial s}\frac{\partial^2 \upsilon(s,t)}{\partial s^2}]\}}{\frac{\partial^2 \upsilon(s,t)}{\partial t^2}}$	$\frac{\frac{1}{2}\frac{\partial}{\partial s}\{\frac{\partial \upsilon(s,t)}{\partial s}\int_l^s \frac{\partial^2}{\partial t^2}\int_0^s [\frac{\partial \upsilon(s,t)}{\partial s}]^2 dsds\}}{\frac{\partial^2 \upsilon(s,t)}{\partial t^2}}$
$a_b = 0.08g$	$O(\varepsilon^2)$ $\varepsilon = 0.12$	$O(\varepsilon^2)$ $\varepsilon = 0.087$
$a_b = 0.04g$	$O(\varepsilon^2)$ $\varepsilon = 0.072$	$O(\varepsilon^2)$ $\varepsilon = 0.054$
$a_b = 0.02g$	$O(\varepsilon^2)$ $\varepsilon = 0.044$	$O(\varepsilon^2)$ $\varepsilon = 0.033$

Evaluate at $s = 0$	$\frac{EI}{\rho A}\frac{\partial}{\partial s}\{\frac{\partial \upsilon(s,t)}{\partial s}\frac{\partial}{\partial s}[\frac{\partial \upsilon(s,t)}{\partial s}\frac{\partial^2 \upsilon(s,t)}{\partial s^2}]\}$	$\frac{1}{2}\frac{\partial}{\partial s}\{\frac{\partial \upsilon(s,t)}{\partial s}\int_l^s \frac{\partial^2}{\partial t^2}\int_0^s [\frac{\partial \upsilon(s,t)}{\partial s}]^2 dsds\}$
$a_b = 0.08g$	-2.1	-0.64
$a_b = 0.04g$	-0.51	-0.15
$a_b = 0.02g$	-0.11	-0.034

Evaluate at $s = 0$	$\frac{\frac{EI}{\rho A}\frac{\partial}{\partial s}\{\frac{\partial \upsilon(s,t)}{\partial s}\frac{\partial}{\partial s}[\frac{\partial \upsilon(s,t)}{\partial s}\frac{\partial^2 \upsilon(s,t)}{\partial s^2}]\}}{\frac{\partial^2 \upsilon(s,t)}{\partial t^2}}$	$\frac{\frac{1}{2}\frac{\partial}{\partial s}\{\frac{\partial \upsilon(s,t)}{\partial s}\int_l^s \frac{\partial^2}{\partial t^2}\int_0^s [\frac{\partial \upsilon(s,t)}{\partial s}]^2 dsds\}}{\frac{\partial^2 \upsilon(s,t)}{\partial t^2}}$
$a_b = 0.08g$	$O(\varepsilon^2)$ $\varepsilon = 0.15$	$O(\varepsilon^2)$ $\varepsilon = 0.083$
$a_b = 0.04g$	$O(\varepsilon^2)$ $\varepsilon = 0.094$	$O(\varepsilon^2)$ $\varepsilon = 0.051$
$a_b = 0.02g$	$O(\varepsilon^2)$ $\varepsilon = 0.057$	$O(\varepsilon^2)$ $\varepsilon = 0.031$

Moment $[[N*m]$	$EI\frac{\partial^2}{\partial s^2}\upsilon(0,t)$	$k_1\frac{\partial}{\partial s}\upsilon(0,t)$	$k_3[\frac{\partial}{\partial s}\upsilon(0,t)]^3$
$a_b = 0.08g$	0.22	0.22	-0.34
$a_b = 0.04g$	0.14	0.14	-0.22
$a_b = 0.02g$	0.085	0.085	-0.12

	$\frac{EI\frac{\partial^2}{\partial s^2}\upsilon(0,t)}{EI\frac{\partial^2}{\partial s^2}\upsilon(0,t)}$	$\frac{k_1\frac{\partial}{\partial s}\upsilon(0,t)}{EI\frac{\partial^2}{\partial s^2}\upsilon(0,t)}$	$\frac{k_3[\frac{\partial}{\partial s}\upsilon(0,t)]^3}{EI\frac{\partial^2}{\partial s^2}\upsilon(0,t)}$
$a_b = 0.08g$	1	$O(1)$	$O(\varepsilon^2)$ $\varepsilon = 1.2$
$a_b = 0.04g$	1	$O(1)$	$O(\varepsilon^2)$ $\varepsilon = 1.2$
$a_b = 0.02g$	1	$O(1)$	$O(\varepsilon^2)$ $\varepsilon = 1.2$

	f_0 (hz)	$\xi = \frac{c_\upsilon}{2\omega\rho A}$	$\frac{\overline{c}}{\rho A}[\frac{1}{m}]$	Nonlinear factor α	$k_1\,[N*m]$	$k_3\,[N*m]$
$a_b = 0.08g$	12.55	0.00420	3.18	$-2.5*10^6$	114	$-4.6*10^7$
$a_b = 0.04g$	12.56	0.00420	2.18	$-7.5*10^6$	120	$-1.4*10^8$
$a_b = 0.02g$	12.60	0.00420	0	$-1.8*10^7$	137	$-5.2*10^8$

Modal space order analyses

Unit $[m^2/s^2]$	Term 1	Term 2	Term 3	Term 4	Term 5	Term 6	Term 7
$a_b = 0.08g$	26	0.22	0.067	26	0.35	-0.18	0.030
$a_b = 0.04g$	16	0.14	0.018	16	0.17	-0.035	0.0071
$a_b = 0.02g$	9.8	0.083	0	9.8	0.083	-0.0079	0.0016

	$\frac{\text{Term 2}}{\text{Term 1}}$	$\frac{\text{Term 3}}{\text{Term 1}}$	$\frac{\text{Term 4}}{\text{Term 1}}$	$\frac{\text{Term 5}}{\text{Term 1}}$	$\frac{\text{Term 6}}{\text{Term 1}}$	$\frac{\text{Term 7}}{\text{Term 1}}$
$a_b = 0.08g$	$O(\varepsilon^2)$ $\varepsilon = 0.092$	$O(\varepsilon^2)$ $\varepsilon = 0.051$	$O(1)$	$O(\varepsilon^2)$ $\varepsilon = 0.12$	$O(\varepsilon^2)$ $\varepsilon = 0.075$	$O(\varepsilon^2)$ $\varepsilon = 0.034$
$a_b = 0.04g$	$O(\varepsilon^2)$ $\varepsilon = 0.092$	$O(\varepsilon^2)$ $\varepsilon = 0.033$	$O(1)$	$O(\varepsilon^2)$ $\varepsilon = 0.010$	$O(\varepsilon^2)$ $\varepsilon = 0.047$	$O(\varepsilon^2)$ $\varepsilon = 0.021$
$a_b = 0.02g$	$O(\varepsilon^2)$ $\varepsilon = 0.092$	0	$O(1)$	$O(\varepsilon^2)$ $\varepsilon = 0.092$	$O(\varepsilon^2)$ $\varepsilon = 0.028$	$O(\varepsilon^2)$ $\varepsilon = 0.013$

Glare 2 (mode 2)

Unit $[m/s^2]$	$\frac{\partial^2 \upsilon(s,t)}{\partial t^2}$	$\frac{c_\upsilon}{\rho A}\frac{\partial}{\partial t}\upsilon(s,t)$	$\frac{\bar{c}}{\rho A}\frac{\partial}{\partial t}\upsilon(s,t)\lvert\frac{\partial}{\partial t}\upsilon(s,t)\rvert$	$\frac{EI}{\rho A}\frac{\partial^4 \upsilon(s,t)}{\partial s^4}$	$a_b \cos\Omega t$
$a_b = 3g$	$2.6*10^3$	7.8	50	$2.6*10^3$	31
$a_b = 1g$	$1.3*10^3$	4.0	13	$1.3*10^3$	10.3
$a_b = 0.1g$	$2.7*10^2$	0.83	0	$2.7*10^2$	0.98

	$\frac{\frac{\partial^2 \upsilon(s,t)}{\partial t^2}}{\frac{\partial^2 \upsilon(s,t)}{\partial t^2}}$	$\frac{\frac{c_\upsilon}{\rho A}\frac{\partial}{\partial t}\upsilon(s,t)}{\frac{\partial^2 \upsilon(s,t)}{\partial t^2}}$	$\frac{\frac{\bar{c}}{\rho A}\frac{\partial}{\partial t}\upsilon(s,t)\lvert\frac{\partial}{\partial t}\upsilon(s,t)\rvert}{\frac{\partial^2 \upsilon(s,t)}{\partial t^2}}$	$\frac{\frac{EI}{\rho A}\frac{\partial^4 \upsilon(s,t)}{\partial s^4}}{\frac{\partial^2 \upsilon(s,t)}{\partial t^2}}$	$\frac{a_b \cos\Omega t}{\frac{\partial^2 \upsilon(s,t)}{\partial t^2}}$
$a_b = 3g$	1	$O(\varepsilon^2)$ $\varepsilon = 0.055$	$O(\varepsilon^2)$ $\varepsilon = 0.14$	$O(1)$	$O(\varepsilon^2)$ $\varepsilon = 0.11$
$a_b = 1g$	1	$O(\varepsilon^2)$ $\varepsilon = 0.055$	$O(\varepsilon^2)$ $\varepsilon = 0.10$	$O(1)$	$O(\varepsilon^2)$ $\varepsilon = 0.089$
$a_b = 0.1g$	1	$O(\varepsilon^2)$ $\varepsilon = 0.055$	0	$O(1)$	$O(\varepsilon^2)$ $\varepsilon = 0.060$

Evaluate at $s = l$	$\frac{EI}{\rho A}\frac{\partial}{\partial s}\{\frac{\partial \upsilon(s,t)}{\partial s}\frac{\partial}{\partial s}[\frac{\partial \upsilon(s,t)}{\partial s}\frac{\partial^2 \upsilon(s,t)}{\partial s^2}]\}$	$\frac{1}{2}\frac{\partial}{\partial s}\{\frac{\partial \upsilon(s,t)}{\partial s}\int_l^s \frac{\partial^2}{\partial t^2}\int_0^s [\frac{\partial \upsilon(s,t)}{\partial s}]^2 dsds\}$
$a_b = 3g$	218	-248
$a_b = 1g$	28	-32
$a_b = 0.1g$	0.26	-0.30

Evaluate at $s = l$	$\frac{\frac{EI}{\rho A}\frac{\partial}{\partial s}\{\frac{\partial \upsilon(s,t)}{\partial s}\frac{\partial}{\partial s}[\frac{\partial \upsilon(s,t)}{\partial s}\frac{\partial^2 \upsilon(s,t)}{\partial s^2}]\}}{\frac{\partial^2 \upsilon(s,t)}{\partial t^2}}$	$\frac{\frac{1}{2}\frac{\partial}{\partial s}\{\frac{\partial \upsilon(s,t)}{\partial s}\int_l^s \frac{\partial^2}{\partial t^2}\int_0^s [\frac{\partial \upsilon(s,t)}{\partial s}]^2 dsds\}}{\frac{\partial^2 \upsilon(s,t)}{\partial t^2}}$
$a_b = 3g$	$O(\varepsilon^2)$ $\varepsilon = 0.29$	$O(\varepsilon^2)$ $\varepsilon = 0.31$
$a_b = 1g$	$O(\varepsilon^2)$ $\varepsilon = 0.15$	$O(\varepsilon^2)$ $\varepsilon = 0.16$
$a_b = 0.1g$	$O(\varepsilon^2)$ $\varepsilon = 0.031$	$O(\varepsilon^2)$ $\varepsilon = 0.033$

Evaluate at $s=0$	$\frac{EI}{\rho A}\frac{\partial}{\partial s}\{\frac{\partial \upsilon(s,t)}{\partial s}\frac{\partial}{\partial s}[\frac{\partial \upsilon(s,t)}{\partial s}\frac{\partial^2 \upsilon(s,t)}{\partial s^2}]\}$	$\frac{1}{2}\frac{\partial}{\partial s}\{\frac{\partial \upsilon(s,t)}{\partial s}\int_l^s \frac{\partial^2}{\partial t^2}\int_0^s [\frac{\partial \upsilon(s,t)}{\partial s}]^2 dsds\}$
$a_b = 3g$	-212	-307
$a_b = 1g$	-27.6	-40.1
$a_b = 0.1g$	-0.25	-0.37

Evaluate at $s=0$	$\frac{\frac{EI}{\rho A}\frac{\partial}{\partial s}\{\frac{\partial \upsilon(s,t)}{\partial s}\frac{\partial}{\partial s}[\frac{\partial \upsilon(s,t)}{\partial s}\frac{\partial^2 \upsilon(s,t)}{\partial s^2}]\}}{\frac{\partial^2 \upsilon(s,t)}{\partial t^2}}$	$\frac{\frac{1}{2}\frac{\partial}{\partial s}\{\frac{\partial \upsilon(s,t)}{\partial s}\int_l^s \frac{\partial^2}{\partial t^2}\int_0^s [\frac{\partial \upsilon(s,t)}{\partial s}]^2 dsds\}}{\frac{\partial^2 \upsilon(s,t)}{\partial t^2}}$
$a_b = 3g$	$O(\varepsilon^2)$ $\varepsilon = 0.29$	$O(\varepsilon^2)$ $\varepsilon = 0.35$
$a_b = 1g$	$O(\varepsilon^2)$ $\varepsilon = 0.15$	$O(\varepsilon^2)$ $\varepsilon = 0.18$
$a_b = 0.1g$	$O(\varepsilon^2)$ $\varepsilon = 0.030$	$O(\varepsilon^2)$ $\varepsilon = 0.037$

Moment $[[N*m]$	$EI\frac{\partial^2}{\partial s^2}\upsilon(0,t)$	$k_1\frac{\partial}{\partial s}\upsilon(0,t)$	$k_3[\frac{\partial}{\partial s}\upsilon(0,t)]^3$
$a_b = 3g$	0.97	0.97	-61
$a_b = 1g$	0.49	0.49	-14
$a_b = 0.1g$	0.1	0.1	

	$\frac{EI\frac{\partial^2}{\partial s^2}\upsilon(0,t)}{EI\frac{\partial^2}{\partial s^2}\upsilon(0,t)}$	$\frac{k_1\frac{\partial}{\partial s}\upsilon(0,t)}{EI\frac{\partial^2}{\partial s^2}\upsilon(0,t)}$	$\frac{k_3[\frac{\partial}{\partial s}\upsilon(0,t)]^3}{EI\frac{\partial^2}{\partial s^2}\upsilon(0,t)}$
$a_b = 3g$	1	$O(1)$	$O(\varepsilon^2)$ $\varepsilon = 7.9$
$a_b = 1g$	1	$O(1)$	$O(\varepsilon^2)$ $\varepsilon = 5.4$
$a_b = 0.1g$	1	$O(1)$	

	f_0 (hz)	$\xi = \frac{c_\upsilon}{2\omega\rho A}$	$\frac{\overline{c}}{\rho A}[\frac{1}{m}]$	Nonlinear factor α	$k_1\,[N*m]$	$k_3\,[N*m]$
$a_b = 3g$	77.72	0.00152	1.82	$-9.4*10^8$	1081	$-8.3*10^{10}$
$a_b = 1g$	77.78	0.00152	1.84	$-3*10^9$	1622	$-5*10^{11}$
$a_b = 0.1g$	77.90	0.00152	0			

Modal space order analyses

Unit $[m^2/s^2]$	Term 1	Term 2	Term 3	Term 4	Term 5	Term 6	Term 7
$a_b = 3g$	712	2.16	2.56	712	7.29	-12.9	7.9
$a_b = 1g$	361	1.10	0.67	361	2.43	-1.7	1.0
$a_b = 0.1g$	75.9	0.23	0	75.9	0.23	-0.016	0.0096

	$\frac{\text{Term 2}}{\text{Term 1}}$	$\frac{\text{Term 3}}{\text{Term 1}}$	$\frac{\text{Term 4}}{\text{Term 1}}$	$\frac{\text{Term 5}}{\text{Term 1}}$	$\frac{\text{Term 6}}{\text{Term 1}}$	$\frac{\text{Term 7}}{\text{Term 1}}$
$a_b = 3g$	$O(\varepsilon^2)$ $\varepsilon = 0.055$	$O(\varepsilon^2)$ $\varepsilon = 0.060$	$O(1)$	$O(\varepsilon^2)$ $\varepsilon = 0.10$	$O(\varepsilon^2)$ $\varepsilon = 0.13$	$O(\varepsilon^2)$ $\varepsilon = 0.11$
$a_b = 1g$	$O(\varepsilon^2)$ $\varepsilon = 0.055$	$O(\varepsilon^2)$ $\varepsilon = 0.043$	$O(1)$	$O(\varepsilon^2)$ $\varepsilon = 0.082$	$O(\varepsilon^2)$ $\varepsilon = 0.068$	$O(\varepsilon^2)$ $\varepsilon = 0.053$
$a_b = 0.1g$	$O(\varepsilon^2)$ $\varepsilon = 0.055$	0	$O(1)$	$O(\varepsilon^2)$ $\varepsilon = 0.055$	$O(\varepsilon^2)$ $\varepsilon = 0.014$	$O(\varepsilon^2)$ $\varepsilon = 0.011$

Glare 2 (mode 3)

Unit $[m/s^2]$	$\frac{\partial^2 \upsilon(s,t)}{\partial t^2}$	$\frac{c_\upsilon}{\rho A}\frac{\partial}{\partial t}\upsilon(s,t)$	$\frac{\bar{c}}{\rho A}\frac{\partial}{\partial t}\upsilon(s,t)\lvert\frac{\partial}{\partial t}\upsilon(s,t)\rvert$	$\frac{EI}{\rho A}\frac{\partial^4 \upsilon(s,t)}{\partial s^4}$	$a_b \cos\Omega t$
$a_b = 25g$	$1.4*10^4$	46	210	$1.4*10^4$	250
$a_b = 12.5g$	$8.2*10^3$	27	99	$8.2*10^3$	129
$a_b = 5g$	$5.0*10^3$	16	23	$5.0*10^3$	50
$a_b = 0.5g$	$7.6*10^2$	2.5	0	$7.6*10^2$	4.9

	$\frac{\frac{c_\upsilon}{\rho A}\frac{\partial}{\partial t}\upsilon(s,t)}{\frac{\partial^2 \upsilon(s,t)}{\partial t^2}}$	$\frac{\frac{\bar{c}}{\rho A}\frac{\partial}{\partial t}\upsilon(s,t)\lvert\frac{\partial}{\partial t}\upsilon(s,t)\rvert}{\frac{\partial^2 \upsilon(s,t)}{\partial t^2}}$	$\frac{\frac{EI}{\rho A}\frac{\partial^4 \upsilon(s,t)}{\partial s^4}}{\frac{\partial^2 \upsilon(s,t)}{\partial t^2}}$	$\frac{a_b \cos\Omega t}{\frac{\partial^2 \upsilon(s,t)}{\partial t^2}}$
$a_b = 25g$	$O(\varepsilon^2)$ $\varepsilon = 0.057$	$O(\varepsilon^2)$ $\varepsilon = 0.12$	$O(1)$	$O(\varepsilon^2)$ $\varepsilon = 0.13$
$a_b = 12.5g$	$O(\varepsilon^2)$ $\varepsilon = 0.057$	$O(\varepsilon^2)$ $\varepsilon = 0.11$	$O(1)$	$O(\varepsilon^2)$ $\varepsilon = 0.12$
$a_b = 5g$	$O(\varepsilon^2)$ $\varepsilon = 0.057$	$O(\varepsilon^2)$ $\varepsilon = 0.068$	$O(1)$	$O(\varepsilon^2)$ $\varepsilon = 0.10$
$a_b = 0.5g$	$O(\varepsilon^2)$ $\varepsilon = 0.055$	0	$O(1)$	$O(\varepsilon^2)$ $\varepsilon = 0.080$

Evaluate at $s = l$	$\frac{EI}{\rho A}\frac{\partial}{\partial s}\{\frac{\partial \upsilon(s,t)}{\partial s}\frac{\partial}{\partial s}[\frac{\partial \upsilon(s,t)}{\partial s}\frac{\partial^2 \upsilon(s,t)}{\partial s^2}]\}$	$\frac{1}{2}\frac{\partial}{\partial s}\{\frac{\partial \upsilon(s,t)}{\partial s}\int_l^s \frac{\partial^2}{\partial t^2}\int_0^s [\frac{\partial \upsilon(s,t)}{\partial s}]^2 dsds\}$
$a_b = 25g$	$-1.6*10^3$	$2.7*10^3$
$a_b = 12.5g$	-329	543
$a_b = 5g$	-74	121
$a_b = 0.5g$	-0.26	0.42

Evaluate at $s = l$	$\frac{\frac{EI}{\rho A}\frac{\partial}{\partial s}\{\frac{\partial \upsilon(s,t)}{\partial s}\frac{\partial}{\partial s}[\frac{\partial \upsilon(s,t)}{\partial s}\frac{\partial^2 \upsilon(s,t)}{\partial s^2}]\}}{\frac{\partial^2 \upsilon(s,t)}{\partial t^2}}$	$\frac{\frac{1}{2}\frac{\partial}{\partial s}\{\frac{\partial \upsilon(s,t)}{\partial s}\int_l^s \frac{\partial^2}{\partial t^2}\int_0^s [\frac{\partial \upsilon(s,t)}{\partial s}]^2 dsds\}}{\frac{\partial^2 \upsilon(s,t)}{\partial t^2}}$
$a_b =$ $25g$	$O(\varepsilon^2)$ $\varepsilon = 0.34$	$O(\varepsilon^2)$ $\varepsilon = 0.43$
$a_b =$ $12.5g$	$O(\varepsilon^2)$ $\varepsilon = 0.20$	$O(\varepsilon^2)$ $\varepsilon = 0.26$
$a_b =$ $5g$	$O(\varepsilon^2)$ $\varepsilon = 0.12$	$O(\varepsilon^2)$ $\varepsilon = 0.16$
$a_b =$ $0.5g$	$O(\varepsilon^2)$ $\varepsilon = 0.018$	$O(\varepsilon^2)$ $\varepsilon = 0.023$

Evaluate at $s = 0$	$\frac{EI}{\rho A}\frac{\partial}{\partial s}\{\frac{\partial \upsilon(s,t)}{\partial s}\frac{\partial}{\partial s}[\frac{\partial \upsilon(s,t)}{\partial s}\frac{\partial^2 \upsilon(s,t)}{\partial s^2}]\}$	$\frac{1}{2}\frac{\partial}{\partial s}\{\frac{\partial \upsilon(s,t)}{\partial s}\int_l^s \frac{\partial^2}{\partial t^2}\int_0^s [\frac{\partial \upsilon(s,t)}{\partial s}]^2 dsds\}$
$a_b =$ $25g$	$-1.7*10^3$	$-6.8*10^3$
$a_b =$ $12.5g$	-335	-1385
$a_b =$ $5g$	-75	-310
$a_b =$ $0.5g$	-0.26	-1.1

Evaluate at $s = 0$	$\frac{\frac{EI}{\rho A}\frac{\partial}{\partial s}\{\frac{\partial \upsilon(s,t)}{\partial s}\frac{\partial}{\partial s}[\frac{\partial \upsilon(s,t)}{\partial s}\frac{\partial^2 \upsilon(s,t)}{\partial s^2}]\}}{\frac{\partial^2 \upsilon(s,t)}{\partial t^2}}$	$\frac{\frac{1}{2}\frac{\partial}{\partial s}\{\frac{\partial \upsilon(s,t)}{\partial s}\int_l^s \frac{\partial^2}{\partial t^2}\int_0^s [\frac{\partial \upsilon(s,t)}{\partial s}]^2 dsds\}}{\frac{\partial^2 \upsilon(s,t)}{\partial t^2}}$
$a_b =$ $25g$	$O(\varepsilon^2)$ $\varepsilon = 0.34$	$O(\varepsilon^2)$ $\varepsilon = 0.70$
$a_b =$ $12.5g$	$O(\varepsilon^2)$ $\varepsilon = 0.20$	$O(\varepsilon^2)$ $\varepsilon = 0.41$
$a_b = 5g$	$O(\varepsilon^2)$ $\varepsilon = 0.12$	$O(\varepsilon^2)$ $\varepsilon = 0.25$
$a_b = .5g$	$O(\varepsilon^2)$ $\varepsilon = 0.018$	$O(\varepsilon^2)$ $\varepsilon = 0.038$

Moment $[[N*m]$	$EI\frac{\partial^2}{\partial s^2}\upsilon(0,t)$	$k_1\frac{\partial}{\partial s}\upsilon(0,t)$	$k_3[\frac{\partial}{\partial s}\upsilon(0,t)]^3$
$a_b = 25g$	1.9	1.9	-86
$a_b = 12.5g$	1.1	1.1	-35
$a_b = 5g$	0.68	0.68	-11
$a_b = 0.5g$	0.1	0.1	

	$\frac{EI\frac{\partial^2}{\partial s^2}\upsilon(0,t)}{EI\frac{\partial^2}{\partial s^2}\upsilon(0,t)}$	$\frac{k_1\frac{\partial}{\partial s}\upsilon(0,t)}{EI\frac{\partial^2}{\partial s^2}\upsilon(0,t)}$	$\frac{k_3[\frac{\partial}{\partial s}\upsilon(0,t)]^3}{EI\frac{\partial^2}{\partial s^2}\upsilon(0,t)}$
$a_b = 25g$	1	$O(1)$	$O(\varepsilon^2)$ $\varepsilon = 6.8$
$a_b = 12.5g$	1	$O(1)$	$O(\varepsilon^2)$ $\varepsilon = 5.7$
$a_b = 5g$	1	$O(1)$	$O(\varepsilon^2)$ $\varepsilon = 4.1$
$a_b = 0.5g$	1	$O(1)$	

	f_0 (hz)	$\xi = \frac{c_\upsilon}{2\omega\rho A}$	$\frac{\overline{c}}{\rho A}[\frac{1}{m}]$	Nonlinear factor α	$k_1\,[N*m]$	$k_3\,[N*m]$
$a_b = 25g$	214.88	0.00163	1.96	$-9.2*10^{10}$	382	$-7.3*10^{8}$
$a_b = 12.5g$	215.35	0.00163	2.68	$-1.14*10^{11}$	587	$-5.27*10^{9}$
$a_b = 5g$	215.6	0.00163	1.70	$-1.19*10^{11}$	817	$-2.04*10^{10}$
$a_b = 0.5g$	216.25	0.00163	0			

Modal space order analyses

Unit $[m^2/s^2]$	Term 1	Term 2	Term 3	Term 4	Term 5	Term 6	Term 7
$a_b = 25g$	3868	12.6	11.2	3868	35.1	-62	342
$a_b = 12.5g$	2278	7.4	5.3	2278	18.1	-12.7	69
$a_b = 5g$	1385	4.5	1.2	1385	7.0	-2.8	15
$a_b = 0.5g$	210	0.69	0	210	0.69	-0.01	0.054

	$\frac{\text{Term 2}}{\text{Term 1}}$	$\frac{\text{Term 3}}{\text{Term 1}}$	$\frac{\text{Term 4}}{\text{Term 1}}$	$\frac{\text{Term 5}}{\text{Term 1}}$	$\frac{\text{Term 6}}{\text{Term 1}}$	$\frac{\text{Term 7}}{\text{Term 1}}$
$a_b = 25g$	$O(\varepsilon^2)$ $\varepsilon = 0.057$	$O(\varepsilon^2)$ $\varepsilon = 0.054$	$O(1)$	$O(\varepsilon^2)$ $\varepsilon = 0.095$	$O(\varepsilon^2)$ $\varepsilon = 0.13$	$O(\varepsilon^2)$ $\varepsilon = 0.30$
$a_b = 12.5g$	$O(\varepsilon^2)$ $\varepsilon = 0.057$	$O(\varepsilon^2)$ $\varepsilon = 0.048$	$O(1)$	$O(\varepsilon^2)$ $\varepsilon = 0.089$	$O(\varepsilon^2)$ $\varepsilon = 0.075$	$O(\varepsilon^2)$ $\varepsilon = 0.17$
$a_b = 5g$	$O(\varepsilon^2)$ $\varepsilon = 0.057$	$O(\varepsilon^2)$ $\varepsilon = 0.030$	$O(1)$	$O(\varepsilon^2)$ $\varepsilon = 0.071$	$O(\varepsilon^2)$ $\varepsilon = 0.045$	$O(\varepsilon^2)$ $\varepsilon = 0.11$
$a_b = 0.5g$	$O(\varepsilon^2)$ $\varepsilon = 0.057$	0	$O(1)$	$O(\varepsilon^2)$ $\varepsilon = 0.057$	$O(\varepsilon^2)$ $\varepsilon = 0.0068$	$O(\varepsilon^2)$ $\varepsilon = 0.016$

REFERENCES

1. Allemang, R. J. and Brown, D. L., 1996, Experimental Modal Analysis, Chapter 21 in Shock and Vibration HandbookC. M. Harris (ed.), McGraw-Hill, New York.

2. Cady, W.G., 1964, Piezoelectricity. Dover, New York.

3. Gibson, R., 1989, Vibration-test methods for dynamic-mechanical-property characterization. Manual on Experimental Methods for Mechanical Testing of Composites, VII E, R. L. Pendleton and M. E. Tuttle, eds., Society for Experimental Mechanics, Bethel, CT.

4. Lee, C.K., 1992, Piezoelectric laminates theory and experiment for distributed sensors and actuators. Intelligent Structural Systems, Dordrecht Kluwer Academic (pp75-167).

5. Love, A. E. H., 1944, A Treatise on the Mathematical Theory of Elasticity, Dover, New York.

6. Meirovitch, L., 1997, Principles and Techniques of Vibrations, Prentice Hall, Upper Saddle River, New Jersey.

7. Nayfeh, A. H. and Mook, D. T., 1979, Nonlinear Oscillations, Wiley, New York.

8. Srinivasan, A.V. and McFarland, D.M., 2000, Smart Structures: Analysis and Design, Cambridge University Press, Cambridge, UK.

9. Thomson, W. T. and Dahleh, M. D., 1997, Theory of Vibration with Applications, Prentice-Hall, Englewood Cliff, New Jersey.

10. Timoshenko, S. P., 1983, History of Strength of Materials, Dover, New York.

11. Tzou, H.S. 1993, Piezoelectric shells (Distributed sensing and control of continua) Prentice-Hall, Dordrecht Kluwer Academic.

12. Vlot, A. and Gunnink, J.W. (Eds), 2001, Fiber Metal Laminates: an Introduction. Kluwer, Dordrecht, The Netherlands.

13. Anderson, T. J., Nayfeh, A. H., and Balachandran, B., 1996, Experimental verification of the importance of the nonlinear curvature in the response of a cantilever beam, Journal of Vibration and Acoustics, 118, pp. 21—27.

14. Agnes, G. S., 1995, Development of a modal model for simultaneous active and passive piezoelectric Vibration suppression Journal of Intelligent Materials Systems and Structures, 6, 482-487.

15. Agrawal, S. K., Tong, D. and Nagaraja, K., 1994, Modeling and Shape Control of Piezoelectric Embedded Elastic Plates, Journal of Intelligent Materials Systems and Structures,5, 514-521.

16. Agrawal, B. N. and Treanor, K. E., 1999, Shape Control of a Beam Using Piezoelectric Actuators, Smart Materials and Structures, 8, 729-740.

17. Akella, P., Chen, X., Cheng, W., Hughes, D. and Wen, J. T., 1994, Modeling and Control of Smart Structures with Bonded Piezoelectric Sensors and Actuators Smart Materials and Structures, 3, 344-353.

18. Albert, T. E. and Colvin, A., 1991, Observations on the nature of transfer functions for control of piezoelectric laminates, Journal of Intelligent Materials Systems and Structures, 2, 528-541.

19. Aldraihem, O.J. and Wetherhold, R.C., 1997, Mechanics and control of coupled bending and twisting vibration of laminated beams, Smart Materials and Structures, 6, 123-133.

20. Aldraihem, O.J. and Khdeir, A. A., 2000, Smart beams with extension and thickness-shear piezoelectric actuators, Smart Materials and Structures, 9, 1-9.

21. Aldraihem, O.J., Singh, T. and Wetherhold, R.C., 2000, Optimal size and location of piezoelectric actuator/sensors: practical considerations, Journal of Guidance, Control and Dynamics, 23, 509-515.

22. Algrain, M., Hardt, S. and Ehlers, D., 1997, A phase-lock-loop-based control system for suppressing periodic vibration in smart structural systems, Smart Materials and Structures, 6, 10-22.

23. Anderson, E. H. and Hagood, N.W., 1994, Simultaneous piezoelectric sensing/actuation: analysis and application to controlled structures, Journal of Sound and Vibration, 174, 617-639.

24. Ang, K.K., Wang, S.Y. and Quek, S.T., 2002, Weighted energy linear quadratic regulator vibration control of piezoelectric composite plates, Smart Materials and Structures, 11, 98-106.

25. Angelino, M.R. and Washington, G.N., 2002, Design and construction of a piezoelectric point actuated active aperture antenna, Journal of Intelligent Material Systems and Structures, 13, 125-136.

26. Arafat, H. N. and Nayfeh, A. H., 2001, The influence of nonlinear boundary conditions on the nonplanar autoparametric responses of an inextensible beam, in Proceedings of the 2001 ASME Design Engineering Technical Conferences, Pittsburgh, Pennsylvania.

27. Badre-Alam, A., Wang, K.W. and Gandhi, F., 1999, Optimization of enhanced active constrained layer (EACL) treatment on helicopter flexbeams for aeromechanical stability augmentation, Smart Materials and Structures, 8, 182-196.

28. Bai, M.R. and Lin, G.M., 1996, The development of a DSP-based active small amplitude vibration control system for flexible beams by using LQG algorithms and intelligent materials, Journal of Sound and Vibration, 198, 411-427.

29. Bailey, T. and JE Hubbard, Jr., 1985, Distributed piezoelectric polymer active vibration control of a cantilever beamJournal of Guidance, Control and Dynamics, 8, 605-611.

30. Balamurugan, V. and Narayanan, S., 2001, Active vibration control of piezolaminated smart beams, Defence Science Journal, 51, 103- 114.

31. Balamurugan, V. and Narayanan, S., 2001, Active vibration control of smart, shells using distributed piezoelectric sensors and actuators, Smart Materials and Structures, 10, 173- 180.

32. Ball, J. K. and Jones, J. D., 1995, A comparison of shaped piezoelectric actuator for divergence control, Journal of Intelligent Material Systems and Structures, 6, 598-609.

33. Banks, H. T., Ito, K. and Wang, Y., 1993, Computational methods for identification and feedback control in structures with piezoelectric actuators and sensors, Journal of Intelligent Material Systems and Structures, 4, 469-476.

34. Barboni, R., Mannini, A., Fantini, E. and Gaudenzi, P., 1999, Optimal placement of PZT actuators for control of beam dynamics, Smart Materials and Structures, 8, 110-120.

35. Barrett, R., Frye and Scliesman, M., 1998, Design, construction and characterization of a flightworthy piezoelectric solid state adaptive rotor, Smart Materials and Structures, 7, 422-431.

36. Bayon De Noyer, M. P. and Hanagud, S. V., 1998, Single actuator and multi-mode acceleration feedback control, Journal of Intelligent Material Systems and Structures, 9, 522-533.

37. Baz, A., Poh, S. and Fedor, J., 1992, Independent modal space control with positive position feedback, Journal of Guidance, Control and Dynamics, 114, 96-103.

38. Baz, A., 1995, Optimal deflection control of multi-segment traversing beams Smart Materials and Structures, 4, 75-82.

39. Baz, A. and Poh, S., 1996, Modal and physical deflections of beams using distributed wire sensors, Smart Materials and Structures, 5, 261-271.

40. Baz, A. and Ro, J., 1996, Vibration control of plates with active constrained layer damping, Smart Materials and Structures, 5, 272-280.

41. Baz, A. and Hong, J.-T., 1997, Adaptive control of flexible structures using modal positive position feedback, International Journal of Adaptive Control and Signal Processing, 11, 231-253.

42. Baz, A. and Ro, J., 2001, Vibration control of rotating beams with active constrained layer damping, Smart Materials and Structures, 10, 112-120.

43. Beckert, W. and Pfundtner, G., 2002, Analysis of the deformational behaviors of a bimorph configuration with piezoelectric actuation, Smart Materials and Structures, 11, 599-609.

44. Benjeddou, A., Trindade, M. A. and Ohayon, R., 1997, A unified beam finite element model for extension and shear piezoelectric actuation mechanisms, Journal of Intelligent Material Systems and Structures, 8, 1012-1025.

45. Benjeddou, A., Trindade, M. A. and Ohayon, R., 2000, Piezoelectric actuation mechanisms for intelligent sandwich structures, Smart Materials and Structures, 9, 328-335.

46. Bent, A. A., 1997, Piezoelectric Fiber composites with interdigitated electrodes, Journal of Intelligent Material Systems and Structures, 8, 903-919.

47. Berdichevsky, V.L., Kim, W.W., Ozbek, A., 1995, Dynamical potential for nonlinear vibrations of cantilevered beams, Journal of Sound and Vibration, 179, 151-164.

48. Bert, C.W., 1973, Material damping: an introductory review of mathematical models, measures, and experimental techniques, Journal of Sound and Vibration, 29, 129-153.

49. Bhargava, A., Chaudhry, Z., Liang, C. and Roger, C, A, 1995, Experimental verification of optimal actuator location and configuration based on actuator power factor, Journal of Intelligent Material Systems and Structures, 6, 411-418.

50. Bhattacharya, P., Suhail, H. and Sinha, P.K., 1998, Finite element free vibration analysis of smart laminated composite beams and plates, Journal of Intelligent Material Systems and Structures, 9, 20-28.

51. Bin, L. (Li, B.), Li, Y., Yin, X. and Huang, S., 2000, Maximal modal force rule for optimal placement of point piezoelectric actuators for plates, Journal of Intelligent Material Systems and Structures, 11, 512-515.

52. Birman, V., Knowles, G.J. and Murray, J.J., 1999, Application of piezoelectric actuators to active control of composite spherical caps, Smart Materials and Structures, 8, 218-222.

53. Bisegna, P. and Maceri, F., 1996, A consistent theory of thin piezoelectric plates, Journal of Intelligent Material Systems and Structures, 7, 372-389.

54. Bisegna, P. and Caruso, G., 2000, Mindlin-type finite elements for piezoelectric sandwich plates, Journal of Intelligent Material Systems and Structures, 11, 14-25.

55. Brennan, M.J., Garcia-Bonito, J., Elliott, S.J., David, A. and Pinnington, R.J., 1999, Experimental investigation of different actuator technologies for active vibration control, Smart Materials and Structures, 8, 145-153.

56. Bronowicki, A.J., McIntyre, L.J., Betros, R.S. and Dvorsky, G.R., 1996, Mechanical validation of smart structures, Smart Materials and Structures, 5,129-139.

57. Brooks, S. and Heyliger, P., 1994, Static behavior of piezoelectric laminates with distributed and patched actuators, Journal of Intelligent Material Systems and Structures, 5, 635-646.

58. Bruant, I., Coffignal, G., Léné, F. and Vergé, M., 2001, Active control of beam structures with piezoelectric actuators and sensors: modeling and simulation, Smart Materials and Structures, 10, 404-408.

59. Brush, J. C., Sloss, J. M. and Sadek, I. S., 2000, Optimal piezo-actuator location/lengths and applied voltage for shape control of beams, Smart Materials and Structures, 9, 205-211.

60. Burgreen, D., 1951, Free vibrations of a pin-ended column with constant distance between pin ends, Journal of Applied Mechanics, 18, pp. 135—139.

61. Busby, H. R. and Weingarten, V. I., 1972, Non-linear response of a beam to periodic loading, International Journal of Non-Linear Mechanics, 7, pp. 289—303.

62. Butler, R. and Rao, V., 1996, A state space modeling and control method for multivariable smart structural systems, Smart Materials and Structures, 5, 386-399.

63. Cai, C., Liu, G.R. and Lam, K.Y., 2001, A technique for modeling multiple piezoelectric layers, Smart Materials and Structures, 10, 689-694.

64. Cai, D. and Gao, D. Y., 1998, Shear control and analytic solutions for 2-D dynamic smart beam theory, Journal of Intelligent Material Systems and Structures, 9, 182-188.

65. Cannon Jr., R. H. and Rosenthal, D. E., 1984, Experiments in control of flexible structures with noncolocated sensors and actuators, Journal of Guidance, 7,546-553.

66. Carpenter, M. J. 1997, Using energy methods to derive beam finite elements incorporating piezoelectric materials Journal of Intelligent Material Systems and Structures, 8, 26-40.

67. Centolanza1, L.R., Smith, E.C. and Munsky, B., 2002, Induced-shear piezoelectric actuators for rotor blade trailing edge flaps, Smart Materials and Structures, 11, 24-35.

68. Chandra, R. and Chopra, I., 1993, Structural modeling of composite beams with strain-induced actuators, AIAA Journal, 31, 1692-1701.

69. Chandrashekhara, K. and Afarwai, A. N., 1993, Active vibration control of laminated composite plates using piezoelectric devices: A finite element approach, Journal of Intelligent Material Systems and Structures, 4, 496-508.

70. Chandrashekhara, K. and Bhatia, K., 1993, Active buckling control of smart composite plates finite-element analysis, Smart Materials and Structures, 2, 31-39.

71. Chandrashekhara, K. and Tenneti, R., 1995, Thermally induced vibration suppression of laminated plates with piezoelectric sensors and actuators, Smart Materials and Structures, 4, 281-290.

72. Chandrashekhara, K. and Donthireddy, P., 1997, Vibration suppression of composite beams with piezoelectric devices using higher order theory, European journal of mechanics, A/Solid, 4, 709-721.

73. Chandrashekhara, K. and Varadarajan, S., 1997, Active shape control of composite beams with piezoelectric actuators, Journal of Intelligent Material Systems and Structures, 8, 112-124.

74. Chandrashekhana, C. and Stanway, R., 2000, Active constrained layer damping of plate vibrations: A numerical and experimental study of modal controllers, Smart Materials and Structures, 9, 940-952.

75. Charette, F. and Berry, A., 1997, Dynamic effects of piezoelectric actuators on the vibrational response of a plate, Journal of Intelligent Material Systems and Structures, 8, 513-524.

76. Chattopadhyay, A. and Seeley, C.E., 1994, A multiobjective design optimization procedure for control of structures using piezoelectric materials, Journal of Intelligent Material Systems and Structures, 5, 403-411.

77. Chattopadhyay, A. and Seeley, C.E. , 1995, A coupled controls/structures optimization procedure for the design of rotating composite box beams with piezoelectric actuators, Smart Materials and Structures, 4, 170-178.

78. Chattopadhyay, A., Dragomir-daescu, D. and Gu, H., 1999, Dynamics of delaminated smart composite cross-ply beams, Smart Materials and Structures, 8, 92-99.

79. Chaudhry, Z. and Roges, C. A., 1994, The pin-force model revisited, Journal of Intelligent Material Systems and Structures, 5, 347-354.

80. Chee, C.Y.K., Tong, L. and Steven, G.P., 1998, A review on the modeling of piezoelectric sensors and actuators incorporated in intelligent structures, Journal of Intelligent Material Systems and Structures, 9, 3-19.

81. Chee, C.Y.K., Tong, L. and Steven, G.P., 1999, A mixed model for composite beams with piezoelectric actuators and sensors, Smart Materials and Structures, 8, 417-432.

82. Chee, C. I., Napolitano, M. R. and Chen, C.-L., 1992, A new learning algorithm for neural network state estimation in active vibration control, Smart Materials and Structures, 1, 250-257.

83. Chen, C.Q. and Shen, Y.P., 1997, Optimal control of active structures with piezoelectric modal sensors and actuators, Smart Materials and Structures, 6,403-409.

84. Chen, Q. and Levy, C., 1996, Active vibration control of elastic beam by means of shape memory alloy layers, Smart Materials and Structures, 5, 400-406.

85. Chen, S. and Cao, Z., 2000, A new method for determining location of piezoelectric sensor/actuator for vibration control of intelligent structures, Journal of Intelligent Material Systems and Structures, 11, 108-115.

86. Chen, S.-H., Yao, G.-F. and Huang, C., 2000, A new intelligent thin-shell element, Smart Materials and Structures, 9, 10-18.

87. Cheng, J., Qian, C., Zhao, M., Lee, S.W.R., Tong, P. and Zhang, T.Y., 2000, Effects of electric fields on the bending behavior of PZT-5H piezoelectric laminates, Smart Materials and Structures, 9, 824-831.

88. Choi, S. and Lee, J. J.,1998, The shape control of a composite beam with embedded shape memory alloy wire actuators, Smart Materials and Structures,7, 759-770.

89. Choi, W. C. and Kim, N. W., 1996, Experimental study on active vibration control of a flexible cantilever using an artificial neural-network state predictor Smart Materials and Structures, 5, 751-758.

90. Choi, S.B., 1995, Alleviation of chattering in flexible beam control via piezofilm actuator and sensor, AIAA Journal, 33, 564-567.

91. Choi, S.B., Cho, S.S., Shin, H.C. and Kim, H.K., 1999, Quantitative feedback theory control of a single-link flexible manipulator featuring piezoelectric actuator and sensor, Smart Materials and Structures, 8, 338-349.

92. Clark, R.L., Flemming, M.R. and Fuller, C.R., 1993, Piezoelectric actuators for distributed vibration excitation of thin plates: a comparison between theory and experiment, Journal of Vibration and Acoustics, 115, 332-339.

93. Clark, W. W., Robertshaw, H. H. and Warrington, T. J., 1990, A comparison of actuators for vibration control of the planner vibrations of a flexible cantilevered beam, Journal of Intelligent Material Systems and Structures, 1, 289-308.

94. Clark, W. W., 2000, Vibration control with state-switched piezoelectric materials, Journal of Intelligent Material Systems and Structures, 11, 263-271.

95. Cole, D. C. and Clark, R. L., 1994, Adaptive compensation of piezoelectric sensoriactuators, Journal of Intelligent Material Systems and Structures, 5, 665-672.

96. Crespo da Silva, M. R. M., 1978, Flexural-flexural oscillations of Beck's column subject to a planar harmonic excitation, Journal of Sound and Vibration, 60, 133-144.

97. Crespo da Silva, M. R. M., 1978, Harmonic non-linear response of Beck's column to a lateral excitation, International Journal of Solids and Structures, 14, 987-997.

98. Crespo da Silva, M. R. M. and Hodges, D. H., 1986, Nonlinear flexure and torsion of rotating beams with application to helicopter rotor blades. I: Formulation, Vertica, 10, 151-169.

99. Crespo da Silva, M. R. M. and Hodges, D. H., 1986, Nonlinear flexure and torsion of rotating beams, with application to helicopter rotor blades. II: Response and stability results, Vertica, 10, 171-186.

100. Crespo da Silva, M. R. M., Zaretzky, C. L., and Hodges, D. H., 1991, Effects of approximation on the static and dynamic response of a cantilever with a tip mass, International Journal of Solids and Structures, 27, 565-583.

101. Crwaley, E.F. and deLuis, J., 1987, Use of piezoelectric actuators as elements of intelligent structures, AIAA Journal, 25, 1373-1385.

102. Crawley, E.F. and Anderson, E.H., 1990, Detailed models of piezoceramic actuation of beams, Journal of Intelligent Material Systems and Structures, 1, 4-25.

103. Crwaley, E.F., 1994, Intelligent structures for aerospace: a technology overview and assessment, AIAA Journal, 32, 1689-1699.

104. Damle, R., Lashlee, R., Rao, V. and Kern, F., 1994, Identification and robust control of smart structures using artificial neural networks, Smart Materials and Structures, 3, 35-46.

105. Damle, R., Rao, V. and Kern, F., 1997, Robust control of smart structures using artificial neural networks hardware, Smart Materials and Structures, 6, 301-314.

106. D'cruz, J., 1993, The active control of panel vibrations with piezoelectric actuators, Journal of Intelligent Material Systems and Structures, 4, 398-342.

107. De Blonk, B. J. and Lagoudas, D. C., 1998, Actuation of electrometric rods with embedded two-way shape memory alloy actuators, Smart Materials and Structures, 7, 771-783.

108. De Faria, A. R. and De Almeida, S. F. M., 1996, modeling of actively damped beams with piezoelectric actuators with finite stiffness bondJournal of Intelligent Material Systems and Structures, 7, 677-688.

109. Degiorgi, V. G., Lindner, D. K. and Mcdermott, S. H., 1999, Combining modeling methodologies for improved understanding of smart material characteristics, Journal of Intelligent Material Systems and Structures, 9, 509-521.

110. Dimitriadis, E.K., Fuller, C.R. and Rogers, C.A., 1991, Piezoelectric actuators for distributed vibration excitation of thin plates, Journal of Vibration and Acoustics, 113, 100-107.

111. Diwekar, A. M. and Yedavalli, R. K., 1996, Smart structure control in matrix second-order form Smart Materials and Structures, 5, 429-436.

112. Dosch, J.J., Inman, D.J., and Garcia, E., 1992, A self-sensing piezoelectric actuator for collocated control, Journal of Intelligent Material Systems and Structures, 3, 166-185.

113. Dowell, E. H., Traybar, J., and Hodges, D. H., 1977, An experimental-theoretical correlation study of non-linear bending and torsion deformations of a cantilever beam, Journal of Sound and Vibration, 50, 533-544.

114. Doyle, C. and Fernando, G., 1998, Detecting impact damage in a composite material with an optical fiber vibration sensor system, Smart Materials and Structures, 7, 543-549.

115. Du, H., Lau, G. K., Lim, M. K. and Qui, J., 2000, Topological optimization of mechanical amplifier for piezoelectric actuators under dynamic motion, Smart Materials and Structures, 9, 788-800.

116. Eisley, J. G., 1964, Nonlinear vibration of beams and rectangular plates, ZAMP, 15, 167-175.

117. Epps, J. and Chandra, R., 1997, Shape memory alloy actuation for active tuning of composite beams, Smart Materials and Structures, 6, 251-264.

118. Evensen, D. A., 1968, nonlinear vibrations of beams with various boundary conditions, AIAA Journal, 6, 370-372.

119. Fanson, J. L., 1990, Positive position feedback control for large space structures, AIAA Journal, 28, 717-724.

120. Fariborzi, F., Golnaraghi, M.F. and Heppler, G.R., 1997, Experimental control of free and forced structural vibration using a linear coupling strategy, Smart Materials and Structures, 6, 540-548.

121. Frecker, M. and Canfield, S., 2000, Optimal design and experimental validation of compliant mechanical amplifiers for piezoelectric stack actuators, Journal of Intelligent Material Systems and Structures, 11, 360-369.

122. Gao, F., Shen, Y. and Li, L., 2000, The optimal design of piezoelectric actuators for plate vibroacoustic control using genetic algorithms with immune diversity. Smart Materials and Structures, 9, 485-491.

123. Friswell, M. I., 2001, On the design of modal actuators and sensorsJournal of Sound and Vibration, 241, 361-372.

124. Fukuda, T., Takawam, T. and Nakashima, K., 2000, Optimum vibration control of CFRP sandwich beam using electro-rheological fluids and piezoceramic actuators, Smart Materials and Structures, 9, 121-125.

125. Fung, R.-F., Huang, J.-S., and Jan, S.-C., 2000, Dynamic analysis of a piezothermoelastic resonator with various shapes, Journal of Vibration and Acoustics, 122, 244-253.

126. Gao, F., Shen, Y and Li, L., 2000, The optimal design of piezoelectric actuators for plate vibroacoustic control using genetic algorithms with immune diversity, Smart Materials and Structures, 9, 485-491.

127. Garcia-Bonito, J., Brennan, M.J., Elliott, S.J., David, A. and Pinnington, R.J., 1998, A novel high-displacement piezoelectric actuator for active vibration control, Smart Materials and Structures, 7, 31-42.

128. Gaudenzi, P., and Fantino, E., 1998, Genetic algorithm optimization for the active control of a beam by means of PZT actuators, Journal of Intelligent Material Systems and Structures, 9, 291-300.

129. Gaudenzi, P., and Barboni, R., 1999, Static adjustment of beam deflections by means of induced strain actuators, Smart Materials and Structures, 8, 278-283.

130. Gaudenzi, P., Carbonaro, R. and Benzi, E., 2000, Control of beam vibrations by means of piezoelectric devices: theory and experiments, Composite Structures, 50, 373-379.

131. Gawronski, W., 1999, Simultaneous placement of actuators and sensors, Journal of Sound and Vibration, 228, 915-922.

132. Gibbs, G.P. and Fuller, C.R., 1992, Excitation of thin beams using asymmetric piezoelectric actuators, Journal of Acoustic Society of American, 92, 3221-3227.

133. Giurgiutiu, V., 2000, Review of smart-materials actuation solutions for aeroelastic and vibration control, Journal of Intelligent Material Systems and Structures, 11, 525-544.

134. Goh, C. J. and Caughey, T. K., 1985, On the stability problem caused by finite actuator dynamics in the collocated control of large space structures, International Journal of Control, 41, 787-802.

135. Golubin, A.Y. and Kalamkarov, A.L., 2000, Optimal control problems in the theory of smart structures, Smart Materials and Structures, 9, 226-234.

136. Goo, N.S., Kim, C., Kwon, Y-D. and Yoon, K.J., 2001, Behaviors and performance evaluation of a lightweight piezo-composite curved actuator, Journal of Intelligent Material Systems and Structures, 12, 639-646.

137. Gopinathan, S. V., Varadan, V. V. and Varadan, V. K., 2000, A review and critique of theories for piezoelectric laminates, Smart Materials and Structures, 9, 24-48.

138. Ha, S.-K., Keilers, C. and Chang, F.-K., 1991, Analysis of laminated composites containing distributed piezoelectric ceramics, Journal of Intelligent Material Systems and Structures, 2, 59-71.

139. Ha, S.-K., Keilers, C. and Chang, F.-K., 1992, Finite element analysis of composite structures containing distributed piezoceramic sensors and actuators, AIAA Journal, 30, 772-80.

140. Hac, A. and Liu, L., 1993, Sensor and actuator location in motion control of flexible structures, Journal of Sound and Vibration, 167, 239-261.

141. Hagood, N.W., Chang, W. H. and von Flotow, A., 1990, Modeling of piezoelectric actuator dynamics for active structural control, Journal of Intelligent Material Systems and Structures, 1, 327-354.

142. Hagood, N.W. and von Flotow, A., 1991, damping of structural vibration with piezoelectric materials and passive electrical networks, Journal of Sound and Vibration, 146, 243-264.

143. Han, J.H., Rew, K.H. and Lee, I., 1997, An experimental study of active vibration control of composite structures with a piezo-ceramic actuator and a piezo-film sensor, Smart Materials and Structures, 6, 549-558.

144. Han, J.H. and Lee, I., 1999, Optimal placement of piezoelectric sensors and actuators for vibration control of a composite plate using genetic algorithms, Smart Materials and Structures, 8, 257-267.

145. Han, J.H., Cho, K.D., Youn, S.H. and Lee, I., 1999, Vibration and actuation characteristics of composite structures with a bonded piezo-ceramic actuator, Smart Materials and Structures, 8, 136-143.

146. Hashin, Z., 1970, Complex moduli of viscoelastic composites - i. general theory and application to particulate composites, International Journal of Solids and Structures, 6, 539-552.

147. Hashin, Z., 1970, Complex moduli of viscoelastic composites - ii. fiber reinforced materials, International Journal of Solids and Structures, 6, 797-807.

148. Hodges, D. H., Crespo da Silva, M. R. M., and Peters, D. A., 1988, Nonlinear effects in the static and dynamic behavior of beams and rotor blades, Vertica, 12, 243—256.

149. Hollkamp, J.J., 1994, Multimodal passive vibration suppression with piezoelectric materials and resonant shunts, Journal of Intelligent Material Systems and Structures, 5, 49-57.

150. Hollkamp, J.J., 1994, A self-tuning piezoelectric vibration absorber, Journal of Intelligent Material Systems and Structures, 5, 559-566.

151. Hollkamp, J.J. and Gordon, R.W., 1996, An experimental comparison of piezoelectric and constrained layer damping, Smart Materials and Structures, 5, 715-722.

152. Hong, S.Y., Varadan, V.V., and Varadan, V.K., 1998, Implementation of coupled mode optimal structural vibration control using approximated eigenfunctions, Smart Materials and Structures, 7, 63-71.

153. Huang, S.C., Inman, D.J. and Austin, E. M., 1996, Some design considerations for active and passive constrained layer damping treatments, Smart Materials and Structures, 5, 301-313.

154. Hwang, J.K., Choi, C.-H. and Song, C.K., 2000, Phase delay control of a cantilever beam, Journal of Vibration and Control, 6, 257-272.

155. Hwang, W.S., Park, H.C. and Hwang, W., 1994, Vibration control of laminated plate with piezoelectric sensors/actuators: Finite element formulation and modal analysis, Advances in vibration control for intelligent structures, 1, 45-56.

156. Ikegami, R., Wilson, D.G., Anderson, J.R. and Julien, F.J., 1990, Active vibration control using NiTiNOL and piezoelectric ceramics, Journal of Intelligent Material Systems and Structures, 1, 189-206.

157. Im, S. and Atluri, S.N., 1989, Effects of piezoactuator on a finitely deformed beam subjected to general loading. AIAA Journal, 27, 1801-1807.

158. Ip, K.H. and Tse, P.C., 2001, Optimal configuration of a piezoelectric patch for vibration control of isotropic rectangular plates, Smart Materials and Structures, 10, 395-403.

159. Irschik, H., Krommer, M., Belyaev, A.K. and Schlacher, K., 1998, Shaping of piezoelectric sensors/actuators for vibrations of slender beams: Coupled theory and inappropriate shape functions, Journal of Intelligent Material Systems and Structures, 9, 546-554.

160. Jha, R. and Rower, J., 2002, Experimental investigation of active vibration control using neural networks and piezoelectric actuators, Smart Materials and Structures, 11, 115-121.

161. Jha, R. and He, C., 2002, Neural-network-based adaptive predictive control for vibration suppression of smart structures, Smart Materials and Structures, 11, 909-916.

162. JC Bruch, Jr., Sloss, J.M., Adali, S. and Sadek, I.S., 1999, Modified bang-bang piezoelectric control of vibrating beams, Smart Materials and Structures, 8, 647-653.

163. JC Bruch, Jr., Sloss, J.M., Adali, S. and Sadek, I.S., 2000, Optimal piezo-actuator locations/lengths and applied voltage for shape control of beams, Smart Materials and Structures, 9, 205-211.

164. Joshi, S.P., 1992, Non-linear constitutive relations for piezoelectric materials, Smart Materials and Structures, 1, 80-83.

165. Kamada, T., Fujita, T., Hatayama, T., Arikabe, T., Murai, N., Aizawa, S. and Tohyama, K., 1998, Active vibration control of flexural-shear type frame structures using piezoelectric actuators, Smart Materials and Structures, 7, 479-388.

166. Kagawa, Y., Tsuchiya, T. and Wakatsuki, N., 2001, Equivalent circuit representation of a vibrating structure with piezoelectric transducers and the stability consideration in the active damping control, Smart Materials and Structures, 10, 389-394.

167. Kang, Y.K., Park, H.C., Hwang, W. and Han, K.S., 1996, Prediction and measurement of modal damping of laminated beams with piezoelectric sensor/actuator, Journal of Intelligent Material Systems and Structures, 7, 25-32.

168. Kang, Y.K., Kim, M.H., Park, H.C. and Agrawal, B., 1998, Multi-modal vibration control of laminated composite plates using piezoelectric sensors/actuators, Journal of Intelligent Material Systems and Structures, 9, 988-990.

169. Kawiecki, G., 1998, Finite element study of open-section beams actuated by skewed piezoelements, Smart Materials and Structures, 7, 85-94.

170. Kekana, M., 2002, Finite element modeling of laminated piezo-elastic structures: Lyapunov stability analysis, Journal of Sound and Vibration, 256, 463-473.

171. Kelly, J.S., Rao, V.S., Pottinger, H.J. and Clifford, H., 1997, Design and implementation of digital controller for smart structures using field programmable gate arrays, Smart Materials and Structures, 6, 559-572.

172. Khaheour, A, Golnaraghi, M.F. and Morris, K.A., 1997, Modal coupling controller design using a normal form method, Part 1: dynamics, Journal of Sound and Vibration, 205, 657-670.

173. Khaheour, A, Golnaraghi, M.F. and Morris, K.A., 1997, Modal coupling controller design using a normal form method, Part 2: control, Journal of Sound and Vibration, 205, 671-688.

174. Khdeir, A.A. and Aldraihem, O.J., 2001, Deflection analysis of beams with extension and shear piezoelectric patches using discontinuity functions, Smart Materials and Structures, 10, 212-220.

175. Kim, J., Varadan, V.V., Varadan, V.K. and Bao, X. -Q., 1996, Finite element modeling of a smart cantilever plate and comparison with experiments, Smart Materials and Structures, 5, 165-170.

176. Kim, J. and Ko, B., 1998, Optimal design of a piezoelectric smart structure for noise control, Smart Materials and Structures, 7, 801-808.

177. Kim, S.J. and Jones, J.D., 1995, Quasi-static control of natural frequencies of composite beams using embedded piezoelectric actuators, Smart Materials and Structures, 4, 106-112.

178. Kim, S.J. and Jones, J.D., 1995, Influence of piezo-actuator thickness on the active vibration control of a cantilever beam, Journal of Intelligent Material Systems and Structures, 6, 610-623.

179. Kim, Y.S., Wang, K.W. and Lee, H.S., 1992, Feedback control of ER-Fluid-based structures for vibration suppression, Smart Materials and Structures, 1, 130-145.

180. Kim, Y. and Kum, D., 1997, Simultaneous structural/control optimum design of composite plate with piezoelectric actuators, Journal of Guidance, Control and Dynamics, 20, 1111-1117.

181. Kioua, H. and Mirza, S., 2000, Piezoelectric induced bending and twisting of laminated composite shallow shell, Smart Materials and Structures, 9, 476-484.

182. Kondoh, S., Yatomi, C. and Inoue, K., 1990, The positioning of sensors and actuators in the vibration control of flexible structures, JSME International Journal Series III, 33, 145-152.

183. Krommer, M. and Irechlk, H., 1999, On the influence of the electric field on free transverse vibration of smart beams, Smart Materials and Structures, 8, 401-410.

184. Krommer, M., 2001, On the correction of the Bernoulli-Euler beam theory for smart piezoelectric beams, Smart Materials and Structures, 10, 668-680.

185. Lagoudas, D.C. and Bo, Z., 1994, The cylindrical bending of composite plates with piezoelectric and SMA layers, Smart Materials and Structures, 3, 309-317.

186. Lam, K.Y., Peng, X.Q., Liu, G.R. and Reddy, J.N., 1997, A finite-element model for piezoelectric composite laminates, Smart Materials and Structures, 6, 583-591.

187. Lam, K.Y., Ng, T.Y., 1999, Active control of composite plates with integrated piezoelectric sensors and actuators under various dynamic loading conditions, Smart Materials and Structures, 8, 223-237.

188. Lam, M.J. 1997, Vibration control through passive constrained layer damping and active control, Journal of Intelligent Material Systems and Structures, 8, 663-677.

189. Lane, S.A., Griffin, S. and Leo, D.J., 2001, Active structural acoustic control of a launch vehicle fairing using monolithic piezoceramic actuators, Journal of Intelligent Material Systems and Structures, 12, 795-806.

190. Lara, A., Bruch Jr, J.C., Sloss, J.M., Sadek, I.S. and Adali, S., 2000, Vibration damping in beams via piezo actuation using optimal boundary control, International Journal of Solid and Structures, 37, 6537-6554.

191. Law, H.H., Rossiter, P.L., Simon, G.P. and Koss, L.L., 1996, Characterization of mechanical vibration damping by piezoelectric material, Journal of Sound and Vibration, 197, 489-513.

192. Lee, C. K., 1990, Theory of laminated piezoelectric plates for the design of distributed sensors/actuators. Part 1: governing equations and reciprocal relationships, Journal of the Acoustic Society of American, 87, 1144-1158.

193. Lee, C.-W. and Li, H.L., 2000, Computational analysis for the torsional control of an anti-symmetric piezoelectric composite laminate, Journal of Intelligent Material Systems and Structures, 10, 530-533.

194. Lee, C.-Y. and Cheng, C.-C., 1998, Dynamic characteristics of sandwich beam with embedded Electro-Rheological fluid, Journal of Intelligent Material Systems and Structures, 9, 60-69.

195. Lei, C.Y. and Wu, M.H., 1991, Thermomechanical properties of NITI-base shape memory alloys, Smart Structures and Materials, ASME, 24, 73-77.

196. Leitmann, G., 1994, Semiactive control for vibration attenuation, Journal of Intelligent Material Systems and Structures, 5, 841-846.

197. Leng, J. and Asund, A., 1999, Active vibration control system of smart structures based on FOS and ER actuator, Smart Materials and Structures, 8, 252-256.

198. Leo, D.J., 1999, Energy analysis of piezoelectric-actuated structures driven by linear amplifier, Journal of Intelligent Material Systems and Structures, 10, 36-45.

199. Lesieutre, G.A. and Lee, U., 1996, A finite element for beams having segmented active constrained layers with frequency-dependent viscoelastics, Smart Materials and Structures, 5, 615-627.

200. Lewis, J.A., and Inman, D.J., 2001, Finite element modeling and active control of an inflated torus using piezoelectric devices, Journal of Intelligent Material Systems and Structures, 12, 819-833.

201. Liang, C., Rogers, C.A. and Malafeew, E., 1991, Preliminary investigation of shape memory polymers and their hybrid composites, Smart Structures and Materials, ASME, 24, 97-105.

202. Liang, C., Sun, F. and Rogers, C.A., 1995, Determination of design of optimal actuator location and configuration based on actuator power factor, Journal of Intelligent Material Systems and Structures, 6, 456-464.

203. Liang, C., Sun, F. and Rogers, C.A., 1996, Electro-mechanical impedance modeling of active material systems, Smart Materials and Structures, 5, 171-186.

204. Liao, W.H., Chou, J.H. and Horng, I.R., 1997, Robust vibration control of flexible linkage mechanisms using piezoelectric films, Smart Materials and Structures, 6, 457-463.

205. Liaw, B. M., Liu, Y. X., and Villars, E. A., 2001, Impact Damage Mechanisms in Fiber-Metal Laminates, Proceedings, SEM Annual Conference on Experimental and Applied Mechanics, Portland, OR, June 4-6, 36-539.

206. Lim, Y.H., Varadan, V.V. and Varadan, V.K., 1997, Closed loop finite element modeling of active structural damping in the frequency domain, Smart Materials and Structures, 6, 161-168.

207. Lim, Y.H., Gopinathan, S.V., Varadan, V.V. and Varadan, V.K., 1999, Finite element simulation of smart structures using an optimal output feedback controller for vibration and noise control, Smart Materials and Structures, 8, 324-37.

208. Lin, C.-C. and Hsu, C.-Y., 1999, Static shape control of smart beam plates laminated with sine sensors and actuators, Smart Materials and Structures, 8, 519-530.

209. Lin, C.Y. and Crawley, E.F., 1995, Design considerations for a strain actuated adaptive wing for aeroelastic control, Journal of Intelligent Material Systems and Structures, 6, 403-410.

210. Lin, Y.-H. and Chu, C.-L., 1995, A new design for independent modal space control of general dynamic systems, Journal of Sound and Vibration, 180, 351-361.

211. Lindner, D. and Reichard, K.M., 1991, Control systems using modal domain optical fiber sensors for smart structure application, Smart Structures and Materials, ASME, 24, 117-121.

212. Ling, S.F., Du, H. and Jiang, T., 1998, Analytical and experimental study on a piezoelectric linear motor, Smart Materials and Structures, 7, 382-388.

213. Liu, G.R., Peng, X.Q., Lam, K.Y. and Tani J., 1999, Vibration control simulation of laminated composite plates with integrated piezoelectrics, Journal of Sound and Vibration, 220, 827-846.

214. Lobontiu, N., Goldfarb, M. and Garcia, E., 1999, Achieving maximum tip displacement during resonant excitation of piezoelectrically actuated beams, Journal of Intelligent Material Systems and Structures, 10, 900-913.

215. Lu, L.-Y., Utku, S. and Wada, B.K., 1992, On the placement of active members in adaptive truss structures for vibration control, Smart Materials and Structures, 1, 8-23.

216. Mahut, T., Agbossou, A. and Pastor, J., 1998, Dynamic analysis of piezoelectric fiber composite in an active beam using homogenization and finite element methods, Journal of Intelligent Material Systems and Structures, 9, 1009-1016.

217. Malatkar, P. and Nayfeh, A. H., 2003, A parametric identification technique for SDOF weakly nonlinear systems with cubic nonlinearities, Journal of Vibration and Control, 9, 317-336.

218. Malatkar, P., Nonlinear Vibrations of Cantilever Beams and Plates, Ph.D. thesis, Virginia Polytechnic Institute and State University, Blacksburg, Virginia, 2003.

219. Maln, J.A., Garcia, E. and Howard, D., 1994, Optimal placement and sizing of paired piezoactuators in beams and plates, Smart Materials and Structures, 3, 373-381.

220. Manning, W.J., Plummer, A.R. and Levesley, M.C., 2000, Vibration control of a flexible beam with integrated actuators and sensors, Smart Materials and Structures, 9, 932-939.

221. Marissen, R. and Vogelesang, L. B., 1981, Development of a New Hybrid Material: ARALL, Proceedings, 2nd International SAMPE European Conference, Cannes, Frances, 113-122.

222. Martin, T., Hudd, J., Wells, P., Tunicliffe, D. and Das-Gupta, D., 2001, The use of low profile piezoelectric sensors for impact and acoustic emission (AE) detection in CFRC structures, Journal of Intelligent Material Systems and Structures, 12, 537-544.

223. Meyer, J.L., Harrington, W.B., Agrawal, B.N. and Song, G., 1998, Vibration suppression of a spacecraft flexible appendage using smart material, Smart Materials and Structures, 7, 95-104.

224. Miller, S.E. and Abramovich, H., 1995, A self-sensing piezolaminated actuator model for shells using a first order shear deformation theory, Journal of Intelligent Material Systems and Structures, 6, 624-638.

225. Mollenhauer, D.H. and Griffin Jr., O.H., 1994, Induced strain of actuation of surface bonded piezoceramic patches: A numerical and experimental study, Journal of Intelligent Material Systems and Structures, 5, 355-362.

226. Molyet, K.E., Naganathan, N.G. and Dukkipati, R., 1999, Study of induced strain transfer in piezoceramic smart material systems, Smart Materials and Structures, 8, 672-690.

227. Moon, F.C., Holmes, P.J., 1985, Double-poincare sections of a quasi-periodically forced chaotic attractor, Physical Letters A, 111, 157-160.

228. Moon, S.H and Kim, S.J., 2001, Active and passive suppression of nonlinear panel flutter using finite element method, AIAA Journal, 39, 2042-2050.

229. Na, S. and Librescu, L., 1998, Oscillation control of cantilevers via smart materials technology and optimal feedback control: actuator location and power consumption issues, Smart Materials and Structures, 7, 833-842.

230. Nam, C., Kim, Y. and Weisshaar, T.A., 1996, Optimal sizing and placement of piezo-actuators for active flutter suppression, Smart Materials and Structures, 5, 216-224.

231. Newton, D., Garcia, E. and Horner, G., 1997, A linear piezoelectric motor Smart Materials and Structures, 6, 295-304.

232. Nitzsche, F. and Breitbach, E., 1994, Individual blade control of hinged blades using smart structures Smart Materials and Structures, 3, 171-180.

233. Nitzsche, F. and Breitbach, E., 1994, Vibration control of rotary wings using smart structures, Smart Materials and Structures, 3, 181-189.

234. Niezrecki, C. and Cudney, H.H., 2001, Feasibility to control launch vehicle internal acoustics using piezoelectric actuators, Journal of Intelligent Material Systems and Structures, 12, 647-660.

235. Oguamanam, D.C.D., De Almeida, S.F.M. and Hansen, J.S., 1998, Stress stiffening effects in laminated beams with piezoelectric actuators, Journal of Intelligent Material Systems and Structures, 9, 137-145.

236. Oh, I.K., Han, J.H. and Lee, I, 2000, Postbuckling and vibration characteristics of piezolaminated composite plate subject to thermo-piezoelectric loads, Journal of Sound and Vibration, 233, 19-40.

237. Pae, S., Lee, H., Park, H. and Hwang, W., 2000, Realization of higher-mode deformation of beams using shape memory alloy wires and piezoceramics, Smart Materials and Structures, 9, 848-854.

238. Paget, C.A., Levin, K. and Delebarre, C., 2002, Actuation performance of embedded piezoceramic transducer in mechanically loaded composites, Smart Materials and Structures, 11, 886-891.

239. Pai, P. F. and Nayfeh, A. H., 1990, Three-dimensional nonlinear vibrations of composite beams I: Equations of motion, Nonlinear Dynamics, 1, 477-502.

240. Pai, P. F. and Nayfeh, A. H., 1992, A nonlinear composite beam theory, Nonlinear Dynamics, 3, 273—303.

241. Pai, P.F., Nayfeh, A.H., Oh, K. and Mook, D.T., 1993, A refined nonlinear model of composite plates with integrated piezoelectric actuators and sensors, International Journal of Solids and Structures, 30, 1603-1630.

242. Pai, P. F. and Nayfeh, A. H., 1994, A fully nonlinear theory of curved and twisted composite rotor blades accounting for warpings and three-dimensional stress effects, International Journal of Solids and Structures, 31, 1309-1340.

243. Pai, P.F., Wen, B., Naser, A.S. and Schulz, M.J., 1998, Structural vibration control using PZT patches and non-linear phenomena, Journal of Sound and Vibration, 215, 273-296.

244. Pai, P.F., Rommel, B. and Schulz, M.J., 2000, Dynamics regulation of a skew cantilever plate using PZT patches and saturation phenomena, Journal of Intelligent Material Systems and Structures, 11, 642-655.

245. Pan, X. and Hansen, C.H., 1994, Piezoelectric crystal vs point force excitation of beam and plates, Journal of Intelligent Material Systems and Structures, 5, 363-370.

246. Park, C., Walz, C. and Chopra, I., 1993, Bending and torsion models of beams with induced strain actuators, Smart Structures and Intelligent Systems; Proc. SPIE, 1917, 192-216.

247. Park, C.H., 2001, On the circuit model of piezoceramics, Journal of Intelligent Material Systems and Structures, 12, 515-522.

248. Peelamedu, S.M., Yu, Y., Naganathan, N.G. and Dukkipati, R.V., 1999, Active strain-transfer analysis in a piezoceramic system using a finite-element method and experimental investigation, Smart Materials and Structures, 8, 654-662.

249. Peng, X.Q., Lam, K.Y. and Liu, G.R., 1998, Active vibration control of composite beams with piezoelectrics: a finite element model with third order theory, Journal of Sound and Vibration, 209, 635-650.

250. Pereira, A.K.A., Arruda, J.R.F. and Moreira, F.J.O., 2000, Active control of the structural intensity in beans using frequency-domain adaptive method, Journal of Intelligent Material Systems and Structures, 11, 3-13.

251. Poh, S. and Baz, A., 1990, Active control of a flexible structure using a modal positive position feedback controller, Journal of Intelligent Material Systems and Structures, 1, 273-288.

252. Prakah-Asante, K.O. and Craig, K.C., 1994, The application of multi-channel design methods for vibration control of an active structure, Smart Materials and Structures, 3, 329-343.

253. Preiswerk, M. and Venkatesh, A., 1994, An analysis of vibration control using piezoceramics in planar flexible-linkage mechanisms, Smart Materials and Structures, 3, 190-200.

254. Oates, W.S. and Lynch, C.S., 2001, Piezoelectric hydraulic pump system dynamic model, Journal of Intelligent Material Systems and Structures, 12, 737-744.

255. Qu, Z.Q., 2001, An efficient modeling method for laminated composite plates with piezoelectric sensors and actuators, Smart Materials and Structures, 10, 807-818.

256. Quek, S.T. and Wang, Q., 2000, On dispersion relations in piezoelectric coupled-plate structures, Smart Materials and Structures, 9, 859-867.

257. Rahmoune, M., Benjeddou, A., Ohayon, R. and Osmont, D., 1998, New thin piezoelectric plane model, Journal of Intelligent Material Systems and Structures, 9, 1017-1029.

258. Raja, S., Rohwer, K. and Rose, M., 1999, Piezothermoelastic modeling and active vibration control of laminated piezoelectric composite beam, Journal of Intelligent Material Systems and Structures, 10, 890-899.

259. Raja, S., Prathap, G. and Sinha, P.K., 2002, Active vibration control of composite sandwich beams with piezoelectric extension-bending and shear actuators, Smart Materials and Structures, 11, 63-71.

260. Rao, V., Damle, R. and Tebbe, C. and Kern, F., 1994, The adaptive control of smart structures using neural network, Smart Materials and Structures, 3, 354-366.

261. Rastegar, J.S. and Yuan, L., 2001, A systematic method for the design of piezostack actuator integrated robots for high-speed and precision operation, Journal of Intelligent Material Systems and Structures, 12, 835-846.

262. Ray, J. D. and Bert, C. W., 1969, Nonlinear vibrations of a beam with pinned ends, Journal of Engineering for Industry, 91, 997-1004.

263. Ray, M.C., Rao, K.M. and Samanta, B., 1993, Exact solution for static analysis of an intelligent structure under cylindrical bending, Computers and Structures, 47, 1031-1042.

264. Ray, M.C., 1998, Optimal control of laminated plate with piezoelectric sensor and actuator layers, AIAA Journal, 36, 2204-2208.

265. Redmond, J. and Barney, P., 1997, Vibration control of stiff beams and plates using structurally integrated PZT stack actuators, Journal of Intelligent Material Systems and Structures, 8, 525-535.

266. Rhee, S.W. and Koval, L.R., 1999, Comparison of classical with robust control for SMA smart structures Smart Structures and Materials, 2, 162-171.

267. Rivory, J.F., Hansen, C.H. and Pan, J., 1994, Further studies of the dynamic response of a simply supported beam excited by a pair of out-of-phase piezoelectric actuators, Journal of Intelligent Material Systems and Structures, 5, 654-664.

268. Rivière, A., 1993, damping characterization of composite materials by mechanical spectrometry, ibid, 316-322.

269. Robbins, D.H. and Reddy, J.N., 1991, Analysis of piezoelectrically actuated beams using a layer-wise displacement theory, Computers and Structures, 41, 265-279.

270. Robbins Jr, D.H. and Reddy, J.N., 1996, An efficient computational model for the stress analysis of smart plate structures, Smart Structures and Materials, 5, 353-360.

271. Sadri, A.M., Wright, J.R. and Wyne, R.J., 1999, Modeling and optimal placement of piezoelectric actuators in isotropic plates using genetic algorithms, Smart Structures and Materials, 8, 490-498.

272. Sadri, A.M., Wright, J.R. and Wynne, R.J., 2002, LQG control design for panel flutter suppression using piezoelectric actuators, Smart Materials and Structures, 11, 834-839.

273. Saravanos, D.A. and Heyliger, P.R., 1995, Coupled layerwise analysis of composite beams with embedded piezoelectric sensors and actuators, Journal of Intelligent Material Systems and Structures, 6, 350-363.

274. Saravanos, D.A., 1997, Passively damped laminated piezoelectric shell structures with integrated electric networks, AIAA Journal, 38, 1260-1268.

275. Saravanos, D.A., 1997, Mixed laminate theory and finite element for smart piezoelectric composite shell structures, AIAA Journal, 35, 1327-1333.

276. Sato, K., Saito, H., and Otomi, K., 1978, The parametric response of a horizontal beam carryinga concentrated mass under gravity, Journal of Applied Mechanics, 45, 643-648.

277. Schafer, J. and Janocha, H., 1995, Cancellation of periodic forces with solid-state actuators, Journal of Intelligent Material Systems and Structures, 6, 140-145.

278. Saunders, W.R., Cole, D.G. and Robertshaw, H.H., 1994, Experiments in piezostructure modal analysis for MIMO feedback control, Smart Materials and Structures, 3, 210-218.

279. Schetky, L.M. and Wu, M.H., 1991, The properties and processing of shape memory alloys for use as actuators in intelligent composite materials, Smart Structures and Materials, ASME, 24, 65-71.

280. Schijve, J., Van Lipzig, H. T. M., Van Gestel, G. F. J. A. and Hoeymakers, A. H. W., 1979, Fatigue Properties of Adhesively-Bonded Laminated Sheet Materials of Aluminum Alloys, Engineering Fracture Mechanics, 12, 561-579.

281. Schultz, A.B. and Tsai, S.W., 1968, Dynamic moduli and damping ratios in fiber-reinforced composites, Journal of Composite Materials, 2, 368-379.

282. Schultz, A.B. and Tsai, S.W., 1969, Measurements of complex dynamic moduli for laminated fiber-reinforced composites, Journal of Composite Materials, 3, 434-443.

283. Schultz, G. and Heimbold, G., 1983, Dislocated actuator/sensor positioning and feedback design for flexible structures, Journal of Guidance, 6, 361-367.

284. Seeley, C.E. and Chattopadhyay, A., 1993, The development of an optimization procedure for the design of intelligent structures, Smart Materials and Structures, 2, 135-146.

285. Seeley, C.E. and Chattopadhyay, A., 1998, Experimental investigation of composite beams with piezoelectric actuation and debonding, Smart Materials and Structures, 7, 502-511.

286. Shah, D.K., Joshi, S.P. and Chan, W.S., 1993, Static structural response of plates with piezoelectric layers, Smart Materials and Structures, 2, 172-180.

287. Shaw, J., 2000, Hybrid control of a cantilevered ER sandwich beam for vibration suppression, Journal of Intelligent Material Systems and Structures, 11, 26-31.

288. Shen, I.Y. 1995, Bending and torsional vibration control of composite beams through intelligent constrained-layer damping treatments, Smart Materials and Structures, 4, 340-355.

289. Shen, M.-H.H., 1994, Analysis of beams containing piezoelectric sensors and actuators, Smart Materials and Structures, 3, 439-447.

290. Shen, Y. and Homaifar, A., 2001, Vibration control of flexible structures with PZT sensors and actuators, Journal of Vibration and Control, 7, 417-451.

291. Shih, H.R., 2000, Distributed vibration sensing and control of a piezoelectric laminated curved beam, Smart Materials and Structures, 9, 761-766.

292. Shu, S.G., Lagoudas, D.C., Hughes, D. and Wen, J.T., 1997, Modeling of a flexible beam actuated by shape memory alloy wires, Smart Materials and Structures, 6, 265-277.

293. Sirohi, J. and Chopra, I., 2000, Fundamental behavior of piezoceramic sheet actuators, Journal of Intelligent Material Systems and Structures, 11, 47-61.

294. Smyser, C.P. and Chandrashekhara, K., 1997, Robust vibration control of composite beams using piezoelectric devices and neural networks, Smart Materials and Structures, 6, 178-189.

295. Smyser, S.D. and Tanaka, N. 1993, A neural network for feedforward controlled smart structures, Journal of Intelligent Material Systems and Structures, 4, 373-378.

296. Song, G., Kelly, B. and Agrawal, B., 2000, Active position control of a shape memory alloy wire actuated composite beam, Smart Materials and Structures, 9, 711-716.

297. Song, G., Schmidt, S.P. and Agrawal, B.N., 2000, Active vibration suppression of a flexible structure using smart material and a modular control patch, Proceeding of Institution of Mechanical Engineers, 214, 217-229.

298. Song, J.K. and Washinhton, G., 2000, Neural network discrimination in intelligent vibration control, Journal of Intelligent Material Systems and Structures, 11, 234-242.

299. Song, O., Librescu, L. and Rogers, C.A., 1994, Active response control of cantilevered thin-walled beams carrying heavy concentrated masses, Journal of Intelligent Material Systems and Structures, 5, 42-48.

300. Spencer, M.G., Sanner, R.M. and Chopra, I., 1998, An adaptive neurocontroller for vibration suppression and shape control of a flexible beam, Journal of Intelligent Material Systems and Structures, 9, 160-170.

301. Steffen V., Jr. and Inman, D.J., 1999, Optimal design of piezoelectric materials for vibration damping in mechanical systems, Journal of Intelligent Material Systems and Structures, 10, 945-955.

302. Stobener, U. and Gaul, L., 2000, Modal vibration control for PVDF coated plates, Journal of Intelligent Material Systems and Structures, 11, 283-293.

303. Strmbi, G., Barboni, R. and Gaudenzi, P., 1995, Pin-force and Euler-Bernoulli models for analysis of intelligent structures, AIAA Journal, 33, 1746-1749.

304. Sugavanam, S., Varadan, V.K. and Varadan, V.V., 1998, Modeling and control of a lightly damped T-beam using piezoceramic actuators and sensors, Smart Materials and Structures, 7, 899-906.

305. Suleman, A., Modi, V.J., Venkayya, V.B., 1995, Structural modeling issues in flexible systems, AIAA Journal, 33, 919-923.

306. Suleman, A. and Venkayya, V.B., 1995, A simple finite element formulation for a laminated composite plate with piezoelectric layers, Journal of Intelligent Material Systems and Structures, 6, 776-782.

307. Suleman, A. and Goncalves, M.A., 1999, Multi-objective optimization of an adaptive composite beam using the physical programming approach, Journal of Intelligent Material Systems and Structures, 10, 56-70.

308. Sun, B. and Huang, D., 2000, Analytical vibration suppression analysis of composite beams with piezoelectric laminae, Smart Materials and Structures, 9, 751-760.

309. Sun, C. T., Dicken, A., and Wu, H. F., 1993, Characterization of Impact Damage in ARALL Laminates, Composites Science and Technology, 49,139-144.

310. Sun, D., Wang, D. and Wu, H., 1999, Distributed piezoelectric element method for vibration control of smart plates, AIAA Journal, 37, 1459-1463.

311. Sun, D., Tong, L. and Wang, D., 2001, Vibration control of plates using discretely distributed piezoelectric quasi-modal actuators/sensors, AIAA Journal, 39,1766-1772.

312. Sung, C.K., Chen, T.F. and Chen, S.G., 1996, Piezoelectric modal actuator/sensor design for monitoring/generating flexural and torsional vibrations of cylindrical shells, Journal of Vibration and Acoustics, 118, 48-55.

313. Tabaddor, M., 2000, Influence of nonlinear boundary conditions on the single-mode response of a cantilever beam, International Journal of Solids and Structures, 37, 4915-4931.

314. Takawa, T., Fukuda, T. and Takada, T., 1997, Flexural-torsion coupling vibration control of fiber composite cantilevered beam by using piezoceramic actuators, Smart Materials and Structures, 6, 477-484.

315. Tani, J., Qiu, J. and Miura, H., 1995, Vibration control of a cylindrical shell using piezoelectric actuators, Journal of Intelligent Material Systems and Structures, 6, 380-388.

316. Tauchert, T. R., 1971, Measurements of the elastic moduli of laminated composites using an ultrasonic technique, Journal of Composite Materials, 5, 549-552.

317. Thompsoni, D.M. and Jr., H.G., 1993, Finite element predictions of active buckling control of stiffened panels, Journal of Intelligent Material Systems and Structures, 4, 243-247.

318. Tong, D. and Williams II, R.L., 1998, Optimal shape control of composite thin plates with piezoelectric actuators, Journal of Intelligent Material Systems and Structures, 9, 458-467.

319. Trindade, M.A., Benjeddou, A. and Ohayon, R., 1999, Parametric analysis of the vibration control of sandwich beams through shear-based piezoelectric actuators, Journal of Intelligent Material Systems and Structures, 10, 377-385.

320. Tsai, M.S. and Wang, K.W., 1996, Control of a ring structure with multiple active - passive hybrid piezoelectrical networks, Smart Materials and Structures, 5, 695-703.

321. Tsai, M.S. and Wang, K.W., 1999, On the structural damping characteristics of active piezoelectric actuators with passive shunt, Journal of Sound and Vibration, 221, 1-22.

322. Tsai, M.S. and Wang, K.W., 2002, A coupled robust control/optimization approach for active-passive hybrid piezoelectric networks, Smart Materials and Structures, 11, 389-395.

323. Tzou, H.S. and Grade, M., 1989, Theoretical analysis of a multi-layered thin shell coupled with piezoelectric shell actuations for distributed vibration controls, Journal of Sound and Vibration, 132, 433-450.

324. Tzou, H.S. and Tseng, C.I., 1990, Distributed piezoelectric sensor/actuator design for dynamic measurement/control of distributed parameter system: a piezoelectric finite element approach, Journal of Sound and Vibration, 138, 17-34.

325. Tzou, H.S. and Fu, H.Q., 1994, A study of segmentation of distributed piezoelectric sensors and actuators part 1: theoretical analysis. Journal of Sound and Vibration, 172, 247-259.

326. Tzou, H S, Zhong, J.P. and Hollkamp, J.J., 1994, Spatially distributed orthogonal piezoelectric shell actuators: theory and applications, Journal of Sound and Vibration, 177, 363- 378.

327. Tzou, H S, Hollkamp, J.J., 1994, Collocated independent modal control with self-sensing orthogonal piezoelectric actuators (theory and experiment), Smart Materials and Structures, 3, 277-284.

328. Tzou, H S and Bao, Y., 1994, Modeling of thick anisotropic composite triclinic piezoelectric shell transducer laminates, Smart Materials and Structures, 3,285-292.

329. Tzou, H S and Bao, Y., 1994, Nonlinear piezothermoelasticity and multi-field actuations, Part 1: Nonlinear anisotropic composite piezothermoelectric shell laminates, Journal of Sound and Vibration, 119, 374-389.

330. Valoor, M.T., Chandrashekhara, K. and Agarwal, S., 2000, Active vibration control of smart composite plates using self-adaptive neuro-controller, Smart Materials and Structures, 9, 197-204.

331. Varadan, V.K., Hong, S.Y. and Varadan, V.V., 1990, Piezoeletric sensors and actuators for active vibration damping using digital control, Smart Materials and Structures, 9, 197-204.

332. Varadarajan, S., Chandrashekhara, K. and Agarwal, S., 2000, LQG/LTR-based robust control of composite beams with piezoelectric devices, Journal of Vibration and Control, 6, 607-630.

333. Vel, S.S. and Batra, R.C., 2000, Three-dimensional analytical solution for hybrid multilayered piezoelectric plates, Journal of Applied Mechanics, 67, 558-567.

334. Vel, S.S. and Batra, R.C., 2000, Cylindrical bending of laminated plates with distributed and segmented piezoelectric actuators/sensors, AIAA Journal, 38, 857-867.

335. Vel, S.S. and Batra, R.C., 2001, Exact Solution for Rectangular Sandwich Plates with Embedded Piezoelectric Shear Actuators, Smart Materials and Structures,10, 240-251.

336. Vipperman, J.S. and Clark, R.L., 1996, Implementation of an adaptive piezoelectric sensoriactuator, AIAA Journal, 34, 2102-2109.

337. Vlot, A., 1993, Impact Properties of Fiber Metal Laminates, Composite Engineering, 3, 911-927.

338. Wada, B.K., Fanson, J.L. and Crawley, E.F., 1990, Adaptive structures, Journal of Intelligent Material Systems and Structures, 1, 157-174.

339. Wagner, U.V. and Hagedorn, P., 2002, Piezo-beam systems subjected to weak electric field: experiments and modeling of non-linearities, Journal of Sound and Vibration, 256, 861-872.

340. Wang, B. -T. and Rogers, C.A., 1991, Modeling of finite-length spatially-distributed induced strain actuators for laminate beams and plates, Journal of Intelligent Material Systems and Structures, 2, 38-58.

341. Wang, B.-T. and Wang, C.C., 1996, Modeling of finite-length spatially-distributed induced strain actuators Feasibility analysis of using piezoceramic transducers for cantilever beam modal testing, Smart Materials and Structures, 6, 106-116.

342. Wang, C.M., Ang, K.K. and Ajit, A., 1999, Shape control of laminated cantilevered beams with piezoelectric actuators, Journal of Intelligent Material Systems and Structures, 10, 164-175.

343. Wang, Q. and Quek, S.T., 2000, Flexural vibration analysis of sandwich beam coupled with piezoelectric actuator, Smart Materials and Structures, 9, 103-109.

344. Wang, Q. and Wang, C.M., 2000, Optimal placement and size of piezoelectric patches on beams from the controllability perspective, Smart Materials and Structures, 9, 558-567.

345. Wang, Q., Quek, S.T., Sun, C.T. and Liu, X. 2001, Analysis of piezoelectric coupled circular plate. Smart Materials and Structures, 10, 229-239.

346. Wang, S.Y., Quek, S.T. and Ang, K.K., 2001, Vibration control of smart piezoelectric composite plates, Smart Materials and Structures, 10, 637-644.

347. Wang, X., Ehlers, C. and Neitzel, M., 1996, Electro-mechanical dynamic analysis of the piezoelectric stack, Smart Materials and Structures, 5, 492-500.

348. Wang, X., Ehlers, C. and Neitzel, M., 1997, An analytical investigation of static models of piezoelectric patches attached to beams and plates, Smart Materials and Structures, 6, -213.

349. Wang, X. and Shen, Y., 1998, On the characterization of piezoelectric actuators attached to structures, Smart Materials and Structures, 7, 389-395.

350. Woinowsky-Krieger, S., 1950, The effect of an axial force on the vibration of hinged bars, Journal of Applied Mechanics, 17, 35—36.

351. Wu, H. F., 1989, Statistical Analysis of Tensile Strength of ARALL Laminates, Journal of Composite Materials, 23, 1065-1080.

352. Wu, H. F., 1990, Temperature Dependence of the Tensile Properties of ARALL-4 Laminates," Journal of Materials Science, 25, 1120-1127.

353. Yalcintas, M., Coulter, J.P. and Don, D.L., 1995, Structural modeling and optimal control of electorheological material based adaptive beams, Smart Materials and Structures, 4, 207-214.

354. Yalcintas, M. and Coulter, J.P., 1998, Electorheological material based non-homogeneous adaptive beams, Smart Materials and Structures, 7, 128-143.

355. Yan, Y.J. and Yam, L.H., 2002, Optimal design of number and locations of actuators in active vibration control of a space truss, Smart Materials and Structures, 11, 496-503.

356. Yang, J.S., Batra, R.C. and Liang, X.Q., 1994, The cylindrical bending vibration of a laminated elastic plate due to piezoelectric actuators, Smart Materials and Structures, 3, 485-493.

357. Yang, J.S. and Tiersten, H.F., 1997, Elastic analysis of the transfer of shearing stress from partially electroded piezoelectric actuators to composite plates in cylindrical bending, Smart Materials and Structures, 6, 333-340.

358. Yang, J.S., 1997, Equations for the flexural motion of elastic plates with partially electroded piezoelectric actuators, Smart Materials and Structures, 6, 485-490.

359. Yang, J.S., 1999, Equations for thick elastic plates with partially electroded piezoelectric actuators and higher order electric fields, Smart Materials and Structures, 8, 73-82.

360. Yang, S.M., 1993, Stability criteria of structural control with systems noncolocated velocity feedback, AIAA Journal, 31, 1351-1353.

361. Yang, S.M. and Lee, Y.J., 1993, Optimization of non-collocated sensor/actuator location and feedback gain in control systems, Smart Materials and Structures,2, 96-102.

362. Yang, S.M. and Lee, Y.J., 1993, Vibration suppression with optimal sensor/actuator location and feedback gain, Smart Materials and Structures, 2, 232-239.

363. Yang, S.M. and Chiu, J.S., 1994, Dither-motor design with concurrent sensing and actuating piezoelectric materials, Smart Materials and Structures, 3, 248-253.

364. Yang, S.M. and Lee, Y.J., 1994, Interaction of structure vibration and piezoelectric actuation, Smart Materials and Structures, 3, 494-500.

365. Yang, S.M. and Lee, Y.J., 1994, Modal analysis of stepped beams with piezoelectric materials, Journal of Sound and Vibration, 176, 289-300.

366. Yang, S.M. and Bian, J.J., 1995, Vibration suppression experiment on composite laminated plates using an embedded piezoelectric sensor and actuator, Smart Materials and Structures, 4, 501-507.

367. Yang, S.M. and Jeng, C.A., 1996, Structural vibration suppression by concurrent piezoelectric sensor and actuator, Smart Materials and Structures, 5, 806-813.

368. Yang, S.M. and Lee, G.S., 1998, An optimal neural network design methodology for fast convergence and vibration suppression, Journal of Intelligent Material Systems and Structures, 9, 999-1008.

369. Yang, Y., Ju, C. and Soh, C.K., 2003, Analytical and semi-analytical solutions for vibration control of a cantilevered column using a piezoelectric actuator, Smart Materials and Structures, 12, 193-203.

370. Yim, W. and Singh, S.N., 2000, Variable structure adaptive force tracking control of a cantilevered column using a piezoelectric actuator, Journal of Vibration and Control, 6, 1029-1043.

371. Young, A.J. and Hansen, C.H., 1994, Control of flexural vibration in a beam using a piezoceramic actuator and an angle stiffener, Journal of Intelligent Material Systems and Structures, 5, 536-549.

372. Yousefi-koma, A. and Vukovich, G., 1999, Optimization of piezoacturator configuration in control of flexible structures, Journal of Intelligent Material Systems and Structures, 10, 787-796.

373. Yousefi-koma, A. and Vukovich, G., 2000, Vibration suppression of flexible beams with bonded piezotransducers using wave-absorbing controllers, Journal of Guidance, Control and Dynamics, 23, 347-354.

374. Yu, Y.Y., 1995, Some recent advances in linear and nonlinear dynamical modeling of elastic and piezoelectric plates, Journal of Intelligent Material Systems and Structures, 6, 237-244.

375. Yuan, S.-Q., Xu, Q.-Y. and Zhang, L., 1999, Application of internal model based controller to active vibration suppression system, Journal of Intelligent Material Systems and Structures, 10, 914-999.

376. Zavodney, L. D., 1987, Can the modal analyst afford to be ignorant of nonlinear vibration phenomena? Proceedings of the 5th International Modal Analysis Conference, London, 154-159.

377. Zeinoun, I.J. and Khorrami, F., 1994, An adaptive control scheme based on fuzzy logic and its application to smart structures, Smart Materials and Structures, 3, 266-276.

378. Zhang, H., Lennox, B., Goulding, P.R. and Leung, A.Y.T., 2000, A float-encoded genetic algorithm technique for integrated optimization of piezoelectric actuator and sensor placement and feedback gains, Smart Materials and Structures, 9, 552-557.

379. Zhang, Q., Shelley, S., Allemang, R.J., 1991, A active damping design of flexible structures based on SISO and SIMO noncolocated sensor-actuator velocity feedback, Journal of Dynamic System, Measurement and Control, 113, 259-266.

380. Zhang, X.D., Rogers, C.A. and Liang, C., 1991, Modeling of two-way shape memory effect, Smart Structures and Materials, ASME, 24, 79-90.

381. Zhang, X.D. and Sun, C.T., 1996, Formulation of an adaptive sandwich beam, Smart Materials and Structures, 5, 814-823.

382. Zhang, X.D. and Sun, C.T., 1999, Analysis of a sandwich plate containing a piezoelectric core, Smart Materials and Structures, 8, 31-40.

383. Zhou, S., Liang, C. and Rogers, C.A., 1995, Integration and design of piezoceramic patch actuators, Journal of Intelligent Material Systems and Structures, 6, 125-133.

384. Zhou, S., Liang, C. and Rogers, C.A., 1995, Integration and design of piezoceramic elements in intelligent structures, Journal of Intelligent Material Systems and Structures, 6, 733-743.

385. Zhou, X., Chattopadhyay, A. and Thornburgh, R., 2000, Analysis of piezoelectric smart composites using a coupled piezoelectric-mechanical model, Journal of Intelligent Material Systems and Structures, 11, 169-179.

386. Zhou, Y.S. and Tiersten, H.F., 1994, An elastic analysis of laminated composite plates in cylindrical bending due to piezoelectric actuators, Smart Materials and Structures, 3, 255-265.

PUBLICATIONS

1. Liu, Jianjun, 1996, Introduction to Foxbase & FoxPro database system, Beijing Science & Technology Publishing House, Beijing, People's Republic of China.

2. Liu, J.J. and Liaw, B., 2001, Dynamic mechanical properties of fiber-metal laminates, ASME International Mechanical Engineering Congress and Exposition, Volume I, 1-6

3. Liu, J.J. and Liaw, B., 2002, Vibration and impulse responses of fiber-metal laminated beams, Proceedings of IMAC-XX: A Conference on Structural Dynamics, Volume II, 1411-1416

4. Liu, J.J. and Liaw, B., 2004, Efficiency of active control of beam vibration using PZT Patches, 2004 SEM Conference & Exposition